OXFORD

Planetary Atmospheres

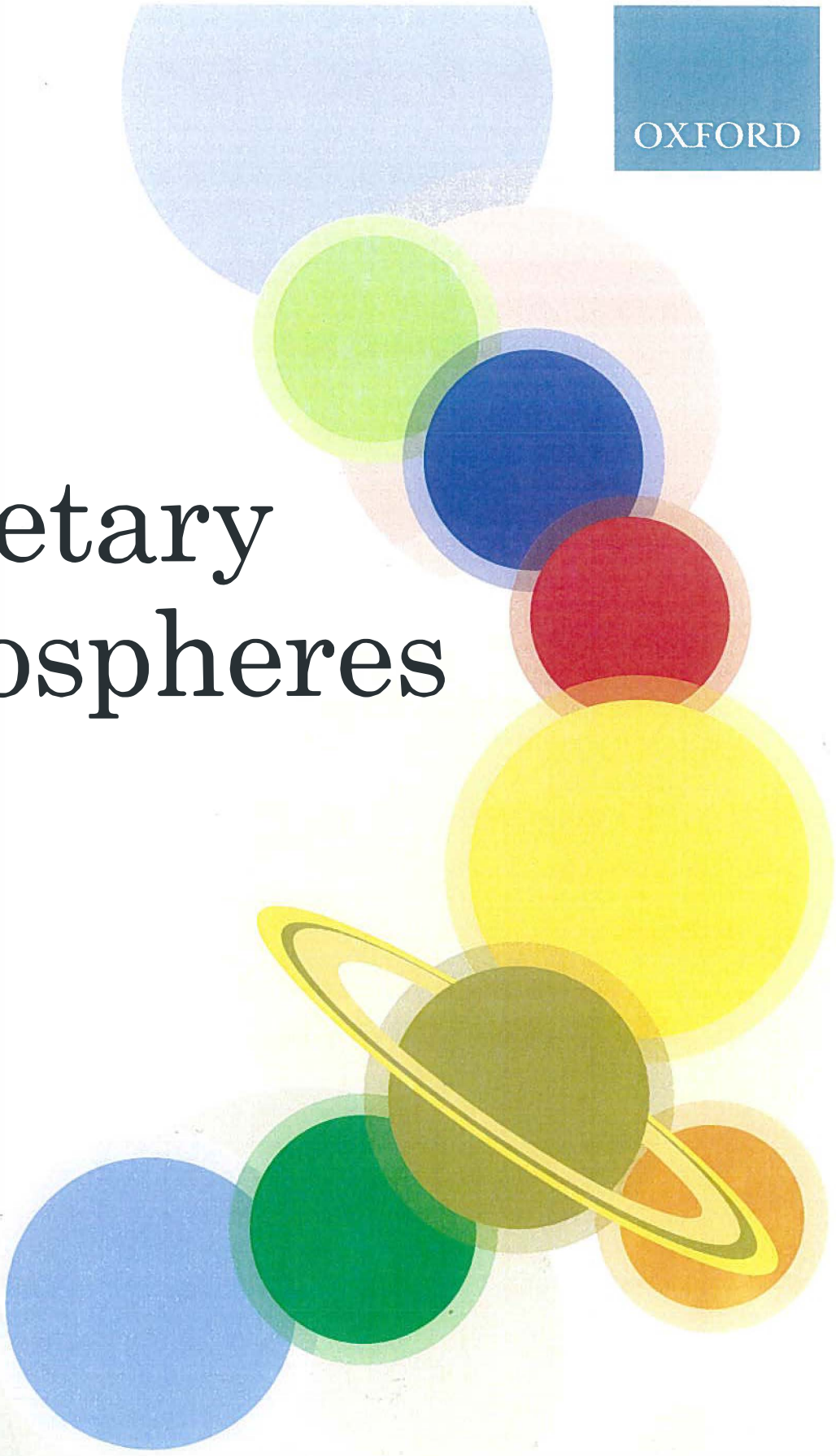

F. W. Taylor

Planetary Atmospheres

F.W. Taylor

Department of Physics
University of Oxford, UK

Original artwork by D.J. Taylor

OXFORD
UNIVERSITY PRESS

OXFORD
UNIVERSITY PRESS
Great Clarendon Street, Oxford OX2 6DP
Oxford University Press is a department of the University of Oxford.
It furthers the University's objective of excellence in research, scholarship,
and education by publishing worldwide in
Oxford New York
Auckland Cape Town Dar es Salaam Hong Kong Karachi
Kuala Lumpur Madrid Melbourne Mexico City Nairobi
New Delhi Shanghai Taipei Toronto
With offices in
Argentina Austria Brazil Chile Czech Republic France Greece
Guatemala Hungary Italy Japan Poland Portugal Singapore
South Korea Switzerland Thailand Turkey Ukraine Vietnam
Oxford is a registered trade mark of Oxford University Press
in the UK and in certain other countries
Published in the United States
by Oxford University Press Inc., New York

First published 2010

British Library Cataloguing in Publication Data
Data available
Library of Congress Cataloging in Publication Data
Data available
Typeset by SPI Publisher Services, Pondicherry, India
Printed in Great Britain
on acid-free paper by
CPI Antony Rowe
ISBN 978–0–19–954742–5 (Hbk)
ISBN 978–0–19–954741–8 (Pbk)
1 3 5 7 9 10 8 6 4 2

Preface

The final year of the Physics undergraduate degree (M.Phys.) course at Oxford University involves specialisation in two areas of Physics, which the student chooses from a list of eleven options. One of these options, called *The Physics of Atmospheres and Oceans*, is further subdivided into short courses on basic Atmospheric Physics and Oceanography, Theory and Practice of Remote Sounding, Weather Forecasting, Climate Change and Chaos, and Comparative Planetology. All of the students, whether they choose this option or not, took, in the previous year, the course called *Climate Physics* which provides a basis for the more advanced material in the *Atmospheres and Oceans* option. A textbook for the Climate Physics course, *Elementary Climate Physics*, was published in 2005.

This book is the text for the *Comparative Planetology* segment of the final year course. The title *Planetary Atmospheres* has been chosen to avoid the confusion that might result when 'comparative planetology' is no longer obviously meant to be in the context of a course about atmospheres and oceans. The coverage is also extended somewhat beyond the boundaries of the Oxford course in order to make it more useful to students elsewhere. The emphasis remains on *comparative* aspects of planetary atmospheres, generally meaning comparison with the Earth, including atmospheric composition, thermal structure, cloud properties, dynamics, weather and climate, and aeronomy. The goal is to look for common processes at work under different boundary conditions in order to reach a fundamental understanding of the physics of atmospheres.

It is appropriate for a short module that forms part of a general Physics course that it should choose to emphasise certain aspects that are of broad topical interest. Here, those are (i) evolutionary processes, setting the Earth in its context as a planet and a member of the Solar System; (ii) the properties of atmospheres that affect the climate near the surface of each planet; and (iii) measurement techniques and models, where the same experimental and theoretical physics is applied under different conditions to investigate and explain atmospheric behaviour. These might be thought of as the astronomical, environmental, and technical sides of the discipline, respectively.

The syllabus for the Oxford course is summarised in the student handbook as:

- *Origins of planetary atmospheres and evolution*;
- *Composition and photochemistry*;
- *Radiative properties and energy balance*;

- *Clouds, dust, and aerosol*;
- *Atmospheres in radiative equilibrium*;
- *Climate and climate change*; and
- *Observation of planetary atmospheres*.

The recommended textbooks used before the present book existed are listed below; it had been a problem that a minimum of five books were needed to support one short course, and that some of those are somewhat out of date, requiring further subsidiary references to cover the course adequately. This book was produced to cover the basics in a single manuscript. Of course, some secondary reading is also appropriate, and the other recommended books are still relevant. In addition, specific references to important sources or seminal papers are given at the ends of the chapters, along with key definitions and some historical background in footnotes and in the Glossary at the end of the book.

The approach is the same as in *Elementary Climate Physics*: an overview, followed by more detailed discussion of key topics, arranged by physical phenomenon and not planet by planet as usually found in this field. There is an emphasis on acquiring and interpreting measurements, including the basic physics of instruments and models. The resulting knowledge about atmospheres is set in the context of simple models that can be manipulated with no more computing power than is available with a simple spreadsheet and which do not obscure the basic physics. A clear, basic discussion sometimes requires a difficult balance between repetition and cross-referencing. Where terms are introduced in the text they appear in italics and are defined and explained in the glossary at the end of the book. Values for important parameters and useful constants are also collected in an appendix. A handy set of simplified reference model atmospheres is also provided, as are some sample questions, mostly from past examinations and tutorials, for which the answers are to be found in the text.

Additional topics that fall outside the Oxford syllabus are covered whenever that gives a more well-rounded treatment of the subject for the benefit of readers who are not at Oxford and not taking this particular course. In this way, it is hoped that this book will be found to be useful for a wide range of students everywhere, or anyone interested in the fundamental science of planetary atmospheres.

Acknowledgements

Thanks are extended to the many colleagues past and present whose work in one way or another contributed to the material presented here. Particular acknowledgement and gratitude is due to Dr D.J. Taylor who drew all of the original diagrams and created the cover image. Ms Jo Barstow, Dr Colin Wilson and Professor Peter Read scrutinised some or all of the manuscript and made very useful suggestions and corrections.

Parts of the chapter on atmospheric dynamics are based on unpublished lecture notes produced by the present author with P.L. Read, R. Hide, and P.J. Gierasch in the 1980s for a graduate course on the subject, and on some current lectures given by Professor Read. Sections 9.5 and 9.8 on the climates of Mars and Titan, respectively, follow the author's books: *The Scientific Exploration of Mars*, Cambridge University Press, 2009, and *Titan: Exploring an Earthlike World*, (with A. Coustenis), World Scientific Publishing, 2008, where more detailed coverage, illustrations and references may be found.

Other major sources and references that will be of value to the student are listed at the end of each chapter or, where needed to bolster a specific point or measurement, in a footnote. Background notes are also provided in footnotes.

Recommended books

The present book assumes knowledge of the material covered in:

F.W. Taylor, *Elementary Climate Physics*, Oxford University Press, 2005, which relates to a course taken by Physics undergraduates in the Third Year at Oxford, i.e., one year before the *Planetary Atmospheres* course. For very important material or derivations a summary is given in this book, with a reference back to the longer discussion in the introductory text for those who find the material unfamiliar.

For further reading, the following general texts are recommended:

N. McBride and I. Gilmour, eds., *An Introduction to the Solar System*, Cambridge University Press, 2004.

J.S. Lewis, *The Physics and Chemistry of the Solar System*, Academic Press, 1995.

J.W. Chamberlain and D.M. Hunten, *Theory of Planetary Atmospheres*, Academic Press, 2nd edition, 1987.

J.T. Houghton, F.W. Taylor, and C.D. Rodgers, *Remote Sounding of Atmospheres*, Cambridge University Press, 1986, republished 2009.

I. de Pater and J.J. Lissauer, *Planetary Sciences*, Cambridge University Press, 2001.

Contents

The Solar System, the planets and their atmospheres

1

1.1 The Solar System

The study of planetary atmospheres helps us to understand the origin, evolution and current properties of the family of planets that orbit the Sun. Of particular interest at the present time is the investigation of the variability and overall stability of these atmospheres, to understand the surface environment and climate. On the best known example, Earth, these depend on a complicated, changing, and far from completely understood balance between radiative, dynamical and chemical processes, all of which have analogues on the other planets. By investigating all of them, we learn more than we would by studying the Earth as an isolated example.

Figures 1.1 and 1.2 show the scale of the Solar System. The planets fall into two groups: four small, rocky inner planets, and four large, fluid outer planets. The satellites and rings of the outer planets give us clues to the origin and evolution of the system as a whole, as do the small rocky and icy bodies concentrated in the asteroid belt between Mars and Jupiter, and the icy Kuiper belt objects that orbit beyond Neptune. These small bodies inform us about the history of the Solar System as a whole, but obviously are less-valuable analogues of the Earth and its climate system than the planets themselves.

Venus, Earth and **Mars,** the inner Solar System planets with substantial atmospheres, are of moderate size when compared to the asteroids and comets on one hand, and the gas giants of the outer Solar System on the other (Table 1.1). All have rocky surfaces, and interiors that contain large abundances of heavy elements, such as iron and nickel. Their atmospheres are geometrically thin compared to the planetary radius, but they are dense enough to be *optically thick* at some wavelengths[1] and to have a profound influence on the radiative energy balance prevailing at the solid surface (a useful definition of a 'thick' atmosphere when studying climate). Earth's atmosphere is optically thin near the peak emitting wavelength of the Sun ($\sim 0.7\,\mu$m), and optically thick near the peak emitting wavelength of the Earth's surface ($\sim 15\,\mu$m).[2]

The four giant or 'Jovian' planets, **Jupiter, Saturn, Uranus,** and **Neptune**, dominate the outer Solar System. They account for 99.6% of the total mass of the planets and have very deep atmospheres and large complements of satellites. The differences in the compositions of

[1] An atmosphere, or any other object, is optically thick at a given wavelength when a photon of that wavelength has only a small chance, typically defined as less than e^{-5} or about 0.67%, of being transmitted without absorption or scattering.

[2] The unit of wavelength most used in the infrared is the micron or micrometre, abbreviated μm, which is one thousandth of a millimetre. The wavelength of visible light ranges approximately from 0.38 to 0.75 μm.

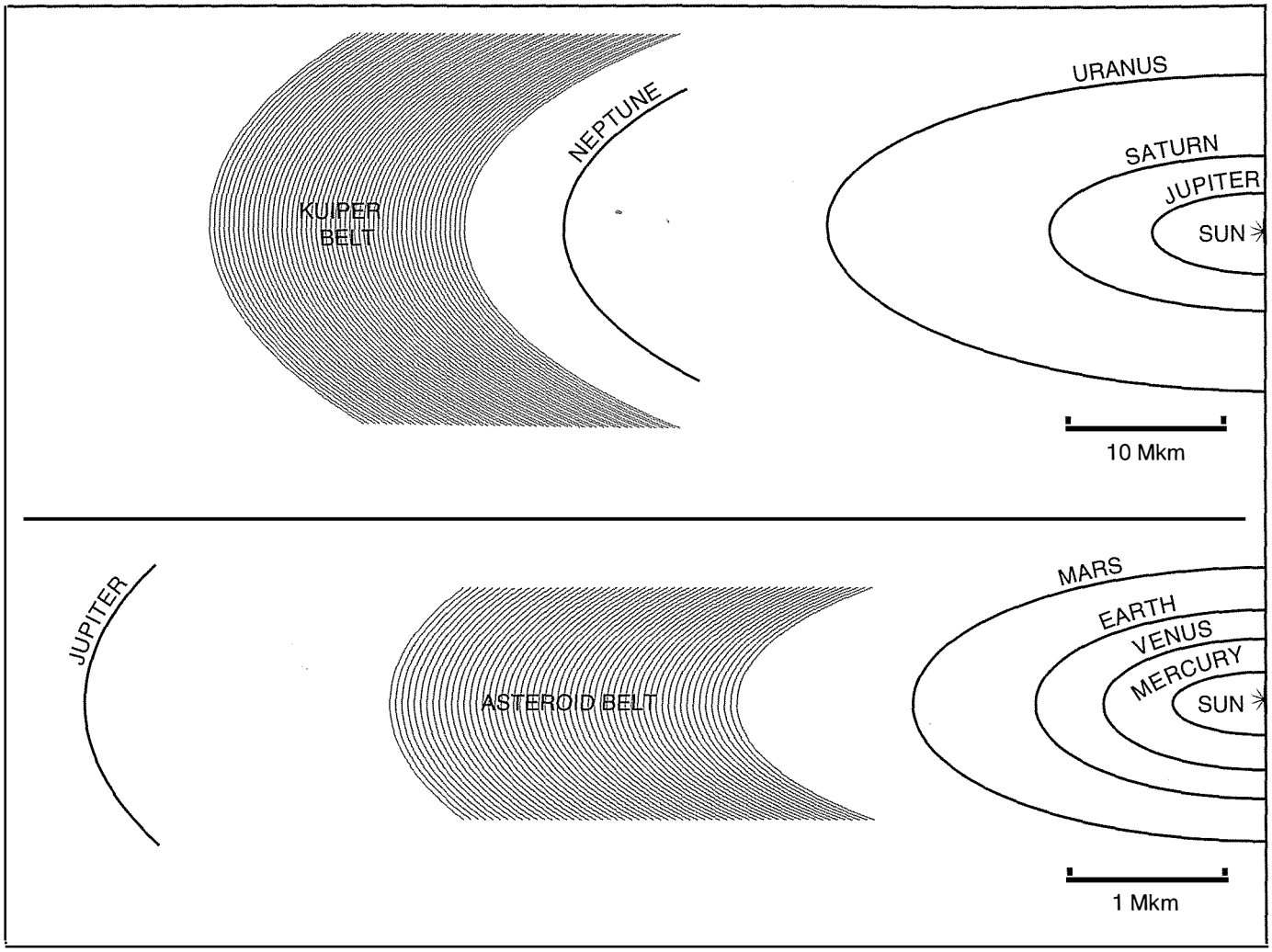

Fig. 1.1
The Solar System: orbital distances. The scale in the lower diagram is ten times smaller than the upper one, in order to display the inner planets and the approximate location of the densest part of the asteroid belt. The upper frame shows the outer planet orbits, and the approximate location of the densest part of the Kuiper belt. The orbit of Jupiter appears in both frames for reference.

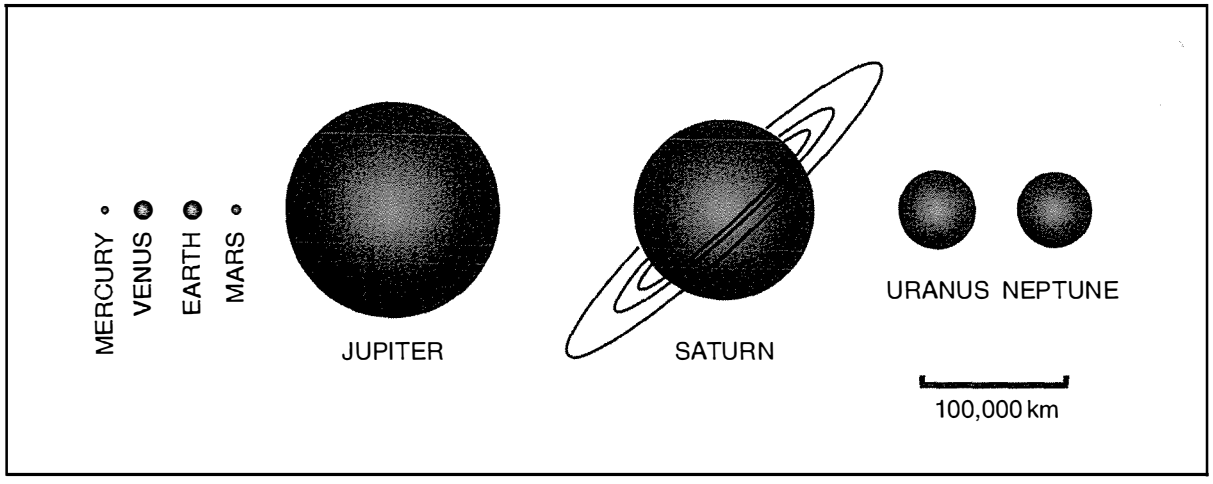

Fig. 1.2
The relative sizes of the planets. By this criterion alone, they clearly form two families.

Table 1.1 The physical properties of the planets, in dimensionless units relative to Earth = 1. For absolute units, see the additional tables in Appendix A.

	Mercury	Venus	Earth	Mars	Jupiter	Saturn	Uranus	Neptune
Solar distance	0.387	0.723	1	1.524	5.2	9.5	19.2	30.1
Orbital period	0.241	0.615	1	1.881	11.9	29.5	84	165
Rotational period	58.8	243	1	1.029	0.411	0.428	0.748	0.802
Orbital eccentricity	12.353	0.412	1	5.471	2.824	3.294	2.706	0.529
Obliquity	0	7.548	1	1.023	0.128	1.151	4.179	1.237
Equatorial radius	0.38	0.95	1	0.53	11.2	9.4	4.0	3.9
Mass	0.055	0.816	1	0.107	318	95	14.5	17.1
Density	0.985	0.950	1	0.714	0.241	0.127	0.230	0.319
Surface gravity	0.283	0.877	1	0.379	2.355	0.928	0.887	1.121
Escape velocity	0.384	0.929	1	0.214	5.232	2.955	1.893	2.259

these bodies, compared with the compositions of the inner planets, indicate that the differences originated in the processes by which the Solar System was formed. The most important of these, as we discuss in Chapter 2, is the distance from the Sun, at the time of planet formation, where the temperature fell below the freezing point of water, allowing the rapid accumulation of mass in the form of icy material. This 'snow line' was evidently between the orbits of Mars, the outermost rocky planet, and Jupiter, the innermost gas giant. The icy protoplanets in the outer Solar System quickly became massive enough to attract and hold large quantities of the elements that remained gaseous, including the most abundant: hydrogen and helium.

The largest satellite of Saturn, **Titan**, is a unique case in our planetary system of a moon with a thick atmosphere (thicker than Earth's, in fact). It is also the only known example, other than Earth, of a body with a substantial atmosphere in which the main component is nitrogen. Thus, although it is in the outer Solar System and is a satellite and not a planet, Titan offers a further example of an Earth-like atmosphere, making a total of four with Venus, Mars and Earth itself.[3]

The innermost planet, **Mercury**, has only a trace of atmosphere, and yet it is not completely negligible for comparative climate studies with the Earth since its polar regions appear to be rich in frozen volatiles, probably mainly water ice. Mercury, with virtually no gaseous envelope, no obvious source of large amounts of water, and in a severe thermal environment, manages to support substantial deposits of ice at its poles.

Pluto, still thought of by many as a member of the family of planets, is now officially excluded from that definition.[4] With a mass of only about one-fifth of Earth's Moon, and a tenth of that of Titan, Pluto is properly considered a member of the Kuiper belt. As such, it is just one of a large number of frozen bodies, some considerably more massive than Pluto, orbiting near the limits of the Sun's influence. Because it was discovered as long ago as 1930, Pluto remains the best studied of the Kuiper belt objects. Pluto has a relatively large satellite, Charon, about one-seventh of the mass of its parent, and a thin atmosphere that derives from frozen nitrogen and other volatiles, including methane, ethane and propane, on its surface. Because Pluto has a very eccentric

[3] The Earth-like atmosphere of Titan, a relatively recent revelation, gives us a problem with terminology. In astronomy, the 'terrestrial planets' are traditionally taken to be the four rocky inner planets: Mercury, Venus, Earth and Mars. So Titan is neither 'terrestrial' nor a planet – although it is part of this family – displacing airless Mercury when we consider the four Earth-like atmospheres in the Solar System. Since Titan is also larger than Mercury, and has more atmosphere than Earth or Mars, it can legitimately be called a 'planetary body' and indeed, in this sense, is sometimes referred to simply as a 'planet' in scientific discourses.

[4] Pluto was discovered in 1930, and designated the ninth planet in the Solar System. However, in 2006, the International Astronomical Union defined a planet as a celestial body that (a) is in orbit around the Sun, (b) has sufficient mass for its self-gravity to overcome rigid body forces so that it assumes a hydrostatic equilibrium (nearly round) shape, and (c) has cleared the neighbourhood around its orbit. Pluto failed test (c), and is now considered to be just one of many dwarf planets (and, since the discovery in 2005 of Xena, now officially renamed Eris, is not even the largest of these).

orbit, its surface pressure cycles from almost nothing at the greatest distance from the Sun (~50 AU), to perhaps a few hundredths of a millibar during its closest approach (~30 AU).[5]

[5] 1 AU = 1.5×10^{11} m = 1 astronomical unit, the mean distance of Earth from the Sun.

1.2 The inner planets

The four inner planets orbit the Sun at mean distances of 57.9, 108.2, 149.6, and 227.9 million kilometres, respectively. The solid bodies of Venus and Earth are of nearly identical size and density and probably fairly similar in bulk composition. Mars is considerably smaller, with a diameter a little more than half that of the other two, and only about one-tenth of the mass. Mercury is smaller still, with about half the mass of Mars.

Mars has high volcanic mountains and deep canyons, representing the largest range of topography in the Solar System, despite its small planetary radius relative to Earth and Venus. The extinct volcano, Olympus Mons, is more than three times as tall as Everest and more then twice as high as Maxwell, these being the highest features on Earth and Venus, respectively. Parts of the Valles Marineris are nearly four times as deep as the Grand Canyon in Arizona, while the canyons in the Ishtar region of Venus are midway between the two. All four inner planet surfaces are modified by volcanism; some of the volcanoes on Earth and probably many more on Venus are still active. There may be remnant volcanic activity on Mars, too, but if so this is limited to geothermal hot 'springs' that allow warm water to seep from underground aquifers onto the surface, where it quickly evaporates or freezes in the thin, cold air. Recent evidence for the localised emission of plumes of methane gas tends to support the idea of warm, wet subsurface chemistry, at least in some isolated locations.

Mars and Earth rotate on their axes with almost the same period, and hence have nearly the same length of day. Venus rotates in the retrograde sense, i.e. east to west,[6] and turns very slowly, only once every 243 days. Thus the planet's angular momentum vector is in the opposite sense to most of the other planets and the Sun; Uranus and Pluto are also anomalous but have their rotation axes close to the ecliptic plane, approximately at right angles to that of the Sun. This is not consistent with any simple theory of the origin of the Solar System. The fact that Venus rotates slowly has a profound effect on its atmospheric circulation and, through its effect, or lack of effect, on the global cloud cover, its surface climate.

[6] In other words, the *obliquity* (the axial tilt or the angle between the rotation vector and the plane of the orbit) of Venus is more than 90°. In fact, it is remarkably close to 180°.

If the rotation axis of a planet is inclined towards the Sun, or the eccentricity of its orbit is significantly different from zero, this will give rise to seasonal behaviour in any atmosphere that is present. On Venus, with obliquity close to 180° and eccentricity near 0.0, only very small Sun-driven seasonal changes would be expected. Mars, however, has a significant axial tilt of 24° and an eccentricity of nearly 0.1, enough to change the solar constant by as much as 18% during the year. Earth has almost the same obliquity as Mars and a smaller, but still significant, eccentricity of 0.0167. The 98° obliquity of Uranus means that the Sun is nearly overhead, at first one pole and then the other, for long periods during the planet's year, implying extreme seasonal behaviour that has yet to be observed in detail.

The year, or time taken to orbit the Sun once, naturally varies with heliocentric distance and is 224.7 (Earth) days for Venus, 365.3 for Earth and 687.0 days for Mars. The rotation period of Venus, at 243 days, is longer than the Venusian year. The solar day, i.e., the time for the Sun to go from noon to noon as seen from the surface of Venus, is about 117 (Earth) days.

1.2.1 Volatiles on Mercury

Mercury (like Earth's Moon, the planet-sized object that it most resembles in appearance, see Fig. 1.3) has only an extremely tenuous atmosphere. It consists of molecules like sodium and helium that are baked out from the surface, and hydrogen and helium captured from the stream of particles that flows outwards from the Sun. The mean free path is such that escape from the planet is more likely than a collision with another molecule (the usual definition of an *exosphere*), meaning the atmosphere is transient. Thus, for purposes of comparing atmospheric physics with the Earth, it is of much less interest than Venus and Mars.

The icy deposits near Mercury's poles are important, however, for what they tell us about the origin and distribution of water in the Solar System. These were detected using radar echoes sent and received by very large radio telescopes on the Earth, in particular that at Arecibo in Puerto Rico. This can produce images with remarkably high spatial resolution (a few kilometres), which have allowed the identification of highly reflective and depolarizing regions inside polar craters, apparently confined to those parts that are permanently shaded from the Sun. The material responsible cannot be definitely identified from the radar data alone, but it has the right reflective properties to be water ice. It is hard to see what other substance could be available in such quantities and behave in this way, although elemental sulphur of internal (volcanic) origin has been proposed as a possibility.

Where, then, does the water come from? Mercury will, like the other rocky inner planets, have emitted large amounts from the interior in its early history. Some of this may have been cold-trapped at the poles and survived there for billions of years. Or perhaps Mercury is still active

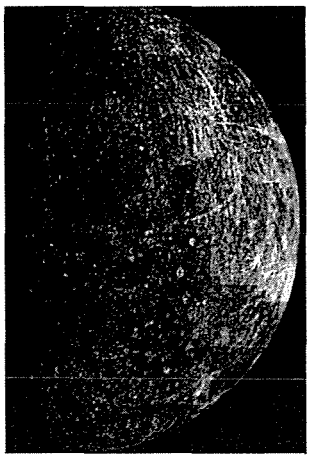

- Diameter 1.4 times Moon
- Much denser than Moon: 5.43 vs. 3.34 g cm^{-3}
- Temperature range 70 to 700 K
- Thin atmosphere: surface pressure ~10^{-15} atm
- Icy polar deposits in shaded craters

Fig. 1.3
Basic facts about Mercury. Its diameter of 1.4 times that of the Moon corresponds to a radius of 2440 km, and the density to a total mass of 3.3×10^{20} kg. The innermost planet orbits the Sun in just 88 Earth days, rotating on its axis in two-thirds of this time. What sort of solar day would this produce for an observer on the surface?[7]

[7] The Sun would take two Mercurian years to go from noon to noon. Another way of looking at it is that daylight would last for one year, and then darkness would prevail for the next year. (A sketch is the easiest way to work this out.)

internally and continues to exhale vapour from cracks and vents in the crust, some of which stays in the thin atmosphere long enough to top up the deposits. This would explain the surprisingly large magnetic field of the planet, but would require unexpectedly large sources of internal heating to prevent such a small body from cooling and solidifying eons ago.

An alternative explanation is that the ice comes from space as a flux of mostly small, but occasionally large, icy bodies (i.e., comets). If a comet as big as Halley[8] had collided with Mercury a few million years ago, the planet would have acquired a temporary atmosphere consisting mostly of steam, some of which would have been deposited as ice in the shaded craters. In this scenario, the ice we see today, which the observers estimate to be at least several tens of metres thick, is the remnant of an event of this kind and will slowly sublime away. However, such large impacts are rare in the current era (based, for instance, on the record on Earth) and instead it may be a large number of very small comets that is responsible; these certainly exist, and although their sizes and numbers are unknown some must collide with each of the planets every day. These impacts must be individually insignificant, since we do not notice their arrival at the Earth, and we would certainly notice something even a fraction of the size of Halley! The upper limit is a diameter measured in centimetres, with most much smaller than that, but there could be such large flux of them that they add up to the equivalent of Halley over a fairly short period of time, like a century.

To evaluate these, and other possible explanations for the phenomenon, we need to compare the rate at which water is lost from deposits inside shaded craters with the estimated rate of supply from different sources. Figure 1.4 shows a simplified model of Mercury, with a single bowl-shaped crater at the north pole containing ice. The sources for this are a mixture of outgassing from the interior and a flux of 'cometesimals' – icy grains. The

[8] Halley is about $8 \times 8 \times 16\,km^3$ and $2 \times 10^{14}\,kg$, formed of a porous aggregate of dust, rock and ice, including some organic material, with a mean density of only $0.6\,g\,cm^{-3}$. The gases emitted while the comet is near the Sun consist mainly (about 80%) of water vapour, indicating that this is the main volatile present.

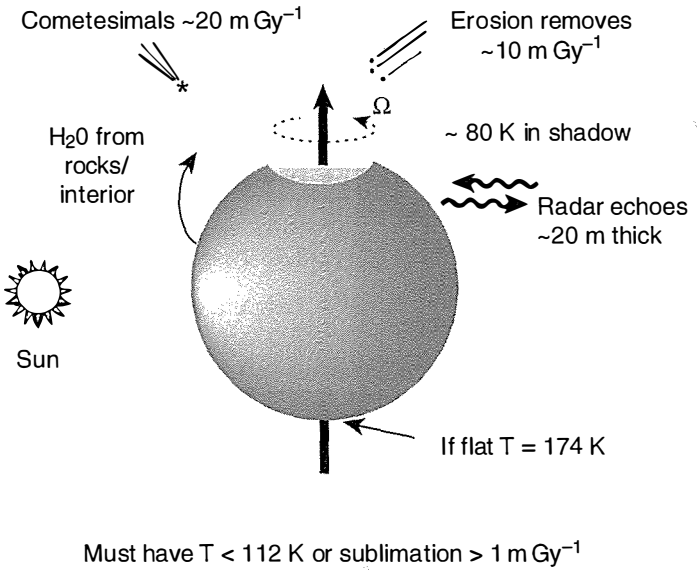

Fig. 1.4
A summary of models that seek to understand the existence of ice deposits some 20 m thick in the permanently shaded craters near the poles of Mercury.

former is impossible to estimate, especially since it depends where on the planet the release takes place. The latter is also quite uncertain, but might be capable of depositing 20 m of ice in one billion years without being inconsistent with our limited understanding of the inventory of icy debris in the Solar System.

The loss processes are sublimation and erosion by micrometeorites. The latter are the rocky equivalents of the icy cometesimals, and their fluxes are such that around 10 m of ice could be vaporised each billion years. Sublimation, of course, is a strong function of temperature, following an expression of the form

$$V \propto p(T)\sqrt{\frac{m}{2\pi kT}}$$

where V is the evaporation rate, p the vapour pressure over the ice at temperature T, and k is Boltzmann's constant. Using this, we find that the sublimation rate reaches 1 metre per billion years for $T \sim 112$ K. Simple radiative energy balance models with the appropriate geometry suggest that the polar region on a smooth, spherical Mercury would have a temperature of around 176 K, while the prevailing temperature in a shaded, bowl-shaped crater with a realistic ratio of depth to diameter of 0.2 would remain under 100 K. (The main factor keeping this from being much lower is scattering of sunlight from the crater rims, so for the realistic case of irregularly shaped craters and walls the precise value is different in every case.)[9]

This simple model suggests that water from icy grains could have accumulated on Mercury in the amounts observed over the 4 billion years or so since the surface of the planet cooled, without the need to invoke current volcanism or massive recent collisions. The question is not answered thereby, of course, and many issues remain, including the fact that some of the craters containing ice behind the Sun-facing wall are far enough from the pole to have minimum calculated temperatures that are as high as ~150 K. Then, if cometesimals are the source, there should be similar deposits on Earth's Moon, which also has permanently shaded craters. This would be great for future lunar bases, but paradoxically it has proved harder to demonstrate the existence of icy deposits on the Moon than it was on distant Mercury.

A small radar device on the Clementine spacecraft, which flew over the lunar south pole in 1994, detected ice-like reflections from the shadowed part of the Aitken basin, which sits right at the pole. A neutron detector on the Lunar Prospector Orbiter confirmed in 1998 a high hydrogen concentration there, and found an even larger signal at the north pole. Despite this, when the spacecraft was crashed into Aitken at the end of its mission, spectral evidence for the expected cloud of water-related molecules like hydroxyl (OH) was not found. However, the impact into the crater Cabeus of the Centaur upper-stage rocket that delivered the Lunar Crater Observation and Sensing Satellite (LCROSS), also watched by instruments on the Lunar Reconnaissance Orbiter just 50 km overhead, achieved a positive result in 2009.

[9] See, for instance, the calculations for idealised craters in 'Near-surface temperatures on Mercury and the Moon and the stability of polar ice deposits' by Ashwin R. Vasavada, David A. Paige, and Stephen E. Wood, *Icarus*, Vol. 141, Issue 2, October 1999, pages 179–193.

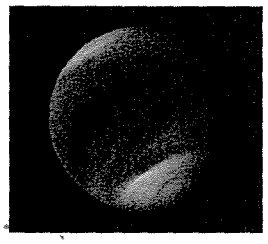

- Covered in thick sulphuric acid clouds
- Very thick CO_2 atmosphere
- Surface pressure of 90 atm
- Surface temperature of 730 K

Fig. 1.5
Venus imaged through an ultraviolet filter by the *Galileo* spacecraft in 1990, and some key facts about the observed climate on the planet.

1.2.2 The atmosphere and climate of Venus

Venus (Fig.1.5) is the closest planet to the Earth, both in terms of distance and in terms of its physical characteristics. The two planets are almost the same size and mean density (see Table 1.2), and, so far as we know and expect, have much the same solid-body composition. The largest external differences appear in the absence of a natural satellite around Venus, the slow, retrograde rotation of the solid body of Venus, and the absence of a measurable Venusian planetary magnetic field. The crust of Venus seems to lack plate tectonics and to be instead much more volcanically active than the Earth.

As the brightest of the planets, Venus has always been a much-noted feature of the night sky near dawn or dusk. Under optimum conditions, Venus can be seen even in the daytime, always within 45° of the Sun due to its inferior orbit relative to the Earth.[10] Many of the parameters listed in Table 1.2 have been known from the early days of scientific observations using telescopes, including the fact that

[10] In astronomy, an 'inferior' orbit is one that is closer to the Sun than that of the Earth.

Table 1.2 Data relevant to climate on the four bodies with Earth-like atmospheres. The atmospheric composition is given as mole fractions, with ppm meaning parts per million, ppb parts per billion, and ~0 meaning undetermined but very small.

	Venus	Earth	Mars	Titan
Mean distance from Sun	1.082×10^8	1.496×10^8	1.524×10^8	1.426×10^9
Eccentricity	0.0068	0.0167	0.0934	0.0288
Obliquity (deg)	177	23.45	23.98	27
Year	0.615	1	1.88	29.41
Rotational period (hours)	5832.24	23.9345	24.6229	382.68
Solar day (days)	117	1	1.0287	16
Solar constant ($kW m^{-2}$)	2.62	1.38	0.594	0.0156
Net heat input ($kW m^{-2}$)	0.367	0.842	0.499	0.0122
Atmospheric:				
Molecular weight (g)	43.44	28.98 (dry)	43.49	29
Surface temperature (K)	730	288	220	95
Surface pressure (bar)	92	1	0.007	1.467
Mass (kg)	4.77×10^{20}	5.30×10^{18}	$\sim 10^{16}$	3×10^{18}
Composition:				
Carbon dioxide	.96	.0003	.95	15 ppb
Nitrogen	.035	.770	.027	.984
Argon	.00007	.0093	.016	.00004
Water vapour	~.0001	~.01	~.0003	8 ppb
Oxygen	~0	.21	.0013	~0
Sulphur dioxide	150 ppm	.2 ppb	~0	~0
Carbon monoxide	40 ppm	.12 ppm	700 ppm	30 ppm
Neon	5 ppm	18 ppm	2.5 ppm	~0

Venus has a very high reflectivity (*albedo*), evidently due to a thick and ubiquitous cloud cover. At $A = 0.76$, the albedo of Venus is two and a half times that of the Earth,[11] more than offsetting the doubling of the solar constant at Venus' mean distance from the Sun in the energy balance equation:

$$(1 - A)\, S\pi R^2 = 4\pi R^2 \sigma (T_E)^4$$

where the quantity of the left-hand side is the solar energy absorbed by the planet of radius R, allowing for the fraction A of the solar constant S that is reflected, and the right-hand side is the energy emitted from the planet of equivalent blackbody temperature T_E, according to the Stefan-Boltzmann law. The value of T_E that results from the application of this simple balance equation is 255 K for Earth, but only about 240 K for Venus (see Chapter 4).

Since Venus absorbs less radiant energy than Earth, there was no particular reason why early practitioners of what we would now call climate modelling should expect the surface temperature to be massively different from our own, and the popular vision of the surface of Venus often included oceans, deserts and steamy jungles. The Sun, presenting a disc twice the area it shows at the Earth, was thought to evaporate water efficiently and produce the thick and extensive cloud deck when the water condensed in the cooler upper atmosphere. When, in 1932, the composition of the atmosphere was shown[12] to be mainly carbon dioxide, soda water oceans became the vogue for Venus.[13]

In the 1950s, it became possible to estimate the surface temperature of Venus for the first time using radio telescopes to measure the intensity of emitted microwave radiation. At wavelengths of a few centimetres, photons emitted from the surface of the planet pass almost unaffected through the cloud layers, and can be measured on Earth. The early results for Venus showed temperatures that were much too hot for free water or plant life. The first space mission to Venus, *Mariner 2*, carried a small microwave radiometer to confirm this measurement from close range and show, by observing limb darkening, that the intense radiation was indeed coming from the surface, and not from a non-thermal source like the ionosphere. Later, the Soviet *Venera* series of spacecraft made a series of landings on the planet's surface, confirming that the temperature was around 730 K, above the melting points of soft metals like lead and tin, and accompanied by a pressure of 92 bars, nearly a hundred Earth atmospheres.

Venera 13 confirmed that the atmosphere is nearly pure carbon dioxide, and obtained a view of a region of the surface of Venus that is typical, featuring volcanic hills and mountains, and fractured lava plains (Fig. 1.6). Radar imaging from orbit shows that there are also flow features of various kinds, including long, sinuous channels. The sky is permanently cloudy, although the thickness varies and the Sun shines dimly through the regions of thinner cloud, with lightning (probably cloud-to-cloud rather than cloud-to-ground as on Earth) generated in the thick, convective clouds.

[11] Planetary albedos are difficult to determine and not very accurately known, even for the Earth. Various values will be found in the literature, corresponding to this uncertainty.

[12] 'Absorption bands in the infra-red spectrum of Venus' by W.S. Adams and T. Dunham, Jr., in *Publications of the Astronomical Society of the Pacific*, Vol. 44, No. 260, pages 243–245, 1932.

[13] As discussed on television by Patrick Moore in *The Sky at Night*, for instance.

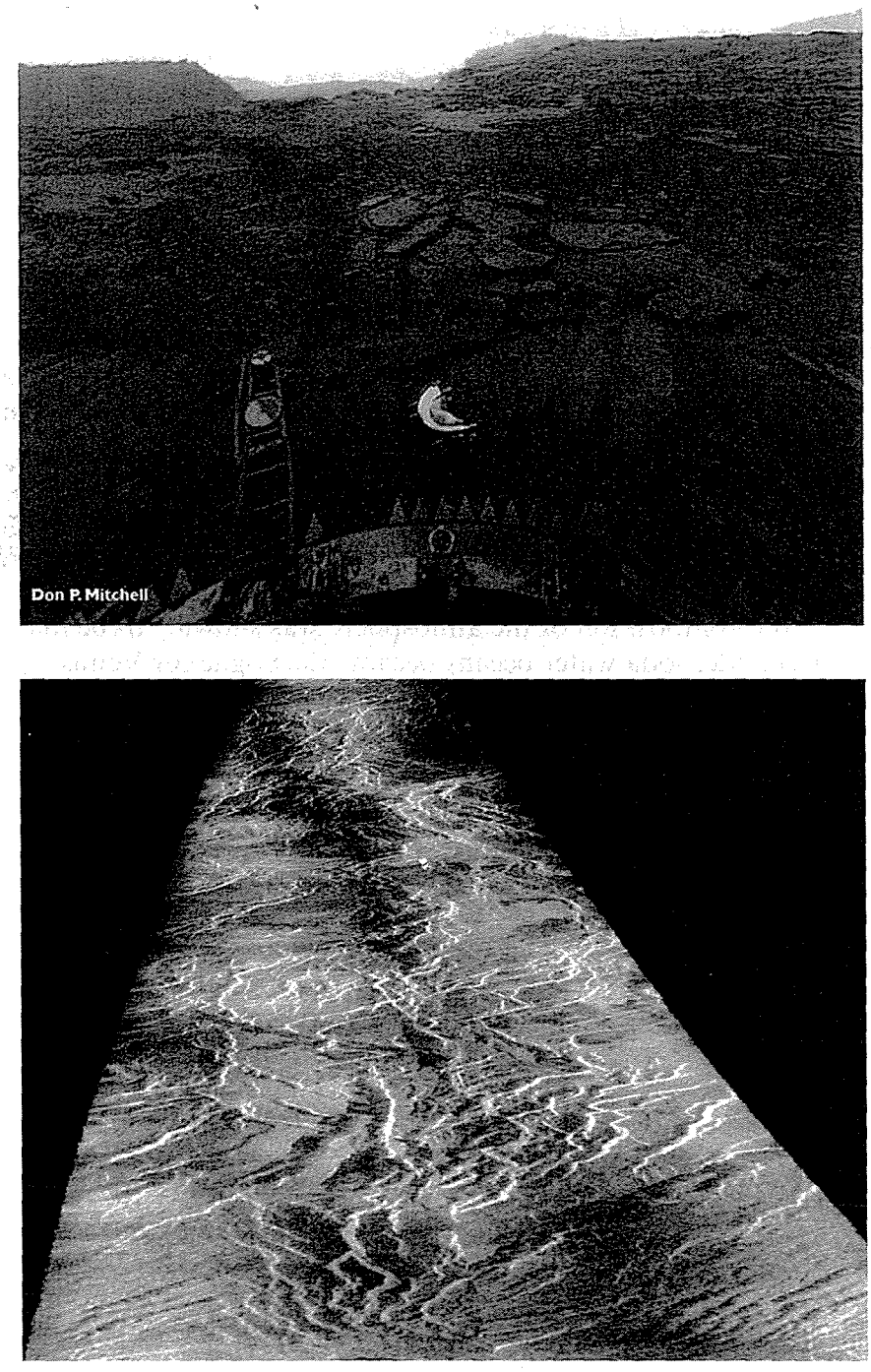

Fig. 1.6
Views of the surface of Venus, from the Soviet lander *Venera 13* sitting on Phoebe Regio in 1975 (top), and the same region seen from aloft some 15 years later by the US *Magellan* orbiting radar imager.

The absence of an internal magnetic field on Venus means that the atmosphere is exposed directly to the stream of very energetic charged particles, mostly protons, that moves radially outwards at high speed from the Sun. The lightest atoms and ions, like hydrogen, formed by the

dissociation of water vapour and other gases by solar ultraviolet radiation, are easily removed from the top of the atmosphere by collisions with these solar wind particles. Oxygen is also removed, at a rate which even today is observed by *Venus Express*[14] to be about half that of hydrogen, supporting the expectation that H_2O is the main source molecule. Over its history, Venus could have lost most of the water it probably had in its early life and, as a direct consequence of this, has retained in its atmosphere huge amounts of carbon dioxide (§6.7). On the Earth, which retained most of its water, corresponding amounts of CO_2 have dissolved in the oceans and formed carbonate rocks. Earth and Venus have retained approximately equal masses of nitrogen, although on the latter this is diluted by the additional carbon dioxide and makes up only 2–3% of the total atmosphere, compared to 79% on Earth.

The effect of a column abundance of CO_2 that is around 1000 km-atm of CO_2 on Venus, compared to 0.001 km-atm on Earth, is a very large 'greenhouse' warming of nearly 500 K, compared to only ~30 K on Earth. Understanding the details of the energy balance at each level requires also investigating the extent and variability of the clouds, and their composition of water, H_2SO_4, and other substances not yet identified. The dynamics and circulation of the global atmosphere are also key components of the climate.

At visible wavelengths, the cloud cover on Venus is complete and impenetrable, with no markings that could be associated with continents, oceans or any of the topographical features which a moderately sized telescope reveals on the other inner planets. Instead, only extremely subtle and ephemeral markings, and some 'scalloping' of the terminator which separates the day and night sides, have been reported by visual observers. If a camera is used instead of the eye, and it is equipped with an ultraviolet filter like that on *Mariner 10* which observed Venus from a distance of 10,000 kilometres in 1973, subtle dark markings appear in the clouds (Fig. 1.5). In the mid 1980s, it was discovered that different patterns with higher levels of contrast can be observed at certain wavelengths in the near-infrared part of the spectrum, originating in the cloud structure at considerably greater depths than those seen in the ultraviolet. Large-scale meteorological activity organises the clouds into patterns, mainly convective near the equator with more laminar flow at higher latitudes (Fig 1.7).

[14] The first European mission to Venus, launched 6 November 2005, arrived on 11 April 2006.

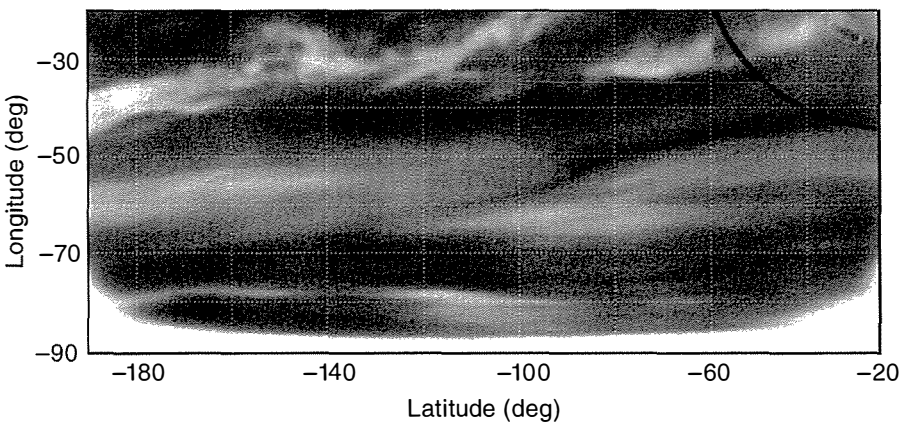

Fig. 1.7
Clouds in the southern hemisphere on the night side of Venus, imaged in the near-infrared 'window' at 1.7 μm wavelength by the VIRTIS spectrometer on *Venus Express* in April 2006. The clouds are illuminated from below by thermal emission from the hot, deep atmosphere and surface. The turbulent region near the equator (towards the top of the image) forms a sharp transition at mid latitudes to laminar flow nearer the pole.

The near-infrared radiation from Venus is most intense within spectral 'windows' between the strong molecular absorption bands of CO_2 and H_2O in the 0.9 to 2.5 μm wavelength region. The clouds provide some attenuation of the flux emitted by the hot lower atmosphere and surface, but the very high single scattering albedo[15] of the cloud droplets in the near infrared means that photons can diffuse to space in the spectral windows between the absorption bands of the main atmospheric constituents. From Earth or from Venus orbit it can be detected only on the night side of the planet, where it is not overwhelmed by the more intense solar flux reflected from the upper clouds (Fig. 1.8).

Spectroscopic analysis of observations of the emission in the near-IR windows by ground-based and spacecraft instruments have been used to investigate cloud particle sizes and optical thickness, and near-IR imaging of the shifting cloud patterns reveals the winds within the middle and lower cloud decks. The cloud features seen in both ultraviolet and near-infrared images move parallel to the equator at speeds as high as 100 m sec^{-1} (around 400 mph) with high vertical shear (i.e., winds that drop off rapidly with height) in the turbulent region, and a gradual decline towards the pole in the laminar flow region. The polar regions themselves are organised into giant polar vortices with a double 'eye' at the centre. These complex dynamics are discussed in Chapter 8.

During the 1991 Venus fly-by of the *Galileo* spacecraft, en route for Jupiter, it was found that the principal topographical features on the surface of the planet could also be discerned in images obtained in the most transparent of the near-infrared windows, those at wavelengths just longer than that of visible light. Unlike the cloud contrasts, which are due to varying cloud thickness, the surface contrasts originate in the temperature lapse rate of the atmosphere. The fall in temperature with height of about 10 K km^{-1} causes high terrain on Venus to appear dark in maps of the thermal emission from the surface. To see these clearly requires a technique for removing the much larger contrasts due to cloud structure, which is possible since the latter vary with wavelength and move rapidly relative to the fixed surface features.

Spectroscopy in the near-IR windows also allows mapping of the abundance of interesting minor constituents of the atmosphere near

[15] The single scattering albedo is the probability that a photon encountering a cloud drop will be scattered rather than absorbed. It is close to 1 in the near infrared for the cloud particles on Venus.

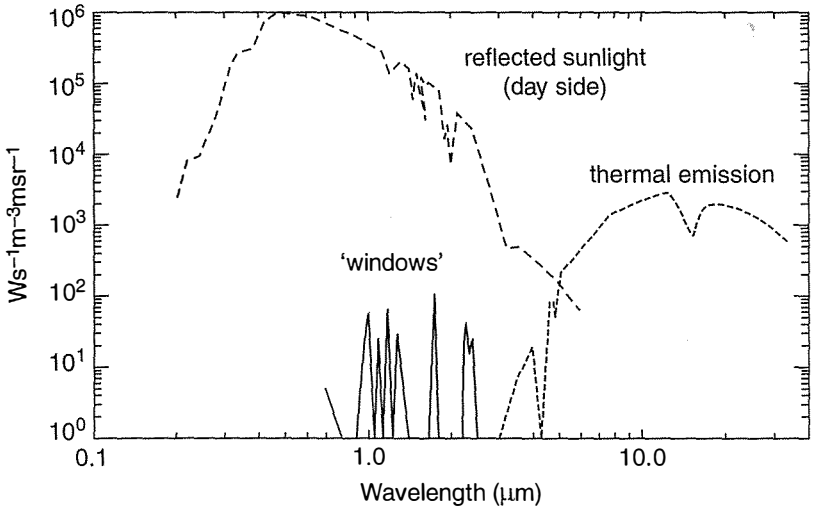

Fig. 1.8
A composite spectrum of Venus[16] showing the reflected solar component (dashed line), the thermally emitted component (dotted line), and the thermal emission in the near-infrared windows (solid line). Obviously, the last of these can only be observed on the night side of the planet, as it is swamped by the reflected solar radiation, about 1000 times brighter, on the day side.

[16] From 'Radiation in the atmosphere of Venus' by D. Titov, M.A. Bullock, D. Crisp, N. Renno, F.W. Taylor, and L.V. Zasova, in *Exploring Venus as a Terrestrial Planet*, ed. by L.W. Esposito, E.R. Stofan, and T.E. Cravens, Geophysical Monograph No. 176, pages 1121—138, American Geophysical Union, 2007.

the surface, including water vapour, halides, carbon monoxide, sulphur dioxide, and carbonyl sulphide. They have provided new information about the near-surface temperature lapse rate, and the deuterium-to-hydrogen ratio. The latter is more than 100 times that on Earth, supporting the idea that Venus has lost large amounts of hydrogen, therefore water, to space, a process that would be expected to produce fractionation between the lighter and heavier isotopes.

The small inclination and eccentricity of Venus' orbit means that we should expect no significant seasonal changes during its annual circuit around the Sun, and none has been observed.

1.2.3 The atmosphere and climate of Earth

A distinctive feature of the Earth in climate terms is that it orbits at a distance from the Sun where water can coexist in each of its three forms. Atmospheric water vapour, the circulating oceans, and the permanent but fluctuating water ice polar caps are all key components of the Earth's variable climate (Fig. 1.9).

Life is also a phenomenon that, on a scale large enough to affect the climate, is probably unique to the Earth, in the Solar System at least. Processes involving living organisms significantly affect the atmospheric composition, including the proportions of oxygen and carbon dioxide. Green plants convert atmospheric carbon dioxide to carbohydrates, releasing oxygen in the process, by the reaction known as photosynthesis, which is essentially:

$$6CO_2 + 12H_2O + h\nu \rightarrow C_6H_{12}O_6 + 6O_2 + 6H_2O$$

i.e., carbon dioxide + water + photons → glucose + oxygen + water.

Carbon dioxide is removed from the atmosphere by dissolving in water and forming carbonic acid

$$CO_2 + H_2O \rightarrow H_2CO_3$$

that can weather silicate rocks, producing ions that are used by marine organisms like coral to make, eventually, insoluble calcium carbonate

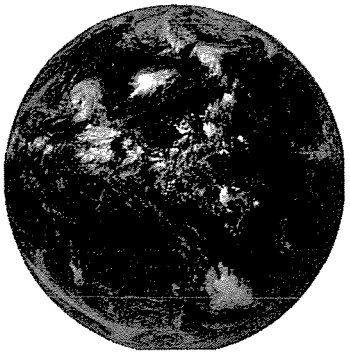

- Water in all three phases
- Widespread water clouds
- 70% liquid H_2O coverage
- N_2–O_2 atmosphere
- Surface pressure 1 bar
- Mean surface temperature 288 k
- Life is part of climate

Fig. 1.9
Planet Earth, and some basic facts about its atmosphere.

$$H_2CO_3 + CaSiO_3 \rightarrow \ldots \rightarrow CaCO_3 + \text{clays}$$

which is stored on the seafloor as layers of limestone (the white cliffs of Dover were produced in this way, for example).

Some of the carbon dioxide is returned to the atmosphere when limestone is carried to hot, deep regions of the crust in subduction zones, where the reaction

$$CaCO_3 + SiO_2 \rightarrow CO_2 + CaSiO_3$$

takes place, followed by outgassing in volcanoes. The current balance between all of these processes results in an atmospheric abundance of carbon dioxide of about 400 parts per million by volume (ppm), much less than Venus or Mars where there is no comparable biosphere and no surface liquid water. The resulting mean surface temperature is both calculated and measured (see Chapter 4) to be around 288 K.

Why is Earth so cool and wet when Venus, a similar-sized planet which formed nearby from the same protostellar cloud, is hot and dry? A clue may be obtained by plotting typical temperature profiles for both atmospheres on a scale where the vertical dimension is represented by log pressure, as shown in Fig. 1.10. In the region where the two profiles overlap, the difference is fairly straightforwardly accounted for by (i) the difference in composition (mostly N_2 on Earth, mostly CO_2 on Venus), (ii) the heating induced by the ozone layer on Earth, which has no equivalent on Venus, and (iii) the difference in solar heating (which is actually greater for Earth, because of Venus' high albedo). The scorching surface temperature on Venus is caused by the additional atmospheric gas, nearly 100 times more than on Earth. It is mostly carbon dioxide, but it need not be – since the atmosphere is already optically thick in the infrared, adding more of any gas, even a non-greenhouse gas, raises the surface temperature. On Venus, the temperature at 1 bar pressure is increasing with depth at a rate approximately equal to the adiabatic lapse rate (about $10\,K\,km^{-1}$), and it must continue to do so

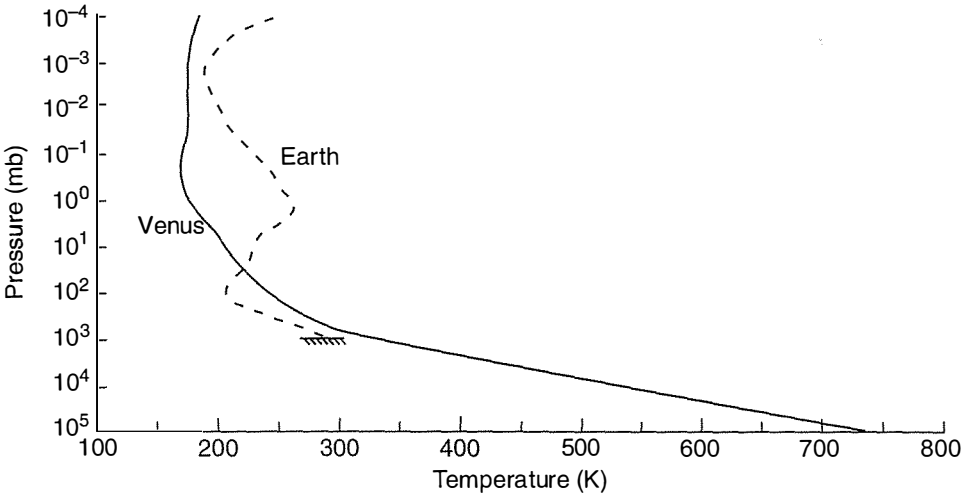

Fig. 1.10
A comparison of measured atmosphere temperature profiles on Earth and Venus, where the vertical scale is pressure in millibars (1000 mb equals the mean surface pressure on Earth). The solid line is derived from remote sounding measurements made by the *Pioneer Venus Orbiter* Infrared Radiometer (Schofield and Taylor, 1983), extrapolated assuming a dry adiabatic lapse rate below 500 mb, and the dashed profile is derived from similar measurements by the Improved Stratospheric and Mesospheric Sounder on the Upper Atmosphere Research Satellite (Taylor *et al.*, 1993).

until the pressure reaches nearly 100 bars at the surface, some 45 km below.

The Earth enjoys its mild, wet climate primarily because the atmospheric pressure is neither too high, as on Venus, nor too low, as on Mars. This in turn is due to the removal of most of the primordial carbon dioxide, leaving only the nitrogen and a few minor constituents like argon, to which life later added the oxygen.

1.2.4 The atmosphere and climate of Mars

Compared to Earth, the atmosphere of Mars is very cold and very tenuous (Fig. 1.11). The composition is mainly CO_2, with very little H_2O vapour, although the low abundance is mainly due to the low temperatures. In fact, the Martian air, although very dry by Earth or even Venus standards, is often close to saturation and water clouds do occur. These are thin and infrequent, however, and upstaged, especially in the polar winters, by clouds of condensed CO_2 (dry ice).

In fact, the most important airborne particles on Mars are neither frozen water nor frozen carbon-dioxide crystals. The main source of aerosol opacity is that due to wind-raised mineral dust, which makes a large contribution to the greenhouse effect and therefore to the surface temperatures on Mars. During exceptionally strong global dust storms that occur typically every two years near the perihelion of Mars, the entire planet can be masked by huge amounts of airborne dust and the meteorological conditions are greatly changed everywhere. After a period of up to a few months, the storms subside as quickly as they begin.

By analogy with Earth and Venus, we would expect Mars to have formed with a much larger inventory of water and carbon dioxide than is apparent now. The oldest terrain on the surface shows ample evidence of running and standing water, clearly visible even from orbit, and supported by the observations of sedimentary deposits on the surface by the recent *Mars Exploration Rovers*. To produce these required not only a lot more water than we can see on Mars at the present time, but also a much thicker atmosphere to raise the temperature enough to keep the water liquid. Mars must have undergone massive climate change over long periods of time in its history.

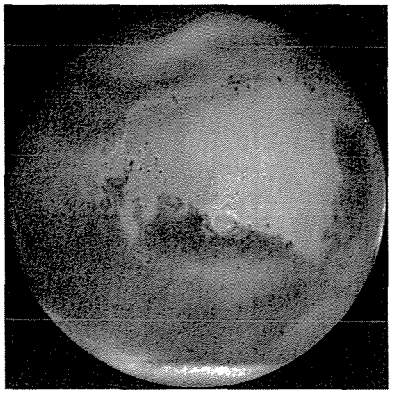

- Thin CO_2 atmosphere
- Thin clouds of CO_2 and H_2O
- Surface pressure ~7 mb
- Surface temperature ~ 250 K
- Dust storms

Fig. 1.11
Mars, and some basic facts about its atmosphere.

The fact that the present surface temperatures and pressures are so close to the triple point of water may provide a clue to how the Martian climate evolved (Fig.1.12). Any oceans on early Mars would have dissolved atmospheric CO_2, just as they do on Earth, producing carbonate deposits as chalk layers that have since been buried under layers of windblown dust and soil. The difference then is that on Mars this process went to the point where liquid water was no longer stable, shutting off further carbonate production. At certain locations, for example, at the bottom of the huge impact basin called Hellas, the pressure is twice the global average and liquid water could still be found, although only during the day when the temperature is above freezing point at 0 °C.[17] In this scenario, the water that once filled oceans and rivers is now frozen below the surface, covered up like the carbonates by centuries of windblown dust deposits, or in the permanent polar caps. The north cap, which seems to contain most of the water, is 1200 km across and up to 3 km thick, which corresponds to about 4% of Earth's polar ice.

[17] The highest measured temperature at the surface of Mars is about 20 °C, and the lowest, −140 °C. The global average is about −60 °C.

At Mars' distance from the Sun, even a thick CO_2 atmosphere might not be enough to warm the planet so it could support liquid water on the surface everywhere (see the discussion in Chapter 9). Here again there is a clue; Mars has several regions dominated by enormous extinct volcanoes, and the Exploration Rovers have found copious deposits of sulphate minerals, apparently produced at the time when the volcanoes were active and filling the atmosphere with sulphurous and other gases and aerosols. Although the details are still to be filled in, the data we have points towards a strong greenhouse effect on Mars that lasted only as long as the active volcanism did, that is, around the first billion years of the planet's history.

1.3 The outer planets

Most of the apparent bulk of the outer planets (Fig. 1.13) is atmosphere: gaseous at the top, becoming liquid lower down where the pressures and temperatures are very high. The visible features are due to multiple layers of cloud of different compositions and colouring (probably four layers according to current models, see Chapter 7, with

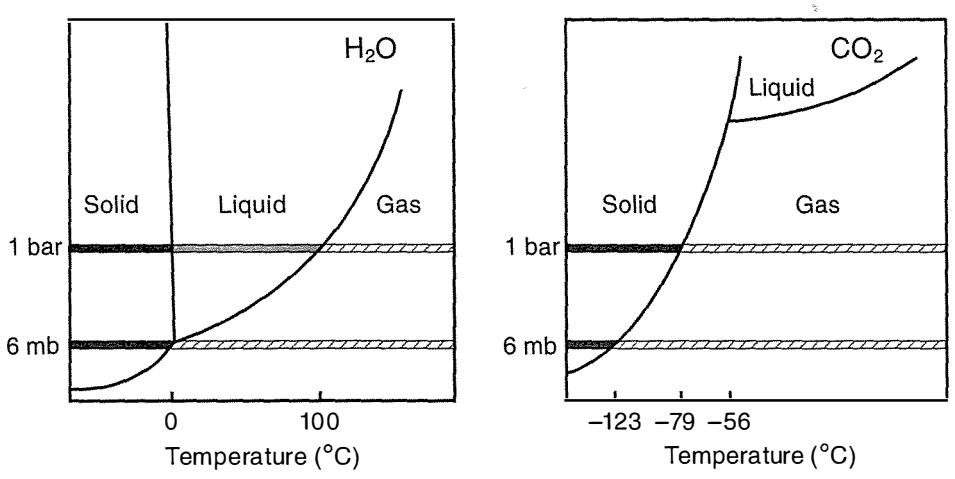

Fig. 1.12
(Left) A phase diagram for water, showing the triple point at 6.1 mb and 0 °C, where solid, liquid and gas coexist. (Right) The corresponding point for carbon dioxide is at 5.11 bars and −56 °C. The horizontal bars show mean pressures on Earth and Mars; the Earth of course has liquid water, while conditions on Mars are against this, but only marginally. Neither planet can have liquid CO_2, except possibly if reservoirs exist at high pressures below the surface.

Fig. 1.13
The giant planets Jupiter, Saturn, Uranus and Neptune, approximately to scale. The small globe at bottom right is the Earth, for comparison.

many more at greater depths where they are not discernable from outside the atmosphere). The heavy elements are concentrated in solid rocky and metallic cores that occupy only a fraction of the visible diameter. For instance, based on theoretical models and the observed mean density, the core of Neptune is thought to be about the size of the Earth, although its gaseous envelope is 4 times greater in diameter. For the larger giant planet Jupiter, the mass of the core is also larger, but still only roughly 10 times the mass of the Earth.

1.3.1 The atmosphere of Jupiter

Jupiter (Fig.1.14) is the largest and most massive of the planets in the Solar System. Its mean diameter is about 11 times greater than that of Earth, so it is more than 1000 times larger in volume. The rapid rotation flattens the planet by about 6 percent of its polar diameter, giving it a perceptibly oval shape. Jupiter's mass of 1.9×10^{27} kg is more than 300 Earth masses, and 2.5 times the combined total of all the other bodies orbiting the Sun. Since the mean density is about one-fourth that of the Earth, it follows that 95% of the mass of Jupiter is atmosphere, with the heavier elements concentrated in a relatively small core with a diameter less than 10% of that of the visible disc. At the interface between the core and the highly compressed fluid

- First gas giant
- Mass 300 × Earth
- Radius 11 × Earth
- Density 0.24 × Earth
- Atmosphere H_2 + He
- ≤1% NH_3 + CH_4
- Temp. 165 K at 1 bar

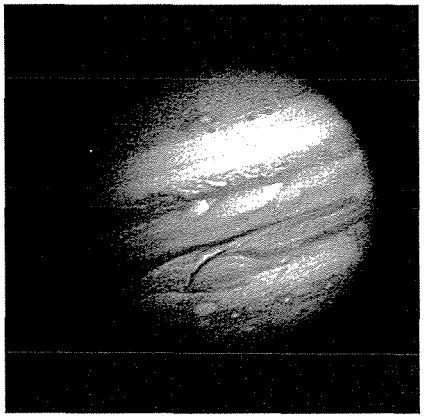

Fig. 1.14
General appearance and defining characteristics of Jupiter, the largest, closest and best studied of the four giant outer planets.

(predominantly liquid metallic hydrogen)[18] at the base of the atmosphere, estimates from models predict temperatures in excess of 10,000 K and pressures of over 4 million bars.

The visible surface of Jupiter consists of layers of cloud appearing as alternating dark and light bands parallel to the equator; the darker reddish and brown coloured bands are called belts, and the lighter yellow and white regions are known as zones. The banding is the result of convective motions forced by a large internal heat source of approximately equal magnitude to the solar heating. This internal energy probably comes from the slow collapse of Jupiter's fluid bulk in response to its huge gravitational field, converting potential energy into heat.

Jupiter's deep atmosphere probably contains hundreds of layers of cloud, each with a different composition (see Chapter 7). Moist air, rising in the cloudy zones from a great depth, contains many minor constituents, each of which condenses at the appropriate level as the temperature falls with height. Only the top three layers have actually been observed – water clouds at about 273 K and 3 bars, ammonium hydrosulphide (NH_4SH, formed by the combination of ammonia, NH_3 and hydrogen sulphide, H_2S) at about 230 K and 1.5 bars, and ammonia ice at 135 K and 0.5 bars. All of these materials are white in the laboratory, but on Jupiter almost certainly contain impurities, especially NH_4SH, which appears to be responsible for the yellow and brown colours that dominate the appearance of Jupiter. It is still not known of what these 'chromophores' consist; various forms of elemental sulphur and its compounds are the most likely candidates.

The fast rotation, the great depth of the atmosphere, and the influence of an internal source of heat, in addition to that arriving from the Sun, make for a very dynamic atmosphere. Superimposed on the basic belt–zone cloud patterns are very high winds and wind shears, and a variety of giant eddies. These are compact, circulating air masses roughly comparable to terrestrial hurricanes, but often much larger. The most striking of all the atmospheric features is the Great Red Spot, which has been observed off and on for at least 300 years, and exceeds the Earth in diameter. The red colour indicates a composition different from the rest of the clouds. It seems likely that the GRS is a deep vortex that draws up material from deep in the atmosphere up to higher levels where it condenses or reacts to form a cloud cap, with additional constituents not found elsewhere across the planet. Truly red cloud materials are fairly rare; the simplest possibility is elemental phosphorus, while more exotic candidates include an almost infinite range of complex organic substances of many colours.

1.3.2 The atmosphere of Saturn

Saturn (Fig.1.15) is second among the planets in terms of mass and size. The mean diameter of the globe is almost ten times that of the Earth, and its rapid rotation (a period of a little over 10 hours) and low density give it more polar flattening than any other planet – about 11 per cent. Saturn's axis of rotation is inclined by 29° to its orbital plane.

[18] 'Metallic' in this context means that the gases, under extreme pressure, have a high proportion of electrons that are not attached to individual atoms or molecules, but can migrate through the entire medium, as in a metal under familiar laboratory conditions. The hydrogen is then highly conducting and this makes it easier to explain Jupiter's high magnetic field.

- Second gas giant
- Mass 95 × Earth
- Radius 9 × Earth
- Density 0.13 × Earth
- Atmosphere H_2 + He
- ≤1% NH_3 + CH_4
- Temp. 134 K at 1 bar

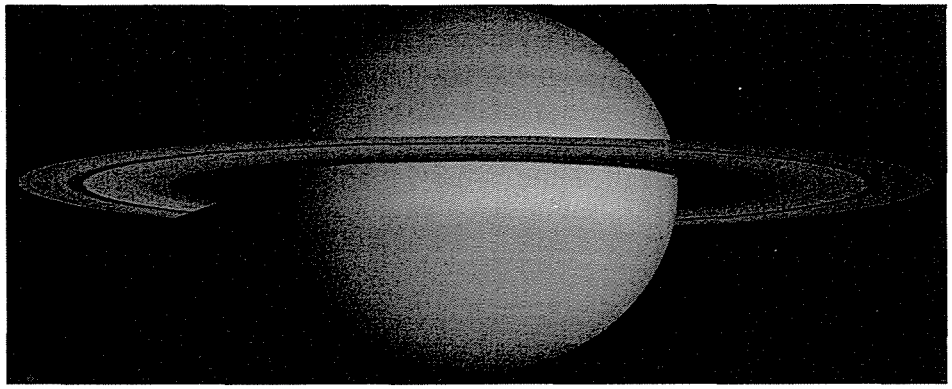

Fig. 1.15
General appearance and defining characteristics of Saturn. Note the remarkably low density compared to its neighbours, indicating a lower proportion of heavier elements in Saturn's overall makeup than the other three outer planets. The rings are made of a large number of icy and rocky moonlets, with sizes up to a few tens of metres in diameter.

Since the plane of its rings is perpendicular to its rotation axis, the rings do not lie in the orbital plane and therefore present a varying aspect to Earth as the planet goes through its roughly 30 year orbit. When seen almost edgewise, every 15 or so years, the rings almost disappear from sight, indicating that they are very flat. Observations from spacecraft at Saturn show that the particles that make up the rings are in fact confined to a layer about 1 km thick.

While Saturn's mass is nearly 100 times greater than Earth's, its density of 0.69 g cm^{-3} is the lowest of any planet. At the same time, the gravitational field, determined by tracking spacecraft passing or orbiting the planet, indicates that more of Saturn's mass is concentrated near the centre than is the case for Jupiter; about 25% as opposed to about 5%. Outside the core, Saturn must be composed primarily of hydrogen and helium, with a metallic layer occupying the innermost half of the radius of the planet. Above the pressure level at about 1 million bars the mixture ceases to be metallic, but has the properties of a liquid up until the 1000 bar level is reached at a depth about 1000 km below the visible clouds, where the temperature is around 1000 K.[19]

The outermost layer of atmosphere consists, like Jupiter, mostly of H_2 and He, with a small component (<1%) of the fully hydrogenated compounds of the common elements, especially CH_4, H_2O and NH_3. Again, like Jupiter, these condense to form the observable cloud layers.

Saturn, and to a lesser extent Uranus and Neptune, may be thought of as a smaller, cooler version of Jupiter where meteorology is concerned. The markings on the disc of Saturn resemble the banded cloud structure of Jupiter's atmosphere, but with much less contrast and more subtle colours. Giant eddies and ribbon-shaped clouds do occur, and on rare occasions, extensive irregular storm systems appear, greater in area than anything seen on Jupiter. Like Jupiter, Saturn has an internal heat source that is comparable to the solar input (Table 1.3), so the atmosphere is heated by about the same amount from above and from below, and is highly convective.

[19] Obviously, these numbers are rounded to reflect the uncertainty in our knowledge of the interior structure of Saturn and the other outer planets.

Most of Saturn's satellites lie in the same plane as the rings, the planet's equatorial plane, and orbit outside the rings. Most of the mass of the satellite and ring system is concentrated in Titan, which is the second-largest satellite in the Solar System after Jupiter's Ganymede. Titan is the only moon to possess a thick atmosphere and is therefore of especial interest (§1.4).

1.3.3 Uranus and Neptune

Uranus (Fig.1.16) and Neptune (Fig. 1.17) are similar in size to each other, with radii about four times larger than Earth, and masses that are 14 and 17 times greater (which makes them just 5% and 6%, respectively, of the mass of Jupiter). Whereas Jupiter and Saturn are composed primarily of hydrogen and helium, the total mass of carbon, nitrogen, oxygen, and possibly silicon, iron, and other heavy elements, must be comparable to or greater than that of the light gases in Uranus and Neptune. For this reason, they have come to be called 'ice giants' rather than gas giants like their larger siblings, where ice means any condensed compound and not just frozen H_2O.

All of the giant planets are fluid to a great depth and can contract to release internal energy as heat. However, when all four are compared, we see that they do not follow a consistent pattern. The heat radiated from Uranus, in particular, apparently does not significantly exceed that

Fig. 1.16
General appearance and defining characteristics of Uranus. In this view the contrast has been stretched to show the tenuous ring system and faint cloud features in the atmosphere. It can then be seen how Uranus' axis of rotation is tipped close to the ecliptic plane, which is nearly horizontal in this view.

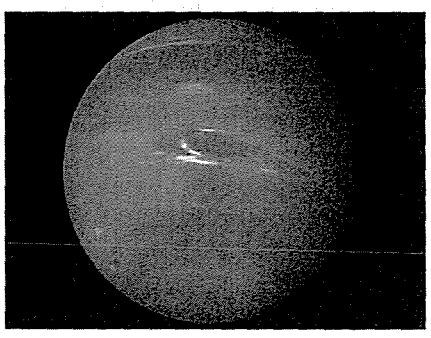

Fig. 1.17
General appearance and defining characteristics of Neptune. The bright cloud features are probably frozen methane.

Table 1.3. Data relevant to climate on the four bodies with non-Earth-like atmospheres, the gas giants of the outer Solar System. The atmospheric composition is given as mole fractions.

	Jupiter	Saturn	Uranus	Neptune
Distance from Sun (km)	7.78×10^8	1.43×10^9	2.87×10^9	4.50×10^9
Eccentricity	0.0489	0.0565	0.0457	0.0113
Obliquity (deg)	3.13	26.73	97.77	28.32
Orbital period (years)	11.857	29.42	84.01	164.79
Solar day (hours)	9.92	10.65	17.24	16.11
Solar constant ($W m^{-2}$)	50.5	14.9	3.71	1.51
Bond albedo	0.343	0.342	0.30	0.29
Total energy output Solar energy input	1.67	1.78	1.06	2.52
Atmospheric:				
Molecular weight (g)	2.22	2.07	2.64	2.6
Temperature at 1 bar (K)	165	134	76	72
Scale height (km)	27	59.5	27.7	20
Composition:				
Hydrogen	0.898	0.936	0.825	0.80
Helium	0.102	0.325	0.152	0.19
Methane	0.003	0.0045	0.023	0.015
Ammonia	0.000 26	0.000 125	?	?

which it receives from the Sun, while its more distant twin Neptune has a substantial internal source, like Jupiter and Saturn (Table 1.3). When the magnitudes of these sources are compared to each other and to the mass of each planet, it becomes clear that the simple 'contraction' model described above and in §4.6 for Jupiter cannot fit all of them without modification. What is probably happening is internal gravitational separation of specific species, again releasing potential energy as heat, rather than just an overall shrinking of the whole planet. For Saturn, which actually radiates more energy than Jupiter, despite being smaller, it has been suggested that the pressure and temperature at certain depths are particularly suitable for the formation of drops of liquid helium, which then 'rain' out towards the centre. What accounts for the difference between Uranus and Neptune is still not known, although a number of speculative models have been developed.

Uranus' rotation is peculiar in that its axis is tilted 98° to the perpendicular to its orbital plane – that is, it lies almost on its side – and has retrograde rotation. The spin axis can point almost directly at the Sun, so regions near the poles spend half of the long orbit alternately in sunlight or darkness. The effect this has on the structure and global circulation of the atmosphere, compared to its similarly sized but more normally aligned neighbour Neptune, is difficult to know at present because there are so few relevant observations. What we do know comes mainly from the *Voyager 2* spacecraft, which observed Uranus at a time when the south pole was pointed almost directly at the Sun. Perhaps surprisingly, the measured temperatures near the cloud tops were not very different between the illuminated and dark polar regions, and the cloud patterns suggested zonal east–west winds similar to those on the other three giant planets.

Neptune's orbital period is almost 165 years and it has not quite completed an orbit of the Sun since its discovery in 1846. It has one large satellite, Triton (2710 km in diameter), which is in an odd retrograde orbit with an inclination of 159°. This suggests that Triton was a drifting object in the Kuiper belt before it was captured by Neptune, which is remarkable in view of its size. Neptune itself has an axial inclination of 29°, not very different from Earth's 23.5°.

The visible atmosphere of Uranus is almost featureless and is green–blue in colour. Occasional discrete faint white clouds are observed at midlatitudes and there is a layer of high haze, presumably photochemically produced, over the sunlit south pole. Neptune is much bluer than Uranus and has more pronounced features, including the streaky, bright white clouds that appear at all latitudes, and dark oval features reminiscent of those on Jupiter. The difference in colour between Uranus and Neptune at visible wavelengths is due mainly to the different path lengths of methane in each atmosphere, varying opacity in the weak methane absorption bands at the red end of the visible spectrum.

Although Neptune receives less sunlight than Uranus, it appears to radiate about the same amount of infrared energy, and to have temperatures in the upper atmosphere that are very similar. The minimum temperature at the tropopause is about 55 K on both planets, increasing with depth along an adiabat.[20] Both have relatively warm upper atmospheres due to absorption of sunlight by hydrocarbons and hazes, but more distant Neptune is actually warmer by as much as 40 K, presumably due to a higher concentration of absorber. The atmospheres of both planets are cold enough for white clouds of methane ice to form near the 1 bar level, with extensive polar hazes above and a main cloud deck at approximately 3 bars below. The composition of the latter is uncertain; microwave observations show that water condenses well below this level, as would be expected from the temperature profile. They also show both atmospheres to be severely depleted in ammonia, which would otherwise have been a candidate for forming a substantial condensate cloud at the observed pressure level. This leaves hydrogen sulphide, H_2S, as the most reasonable guess for the composition of the main cloud decks on Uranus and Neptune, although this has still to be confirmed.

[20] Ignoring condensation effects, the dry adiabatic temperature profile g/C_p (see Chapter 5) for Uranus is 0.68 K km^{-1} and, for Neptune, 0.85 K km^{-1}.

The 'missing' ammonia in the atmospheres of Uranus and Neptune is probably a consequence of radically different interior structures compared to Jupiter and Saturn. Somewhere in each planet there has to be a high concentration of ammonia, or of nitrogen in some other form, since it is unlikely that large objects like Uranus and Neptune could have accreted without acquiring at least approximately cosmogonic proportions of such a common element. In models of their interiors, the pressures and temperatures inside the smaller giant planets are not high enough for hydrogen to become metallic; instead, a conducting mantle of water containing ammonia and other impurities forms around the roughly Earth-sized rocky core at the centre of each planet. It is probably here that their magnetic fields are generated.

1.4 Titan: a satellite with an atmosphere and a climate

Titan (Fig. 1.18) is Saturn's biggest moon and is larger than the planet Mercury. Although Jupiter's moon Ganymede has a slightly greater diameter, Titan looks bigger when measured optically because it is surrounded by an extensive and cloudy atmosphere, while Ganymede has none. Titan's atmosphere is predominantly composed of nitrogen, like Earth's, but with a higher surface pressure, despite the significantly lower gravity. Why this satellite should be endowed with a thick atmosphere while that on larger, volatile-rich Mars is so much less, and the similarly sized Jovian satellites Ganymede and Callisto are essentially airless, is a mystery. The answer must involve the low temperature at Saturn's distance from the Sun, and Titan's relatively large distance from its parent, in the early days of the formation of the planetary system.

The nitrogen on Titan probably started out as ammonia (NH_3), which is easily photochemically dissociated followed by the escape to space of most of the hydrogen. Today, N_2 forms about 95% of the atmosphere. The remainder is mostly methane, CH_4, which is also subjected to dissociation by solar ultraviolet radiation and energetic particles from Saturn's radiation belts, the Sun, and cosmic rays. There has to be a source of methane on Titan to explain its continued presence, because at the present rate of destruction it would all vanish in only about one million years. Titan has a low mean density ($1.88\,g\,cm^{-3}$) so the interior must contain a lot of ice. Some of this would be expected to be frozen methane and ammonia, along with water and other ices. At the high pressures in the interior, and assisted by small amounts of radioactive and tidal heating, the methane could vaporise and escape though cracks and vents in the crust. The *Cassini* spacecraft in orbit around Saturn has obtained some visual evidence for these 'cryovolcanoes' during close passes over Titan.

The decomposing methane in the upper atmosphere is likely to be the main source of the thick layer of orange haze that dominates the visual appearance of Titan. Although its detailed composition is still not known, despite the attentions of several instruments on the *Cassini* Saturn orbiter and the *Huygens* Titan probe, it apparently consists of drops of oily hydrocarbons, produced by a chain of reactions that start

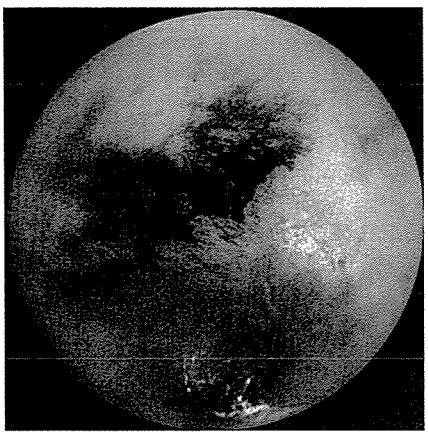

- N_2 atmosphere, 5% CH_4
- Surface pressure 1.6 bar
- Surface temperature 95 K
- Photochemical hydrocarbon haze
- Methane cumulus clouds
- Organic drizzle, CH_4 rain
- Surface run-off, lakes

Fig. 1.18
General appearance and defining characteristics of the atmosphere of Titan.

with the dissociation of methane and nitrogen by solar ultraviolet photons. The ethane, acetylene, ethylene, hydrogen cyanide and other trace constituents that have been detected spectroscopically in the atmosphere are part of this process. As larger and larger molecules are synthesised, condensation occurs, forming aerosol particles that can grow by coalescence. Model calculations of the haze formation predict production and growth rates that are quite rapid and also irreversible, so eventually large droplets drizzle onto the surface to form tarry deposits of condensable hydrocarbons and nitriles.

Ultraviolet photons tend not to penetrate to the lowest 50 km or so of the atmosphere, so photochemistry here is less important and temperatures are lower. There, even relatively simple molecules like methane and ethane can also condense, their high abundances resulting in dense white stratus and cumulus-type clouds in favourable situations, such as strong moist updrafts. Spectacular weather systems marked by clusters of these bright condensate clouds occur sporadically at various preferred locations and seasons on Titan, and some of them apparently release monsoon-type rains, to judge by the appearance of extensive channels and other fluvial features on the surface. Most of the channels and basins are dry most of the time, so the liquid soon evaporates or soaks into the surface, but some extensive lakes have been found as well.

Titan's surface temperature is about −178 °C (95 K). Other statistics are given in Figure 1.19 and in Table 1.4.

Two other satellites, Io (Jupiter) and Triton (Neptune), have thin, transient atmospheres fuelled by volcanoes, expelling mainly sulphur dioxide and hydrogen sulphide on Io, and nitrogen on Triton. The volcanoes are driven by tidal heating of the interior of the body in both

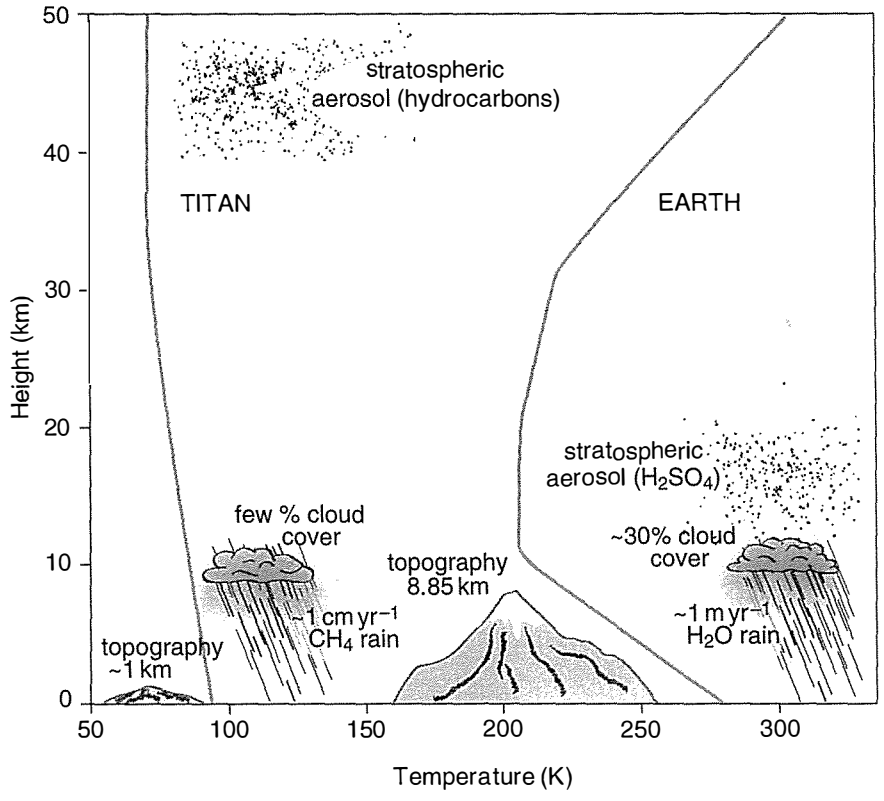

Fig. 1.19
Titan's atmosphere compared to Earth. The relatively low temperatures on Titan are of course due primarily to its tenfold greater distance from the Sun. The relatively small lapse rate results from Titan's low gravity (about one-seventh of Earth). However, the surface pressure is nearly the same for both (actually 50% higher on Titan than on Earth).

Table 1.4 Data on Titan, the largest moon of Saturn. Except for the low temperature, the climate at the surface is Earth-like, even featuring clouds and rain.

Mass	1.35×10^{23} kg ($0.0226 \times$ Earth)
Equatorial radius	2575 km ($0.40 \times$ Earth)
Mean density	1.88 g cm^{-3}
Mean distance from Saturn	1.22×10^{6} km
Rotational period	15.94 days
Orbital period	15.94 days
Orbital eccentricity	0.029
Orbital inclination	0.33°
Atmospheric bulk composition	95% N_2, 5% CH_4
Mean surface temperature	95 K
Surface atmospheric pressure	1.467 bars

cases, rather than by primordial and radioactive heat as with the Earth.[21]

[21] Tidal heating occurs when the solid planet or moon is flexed by gravitational forces acting unequally on different parts of its mass, for instance, if its orbit is eccentric, or regularly perturbed by a third object nearby.

1.5 Comparative climatology

In the last four decades, we have experienced the first close-up exploration of the planets of the Solar System. American, Russian, and (increasingly) European planetary space missions have now explored the atmospheres and environments of all of the planets, some many times. As never before, the data produced places the Earth in its wider context, among the terrestrial planets of the Solar System. Common aspects are revealed, not only of their contemporaneous origin and evolution, but also of their atmospheric structure and surface conditions.

Comparative planetary climatology is still a young discipline, limited by many unknowns, but capable of producing useful first-order insights, and listing key questions that can be addressed by anticipated new measurements. Progress is driven, not only by scientific interest in planetary-scale phenomena and the common evolutionary history of the planetary system, but also by concern about climate change on the Earth, and a consequent interest in all aspects of climate physics.

Comparative planetary climatology addresses the physical processes that determine

- current environmental conditions on Earth-like planets,
- the stability in each case against climate change,
- the development of models to simulate past and future climate,
- new experiments to further investigate these and improve the models.

By comparing the effects of similar processes at work on Mars, Venus and Titan to those on our own planet, we may gain a deeper understanding of global change on the Earth, the origin and evolution over the long term of an habitable world, and the realities behind threats such as greenhouse warming. To do this we construct models which give a description of the state of the climate for all four of the terrestrial planet atmospheres in terms of simple physics. These can be tested and

refined using measurements, and then employed to study, and eventually to answer, questions of climate stability and change, such as:

- What do the climate systems on all four planets have in common?
- How stable are their current climates, and what controls their stability?
- What change has taken place, why, and on what timescale?
- Can we make plausible predictions of future change?

Venus, Earth and Mars all have in common greenhouse warming by CO_2, H_2O and other gases, plus clouds and aerosols, which enhances the surface temperature considerably in each case. On Mars, there is dramatic evidence of past climate change; this, too, has analogous behaviour on the Earth, probably on Venus, and perhaps also on Titan, the large satellite of Saturn, which has one of the most Earth-like atmospheres yet discovered. In particular, Titan's surface pressure is the closest to Earth's of any known planet, and its atmospheric composition has the same main constituent, molecular nitrogen.

Current thinking about the data obtained to date suggests that Mars, Venus and Earth were all more similar to each other when they formed than they are today. It is likely that all three had enough water to form substantial oceans, strong internally generated magnetic fields, and active volcanism on a scale sufficient to create and maintain thick atmospheres. But to what extent were they really the same? Obviously, distance from the Sun is one variable that must have made a difference and been a factor in the disappearance of the oceans on Venus and Mars. The dominant mechanisms of loss may have been the same, but scaled by solar distance and other factors (size, in the case of Mars) to produce different evolutionary paths leading to the present diversity. For instance, it seems likely that most of the water on Venus was lost to space, while that on Mars was frozen below the surface. Venus may never have had liquid water on its surface. If, as seems likely, the surface of the planet was always very hot, its 'ocean' could have outgassed from the interior and resided in the atmosphere as vapour, until it dissociated and escaped without ever condensing.

Measurements of ordinary and heavy water vapour abundances have provided D/H ratios and other evidence that can be used to measure loss rates and extrapolate back over time. Differences and changes in magnetic fields with time can, in principle, be simulated with computer models of planetary interiors, although in practice this is proving a challenge. The actual effect of a magnetic field on atmospheric erosion by the solar wind also remains controversial, although progress is being made.

All of this is discussed further in later chapters. The methodology may be summarised as:

- Uncover the common origin of the Solar System and planets
- Identify their divergent evolutionary paths
- Explain current similarities and differences
- Define the mysteries that remain and make plans to address them through new experiments.

While this approach is, initially at least, most fruitfully applied to those planets nearest to the Earth in size and behaviour, we should not overlook less-likely siblings such as Mercury and the Moon. Mercury, which in terms of its geology and place in the inner Solar System is undoubtedly a terrestrial planet, has an atmosphere that is so thin that it more resembles the terrestrial exosphere. This tenuous region, on the fringe of space, has a long-term relationship to the climate at the Earth's surface through the atmospheric escape processes that occur there. However, the investigation of thick polar deposits on Mercury, apparently of water ice, is likely to yield answers that will lead to a better understanding of the origin of water on all the planets.

Likewise, the deep, hydrogen atmospheres of the gas giants Jupiter, Saturn, Uranus and Neptune, although the seat of fascinating dynamical behaviour and holding many clues about the formation of the Sun and planets, are not simple analogues for the Earth's climate system in any obvious way. Yet even here we find points of fruitful comparison. One example is the vertical temperature profiles: despite the great depth of the outer planet atmospheres, and the existence of internal sources of heat that match or in some cases exceed heating by the Sun, we find that the atmospheric vertical temperature profiles tend to take on the same overall character as those of Earth, Mars and Venus. In particular, they all have a *troposphere* characterised by an adiabatic lapse rate, overlaid by a quasi-isothermal *stratosphere*. These are expected on theoretical grounds when the dominant mode of vertical heat transfer is by convection at depth and by radiation above some level where radiative cooling to space becomes important (see Chapter 5). Radiative transfer theory, accompanied by knowledge of the composition of the atmosphere (including the most important infrared absorbers and emitters, which may be present in quite small proportions) and the properties of the cloud layers, should in principle allow all of the atmospheres of the Solar System to be reconciled, in terms of explaining their temperature structure. This is generally what we find, although many details remain to be worked out.

Progress in understanding these and other climate-related questions on all of the planets, including Earth, comes mainly from space missions. For instance, more than 30 spacecraft have visited Venus alone, and many more will be required before a clear picture emerges of even this, the closest and most Earth-like body in the Solar System. The climate system of a planet involves many interacting processes and feedbacks, so the interpretation of most of the data requires the use of models. When dealing with planets other than Earth, these models are necessarily quite simple, since, despite recent progress and new missions to Mars, Venus and Titan, our knowledge of these bodies and their atmospheres is still relatively scanty.

A goal of model studies is not just to understand the data we already have, but also, crucially, to help define what else can be done that will substantially increase, not just our knowledge, but also our understanding. Given the high cost and relative infrequency of missions to any particular planet, this is not just a scientific question; new technology, or a specific large and difficult mission may be called for. This

could involve the return of atmospheric, surface or deep-drilled core samples, or even human exploration on the surface of Mars (and, eventually, Venus and Titan). Before embarking on such as these, we have to be sure we have understood the problems we are trying to solve with existing data, to the maximum extent possible. Then we have to set realistic, convincing and economical goals. It is easy for this fairly self-evident philosophy to be overlooked, as in the current drive to mount missions to look for life on Europa, one of the large moons of Jupiter. While there does exist a high probability that Europa is home to a liquid water ocean, below several kilometres of icy crust that it exposes to space, the difficulties of exploring beneath the ice are enormous, while the chances of finding anything but dirty water must be extremely small.

What are the top priorities for future space missions? No two leading researchers would give the same answer, but here are some candidates that would be on most lists.

For Mars, a pressing issue is to trace the origins of the methane that has been detected in the atmosphere. If, as expected, this is associated with hydrothermal vents, where warm, liquid water is also to be found just below the surface, then this represents the long-sought opportunity to find life, or answer the question of whether Mars is now, or ever was, habitable by microorganisms recognisable to terrestrial biologists. In what ways will they differ, and why? Sophisticated robots equipped with drills and analytical laboratories – and deployed in the right place – will probably answer these questions before the first human explorers arrive.

The search to discover the nature and extent of volcanic activity on Venus is already underway, but requires new approaches to make major progress. Navigable floating stations ('submarines') in the deep, dense atmosphere will survey the terrain and measure the gaseous emissions in volcanic plumes. They will have to survive high temperatures and pressures, requiring a new generation of electronic devices that likes to run hotter than our current computers and power supplies. Measurements made *in situ* of noble gases and samples from the surface and below will provide geological evidence for past climates, but again are difficult to collect and mostly belong in some future epoch of exploration just over the horizon. No one talks seriously of a search for life on Venus, although some have suggested microbes may survive happily in the clouds, where the temperatures are equitable and there is plenty of water and energy, but it may make sense to ask whether Venus was habitable in the distant past.

In the shorter term, an equally exciting if slightly less exotic goal would be to develop integrated climate models for Venus, Earth and Mars. A single, very large general-circulation model, with all relevant physics included, must be able to simulate the present-day climate of all three planets if it is correctly formulated. Then, never entirely reliably but at least on a firm foundation, experiments to 'hindcast' the past climates and forecast the future would also stand to be optimised, as represented in Figure 1.20. Unfortunately for the inhabitants, the Earth is running a climate-change experiment on such a short timescale that understanding threatens to come too late.

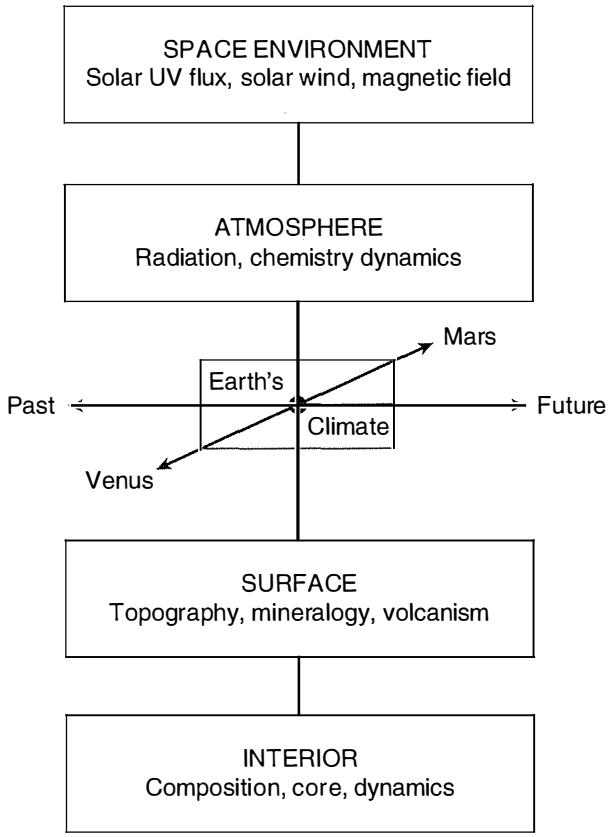

Fig. 1.20
A summary of the key processes controlling climate on the Earth, and their principal interactions in the vertical dimension. The other key dimensions are time, relating the current climate to the past, and space, relating the Earth to its neighbours Venus and Mars, and potentially to other Earth-like planets elsewhere in the universe.

1.6 References and further reading

Recommended introductory reading for the exploration and general properties of the planets and their atmospheres may be found in the following:

Coustenis, A., and F.W. Taylor. *Titan: Exploring an Earthlike World.* World Scientific Publishing, 2008.

Grinspoon, D.H. *Venus Revealed: A New Look Below the Clouds of our Mysterious Twin Planet.* Addison-Wesley, 1997.

Irwin, P.G. *Giant Planets of our Solar System: An Introduction.* Springer, 2006.

Read, P.L., and S.R. Lewis. *The Martian Climate Revisited: Atmosphere and Environment of a Desert Planet.* Springer-Praxis, 2004.

Schofield, J.T., and F.W. Taylor. Measurements of the mean solar-fixed temperature and cloud structure of the middle atmosphere of Venus. *Q. J. Roy. Meteorol. Soc.*, **109,** 57–80, 1983.

Taylor, F.W., C.D. Rodgers, J.G. Whitney, S.T. Werrett, J.J. Barnett, G.D. Peskett, P. Venters, J. Ballard, C.W.P. Palmer, R.J. Knight, P. Morris, T. Nightingale, and A. Dudhia. Remote sensing of atmospheric structure and composition by pressure modulator radiometry from space: The ISAMS experiment on UARS. J. *Geophys. Res.*, **98**, 10 799–10 814, 1993.

Taylor, F.W., D. Crisp, and B. Bézard. Near-infrared sounding of the lower atmosphere of Venus. pp. 325–351, in *Venus 2*, ed. by S.W. Bougher, D.M. Hunten, and R.J. Phillips, University of Arizona Press, Tucson, AZ, 1997.

Taylor, F.W. *The Scientific Exploration of Mars.* Cambridge University Press, 2009.

2 Origin and evolution of planetary atmospheres

The present climates on all of the planets are the result of a multi-stage process, which began when the protosolar cloud formed out of a concentration of interstellar gas and dust and then collapsed under gravity to form the Sun. Most, but not all of the mass of the cloud ended up in the young star, the remainder forming a flat disc of orbiting material in which most of the angular momentum of the system resided. The disc in turn aggregated into progressively larger bodies, which eventually formed the planetary system that we see today.

The planetary masses closest to the star were composed mainly of rocky and metallic material, but included gas and volatiles trapped in their interiors that gradually escaped and formed their modern atmospheres. In the outer Solar System, temperatures were low and ice accreted along with metal and rock, forming massive planets that were able to trap protosolar material, including large amounts of hydrogen and helium that the smaller, hotter inner planets could not retain.

2.1 The origin of the Solar System

Any theory of planetary formation that is more detailed than the bare outline given above must seek to explain why our own planetary system has the contents (Table 2.1) and properties (Table 2.2) that it does. It must also account for the variations on that familiar theme being discovered elsewhere in the Universe. These variations have long been known to include multiple stars, and are recently found to include enormous planets orbiting very rapidly, very close to their respective suns. Systems that include Earth-like planets are harder to detect, but it seems certain that these will be revealed in the next few decades by advanced methods and instruments now being planned. Meanwhile, we have to work mainly with what we know about our own planetary system.

In addition to the inventory listed in Table 2.1, we have the basic properties summarised in Table 2.2 which must be explained by some plausible and probable mechanism that can be modelled using known physics. The question of the origin of the Solar System, and its evolution

Table 2.1 The main contents of the Solar System, and the fraction each contributes to the total mass. In the case of comets (defined here to include all small icy bodies, i.e., Kuiper belt and Oort cloud objects) the total mass is very uncertain. Similarly, the total number of asteroids (small rocky bodies, most of which are in the belt between Mars and Jupiter) is not known very well, but their combined mass is certainly less than that of Earth's Moon.

1 star (99.85% of the Solar System by mass)
8 planets (0.135%)
4 planetary ring systems (~0)
~60 natural satellites (0.000 05%)
~6000 asteroids (~0)
$\sim 10^{12}$ comets (0.015%?)
interplanetary gas and dust (~0)

Table 2.2 Key properties of the Solar System. The 'heavy' elements referred to in item (8) mean anything heavier than helium. The variation is large: from 3 × solar abundance for Jupiter to ~40 × solar for Neptune.

1. Planetary orbits are all in nearly the same plane
2. Planetary orbits are nearly circular
3. Planets orbit the Sun in the same sense
4. Planets spin in the same sense as their orbits (but not Uranus or Venus)
5. Angular momentum of Sun small compared to planets
6. Two families of planets, rocky near the Sun, gas giants far from Sun
7. Atmospheric compositions and isotopic ratios are different
8. Heavy elements in the giant planets are more abundant with distance
9. Orbital radius increases with distance as $4 + n$, where $n = 0, 3, 6, 12, \ldots$[22]
10. Existence of satellite families, Kuiper belt, Oort cloud, comets, etc.

to its present state, is one that has held the attention of many major figures in science at various times (Newton, Laplace, Fourier, Gauss, Kelvin, Helmholtz, Poincaré, Maxwell, and Einstein, to name but a few). Because some of the larger questions, not to mention many of the details, remain unresolved (not least because of the recent first indications of the nature of extrasolar planetary systems mentioned above), it is instructive to consider how the subject has evolved over time.

2.2 Planetary system formation theories

There are two main types of planetary system formation theories:

- those that invoke an infrequent, catastrophic event, such as a near collision between the Sun and another star, and
- those that involve natural processes such as might occur at the birth of any star without external intervention.

Both theories have had distinguished advocates over the centuries, and both sides pointed out that if we knew the answer it would have profound implications for the number of planetary systems likely to exist in the universe. Progress in modelling and observations, particularly the discovery that extrasolar planetary systems appear to be common, has swung opinion decisively towards non-catastrophic models in recent years.

[22] This is usually known as Bode's law, after German astronomer Johann Bode, who published this empirical law in 1766. Bode attributed it to work by Johann Titus two years earlier, although the latter may have taken it from David Gregory's book, *The Elements of Astronomy*, published in 1715. The law is good to within a few per cent for all planets except Neptune, for which it predicts 30.1 AU when the true value is 38.8 AU. Its theoretical basis is still debated.

2.2.1 The Kant-Laplace nebular hypothesis

The philosopher Immanuel Kant[23] espoused the idea that the Solar System formed from a rotating gaseous nebula as it slowly underwent gravitational collapse. Such nebulae certainly are observed throughout the local Galaxy, many of them of great size, and much larger than the Solar System. Kant, in his search for rational explanations of the visible universe, went on to suggest that a similar process of collapse might be responsible for the formation of the Milky Way itself. Some 40 years later, Laplace fleshed out the theory. He showed theoretically how the solar nebula, rotating faster and faster as it contracted, could have flattened into a flat, equatorial disc of hot dust and gas under the action of gravity and the conservation of angular momentum. When the centrifugal force acting on the outer edge of the nebula exceeded the gravitational force, he postulated, a ring of matter separated off and condensed into a planet. The remaining, smaller disc repeated the process inside this ring until all eight planets had formed, then the central portion condensed to become the Sun.

The main problem with Laplace's theory has always been its failure to account for the fact that the Sun has 99% of the mass of the Solar System, but 99% of its angular momentum resides in the orbital and rotational motions of the planets. Recent computer modelling of a large number of small masses in a cloud has shown how difficult it is to reproduce the observed angular momentum distribution by any plausible mechanism in such a system. It also shows that the kind of spin-off envisioned by Laplace would not form planet-sized rings of matter. Instead, material would disperse into space before gravity could pull it together to form a planet.

[23] Immanuel Kant (1724–1804) was the author of *The Critique of Pure Reason* and other seminal and important books, in which he defines the philosophy of science in terms of the relationship between experience and knowledge. His theory of the Solar System was published in *Universal Natural History and Theory of Heaven* when he was 31 years old.

2.2.2 Encounter theories

Georges Buffon[24] proposed in 1745 that the material ripped from the Sun by a collision with a large comet had condensed into the planets. The idea that the cause was not a direct collision but the gravitational attraction of a passing star was proposed by Chamberlin and Moulton,[25] in the USA, and developed in detail using tidal theory by Harold Jeffreys and James Jeans in England.[26] The theory explains why the largest planets are at middling distances from the Sun, the common direction of planets' orbital motion, the Sun's rotation, and the planets' nearly circular and coplanar orbits. However, it still cannot explain how matter drawn from the Sun could have acquired sufficient angular momentum, or how the hot gas condensed into planets. There is also the problem that the probability of a suitable encounter between stars is incredibly small.

[24] Georges-Louis Leclerc, Comte de Buffon (1707–1788) was a French naturalist, known today mainly for his reflections on the origins of species a century before Darwin.

[25] Thomas Chamberlin (1843–1928) held the chair in Geology at the University of Chicago. Forest Moulton, later a professor there, was Chamberlin's graduate student at the time he started work on the mathematical modelling of the Solar System.

[26] Harold Jeffreys (1891–1989) was Plumian Professor of Astronomy at Cambridge. James Jeans (1877–1946) was also at Cambridge, and then moved to Mt. Wilson Observatory in California, where he became one of the originators of the continuous creation theory of the universe.

2.2.3 The protoplanet theory

By the 1930s, it was known that dust particles existed in the cool interstellar gas clouds of hydrogen and helium where star formation

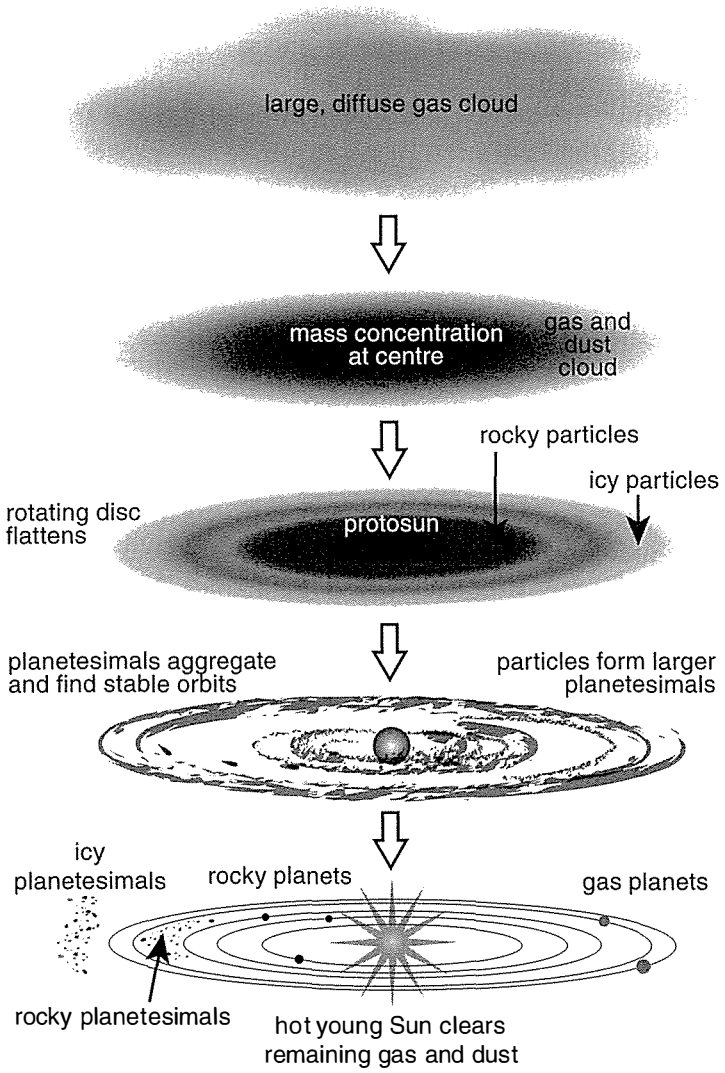

Fig. 2.1
A schematic of the stages in the development of the Solar System from a protosolar cloud. Most current theories have this progression in common, but the details remain uncertain.

takes place. The idea that the dust could condense into larger aggregates that grow to form large 'protoplanets' formed the basis for the 'core-accretion' theory, originally formulated by von Weizsäcker in 1945 and extended by Kuiper in 1951.[27] A key feature was the formation of eddies to start the accretion process that could lead to gravitational collapse.

Gravity makes the protosolar cloud collapse in the direction parallel to the axis of rotation, while centrifugal forces distribute the material that has sufficient orbital velocity into a relatively thin disk of solids within a thicker, more diffuse disc of gases. Inhomogeneities in mass and velocity within the dust layer led to collisions, and because grains formed in space will have a sticky, feathery structure, this frequently resulted in coalescence. The collisions could also cause the angular momentum of the growing fragments to increase with the contraction of the solar nebula. Eventually the fragments reach a critical mass, capable of drawing in nearby material by gravitational attraction. This process became more efficient with size, so growth accelerated and diffuse conglomerations became more compact, leading to asteroid-sized

[27] Carl Friedrich von Weizsäcker (1912–2007) developed his model for the formation of the Solar System while working, reluctantly, on nuclear weapons for the Nazis during WW2. At about the same time, Gerard Kuiper (1905–1973) of the University of Chicago made the first detection of carbon dioxide on Mars and of methane on Titan. He published *On the Origin of the Solar System* in 1951.

'planetesimals' orbiting the dense centre of the solar nebula. Temperature and fractionation effects might mean differences in chemical composition, depending on factors like distance from the young star.

As the central portion of the solar nebula continued to contract, its temperature became hot enough to vaporise the more volatile compounds in the inner disk, leaving mainly the rocky materials, while the outer disk remained relatively cool. The terrestrial planets therefore formed close to the Sun, and contain relatively little volatile icy and gaseous material, although they are rich in metals and rocky materials. The Jovian planets, formed far from Sun beyond the 'snow line' where water froze to form ice, contain more icy material. They would have formed more quickly than rocky planetesimals and grown larger and faster, gravitationally attracting not only rock and ice but also the lighter gases as well. The large relative abundances of hydrogen and helium in the nebula meant these gases were particularly well represented in the giant planets.

Thus most of the properties listed in Tables 2.1 and 2.2 can be explained by the model summarised in Fig. 2.1. As Kuiper wrote more than fifty years ago, 'the common direction of revolution and the low relative orbital inclinations are accounted for by the flatness of the solar nebula. The internal viscosity of the nebula accounts for the near-circular orbits. The direct rotation of the planets is attributed to solar tidal friction on the proto-planets... The latter cause has a secular effect on the obliquities; it has been shown that they will increase some three or fivefold, from initial obliquities of the order of 30 (expected from the turbulent solar nebula, and consistent with the relative orbital inclinations) to the present values. The largest obliquity to which this process can lead is 90°; retrograde rotation cannot arise by the processes considered. It is not clear why Uranus has passed the upper limit by 7°; possibly some extraneous object has moved through the Solar System. The present periods of rotation have not yet been accounted for quantitatively. This appears to be a very complex problem, with physics, chemistry and dynamics all playing a role. We have here perhaps the most important potential source of information still unused in the reconstruction of the planetary condensation processes.'

It is still unused, and indeed our understanding of the formation process has in some ways moved backwards in the intervening fifty years. While Kuiper's summary explains most of the observed differences between the planets in our own Solar System, it has been difficult to reconcile current theory with recent discoveries of 'hot Jupiters' orbiting other stars. These large planets often have remarkable orbital parameters[28] that cannot be explained without some major refinements to our already deficient understanding of the processes involved in planetary formation. Some progress towards a theory with universal applicability is being made with a gravitational instability model, where turbulence in the accretion disc is increased to cause lumps of gas and dust to condense very quickly into Jupiter-plus-sized planets. Such a model leads to very similar compositions for all the giant planets in a stellar system, however, so it is probably not the mechanism

[28] WASP-3b, a rather extreme example, was discovered in 2007 by a consortium of observers operating a programme called Wide Angle Search for Planets. It is 727 light years away in the constellation Lyra, has a mass 1.76 times that of Jupiter, and orbits its star at a distance of only 0.0317 AU in a mere 1.84 days.

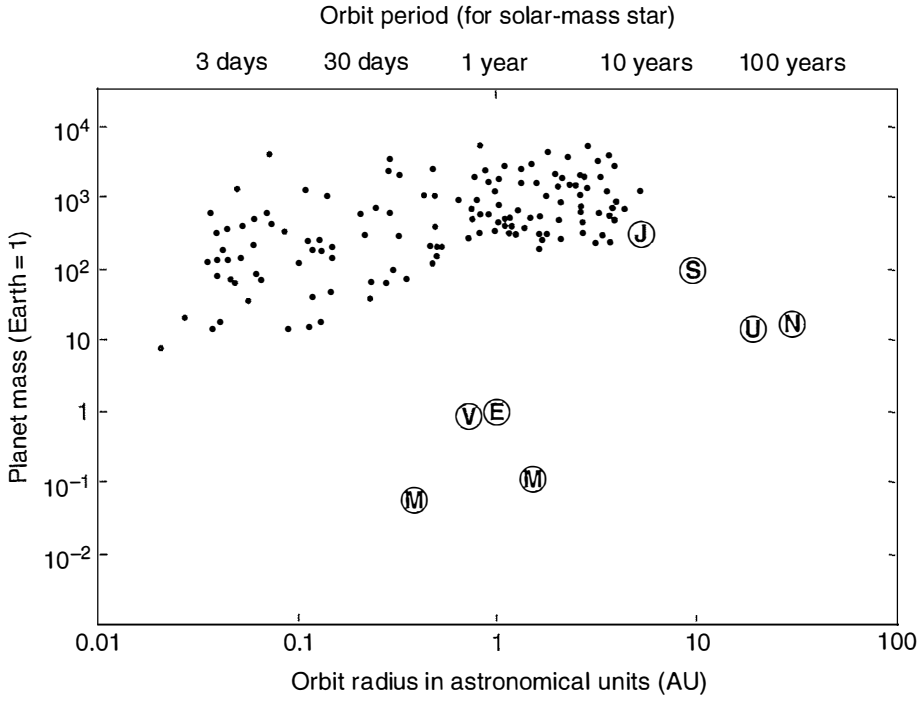

Fig. 2.2
Known exoplanets in January 2006 (planet.iap.fr/OB05390.news.html), at the time of the discovery of the first cool, rocky planet outside the Solar System, OGLE-2005-BLG-390Lb (estimated to be 5.5 Earth masses at 2 AU from its star). The labelled discs are the planets of our Solar System. The reason the exoplanets are relatively large is, of course, because large objects are easier to detect, and not because they are necessarily more numerous in the Galaxy.

that dominated the formation of our own giant planets, which show large variations (Fig. 2.2, Table 2.2).

2.3 Models of planet formation

While bearing in mind that the centuries-long search for a complete theory of planetary system formation is far from over, we now look in more detail at some of the processes believed to have been involved. Following the work of Jeans and others, simple numerical models can be constructed that give useful insights.

2.3.1 Collapse criteria for the protosolar nebula

An isothermal cloud of mass M will undergo gravitational collapse if its gravitational potential energy is greater than its internal thermal energy.

The thermal energy of the cloud is

$$E = \frac{3}{2}NkT = \frac{3M}{2\mu m_H}kT$$

where μ is the molecular weight of the material in cloud, m_H is the mass of the hydrogen atom, M the mass of the cloud, and N the total number of atoms in the cloud.

The gravitational binding energy of the cloud is $E_g = \frac{GM^2}{R}$ and the stability/instability boundary occurs where:

$$\frac{3MkT}{2\mu m_H} = \frac{GM^2}{R}$$

now $M = \frac{4}{3}\pi\rho R^3$, hence

$$R = \left(\frac{M}{2\pi\rho}\right)^{\frac{1}{3}}$$

giving

$$\frac{kT}{\mu m_H} = G(2M^2\pi\rho)^{\frac{1}{3}}$$

By rearrangement we get *Jeans' criterion* for the minimum mass of cloud of temperature T and radius R that will collapse:

$$M_J \approx \frac{1}{\sqrt{\rho}}\left(\frac{kT}{G\mu m_H}\right)^{\frac{3}{2}}$$

Typical values might be: $T = 20\,\text{K}$, $\rho = 10^{10}$ H atoms $(10^{-17}\,\text{kg})$ m^{-3}, whence $M_J \approx 10^{31}$ kg, which is about 10 solar masses, and $R \approx 40{,}000\,\text{AU}$ or about 1 ly.[29]

[29] 1 ly = 65,000 AU = 1 light year, the distance covered in 1 year at light speed.

2.3.2 Formation of planets

The timescale for Jeans collapse is estimated by considering a particle in free fall at a distance R from the centre of a cloud of mass M. The acceleration of the particle is $\frac{GM}{R^2} \approx \frac{R}{t^2}$, where t is the time to collapse to the centre, and $t \approx \frac{1}{\sqrt{G\rho}}$.

Again, inserting typical values we find $t \sim 10^6$ years, so time is not a problem, but the theory has the difficulty that M_J is much greater than the present mass of the Solar System.

This may be explained by assuming that the protosolar cloud was once ten or more times massive than today's Sun and planets combined, but that the excess mass was loss during the *T-Tauri phase* in the early evolution of the Sun, as discussed below (§2.3.5). In principle, this might also provide a means for slowing down the rotation of the Sun in order to get today's observed angular momentum distribution, but detailed models have trouble making this work in practice. Some sort of electromagnetic force could be invoked if the Sun had a much larger magnetic field in the past than it does now, which dragged against the cosmic background field and slowed the Sun's rotation. However, this substitutes one problem for another, which is how the Sun got rid of this excess magnetic field.

2.3.3 The shape of the solar nebula

Here we take a closer look at how the rotating cloud becomes a flattened disc. It is obvious from conservation of net angular momentum that, as the cloud becomes smaller, it rotates faster and the angular

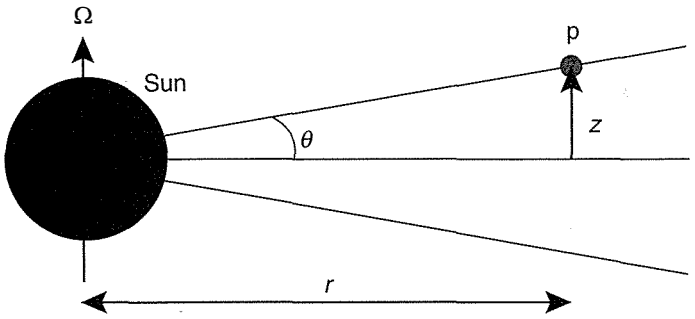

Fig. 2.3
Condensation of the disc occurs as a result of the balance between the centrifugal force of the Sun's rotation at angular velocity, Ω, and gravity, which are balanced in the ecliptic plane but not in the direction z perpendicular to it, causing migration of the particles to the disc. This in turn is balanced by a pressure gradient dp/dz as gas accumulates in the ecliptic plane.

velocity Ω increases. The density distribution of the disc in the direction parallel to Ω, where centripetal forces do not act, is a result of the balance between the pressure gradient force and the gravitational force. Referring to Fig. 2.3, these are given by

$$g_z = g \sin\theta \approx \frac{GM_S z}{r^3}$$

and

$$dp = -\rho g_z dz = \left(\frac{-p\mu}{RT}\right) \times \left(\frac{GM_S z}{r^3}\right) dz$$

In equilibrium,

$$p_z = p_c \exp\left(-\frac{z^2}{H^2}\right)$$

where H is the scale height

$$H = \left(\frac{2RTr^3}{\mu GM_S}\right)^{\frac{1}{2}}$$

This arrangement is stable for gas, but for dust, p is negligible and sedimentation occurs, forming a dust disc in the central plane. This dust layer is not obviously unstable, but in fact observations of many young stars show that their protoplanetary discs last for only a few million years before accreting into larger objects that are less easy to detect. Detailed theories, and there are many of them, account for this by various differences in the orbits of individual dust grains that lead to them colliding with their neighbours and sticking together by chemical, gravitational and electrostatic attraction. Collisions are frequent at first, but become rare by the time that planetesimals with diameters of a kilometre or so, corresponding to a mass $\sim 10^{12}$ kg, have been formed in large numbers.

The comets and asteroids, of which there is still an enormous number in the Solar System, may be remnant planetesimals that did not get absorbed into planets. Most did, however. The segregation of mass into the orbits of the present planets was the result of the original mass

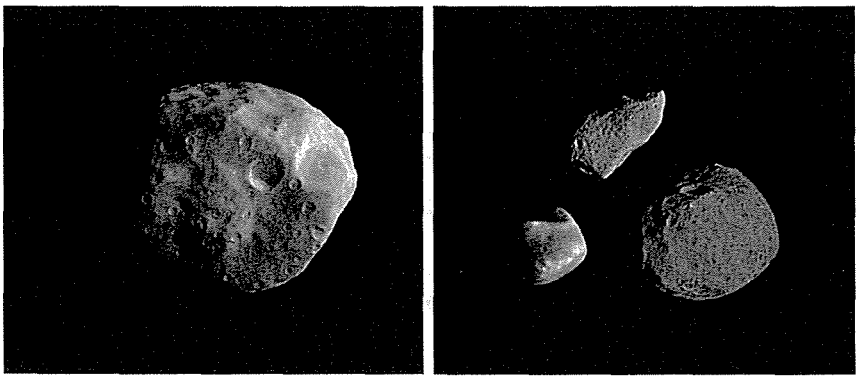

Fig. 2.4
Saturn's satellite Epimetheus, left, is about 100 km across, and an example of a large icy planetesimal. Asteroid 951 Gaspra (top) and the Martian moons Phobos (right) and Deimos (left), shown in the panel on the right on a scale in which the illuminated part of Gaspra is about 17 km long, are all rocky planetesimals more typical of the inner Solar System. Gaspra resides in the asteroid belt between Mars and Jupiter; the others must have encountered Saturn and Mars, respectively, with a trajectory that resulted in capture into orbit, rather than becoming part of the mass of the planet as most of their siblings did.

distribution, combined with the existence of certain stable values of solar distance where objects can orbit without being displaced by resonant interactions with each other, especially with massive, centrally located Jupiter. The planets grew at the expense of planetesimals in unstable orbits, some, perhaps most, of which were non-circular, like the Earth-crossing asteroids that still pass near the Earth and threaten every so often to add to its mass. Comet Shoemaker-Levy did just that to Jupiter in July 1994. All four terrestrial planets show the scars of big collisions late in their formation history:

- The Caloris basin on Mercury is a huge impact crater, 1500 km across, produced by the arrival of a planetesimal so large that damage on the side of the planet opposite to the crater itself, caused by the focussing of seismic waves produced by the collision and transmitted all around the planet, can still be seen.
- Venus rotates slowly backwards, probably the result of one or more large planetesimals with unusual trajectories imparting retrograde angular momentum.
- According to our current understanding, Earth's Moon was produced by the impact of a Mars-sized body after most of the present mass of the Earth was in place.
- The crust on Mars is asymmetric, being thinner over most of the northern hemisphere so that the topography there is several kilometres lower on average relative to the south. This northern basin is probably the result of a glancing blow by a large planetesimal during the early history of the planet. The smaller, but still huge, Argyre and Hellas basins in the southern hemisphere are each the result of a direct hit by an object about 100 km across (cf. the objects in Fig. 2.4).

2.3.4 Compositional variations between planets

In current models of the protoplanetary cloud, the temperature and pressure fall rapidly with distance from the protosun as a result of the energy released during collapse. At the centre, the temperature was very high since the opacity of the surrounding cloud inhibited the escape of heat as radiation, while at the outer edge the temperature

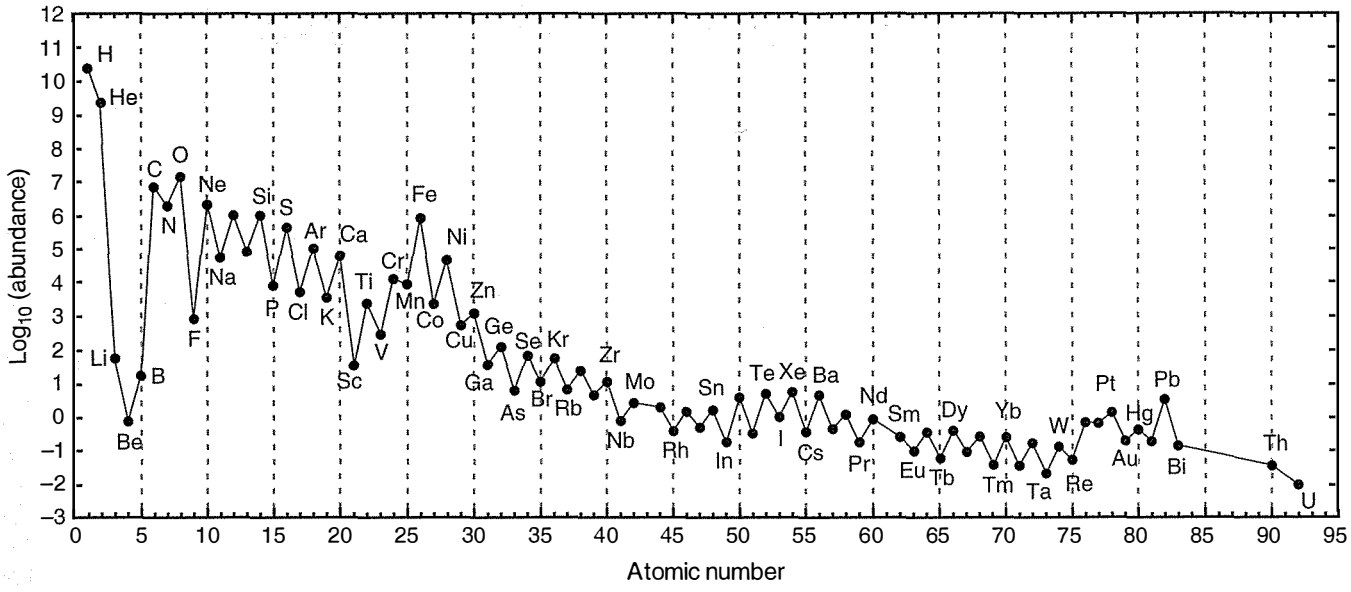

Fig. 2.5
The relative abundances of the elements.[30] Elements with even atomic number Z are systematically more abundant than those with odd Z, with the exception of beryllium.

of the cloud merged into that of cold space. The elemental composition of the cloud as a whole is usually taken to be that given by the cosmic abundance table compiled from spectroscopic studies of molecular clouds and stars, including the Sun. This is shown graphically in Fig. 2.5. The more reactive elements formed simple compounds determined by equilibrium chemistry at the relevant temperature, which varied along the gradient from the centre of the cloud to the edge.

In the region near the protosun, volatile compounds such as water and ammonia remained gaseous, while heavier substances such as iron and silicates condensed. Thus, the inner planets contain a much higher proportion of these less-volatile components. Further from the protosun, the temperatures fell sufficiently to allow ammonia and ice to condense, explaining the increased abundance of these materials further from the Sun. The early disc is thought to have been highly turbulent, with matter transported both outwards and inwards from the main mass concentration near the centre. Some of it ended in the Sun, of course, possibly contributing to a significant transfer of angular momentum that slowed down the rotation of the Sun.

[30] E. Anders and M. Ebihara, 'Solar System abundances of the elements', *Geochimica et Cosmochimica Acta*, **46** (11), 2363–2380, 1982.

2.3.5 The T-Tauri phase of the Sun

Soon after the Sun began to fuse hydrogen and thus became a star, it would have entered its T-Tauri phase, with two to three times its current luminosity and a very dense, high-speed solar wind propelled by a strong magnetic field (Fig. 2.6). Mass loss rates of the order of 10^{-8} solar masses per year extending over 10^7 years would be typical, leading to the loss of a significant fraction of the total mass of the Sun before the activity subsided.

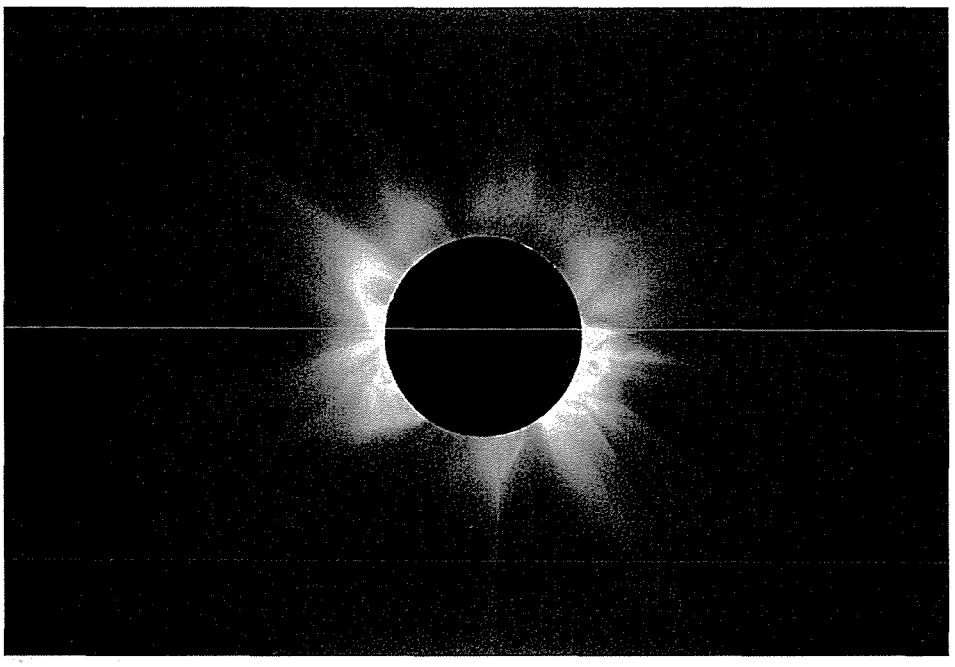

Fig. 2.6
The Sun, like most other stars, emits powerful streams of fast-moving protons and other particles into space, seen as bright rays when the disc is occulted. The solar wind was much more powerful when the Sun was young and in its 'T-Tauri' phase, named after a star that is showing the phenomenon at the present time. T-Tauri is only about 1 million years old and still surrounded by an accretion disc of gas and dust, much of which is being blown away into space. Since T-Tauri was discovered in 1852 the effect has been observed in many young stars and is now believed to be a normal part of stellar evolution. Our Solar System may have lost more than 90% of its original mass in this way.

The principal effect of the T-Tauri solar wind was to sweep away any remaining gas and dust that had not yet formed planets or planetesimals, out to the edge of the solar nebula and into outer space. As we saw above, this must have been about 90% of the mass of the original protosolar cloud. Such a large mass must also have carried away some of the angular momentum of the young star, possibly contributing to the 'despinning' of the Sun. Finally, the two smaller giant planets apparently had not yet become massive enough to complete the gravitational collapse of the nebula in their locality when the T-Tauri phase started. While Jupiter and Saturn acquired large proportions of hydrogen and helium to become gas giants, Uranus and Neptune would remain as 'ice giants'.

2.4 Formation of atmospheres

Once impacts became relatively rare, the planets cooled, and at some stage acquired the atmospheres that evolved to those we see today. Given the formation of a planet in the way we have described, a range of possible processes could have been involved. Did the atmosphere

1. form with the planet out of the solar nebula,
2. outgas later from the interior of the cooling planet,
3. arrive later as solar wind, or
4. arrive later as icy meteorites and comets?

The answer is different for the inner planets, whose original atmospheres could not have survived the T-Tauri phase, than for the outer planet atmospheres, which did (although they stopped accumulating gas from the nebula, especially Uranus and Neptune, at that point). Also, impacts on the inner planets would tend to blast atmospheric gases away, rather than add to them as they would on the giant planets.

Thus the *inner planets* probably lost all of the original gas by solar wind and impacts, but gained a secondary atmosphere later by outgassing from volcanoes and other vents connected to the interior. The expected result is that the elemental ratios of the less-volatile elements are solar, since these were not removed, while the elemental ratios of the primordial (non-radiogenic) noble gases resemble each other and meteorites, but not the Sun. This simple picture is spoiled by a number of important differences between planets, for example the absolute abundance of argon and the ratio of oxygen isotopes. We discuss the implications of these in the later chapters.

If the *outer planets* retained even the light elements from the proto-solar nebula, that would explain why the H_2/He ratios in Jupiter and Saturn resemble those in the Sun. However, again we will see that the picture is not so simple when we look at the detailed composition and much still remains to be learned.

2.5 Atmospheric stability and escape mechanisms

One way in which planetary atmospheres can evolve differently, following a common origin, is by losing some of the original constituents by one or more processes that act differently on planets of different size, or distance from the Sun, for instance. The various possibilities include:

1. Thermal escape to space: all atmospheres are slowly 'boiling' away into space due to the thermal velocities of the molecules near the top of the atmosphere. Any that reaches the escape velocity, in the right direction, without suffering a collision with another molecule, will continue its flight into space and never return.
2. Condensation to form permanent polar caps or permafrost. The latter is frozen, saturated soil that lies at some depth below the surface. A lot of water on both Mars and Earth is in this form.
3. Atmospheric gases can dissolve in large amounts and often this process is at least partly irreversible. Mars and Venus had oceans, or at least oceanic quantities of water in some form, for part of their history, and Earth still does. An important process on Earth is the formation of carbonic acid, H_2CO_3, by atmospheric CO_2 dissolving in rain and oceans, and its subsequent deposition from the oceans by the formation of solid carbonates. It is estimated that all of Earth's atmospheric CO_2 would be removed like this in $\sim$10,000 years if it were not being continuously replaced.
4. The solid-state equivalent of the previous item is absorption and chemical combination of gases regolith. Important examples are the cycling of sulphur compounds between the atmosphere and the crust on both Venus and Mars, and the removal of atmospheric oxygen by the formation of iron oxides ('rusting').
5. Hydrodynamic escape involves sweeping away a relatively heavy atom or molecule in the flow of a lighter one. In hydrogen-rich atmospheres, which may have included early Earth and Mars, the thermal escape of hydrogen may be copious enough to carry

significant amounts of heavier atoms like oxygen with it, although the oxygen atom is too massive to escape by its own thermal energy.

6. Solar wind erosion. We have already seen how a massive flux of particles from the Sun swept away the early atmospheres of the terrestrial planets and removed the residual protoplanetary cloud during the T-Tauri phase early in Solar System history. The solar wind continues at a reduced rate, and is still powerful enough to strip atoms from the top of the atmosphere. The process is particularly efficient on Venus, because it is close to the Sun and because it has no magnetic field to shield the planet from the charged solar wind particles.
7. Impact erosion. Collisions between planetesimals and planets are relatively rare now, but used to be frequent. The impact, especially a glancing blow, can remove huge amounts of atmosphere if the incoming object is large.

Simple physics can be applied to some of these processes, allowing their importance in various situations to be estimated for each planet.

2.5.1 Thermal escape: Jeans formula

The possibility for escape occurs when the thermal energy becomes greater than the gravitational potential energy, i.e., when

$$kT \approx \frac{1}{2}mV^2 > \frac{mMg}{R+z_c}$$

where V = upward velocity of a molecule of mass m, and $R_C = R + z_c$ is the radial distance from the centre of the of the planet of mass M and radius R at which thermal escape first occurs. The latter, known as the *critical level* or *exobase*, is defined as the level where the vertically integrated density above accounts for one mean free path. It falls at altitude z_c above the surface of the planet where

$$\int_{z_c}^{\text{space}} \sigma n_a(z)\mathrm{d}z = \sigma n_a(z_c)H_c = 1$$

and $n_a(z)$ is the number density of all molecules at altitude z, σ is the collisional cross section, and H_c is the overall scale height. For the Earth, the most abundant molecule in the upper atmosphere is molecular oxygen, and thus it is this molecule which largely determines the level of the exobase.[31]

The escape flux (mol m^{-2} s^{-1}) for each particular molecule is then obtained by integrating upwards from this level and over solid angle, assuming isothermal conditions and a Maxwellian distribution. It can be shown[32] that that the upward flux of molecules from the exobase is:

$$F_J = \frac{1}{2}n(z_c)\sqrt{\frac{\alpha}{\pi}}\left(v_c^2 + \frac{1}{\alpha}\right)\exp\left(-\alpha v_c^2\right)$$

[31] See J.T. Houghton, *Physics of Atmospheres*, Cambridge University Press, 2002.

[32] J.W. Chamberlain and D.M. Hunten, *Theory of Planetary Atmospheres*, Academic Press, 1987.

Table 2.3 The characteristic time for escape from Earth's atmosphere by Jeans escape, for four important exospheric constituents. These figures assume that the exobase is at 500 km altitude, that the temperature there is 1480 K, and the gravitational acceleration is 8.43 m s^{-2}.

	H	H_2	He	O
Scale height, H (km)	1460	730	365	91
Most probable speed U (km s^{-1})	4.96	3.51	2.48	1.24
Mean expansion velocity v_e (km s^{-1})	7.32×10^{-2}	8.71×10^{-4}	9.94×10^{-8}	7.14×10^{-32}
Exospheric escape time τ (s)	2.0×10^{4}	8.38×10^{5}	3.67×10^{9}	1.28×10^{33}

Table 2.4 The characteristic Jeans escape times for different gases on several planets and the Moon.

	Moon	Mercury	Mars	Venus	Jupiter
T (K)	300	600	365	700	155
R_c (km)	1738	2439	3590	6255	69 500
$G(R_c)$ (m s^{-2})	1.62	3.76	3.32	8.27	26.2
τ (H) (s)	3.55×10^{3}	3.32×10^{3}	1.39×10^{4}	5.71×10^{5}	5.14×10^{617}
τ (He) (s)	2.03×10^{4}	1.40×10^{5}	2.66×10^{8}	2.85×10^{16}	1.18×10^{2455}
τ (O) (s)	2.25×10^{9}	7.37×10^{13}	1.04×10^{28}	7.87×10^{61}	1.03×10^{9820}
τ (Ar) (s)	3.29×10^{20}	2.57×10^{32}	1.97×10^{68}	6.20×10^{153}	6.61×10^{24522}
τ (Kr) (s)	3.53×10^{41}	9.09×10^{66}	4.45×10^{142}	4.67×10^{322}	3.72×10^{51445}

where $n(z_c)$ is the number density of the molecule in question at the exobase, v_c is its escape velocity, and $a = \frac{m}{2kT} = \frac{1}{U^2}$ where U is the most probable (Maxwellian) speed.

The rate at which the concentration of molecules is reduced may be calculated by considering that the total number of molecules per unit area above the exobase (and thus which may escape) is given by $N = n(z_c)H_c$, where $H_c = kT/mg(r)$ is the scale height of the molecule or atom at the critical level. Writing $F_J = \beta n(z_c) = \frac{\beta N}{H_c}$ we get

$$F_J = \left(\frac{\partial N}{\partial t}\right)_J = -\frac{\beta N}{H_c}$$

and integrating gives

$$N = N_0 \exp\left(-\frac{\beta t}{H_c}\right)$$

so the characteristic escape time is

$$\tau = \frac{H_c}{\beta}$$

Alternatively, we can define an expansion velocity as $\frac{H_c}{\tau} = \beta$. The actual value of dN/dt at the exobase will depend upon the rate of

escape calculated above and upon the rate at which molecules of the gas diffuse up from below.

2.5.2 Hydrodynamic escape

Only light atoms (basically just hydrogen and helium under most relevant conditions at the present time) can escape in significant amounts by Jeans' escape mechanism. However, if the flux of light atoms is large, then heavier atoms may also be driven off by hydrodynamic escape or 'blow off'.

The flux F_2 of the heavier gas of mass M_2, blown off by a flux F_1 of lighter gas molecules of mass M_1 is given by:[33]

[33] See Chamberlain and Hunten, loc. cit., for the derivation.

$$F_2 = \frac{X_2}{X_1} F_1 \left(\frac{M_c - M_1}{M_c - M_2} \right)$$

where X_n is the mole fraction of component n, and $M_c = M_1 + \left(\frac{kTF_1}{bgX_1} \right)$ is called the *crossover mass* which represents the heaviest species which can be removed in this way. The constant b is an empirical diffusion parameter.

Thus the escape rate depends on the mass of both the molecule escaping thermally (usually hydrogen), as well as the total flux of that molecule, which depends in turn on the temperature of the exosphere. The molecule that experiences blow off may be much less abundant than hydrogen, in which case the loss rate can be governed by the rate of supply of the escaping molecule by diffusion from below. In more complex cases, more than two molecules may be escaping, in which case different types of collision can become important. Finally, the energy supply may be augmented by chemistry, dissociation for example, imparting non-thermal velocities to the molecules.

2.5.3 Solar wind erosion

The solar wind is a stream of energetic charged particles, mostly protons and electrons, emitted by the Sun at very high velocities, typically from 400 to 750 km s^{-1}. These impinge on the atmospheres of the planets and blast material away into space. Planets like the Earth that have strong magnetic fields tend to deflect the solar wind particles, directing some away into space and focussing others into the polar regions where the aurorae are produced. Venus and Mars, at least at the present time, do not have the benefit of a magnetic shield of this type, and are generally assumed to be losing atmospheric gas faster than the Earth does, although some recent research has cast doubt on this.

Calculations of atmospheric loss by solar wind erosion are very complex, because the effect not only varies across a large volume of space near the planet, but also with time. On rare occasions, the Sun can fire massive numbers of charged particles into space, in events called coronal mass ejections, which are so much more powerful than

the background solar wind that they may actually dominate the amount of atmospheric erosion that has taken place over long periods in each planet's history. At the Earth, they produce the events known as 'magnetic storms', which disrupt the magnetosphere, affecting radio transmissions and damaging electronic systems on satellites, and even affecting power lines at the surface. The vast amounts of energy that are released undoubtedly rip away a considerable amount of the upper atmosphere, but the quantitative contribution of this effect to the evolution of each atmosphere remains very uncertain.

On Mars, for instance, there is evidence that the planet had a thick atmosphere early on when it also had a magnetic field and active volcanoes. It is tempting to speculate that the loss of the field left the planet unprotected, and the loss of the volcanoes left it without a source of atmospheric renewal, so that it subsequently lost most of its atmosphere to the solar wind, perhaps mainly during the very intense bombardments following coronal mass ejections.

2.5.4 Impact escape

The cratered surface of the Moon is a record of the period of heavy bombardment suffered by all of the inner planets after their formation, and after their surfaces had cooled. In some cases, where the impactor was large and sufficient energy was imparted, some of the atmosphere would have been driven off. This is most important for Mars because of its relatively small size, and in that case even extends to driving off solid material, the so-called SNC meteorites.[34]

M_e, the mass of escaping gas that is driven off by an impactor of radius R, is given by

$$M_e = \frac{\pi R^2 M_a v_s^2}{v_e^2}$$

where M_a is the mass of the atmosphere per unit area, v_e is the planetary escape velocity, and v_s is the impact velocity.

This process, unlike the others, does not discriminate with respect to mass, so it does not cause fractionation of species or their isotopes. Furthermore, solid-body impacts are not fended off by any early magnetic field, no matter how strong. Impacts certainly have occurred and were more common, and more violent, in the early history of the Solar System, so this process has to be taken into account in considering early atmospheric evolution.

An interesting debate is still going on as to whether the impacts that produced the scarred face of Mars were sufficient to reduce its surface atmospheric pressure from the 1 or more bars that would have been needed to produce the warm, wet phase in the planet's early history to the present 0.006 bars or so, or whether some other process (such as solar wind erosion) had a larger role. Obviously both must have been active, and thermal escape as well, but values for the net budget for each remain elusive.

[34] Of the thousands of meteorites that have been recovered on Earth, 34 so far have been shown to have originated on Mars, and are known as SNC (for Shergottite, Nahklite, and Chassignite) meteorites because the earliest falls were at the eponymous locations, in India, Egypt, and France, respectively.

2.6 References and further reading

Brush, S.G. *A History of Modern Planetary Physics.* Cambridge University Press, 1996.
Volume 1, *Nebulous Earth: The Origin of the Solar System and the Core of the Earth from Laplace to Jeffreys.* 354pp.
Volume 2, *Transmuted Past: The Age of the Earth and Evolution of the Elements from Lyell to Patterson.* 144pp.
Volume 3, *Fruitful Encounters: The Origin of the Solar System and of the Moon from Chamberlin to Apollo.* 324pp.
Chamberlain, J.W., and D.M. Hunten. *Theory of Planetary Atmospheres.* Academic Press, 2nd edition, 1987.
Woolfson, M.M. The origin and evolution of the Solar System. *Astron. Geophys.*, **41**, 1, 12–19, 2001.

2.7 Questions

1. What are the key properties of the Solar System that need to be explained by any theory of its origin? What are the main features of the two main classes of theory, and the main reasons for discounting the less popular of these?

2. Show that the energy liberated during the collapse of a sphere of mass M and uniform density from infinity to radius R is given approximately by:

$$E = -\frac{GM^2}{R}$$

3. Using the above result, derive the expression

$$M_J \cong \left(\frac{kT}{G\mu m_H}\right)^{\frac{3}{2}} \frac{1}{\rho^{\frac{1}{2}}}$$

for the critical mass for gravitational collapse of an isothermal cloud of mass M_J, temperature T, and density ρ (k = Boltzmann's constant, μ = molecular weight, M_H = mass of hydrogen atom).

4. Using the previous result, evaluate the crtitical mass and the timescale for gravitational collapse of an isothermal cloud with $T = 20\,\mathrm{K}$ and $\rho = 10^{10}$ hydrogen atoms m^{-3}, and comment on the results with respect to the age and mass of the Solar System.

5. Assuming an isothermal atmosphere, show that the number of molecules N per unit area above a level of altitude z_0 is:

$$N(z_0) = \int_{z_0}^{\infty} n(z)\,\mathrm{d}z = n(z_0)H$$

where $n(z)$ is the number density (molecules m^{-3}) of the atmosphere at altitude z, H is the scale height given by $H = RT/Mg$, R is the gas constant, T the mean temperature, M the molecular weight, and g the gravitational acceleration.

6. Define what is meant by the exobase or critical level Z_c for thermal escape.

7. Assuming a Maxwell-Boltzmann distribution of molecular speeds, the probability that a molecule will have a speed in the range c to $c+dc$ is:

$$P(c)dc = 4\left(\frac{\alpha^3}{\pi}\right)^{\frac{1}{2}} c^2 \exp -(\alpha c^2)dc$$

where $\alpha = m/2kT$. The upward flux of molecules at the exobase with speeds in the range c to $c+dc$ is then:

$$dF = \frac{1}{4} n(z_c) c P(c) dc$$

Assuming that all such molecules with speed greater than the escape velocity v_e at the exobase will escape the atmosphere, show that the escaping Jeans flux is:

$$F_J = \frac{1}{2} n(z_c) \left(\frac{a}{\pi}\right)^{\frac{1}{2}} \left(v_e^2 + \frac{1}{\alpha}\right) \exp\left(-\alpha v_e^2\right)$$

or

$$F_J = \frac{n(z_c) U}{2\sqrt{\pi}} \left(\frac{a}{\pi}\right)^{\frac{1}{2}} \left(1 + \frac{v_e^2}{U^2}\right) \exp\left(-v_e^2/U^2\right)$$

where the most probable speed $U = \sqrt{2kT/m}$.

8. By considering the rate of loss of molecules from a cylinder of unit cross-sectional area above the exobase, show that

$$F_J = -\frac{dN(z_c)}{dt} = \frac{\beta}{H_c} N(z_c)$$

where $\beta = \dfrac{U}{2\sqrt{\pi}} e^{-\lambda}(\lambda + 1)$, $\lambda = v_e/U$, H is the scale height and $N(z_c)$ is the total number of molecules per unit area above the exobase.

9. Using the preceding result show that the characteristic escape time is H_c/β and the expansion velocity is $1/\beta$. Calculate these quantities for hydrogen and oxygen on Mars and Jupiter using these data:

	Thermospheric temperature (K)	Radius at exobase (km)	Gravitational acceleration at exobase (m s^{-2})
Mars	365	3590	3.32
Jupiter	155	69,500	26.2

3 Observations of planetary atmospheres

3.1 Planetary missions

Most of the important progress on understanding planetary atmospheres and climate in the last 50 years has been made by space missions, starting with simple fly-bys and progressing to orbiters and landers. The instrument packages they carried to the planet make either remote measurements using imaging and spectroscopy, or direct sampling during descent through the atmosphere and after a landing on the surface. Remote measurements offer extended global coverage, while direct measurements achieve higher spatial and temporal resolution (for example, in vertical temperature profiles or the abundance and distribution of trace constituents) and are usually simpler to interpret.

Here we give a short history of some of the more notable missions to the planets with atmospheres,[35] and the instruments used to study atmospheric properties and processes, leading to a discussion of the methods and techniques they used and will use in the future. The key discoveries and significant progress they made will be covered in later chapters.

3.2 Venus exploration

3.2.1 *Mariner* 2 (1962) and the *Venera* series (1961–1984)

Mariner 2 (Fig. 3.1) was the first successful interplanetary probe to any destination.[36] It flew past Venus on 14 December 1962, and made measurements of the temperature on the planet using a microwave radiometer to detect the thermal emission from the surface. The long wavelengths used by this radiometer (~1 cm) penetrated the cloud cover, and the high intensities and limb darkening[37] that it measured showed it was unlikely to be an atmospheric or ionospheric effect, confirming indications from Earth-based radio telescopes that the surface of Venus must be very hot. The first estimates were in the region of 1000 K, later refined to nearer the true value of about 735 K.

The *Venera* series of landers sent by the Soviet Union between 1961 and 1984[38] achieved direct measurements of this high temperature, and the high pressure of nearly pure CO_2 that is responsible. By insulating

[35] For a complete listing of all deep-space missions, including unsuccessful ones, see http://nssdc.gsfc.nasa.gov/planetary/projects.html.

[36] *Mariner* was the name given to a series of planetary probes sent to Venus and Mars in the early years of the US National Aeronautics and Space Administration. NASA was created in 1958 and has several large centres that develop various aspects of its space programme. Most of the missions that NASA has sent to the other seven planets beyond the Earth were managed by the Jet Propulsion Laboratory in Pasadena, near Los Angeles, California. Most scientific Earth-observing space missions (unmanned) are the responsibility of the Goddard Space Flight Center in Greenbelt, Maryland, near Washington DC.

[37] The intensity of emission from the atmosphere tends to increase from the centre of the disc to the edge, due to the longer slant path length; the opposite effect is expected for emission from the surface.

[38] The USSR made nine successful landings on Venus with spacecraft that transmitted data from the surface. They also deployed two balloon probes in the atmosphere. *Venera 4* was the first man-made device to enter the atmosphere of another planet (18 October 1967), *Venera 7* the first to make a soft landing on another planet (15 December 1970), and *Venera 9* the first to return images from the surface (8 June 1975).

the electronics and other critical systems from the searing heat outside, some of the landers operated successfully on the surface of Venus for periods of up to about an hour, and photographed their surroundings.

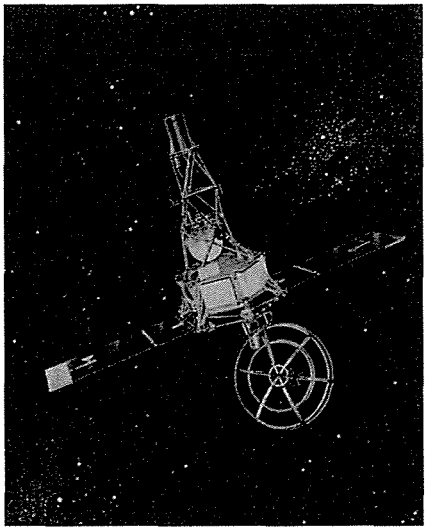

Fig. 3.1
Mariner 2, the world's first successful interplanetary spacecraft. Launched 27 August 1962, on an Atlas-Agena rocket, *Mariner 2* passed within about 34,000 kilometres of Venus, and recorded a surface temperature of about 500 °C.

3.2.2 *Pioneer Venus* (1979)

With the *Pioneer Venus* project, NASA delivered no less than six spacecraft to Venus in December 1979 in a concerted attempt to understand the planet's atmosphere and the extreme climate. One large and three small entry probes, plus the instrumented bus that had carried them from Earth, descended through the atmosphere, making measurements as they went, while a separately launched orbiter operated above. Among many achievements, *Pioneer Venus* obtained the most comprehensive data to date on the temperature and cloud structure and variability of the atmosphere, and discovered dynamical phenomena, including the dipolar nature of the north polar vortex.

3.2.3 *Venus Express* (2006)

The first European mission[39] to Venus went into orbit around the Earth's nearest neighbour on 11 April 2006 (Fig. 3.2). Among the early results were multilevel wind measurements that show three distinct dynamical regimes at low, middle and high latitudes on the planet. High-resolution infrared images of the south polar dipole reveal it to be made up of twin, coupled vortices on a vast scale.

3.2.4 *Future observations*

Understanding the climate system on Venus is a complex task that will proceed gradually, in tandem with the similar undertaking for the Earth, but with an especial need for much more data. This will come mainly from planetary missions, including the current *Venus Express*, the Japanese *Venus Climate Orbiter* now under construction, and whichever of those future missions presently under discussion that eventually fly. Survival in the hostile conditions on Venus is difficult, but new missions must in time include landed and buoyant probes of long duration, which can make very precise measurements of atmospheric composition, surface and cloud properties. Further off, but also essential, are the missions that will sample the geochemistry of the surface and probe the deep interior using seismic measurements and drills. It is profoundly to be hoped that progress towards these goals will be faster during the next few decades than it has been in the last two, when *Venus Express* ended a long period of benign neglect of a nearby Earth-like world that is uniquely instructive for so many of our crucial environmental issues.

[39] The European Space Agency was established in 1974, with its headquarters in Paris and its technical centre in Noordwijk, near Amsterdam. ESA's first planetary project was the *Huygens* Titan probe (delivered by NASA) in 1997; the first fully European mission was *Mars Express* in 2003. A mission to Mercury is in preparation.

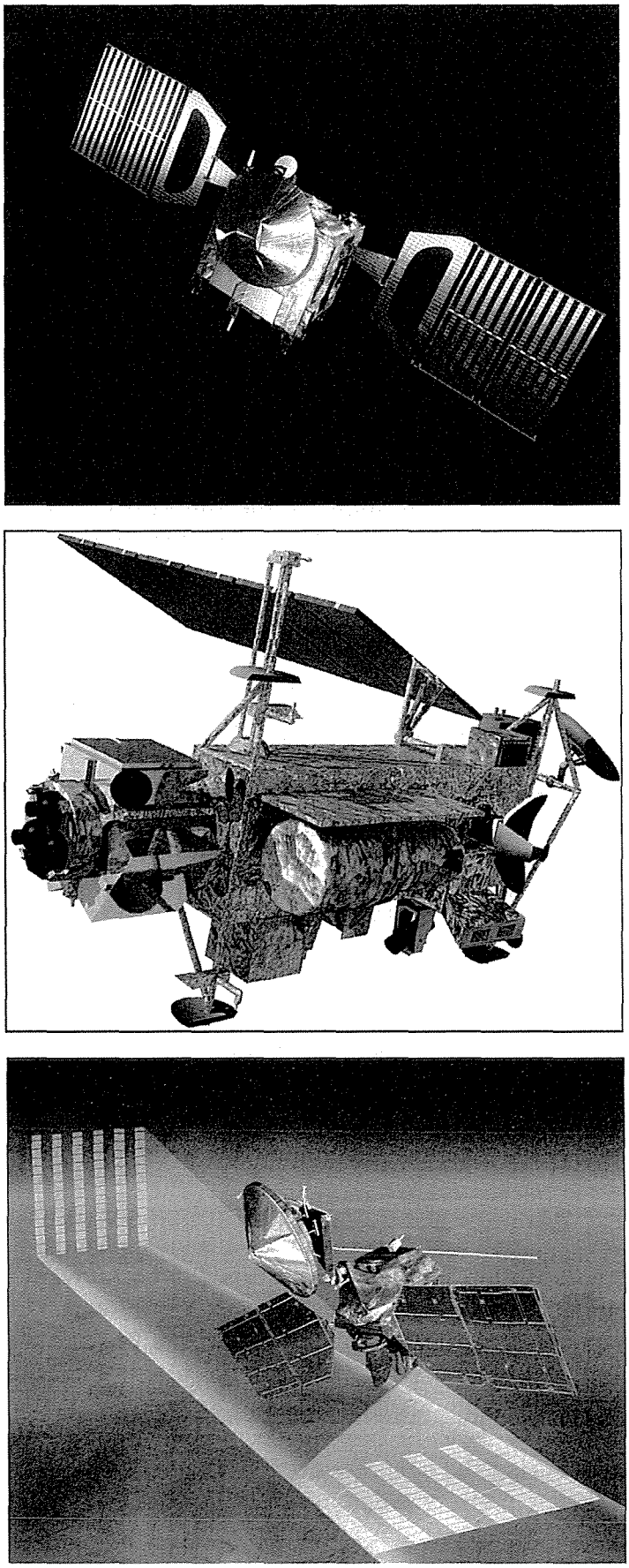

Fig. 3.2
Modern spacecraft for climate research. The Upper Atmosphere Research Satellite (centre), launched into Earth orbit in 1991, was about 10 m long and had a mass of nearly 8 tonnes. For comparison, *Venus Express* (top) and *Mars Reconnaissance Orbiter* (below) are about 1 and 2 tonnes, respectively, and *Mariner 2* (Fig. 3.1) was 0.2 tonnes. The exact mass in each case depended on the amount of fuel for manoeuvres that remained on board at a given stage of the mission.

3.3 Mars exploration

3.3.1 *Mariner 9* (1971)

After mixed success with a number of exploratory fly-by missions, NASA's *Mariner 9* became the first artificial satellite of Mars on 13 November 1971. Among its payload of scientific instruments it carried the Infrared Interferometer Spectrometer (IRIS), developed from a successful Earth observation instrument of the same name. An interferometer was chosen because it could record a wide spectral range in the thermal infrared[40] to look for spectral bands of new species, as well as use established techniques to investigate atmospheric temperatures and humidity.

[40] The 'near infrared' is the part of the infrared spectrum of a planet that is mostly dominated by reflected sunlight, which typically means wavelengths from the visible to about 5 μm (2000 cm^{-1}. The 'thermal infrared' is dominated by radiation emitted at the characteristic temperatures of the planet itself and typically ranges from 5 to 1000 μm (2000 to 10 cm^{-1}).

3.3.2 *Viking* (1976)

Viking was a combined orbiter/lander mission, the primary goal of which was to search for evidence of microbial life on the surface. Among the orbiter instruments sensing the atmosphere was the Mars Atmospheric Water Detector (MAWD), which measured the column abundance of water vapour by observing absorption features in the spectrum of sunlight reflected from the surface. The Infrared Thermal Mapper (IRTM) was a six-channel filter radiometer with four thermal IR channels and two reflected sunlight channels, used to investigate surface composition and atmospheric temperature.

3.3.3 *Mars Express* (2003)

ESA's first mission to Mars was launched on 2 June 2003 and arrived in orbit around the red planet on Christmas Day the same year. Its goals were to image the surface at high resolution (up to two metres per pixel); produce a map of the mineral composition of the surface at 100 metres resolution; map the composition of the atmosphere and determine its global circulation; determine the structure of the subsurface to a depth of a few kilometres; determine the effect of the atmosphere on the surface; and determine the interaction of the atmosphere with the solar wind. *Mars Express* also delivered the unsuccessful *Beagle 2* lander.

3.3.4 *Mars Reconnaissance Orbiter* (2006)

Following the failures of *Mars Observer* in 1992, which blew up on approach to Mars, and *Mars Climate Orbiter* in 1999, which crashed into the planet due to a small but fatal navigation error,[41] an infrared atmospheric sounding experiment called Mars Climate Sounder (MCS) was finally successfully deployed in Mars orbit on *Mars Reconnaissance Orbiter* in 2006 (Fig. 3.2). MCS is the main atmosphere-observing experiment on the largest spacecraft ever to go to Mars, the

[41] This was the infamous mix-up between metric and imperial units – the navigation team calculating the thrust to be applied was working in pounds force, while the spacecraft software expected figures in newtons (1 lbf = 4.45 N).

rest of the payload being mainly dedicated to high-resolution mapping of the surface to find safe and interesting sites for future landings. MCS scans the atmosphere vertically, at the limb, with a spectral range designed to distinguish between gaseous and particle absorption and so obtain high vertical resolution global profiles of temperature, water vapour and dust over the Martian seasons.

3.4 Outer planets: Jupiter and Saturn exploration

3.4.1 *Voyager 1 and 2* (1979)

The *Voyagers* were fly-by missions, hence could obtain only a limited amount of data as they flew rapidly past the planet. However, they carried a version of the IRIS instrument previously deployed in Earth and Mars orbit to cover a wide spectral range (100–2300 cm^{-1}) in the thermal infrared to measure composition and investigate atmospheric temperatures. The 'window' region in the spectrum near 5 μm, which is free from strong absorptions by any of the major species, allowed the deep atmosphere to be probed, down to about the 3 bar level in regions where the cloud opacity was small. IRIS data are still being used to determine atmospheric composition and cloud properties.

3.4.2 *Galileo* (1996)

Galileo was the first, and is so far the only spacecraft to orbit Jupiter. It also delivered the first and only probe into a gas giant atmosphere at Jupiter on 7 December 1995. The orbiter carried the Near Infrared Mapping Spectrometer (NIMS), a spectrometer with a detector array and scanning telescope for better spatial coverage, and cooled detectors for high sensitivity. NIMS covered a spectral range of 0.7–5.2 μm (1900–14,300 cm^{-1}), and hence viewed both thermal emission from the deep atmosphere and sunlight reflected from the cloud tops. Since this range includes the 5 μm window also observed by IRIS, the vertical range extended down to a pressure level of about 3 bars, where the temperature is about 273 K and a thick cloud composed mainly of water liquid and ice particles was encountered.

3.5 Titan

Titan is of special interest because, although it is a moon and not a planet, it is a planetary-sized body with an atmosphere and climate system, both of which stand comparison with the Earth. Only two space missions have made detailed studies of Titan: *Voyager 2* in 1981, and *Cassini*, which arrived in Saturn orbit in 2004. Cassini's programme of measurements was initially scheduled to last at least 5 years, but is still operating, and now looks like doubling that lifetime. One of the largest and most complex deep-space missions ever flown, *Cassini* (Fig. 3.3) carried the *Huygens* probe, which descended to the surface of Titan on 14 January 2005 and made detailed measurements

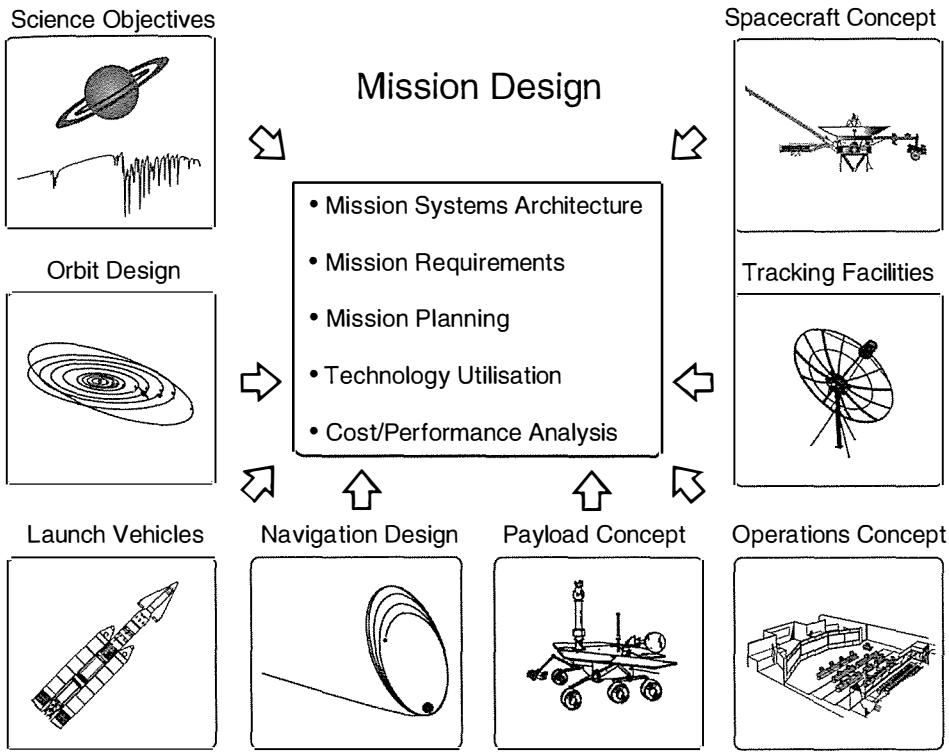

Fig. 3.3
This schematic from the Jet Propulsion Laboratory in Pasadena, California, where NASA's planetary missions are developed and managed, gives an idea of the various technical components involved in a project like the *Cassini* Saturn orbiter.

of atmospheric temperature, composition and cloud structure. It also took spectacular images of the surface terrain, which revealed fluvial features that, along with images of clouds and lakes from the orbiter, are indicators of precipitation and other aspects of a terrestrial-style climatology on Titan.

3.6 Infrared remote sounding instruments

The radiometric instruments on planetary probes are generally derived from their counterparts used on Earth-observing satellites,[42] and typically have the components and general layout shown in Figure 3.4. The components gather, focus, modulate, filter, detect, amplify and calibrate the signal from a well-defined field of view in the atmosphere. The on-board blackbody, at a known temperature T_{BB} ($T_{BB} > T_{Earth} > T_{space}$), is one of two calibration targets, the other being a view to cold space (zero radiance). By design, most instruments have a linear response, i.e., the signal at the output is proportional to the radiance R entering the aperture and a plot of signal S against incoming radiance R is a straight line,

$$S = gR + S_0$$

where the gain g and offset S_0 are obtained by measurements of the calibration blackbody and cold space.

The radiometer optics focus the energy onto the detector, and define the field of view of the instrument. An intermediate focus is usually provided for the modulator (often a rotating or vibrating blade, called a 'chopper') that is used to label the source radiation to distinguish it from the background emission, and to generate an alternating signal at the detector that is simpler to amplify and filter (to reduce noise) than a

[42] See *Elementary Climate Physics*, Chapter 9; this section is a summary of that chapter.

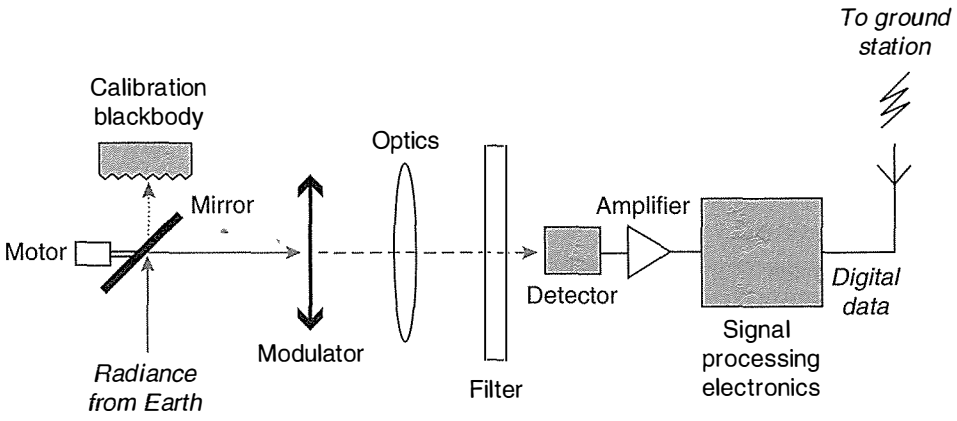

Fig. 3.4
A schematic diagram of an infrared radiometer, showing the main subsystems. The filter isolates the desired spectral passband, defined by a central wavelength λ and width $\Delta\lambda$. In a spectrometer, λ can be varied over a range $\gg\Delta\lambda$.

DC signal. Spectral selection of the set of channels or wavelength ranges to which the instrument is sensitive is by interference filters (solid-state Fabry-Perot etalons), gratings, or interferometric methods.

The detectors may be thermal devices that respond to the heating effect of the radiation, such as thermistors, thermocouples or pyroelectric bolometers. Thermal detectors are less sensitive than photon detectors, but they cover a wider wavelength range and usually do not require cooling to operate at close to their maximum sensitivity. Photon detectors are either photoconductive devices, which measure the change in current due to carriers excited by the incident photons into the conduction band when the detector has a bias voltage across it, or photovoltaic, which measure the induced voltage in a detector without voltage bias. Both types of detector require cooling to suppress the thermal excitation of transitions, which would otherwise completely mask any contribution by the photons, particularly in the infrared, where the energy carried by each photon is relatively small.

3.7 Radiometric performance

The performance of a measurement system can be represented in a number of ways that help experimenters to decide whether a particular design will achieve their scientific objectives. Usually, the investigators will be interested in three things:

1. the spectral resolution, which limits the detection of specific features in the measured spectrum and hence the ability to measure composition, or to resolve temperature structure;
2. the spatial resolution, which determines the detail that can be observed in the target;
3. the signal-to-noise ratio, which determines the error in the measurement.

For example, a weather satellite orbiting the Earth and measuring vertical temperature profiles for forecasting purposes by sensing the emission from the 15 μm CO_2 band needs to be able to resolve the different parts of the band that correspond to weak, strong and intermediate absorption. The width of the CO_2 band is roughly 1 μm (i.e., it extends from about 14.5 to 15.5 μm) and so a reasonable guess at the

resolution required would be $\Delta\lambda \approx 0.1\ \mu$m ($\Delta\nu$ of the order of 10 cm^{-1} in wavenumber units).

A reasonable spatial resolution on the surface of the Earth might be 100 km or better, since this is the scale of weather systems. If the satellite altitude is 1000 km, this corresponds to a field of view of 0.1 radians, i.e., a solid angle Ω of the order of 0.01 steradians. The signal-to-noise ratio obviously has to be significantly greater than unity for a meaningful measurement; S/N $\geq$ 100 is usually taken to be reasonable. To refine this last criterion, it might be better to specify the accuracy with which the temperature of the target can be measured; studies with forecasting models suggest that each channel needs to measure to about 1 K or better for good performance.

These three criteria can be traded off against each other, of course. A wider field of view would result in a larger signal-to-noise ratio if all other parameters remained the same. However, the investigators will normally want to achieve all three without undue compromise. Then, the parameters that are available to them are:

1. The choice of detector (for instance, replacing an ambient temperature detector with a cooled one usually results in a reduction in the noise level in the signal).
2. The size of the entrance aperture, A, of the optics, although a larger telescope will increase the size and weight of the instrument, a crucial consideration if it is to be carried on a spacecraft.
3. The 'dwell' time, i.e., the time spent integrating the signal during each measurement. The signal-to-noise ratio is improved in proportion to the square root of the dwell time if the noise is random, as usually is the case. However, this reduces the spatial resolution, since the field of view of the instrument is continuously smeared by the motion of the spacecraft (about 7 km s^{-1} for an Earth satellite) unless the instrument can scan to compensate (again, increasing mass and complexity).

The solution to the choice of an optimum design is different in every case, particularly for planetary measurements where the properties of the targets vary so much, and where low-resolution measurements might be useful when investigating a region or process for the first time.

3.7.1 *The radiative transfer equation*[43]

The first step in evaluating the expected performance of an instrument to be deployed on a planetary mission is to estimate the strength of the radiation flux it needs to measure. This involves solving the *radiative transfer equation* for a model atmosphere that represents the conditions expected on the planet. Where planetary atmospheric measurements are concerned, we also wish to know which part of the atmosphere the signal originates; i.e., we require knowledge of the *weighting function.*

The radiative transfer equation is

[43] For an advanced discussion, see I.M. Vardavas and F.W. Taylor, *Radiation and Climate*, Oxford University Press, 2007.

$$R_\infty = \int_0^1 B \mathrm{d}\mathcal{T}$$

$$= \int_0^\infty B \frac{\mathrm{d}\mathcal{T}}{\mathrm{dz}} \mathrm{d}z + e_0 B_0 \mathcal{T}_0$$

The first term is the emission from the atmosphere and the second represents the emission from the surface, with emittance e_0 at temperature $\mathcal{T}_0$, where $B_0 = B(T_0)$ and T_0 is the transmittance of the whole atmospheric column. The radiance leaving the top of the atmosphere is just the weighted mean of the Planck function, and the weighting function is the derivative with respect to height of the transmittance of the atmosphere along a vertical path.

The height of the peak in the weighting function $d\mathcal{T}/dz$ depends on the choice of spectral interval, being higher where the atmospheric absorption is stronger, and vice versa. By choosing a series of adjacent spectral intervals along the edge of an atmospheric absorption band, where the absorption coefficient changes rapidly with wavelength, it is possible to select a set of weighting functions that spans the atmospheric region of interest.

The weighting functions depend on the abundances of the principal absorbers in the spectral intervals chosen for the sounding instrument; a band of a gas of known abundance, such as carbon dioxide, can be used to retrieve the temperature profile, and then bands of other species of interest chosen to measure their abundance profiles using this temperature information.

3.7.2 *Signal-to-noise ratio and errors*

The signal S at the output of the radiometer is a linear function of the radiance R_λ at the input aperture, given by

$$S = gA\Omega \int_0^\infty a_\lambda R_\lambda \mathrm{d}\lambda + const.$$

$$= gA\Omega \bar{R} \Delta\lambda + const.$$

$$= g' \bar{R} + S_0$$

Here the radiance (in units of W m^{-2} sr^{-1} $\mu\mathrm{m}^{-1}$) is multiplied by the filter transmission a_λ at each wavelength and integrated over wavelength, then multiplied by the product of the input aperture of the telescope A (m^2) and its angular field of view Ω (in steradians, sr) to obtain the energy (W) falling on the detector. The conversion from watts to volts in the detector is represented by the gain factor g. Over a small spectral range ($\Delta\lambda << \lambda$) the radiance can be assumed to be nearly constant with mean value $\bar{\mathrm{R}}$, and the integral over the filter response $\int_0^\infty a_\lambda d\lambda$ can be replaced with the equivalent width of the filter, $\Delta\lambda$.

If the noise in a measurement of duration Δt is assumed to be random, its mean value is proportional to $1/\sqrt{\Delta t}$. The *noise equivalent power* or NEP, which has units of W $Hz^{-1/2}$, or W $s^{1/2}$, is the power in watts that will produce a signal equal to the rms noise for an observation or 'dwell' time of $t = 1$ second. It generally varies with the square root of the area A_d of the detector, so the *specific detectivity* D^* (m W^{-1} $Hz^{1/2}$) of a detector type is defined by

$$\text{NEP} = \frac{\sqrt{A_d}}{D^*}$$

The NER or *noise equivalent radiance* of an instrument is the change in target radiance that changes the signal by an amount equal to the noise (in radiance units) for the system as a whole, with units of radiance per $\sqrt{\text{Hz}}$ or W m^{-2} sr^{-1} μm^{-1} $s^{1/2}$. The related quantity, *noise equivalent temperature* NET or NEΔT, is the change in target *temperature* that produces a signal change equal to the noise. If the instrument is viewing a target with equivalent blackbody (or 'brightness') temperature T_B (K) then it follows that

$$\frac{\partial B(\lambda, T_B)}{\partial T}\,\text{NET} = \text{NER}$$

The *signal-to-noise ratio* is

$$\text{S/N} = \frac{B(T_B)}{\text{NEP}} A\Omega\Delta\nu\sqrt{\Delta t}$$

The NER is, by definition, the value of the radiance when S/N is unity, so

$$\text{NER} = \frac{\text{NEP}}{A\Omega\Delta\nu\sqrt{\Delta t}}$$

and the NET, also by definition, is

$$\text{NET} = \frac{\text{NER}}{(dB(T_B)/dT)}$$

and

$$\text{S/N} = \frac{B(T_B)\sqrt{t}}{\text{NER}}$$

where $B(T_B)$ is the radiance from the target with *brightness temperature* T_B. If the actual temperature of the target is T, then

$$R_\lambda(T) = B_\lambda(T_B) = e_\lambda B_\lambda(T)$$

where e_λ is the spectral emissivity of the material making up the target.

3.7.3 *Retrievals*

Since most of the radiation originates near the peak of the relevant weighting function, a set of radiance measurements contains information about the variation with temperature or composition with height. A set of measurements can be used to reconstruct or 'retrieve' the temperature profile, with a vertical resolution that is related to the number and width of the weighting functions, by solving N versions of the radiative transfer equation for N spectral channels, each selecting different wavelength intervals.

The simplest of a number of methods that has been developed for the purpose[44] is the relaxation technique, which initially makes the simplifying assumption that all of the radiation in a spectral channel comes from the atmospheric level corresponding to the peak of the weighting function. Then, the radiative transfer equation for each channel becomes simply the inverse of the Planck function. The temperature can be obtained directly, yielding a first-order solution for the profile in the form of a set of temperatures at each of the weighting function peaks. At each other point in the profile, the temperature is taken to be the weighted mean of all of the channels, giving a smooth profile.

[44] See *Elementary Climate Physics*, §6.10.

The next step is to calculate the radiances R'_n from this temperature profile using the radiative transfer equation, and compare them to the measured radiances R_n in each channel. If they are the same within the uncertainty in the measurement, usually determined from the instrumental signal-to-noise ratio, the solution is complete. Usually, however, it is necessary to make an improved estimate by multiplying by the ratio of measured to calculated radiances and iterating until the solution converges to within the measurement noise. Examples of this approach applied to Venus and Mars appear in the sections that follow below.

Temperature and composition profiles can also be estimated by least-squares fitting of measured to calculated radiances, and this is a particularly good way to proceed when a continuous spectrum has been measured. In one of the examples below, the spectrum of Jupiter obtained by the IRIS interferometer on the *Voyager* mission is used to obtain temperature, energy balance, and major and minor constituent information, all from the same measurement. A very advanced retrieval method that is also discussed later is assimilation into models. This uses a sophisticated general circulation model of the planetary atmosphere, which is continuously updated by feeding in measurements as they become available. This technique is becoming standard for terrestrial weather forecasting, although in planetary science it has so far only been applied to Mars.

3.8 Venus experiments

3.8.1 *Mariner 2 microwave radiometer*

Mariner 2 passed by Venus at a distance of 34,350 km on 14 December 1962, 110 days after leaving Earth. Apart from successfully demonstrating interplanetary flight, it had a key scientific goal: to measure the surface temperature on Venus. Radio telescopes on the Earth had

measured the temperature of Venus to be as high as 630 ± 130 K at 21 cm wavelength, and a vigorous debate was raging as to whether this was the true surface temperature or some kind of non-thermal effect, perhaps originating in the ionosphere or magnetosphere of Venus. One way to resolve the issue was to look for centre-to-limb variations in the emission: this would show brightening towards the limb if it was of upper-atmospheric or magnetospheric origin, and limb darkening if it was indeed thermal emission from the surface. Since even the largest Earth-based dishes could not resolve the disc of Venus at radio wavelengths, an instrument on a space mission to the planet would be needed.

To achieve this, *Mariner 2* carried a two-channel microwave radiometer, with a 48.5 cm diameter dish, capable of scanning over 120° in one dimension, feeding radiometers operating at wavelengths of 1.9 and 1.35 cm. The half-power points for the accepted beam had an angular width of approximately 2°, designed to resolve about one-tenth of the radius of Venus from a planned closest approach 15,000 km away. In the event, *Mariner 2* did not get that close to Venus, but it did resolve the disc.

The choice of the wavelengths at which to observe Venus was based on the best atmospheric models available at the time. The scientists in charge of the experiment selected a most likely composition of 75% CO_2, 24% N_2, and 1% H_2O. Figure 3.5 shows their calculations of the microwave spectrum of Venus for such a composition, as a function of surface pressure in the range 2 to 20 bars (they thought it 'fairly certain that the surface pressure is at least 4 times the terrestrial value and possibly as much as 30 times').[45] The main reason for the choice of this surface pressure range was the Earth-based observations, shown in the figure. In effect, they overestimated the water absorption and under-

[45] A.H. Barrett *et al.*, JPL Technical Report No. 32–156, August 1961.

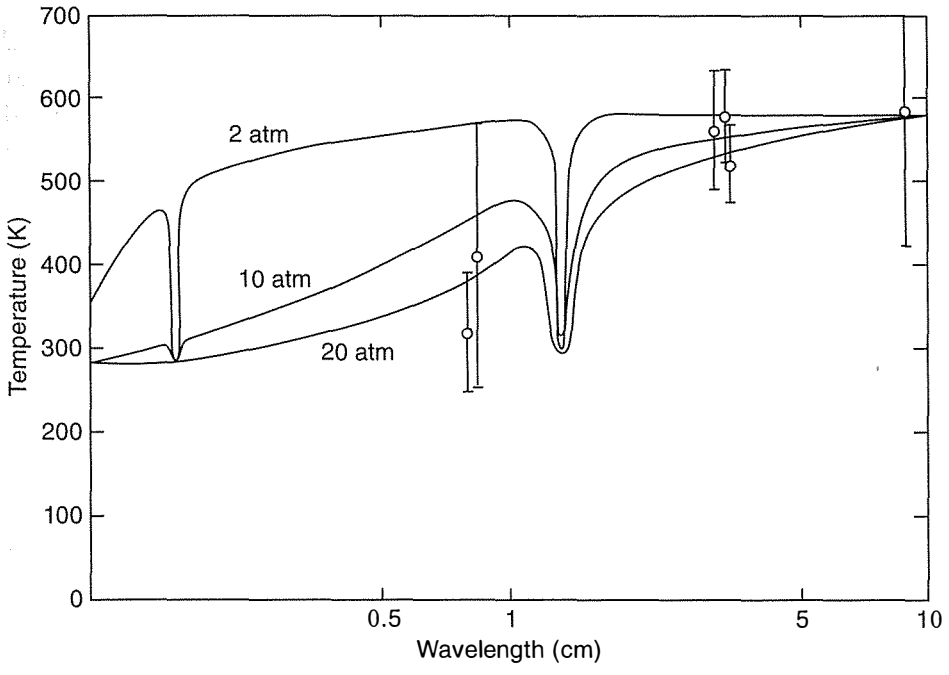

Fig. 3.5
Theoretical microwave spectra for Venus, with an assumed atmospheric composition of 75% CO_2, 24% N_2, and 1% H_2O, and a surface temperature of 600 K, from Barrett *et al.*, 1961. The three curves correspond to surface pressures of 2, 10 and 20 bars; the points with error bars are measurements of the brightness temperature of Venus by Earth-based radio telescopes. The sharp features are lines in the pure rotational spectrum of atmospheric water vapour.

Table 3.1 *Mariner 2* microwave radiometer measurements of the brightness temperature of Venus at two wavelengths and three places on the disc. The measurement errors, estimated from an on-board source and view of cold space, are about 5% (~30 K) for Channel 1 and 25% (~100 K) for Channel 2.

Channel	Scan	Temperature T_B
1 (λ = 1.9 cm)	1 (night-side limb)	480
"	2 (centre of disc)	590
"	3 (day-side limb)	460
2 (λ = 1.35 cm)	1 (night-side limb)	393
"	2 (centre of disc)	400
"	3 (day-side limb)	396

estimated the amount of carbon dioxide, although it was a very creditable attempt for the time.

Expecting the main absorber to be water vapour, the two channels were placed at the centre of a strong water line (1.35 cm) and in the continuum nearby (1.9 cm), where most of the radiation was expected to come from the surface.[46] A somewhat longer wavelength for the latter – say 10 cm – would have been better in terms of avoiding the wing of the water line, but then the field of view would have been wider and the essential spatial resolution on Venus' disc would not have been obtained.

After many adventures, the instrument succeeded in obtaining three scans across the disc of Venus (of the 15 that had been planned); fortunately, one intersected the dark-side limb, another the day-side limb, and the third the centre of the disc, near the day–night terminator, making them suitable for discriminating limb darkening from brightening. The temperatures that were measured are shown in Table 3.1. Channel 1, observing the surface, shows unambiguous limb darkening. Channel 2, observing the atmosphere in a strong water-vapour line, does not.

This groundbreaking experiment (bearing in mind that *Mariner 2* was the first successful probe to any planet) convinced many that Venus did indeed have a very hot surface.[47] Others remained sceptical until the first successful Venus landing by the Soviet Union with *Venera 7*, on 15 December 1970, used thermistor sensors to measure the air temperature directly. It found the temperature was 738 K and the pressure 90 bars at its landing site on the plains between Guinevere Planitia and Alpha Regio, just south of the equator.

[46] Two more channels, at 0.8 and 0.4 cm wavelength, were originally planned, but they had to be abandoned because the spacecraft would have been too heavy for the available launch vehicle. *Mariner* was designed to use the Atlas-Centaur combination then under development, but the Centaur stage fell behind schedule and a smaller Atlas-Agena had to be used. The radiometer weighed about 20 lb; with four channels it would have been nearly twice this.

[47] Carl Sagan had already been convinced by the Earth-based results. In his doctoral thesis at the University of Chicago, submitted in June 1960, he wrote that 'a surface temperature of 600 K demands a very efficient greenhouse effect'.

3.8.2 *Pioneer Venus Orbiter Radiometric Temperature-Sounding Experiment (VORTEX)*

The first dedicated temperature-sounding experiment to be deployed at Venus was launched on 20 May 1978 on board the *Pioneer Venus* orbiter. The instrument had eight spectral channels, five of which measured temperature in the 15 μm band of CO_2 and the remainder of which measured cloud properties and atmospheric water vapour

Table 3.2 Spectral channels for the VORTEX radiometer on *Pioneer Venus* orbiter.

Channel number	Spectral resolution (cm^{-1})	Field of view (deg)	Central wavenumber (cm^{-1})	Principal function
1	0.08	5	667	Mesospheric temperature
2	10.6	1.25	679.4	Stratospheric temperature
3	13.6	1.25	727.2	"
4	14.4	1.25	764.4	"
5	21.5	1.25	869.5	Cloud top temperature
6	170	1.25	4926	Cloud morphology
7	23,000	1	3700	Albedo
8	100	1	222	Water vapour

(Table 3.2). Figure 3.6 shows the calculated weighting functions corresponding to the sounding channels.

The instrument layout is shown in Fig. 3.7. The optical design uses a series of mirrors and dichroic beam splitters[48] to feed radiation of the appropriate wavelength to each channel. Filters in front of each detector completed the definition of the spectral range measured by each channel. The detectors themselves were deuterated triglycine sulphate

[48] A dichroic beam splitter is a device, made of multiple layers of different materials, that transmits all wavelengths longer (or shorter, depending on type) than a critical value, and reflects the rest.

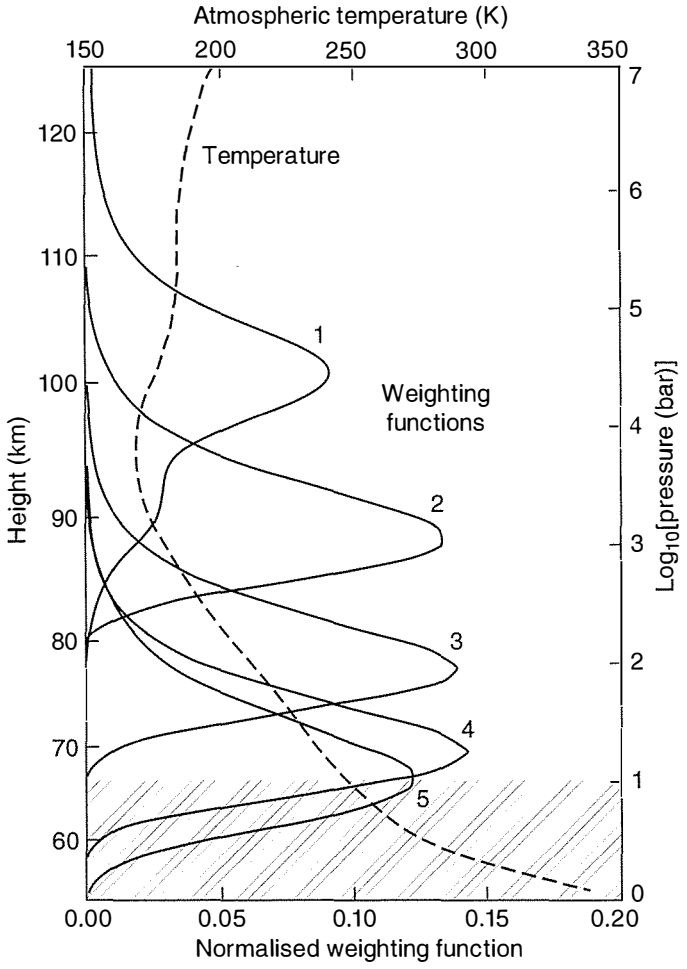

Fig. 3.6
Weighting functions for the temperature sounding channels of the *Pioneer Venus* radiometer. The numbers correspond to the channel numbers in Table 3.2; the shaded region is the approximate location of the uppermost cloud, which does not have a sharp upper boundary but falls off with a scale height of a few kilometres.

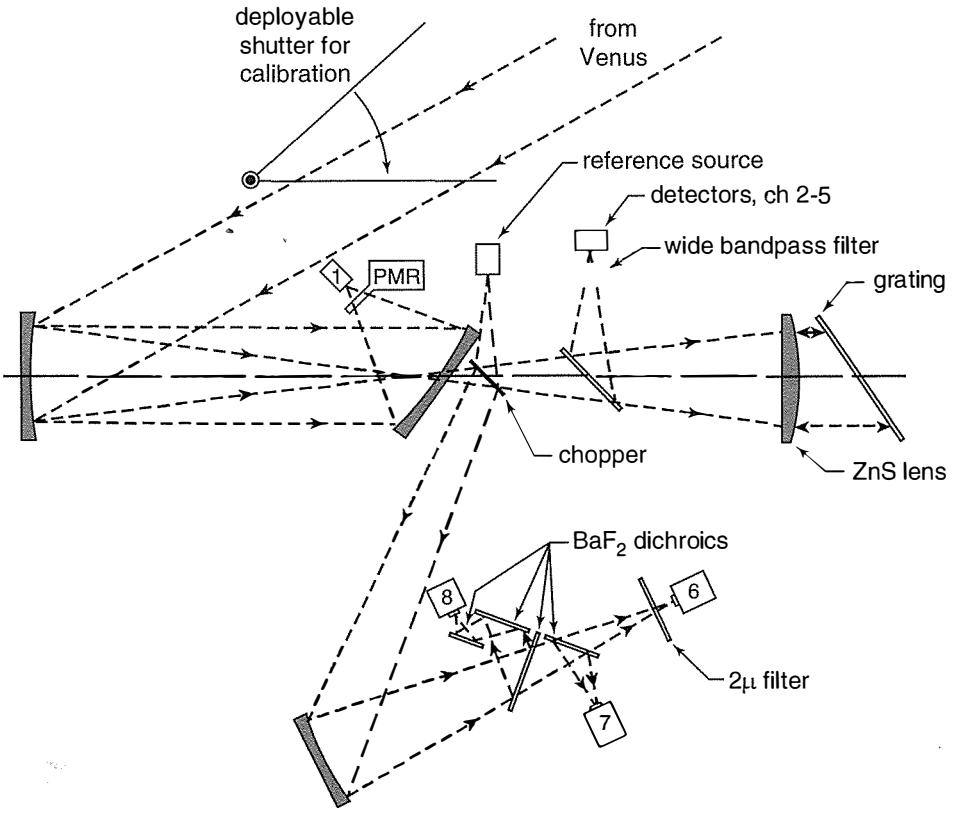

Fig. 3.7
Schematic diagram of the optical system for the *Pioneer Venus* VORTEX radiometer. This is not as complicated as it looks at first sight: the first two mirrors form a telescope that defines the fields of view (5° for channel 1 and 1° for the rest); then a dichroic (wavelength-selective) beam splitter separates the 15 μm temperature-sounding channels, defined by the diffraction grating, from those using transmission and reflection filters to define the spectral bands. This arrangement was designed to maximise the throughput of energy to each detector and so optimise the signal-to-noise ratio.

pyroelectric devices, operated at instrument ambient temperature (35 °C).

With the data given in Table 3.2, the signal-to-noise ratio for each channel could be calculated assumed an instrument aperture of 20 cm^2, an optical efficiency of $2\sqrt{2}$, and detector NEP of 1.7×10^{-10} (3.5×10^{-10} for channel 1) W $Hz^{-1/2}$. In Table 3.3, the resulting figures are compared to those that were measured for the real instrument, using a blackbody target in a thermal vacuum chamber.

The structure and variability of the middle atmosphere of Venus (60 to 140 km) were studied for most of one Venus year, at wavelengths selected to allow the vertical temperature profile, the albedo, the cloud opacity profile, and the far-infrared opacity due to water vapour to be inferred from the data. The measured temperature field has been used

Table 3.3 Signal-to-noise ratios, measured and calculated, for the channels of the VORTEX radiometer.

Channel number	Wavelength (μm)	Dwell time (ms)	Measured S/N	Design S/N
1	15	200	55	54
2	14.68	30	90	78
3	13.72	30	91	103
4	13.09	30	108	119
5	11.47	30	120	137
6	2.03	30	48	89
7	0.2–4.5	30	10,000	10,000
8	35–60	30	117	182

to model the dynamics of the region (§8.3), and the thermal and solar fluxes have been used to compute the planetary radiation budget (§4.4).

3.8.3 *Venus Express VIRTIS*

Venus Express entered Venus orbit in April 2006. On board are seven science instruments devoted to observing the atmosphere and surface of Venus from UV to infrared and radio wavelengths. VIRTIS, the Visible and Infrared Thermal Imaging Spectrometer, is in two parts. The non-imaging VIRTIS-H spectrometer covers the spectral range from 1.84 to 4.99 μm, with a resolution of 1 nm, and the imaging VIRTIS-M covers the UV, visible and infrared wavelengths from 0.27 to 5.19 μm at a lower spectral resolution of approximately 2 nm and 10 nm for the UV-VIS and IR channels, respectively. The VIRTIS-M instantaneous field of view is 0.2×64 mrad divided into 256 spatial pixels. At the maximum orbital distance of 66,000 km, this instantaneous field of view spans one-third of the diameter of Venus. Using a scan mirror with 256 step positions, the field of view expands to 64×64 mrad. Therefore, at apoapsis, a full image of the Venus disc is created when nine images are taken sequentially to create a 3×3 mosaic.

The VIRTIS instrument has proved a powerful tool for studying the atmospheric composition and dynamics, for instance mapping the distribution of trace gases like carbon monoxide and water vapour below the clouds, measuring winds by cloud tracking, and by calculating thermal winds from temperature measurements.

3.9 Mars experiments

3.9.1 *Mariner 4 radio occultation*

Mariner 4 made the first successful measurements of atmospheric properties by the technique known as radio occultation. This works by monitoring the radio signals sent to Earth as the spacecraft's trajectory carries it out of sight behind the planet. The beam passes through the Martian atmosphere, which acts to slow down the radio waves, lengthening the path, and slightly altering the frequency and wavelength. By measuring these changes with extreme precision, which requires a good clock on board the spacecraft, the temperature and pressure of the atmospheric column that the signal travelled through can be reconstructed.

The current state-of-the-art equipment for this technique is capable of measuring differences as small as 0.2 mm in the several-million-kilometre path that the radio signal follows. This corresponds to resolving changes in atmospheric pressure and temperature of less than 0.1% and 0.1 K respectively. In 1964, the pioneering experiment on *Mariner 4* did not achieve this level of precision, but did well enough to confirm the low surface pressure of 4.1 to 7.0 mb on Mars that had been controversially deduced by some ground-based observers using infrared spectrometers mounted on large telescopes.

3.9.2 *Mariner 9 Infrared Interferometer Spectrometer (IRIS)*

Starting in November 1971, the *Mariner 9* infrared interferometer spectrometer provided the first long-term, high-resolution monitoring of the composition, abundance, and distribution of atmospheric gases and aerosols in the Martian atmosphere. IRIS covered the spectral range 5–50 μm (200–2000 cm^{-1}) at a resolution of 2.4 cm^{-1}. It used measurements of the CO_2 15 μm band to determine pressure–temperature profiles, from which the wind field could be inferred, as well as atmospheric water vapour content and dust aerosol composition. The spectra enabled the identification of water ice clouds, made possible the identification of CO_2 in the residual south polar cap, set upper limits on many atmospheric gases, and established the carbon and oxygen isotopic composition of the atmosphere.

3.9.3 *Mars Express Fourier Spectrometer (PFS)*

PFS is a Fourier spectrometer, like IRIS, capable of measuring the distribution and seasonal variability of the major gaseous components of the atmosphere, the vertical distribution of temperature and pressure, and the properties of airborne dust. By averaging many spectra, PFS is also capable of detecting minor gaseous species present in very small amounts. In this way, PFS made the first measurements of methane in the atmosphere of Mars, and claimed some tentative indications of traces of formaldehyde, both possible indicators of life under the surface.

3.9.4 *Mars Climate Sounder*

The 1993 *Mars Observer*, 1999 *Mars Climate Orbiter*, and 2006 *Mars Reconnaissance Orbiter* spacecraft all carried similar infrared sounders to study the Martian climate and meteorology, although technical problems meant that only the last of these was successful. The plan was to obtain high vertical resolution (5 km or better) profiles of pressure, temperature, water vapour, dust, and condensates with global coverage and a duration of at least one complete Martian seasonal cycle, and preferably (since Mars shows marked inter-annual variability) over more than one. During this time the instrument stares at the atmosphere at the limb of the planet, and the orbit is such that a full range of latitudes, from pole to pole, can be observed. To fill in the coverage between orbits, the instrument uses commandable pointing that allows nadir and intermediate, as well as limb, scanning.

The instrument that finally achieved this, called Mars Climate Sounder, is described by the parameters listed in Table 3.4 and the selection of spectral channels in Table 3.5. The instrument has two telescopes, each serving half of the complete set of spectral channels, and containing relay optics, optical filters, and detector arrays. This simple and compact design is possible because of the recent develop-

Table 3.4 Mars Climate Sounder instrument specifications. IFOV is instantaneous field of view.

Parameter	Property / Performance
Spectral range	0.3 to 50.0 μm in nine spectral channels
Telescopes	Two 4-cm aperture, f/1.6 telescopes
Detectors	Nine, 21-element, linear thermopile arrays at 300 K
Detector IFOV	3.6 × 6.2 mrad, equivalent to 5.0 × 8.6 km at limb
Array IFOV	75 × 75 mrad, equivalent to 105 × 105 km at limb
Pointing	Two-axis azimuth/elevation
Range/resolution	Azimuth: 270/0.1 degrees Elevation: 270/0.1 degrees
Signal integration period	2 seconds
Observation strategy	Limb staring; Limb, nadir, and off-nadir scanning In-track, cross-track, and off-track viewing

Table 3.5 Mars Climate Sounder spectral channel characteristics and functions. A and B refer to the two telescopes.

Channel	Wavelength (μm)	Bandpass (cm^{-1})	Measurement
A1	16.5	595–615	Temperature 20–40 km
A2	15.9	615–645	Temperature 40–80 km, pressure
A3	15.4	635–665	Temperature 40–80 km, pressure
A4	11.8	820–870	Dust and condensate 0–80 km
A5	22.2	400–500	Temperature, dust and cloud 0–20 km
A6	1.65	3300–33,000	Polar radiative balance, albedo
B1	31.7	290–340	Temperature, dust and cloud 0–20 km
B2	41.7	220–260	Water vapour, dust and cloud 0–40 km
B3	42.1	230–245	Water vapour, dust and cloud 0–40 km

ment of sensitive room-temperature thermopile detectors in the USA, and miniature high-resolution interference filters in the UK.

As the first dedicated limb temperature sounding experiment for Mars, MCS required a narrow field of view capable of resolving a thin layer of atmosphere at the limb, 5 km or half a pressure scale height in the vertical direction. A wider value suffices in the horizontal direction since radiance changes less rapidly. In solid-angle terms, this means a field of view measured in microsteradians, which normally would force the telescope aperture to be large to improve the energy grasp, and probably also require cooled detectors for a low noise level. However, the mass available meant that neither of these options was available, and the solution was a new generation of detectors that offered low NEP without cooling.

The detectors use a modern development of very old technology, the thermocouple. Micro-machining techniques are used to produce 0.5-micron-thick silicon nitride membranes carrying arrays of twenty detectors that each consist of twelve Bi–Te and Bi–Sb–Te (bismuth–antimony–tellurium) thermocouples. These achieve a nominal D^* of 8×10^8 cm W^{-1} $Hz^{1/2}$ and response times less than 100 ms, corresponding to an NEΔT of about 0.1 K in the lower part of the Martian atmosphere when viewing at the limb (Fig. 3.8). The detectors are closely spaced in a linear array (one per spectral channel) that is

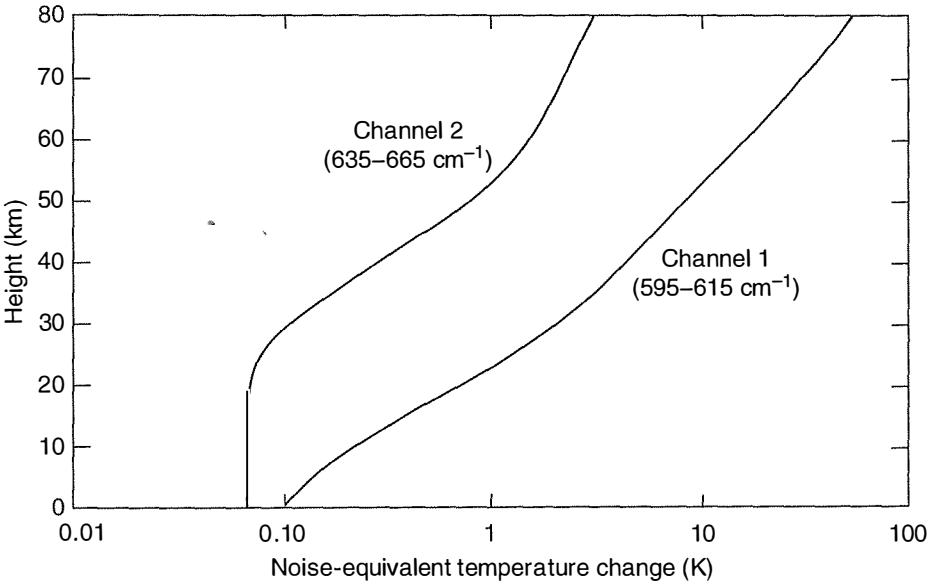

Fig. 3.8
Noise equivalent temperature change (NEΔT) profiles for two channels of the Mars Climate Sounder, with the spectral bands $\Delta\nu$ in wavenumbers indicated on the curves. For simplicity, these were calculated assuming the atmosphere has a constant temperature of $T = 140$ K at every level. The NEΔT increases with height as the atmosphere becomes more transparent; the radiance emitted is $eB(\Delta\nu, T)$ where the emissivity e falls from 1 near the surface to 0 at the top of the atmosphere.

aligned in flight along the vertical direction, so that profiles of radiance can be measured over a 100 km height range in a single two-second measurement.

The MCS obtains close-packed, repetitive temperature, dust, water vapour and cloud profiles, with an extended vertical range and improved altitude resolution compared to previous measurements, and with nearly continuous coverage. This allows global monitoring of the properties of the Martian climate with respect to atmospheric circulation, seasonal changes, and inter-annual climate variability. In addition, the measurements allow the examination of the annual dust and water cycles. Nadir sounding of infrared radiance and broadband solar reflectance from the surface characterises the thermal properties of the lithosphere, the net polar radiative balance, and the annual carbon dioxide frost budget.

3.10 Jupiter experiments

3.10.1 *Pioneer 10 and 11 Infrared Radiometer (IRR)*

The first space mission to a planet in the outer Solar System was *Pioneer 10*, which flew by Jupiter on 3 December 1973 at a distance of 131,000 km. On board were a number of small instruments, including an infrared radiometer operating in two spectral bands, 14 to 25 μm and 30 to 56 μm. These long wavelengths were chosen to meet the challenge of getting reasonable signals from a very cold target: Jupiter's atmosphere at the levels measured is only about 130 K as seen from the Earth, and could have been considerably colder at the poles, which at the time had never been observed.[49]

The instrument was restricted to a mass of 2 kg and a power consumption of 1.2 W, making large apertures and detector cooling difficult. Furthermore, *Pioneer* was a spin-stabilized spacecraft turning at 5 revolutions per minute, allowing only 38 ms for a measurement to

[49] The experimenters felt they needed to allow for the possibility that clouds of frozen methane might be present at the pole, at a temperature of 88 K.

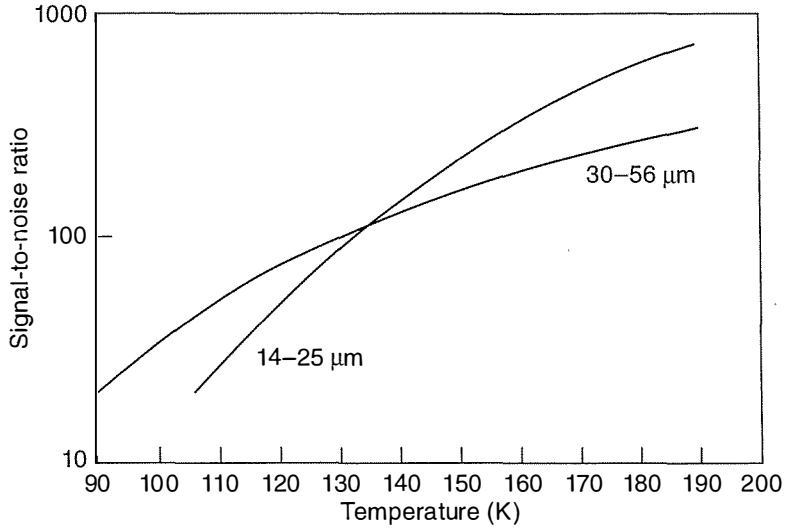

Fig. 3.9
Signal-to-noise ratio as a function of planet brightness temperature for the two channels of the *Pioneer 10* radiometer, which covered the spectral intervals shown (after Bender *et al.*, 1974).

avoid excessive smearing of the $0.3° \times 1.0°$ field of view. The latter was chosen to resolve about 1% of the diameter of the planet, much better than was possible using Earth-based telescopes.

The detector was an 88-junction antimony–bismuth thermopile, 1.27 mm in diameter, which achieved a D^* value about ten times poorer than the more advanced types in Mars Climate Sounder (§3.9.4). The diameter of the entrance aperture to the instrument was 7.62 cm. These parameters allow the signal-to-noise ratio expected for typical Jovian temperatures to be calculated, as shown in Fig. 3.9; the experimenters claimed an NEΔT of 1 K at 90 K for the 30 to 56 μm channel, and 0.1 K at 180 K for the shorter wavelength channel.

The most important result to emerge from the *Pioneer* IRR was confirmation that Jupiter and Saturn have large internal energy sources, comparable to the solar input into their atmospheres (§ 4.6).

3.10.2 *Voyager Infrared Interferometer Spectrometer (IRIS)*

The *Pioneer 10* radiometer obtained adequate signal by using wide spectral pass bands, an option that involves abandoning any chance of investigating the composition of Jupiter's atmosphere, for which high-resolution spectroscopy is essential. On the next mission to Jupiter, called *Voyager*, an infrared interferometer spectrometer (IRIS) was selected. This was designed with a spectral resolution of 4.3 cm^{-1}, high enough to resolve individual spectral features, and so identify minor constituents and estimate their abundance. This admits a factor of $\sim$100 less energy to the detector, still an uncooled thermoelectric device, compared with *Pioneer 10*, and so all other things being equal, would result in an inadequate S/N of around unity.

To compensate, the IRIS experimenters adopted a huge aperture of 50 cm diameter, more typical of a ground-based telescope than a space instrument (Fig. 3.10). This increased the signal relative to *Pioneer* by $\sim$50, restoring a good SNR, at the cost of making object-space cali-

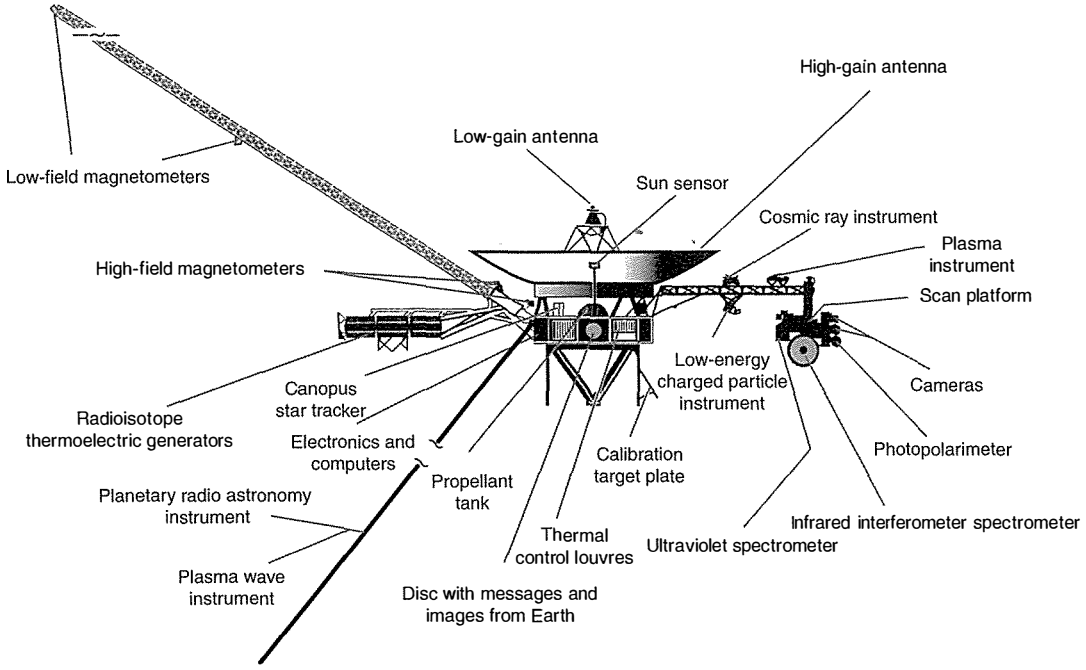

Fig. 3.10
The IRIS spectrometer can be seen at lower right on the *Voyager* spacecraft. The main communications dish at top centre is 3.7 metres in diameter.

bration, where the reference target is placed in front of the whole optical chain, difficult. The space view was not a problem, but a blackbody target that filled such a large aperture was not feasible without a large mass penalty. Instead, the IRIS team devised an ingenious scheme in which the residual emissivity of the large telescope mirror itself was used as a source, by varying its temperature using electrical heating.

The broad spectral coverage of *Voyager* IRIS allowed a wide-ranging scientific investigation, including determination of atmospheric vertical thermal structure and modelling of atmospheric dynamics, measurement of the abundances of the major and minor constituents, including hydrogen and helium and their ratio for comparison with that in the primitive solar nebula, and determination of the balance of energy radiated to that absorbed from the Sun, to help investigate planetary origin, evolution, and internal processes (Fig. 3.11).

3.10.3 *Galileo Near Infrared Mapping Spectrometer (NIMS)*

The successor to IRIS, NIMS made infrared observations of Jupiter from the *Galileo* orbiter, the first artificial satellite of any outer planet. A progressive feature of the new instrument was the use of detector arrays to make simultaneous measurements in several fields of view, building up 'cubes' of data in which the three dimensions were the two spatial directions and wavelength. The need for high spatial resolution and short dwell times to make maps, while retaining a reasonable

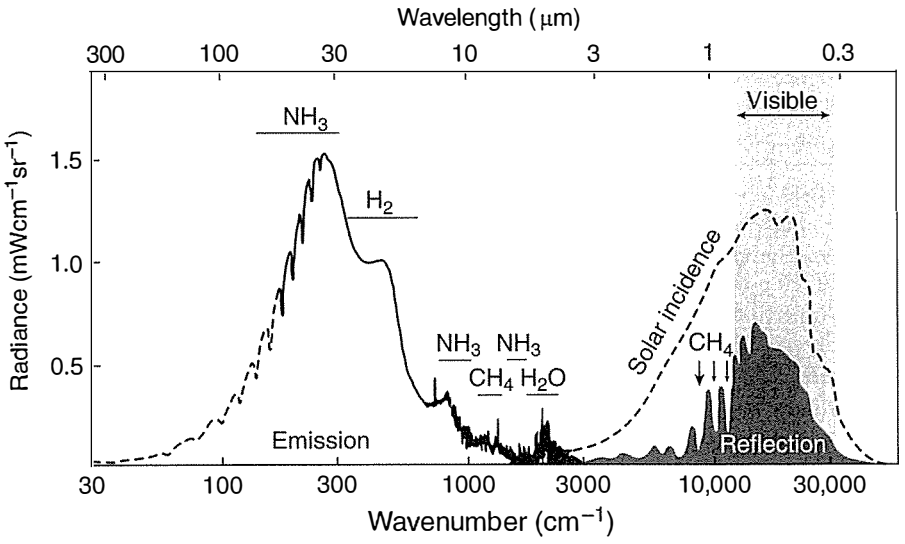

Fig. 3.11
The spectrum of Jupiter, based on *Voyager* IRIS measurements.

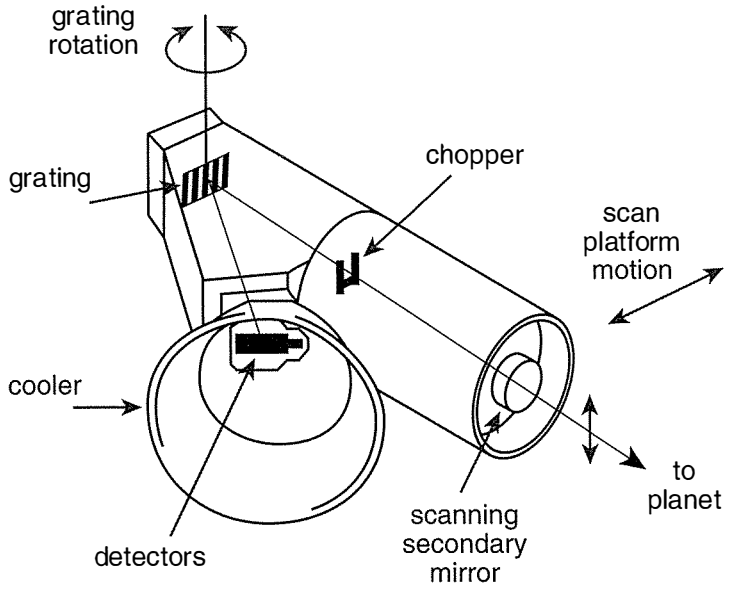

Fig. 3.12
The Near Infrared Mapping Spectrometer, NIMS, used on the *Galileo* Jupiter orbiter. Three scanning mechanisms – one to move the grating, and hence scan in wavelength, and two spatial scans – are used to build up spectral image 'cubes'. The cooler is a conical reflector with a black plate at the base, to which the detectors are thermally connected. By pointing the axis of the cone at cold space, the detectors are passively cooled to around the temperature of liquid nitrogen, 77 K. A similar instrument, VIMS, was built for the *Cassini* Saturn orbiter.

spectral resolution, too, placed extra demands on sensitivity. The solution in this case was a moderately large aperture (140 cm^2) combined with the use of cooled detectors for the first time for an infrared instrument in the outer Solar System.

The cooling was achieved by a passive radiative cooler (Fig. 3.12). This device uses no electrical power; in essence, it is simply a shielded black plate that points continuously at cold space and radiates heat away across the entire infrared spectrum. Even with the heat leak represented by the focal plane array, attached to the back of the cooler and containing the detectors, the cooler still achieves a temperature in the region of 77 K. This is the temperature of liquid nitrogen, the cryogen most commonly used to cool infrared detectors in the laboratory. The 17 detectors (made of indium antimonide, a popular material for near-infrared detectors, except for two silicon diodes in the visible region) form a linear array in the plane of dispersion of the diffraction grating, which is rotated to cover the spectral range from 0.7 to 5.2 μm. The field of view of the detector array is scanned across the

Table 3.6 NIMS signal-to-noise ratio (S/N) calculation. The angular field of view per detector is the acceptance angle (in milliradians) that determines the spatial resolution at a given distance from the target. The etendue or energy grasp is the product of the area of the entrance aperture (in cm^2) and the solid angle (in steradians) defining the cone of rays entering the aperture that can reach the detector.

Angular field of view per detector	0.5 mr
Entrance aperture	140 cm^2
Spectral resolution	0.025 μm
Scan time (20 pixels, 204 wavelengths)	4.3 s
Etendue (aperture × solid field of view)	1.1×10^{-4} cm^2 sr
System optical efficiency	0.5
Detector D^*	3×10^{13} cm W^{-1} $Hz^{1/2}$
Detector NEP	1×10^{-14} W $Hz^{-1/2}$
Noise equivalent radiance at 3 μm	1.2×10^{-9} W cm^{-2} sr^{-1}
S/N for albedo 0.075 at 3 μm	100

planet in two perpendicular directions by small movements of the secondary mirror in the telescope, and by pointing the whole instrument using the spacecraft scan platform.

The spectral range of NIMS was optimised for studying Jupiter and its satellites mainly in reflected solar energy, although the planet shows strong thermal emission in a broad 'window' region near 5 μm, where the main constituents are nearly transparent and radiation from the hot, deep atmosphere can be sensed in regions of low cloud cover. Table 3.6 shows the parameters of the instrument that are needed to calculate the signal-to-noise ratio as a function of wavelength.

NIMS made measurements of temperature, cloud structure, and atmospheric composition on Jupiter for over six years. It revealed complex vertical and horizontal structure, and dramatic temporal variations, many of which we will discuss in the following chapters.

3.11 Titan experiments

3.11.1 *Cassini Composite Infrared Spectrometer (CIRS)*

Cassini was launched in 1997, and made a Jupiter fly-by in 2000 en route for arrival at Saturn in 2004, where it has operated in orbit around the ringed planet for more than five years. On the payload are a Visible and Infrared Mapping Spectrometer (VIMS), with spectral range 0.35 to 5.1 μm (1960 to 28,500 cm^{-1}), a development of *Galileo* NIMS, and the Composite Infrared Spectrometer (CIRS), a much more advanced version of IRIS on *Voyager*. Figure 3.13 shows a schematic of the CIRS instrument and Table 3.7 lists its performance parameters.

CIRS uses twin interferometers, driven by a single scan mechanism to save weight and power, to obtain spectral ranges from 7 to 17 μm and from 17 to 1000 μm (10 to 600 cm^{-1} and 600 to 1430 cm^{-1}). Its spectral resolution, at 0.5 cm^{-1}, is an order of magnitude better than IRIS, and at the same time it obtains better sensitivity through the use of cooled infrared detectors. In addition, CIRS can obtain much better spatial resolution on its target, including an improvement of a factor of 2–3 over *Voyager* in the vertical (height) dimension, due to its better

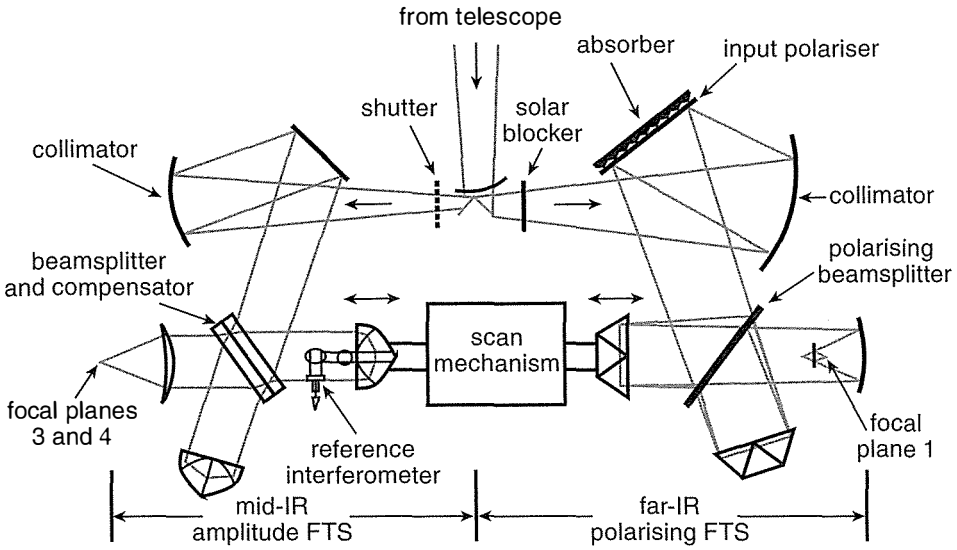

Fig. 3.13
The Composite Infrared Spectrometer (CIRS) instrument on the *Cassini* Saturn orbiter uses two Michelson interferometers to extend its wavelength coverage out to 1000 μm.

optics and six times closer approach to Titan than *Voyager*. Finally, it samples many different regions on Titan by making dozens of separate encounters on different orbits of Saturn.

In addition to improved sensitivity and vertical resolution, the long wavelengths accessible to CIRS allow sounding deeper into Titan's atmosphere than was possible with IRIS. The high performance of CIRS enables several key objectives, including global mapping of the vertical distribution and temporal variation of gaseous species, temperature and clouds in both the troposphere and stratosphere with latitude, longitude and height, as well as allowing the possibility of discovery of previously undetected chemical species. New information on some species in Jupiter's atmosphere, particularly tropospheric ammonia (NH_3) and phosphine (PH_3) and stratospheric acetylene (C_2H_2), and ethylene (C_2H_6), were obtained during the Jupiter fly-by in December 2000.

To give some idea of what a powerful instrument like this can achieve, here are some highlights of the results obtained at Titan from the spectra provided by CIRS:

Table 3.7 CIRS instrument parameters. See notes to Table 3.6. HgCdTe (mercury cadmium telluride) is a common detector material, an amalgam of the three metals in which the proportions of each determine the energy gap of the resulting semiconductor. This allows the detector to be tuned to perform optimally in the wavelength range of interest.

Telescope diameter	50 cm			
Spectral range	Polarising inteferometer:	10–300 cm^{-1}	Michelson interferometer	200–1400 cm^{-1}
Spectral resolution		0.5 to 20 cm^{-1}		0.5 to 20 cm^{-1}
Integration time		50 s		50 s
Focal Planes	*FP1*	*FP2*	*FP3*	*FP4*
Spectral range (cm^{-1})	10–300	200–650	600–1100	1100–1400
Detector type	Thermopile	Thermopile	HgCdTe	HgCdTe
Field of view (mr)	4.3	4.3	0.2	0.2
Etendue (cm^2 sr)	0.03	0.03	8×10^{-15}	8×10^{-15}
D^* (cm $Hz^{-1/2}$ W^{-1})	3×10^{9}	2×10^{9}	3×10^{10}	5×10^{11}
NEP (W $Hz^{-1/2}$)	3×10^{-11}	5×10^{-11}	8×10^{-13}	5×10^{-14}
NER (W Sr^{-1} cm^{-1})	4×10^{-9}	6×10^{-9}	4×10^{-10}	2×10^{-10}

- the global and height distributions of many species, including hydrocarbons, nitriles, and CO_2;
- the first detection of an aromatic compound, benzene (C_6H_6), on Titan;
- data on the atmospheric temperature and composition, and their vertical and horizontal variation, revealed photochemical and radiative processes, and the formation of clouds and hazes;
- the D/H ratio determined from the band of deuterated methane (CH_3D) at 1156 cm^{-1} was found to be consistent with models featuring outgassing of methane from Titan's interior;
- relative elemental abundances and their isotopic ratios in Titan's stratosphere test models of the formation and evolution of the Saturnian system and the Solar System as a whole;
- global temperature structure data retrieved from the inversion of the emission from atmospheric methane at wavelengths near 7 μm diagnose the circulation and dynamics of the atmosphere;
- compositional data records transport between sources and sinks, so short-lived species are additional tracers of the dynamical motions and their timescales.

All of these are discussed in the relevant parts of the later chapters.

3.12 References and further reading

Bender, M.L. *et al.* Infrared radiometer for the *Pioneer 10* and *11* missions to Jupiter. *Applied Optics*, **13**, 11, 2623–2628, 1974.

Carlson, R.W., F.W. Taylor, *et al.* Near Infrared Mapping Spectrometer experiment on *Galileo. Space Sci. Rev.*, **60**, 457, 1992.

Coustenis, A. *et al.* The composition of Titan's stratosphere from *Cassini/* CIRS mid-infrared spectra. *Icarus*, **189**, 1, 35–62, 2007.

Coustenis, A., and F.W. Taylor. *Titan: Exploring an Earthlike World.* 330pp. World Scientific Publishing, 2008.

Drossart P., G. Piccioni *et al.* Scientific goals for the observation of Venus by VIRTIS on ESA/*Venus Express* mission. *Planet.Space Sci.*, **55**, 1653–1672, 2007.

Flasar, F.M., V.G. Kunde *et al.* Exploring the Saturn system in the thermal infrared: The Composite Infrared Spectrometer. *Space Sci. Rev.*, **115**, 169–297, 2004.

Foote, M.C., T.R. Krueger, J.T. Schofield, D.J. McCleese,T.A. McCann, E.W. Jones, and M.R. Dickie. Space science applications of thermopile detector arrays. In *Quantum Sensing: Evolution and Revolution from Past to Future*, ed. by M. Razeghi, and G. Brown. *J. Proc. SPIE*, **4999**, 443–447, 2003.

Formisano V. *et al.* Detection of methane in the atmosphere of Mars. *Science*, **306**, 5702, 1758–1761, 2004.

Kliore, A.K., D.L. Cain, G.S. Levy, V.R. Eshleman, G. Fjeldbo, and F.D. Drake. Occultation experiment: Results of the first direct measurement of Mars' atmosphere and ionosphere. *Science*, **149**, 1243–1248,1965.

Hanel, R.A., *et al.* Infrared spectroscopy experiment on the *Mariner 9* mission: Preliminary results. *Science*, **175**, 305–308, 1972.

Hanel, R.A., D. Crosby, L.W. Herath, D. Vanous, D. Collins, H. Creswick, C. Harris, and M. Rhodes. Infrared spectrometer for *Voyager. Applied Optics*, **19**, 1391–1400, 1980.

Hanel, R.A., B.J. Conrath, D.E. Jennings, and R.E. Samuelson. *Exploration of the Solar System by Infrared Remote Sensing*. Cambridge University Press, 534 pp., 2003.

McCleese, D.J., J. Schofield, S. Calcutt, M. Foote, D. Kass, C. Leovy, D. Paige, P. Read, M. Richardson, F. Taylor, and R. Zurek. Mars Climate Sounder: An investigation of thermal and water vapor structure, dust and condensate distributions in the atmosphere, and energy balance of the polar regions. J. *Geophys. Res.*, **112**, E05S06, 2007.

Taylor, F.W., F. Vescelus, P.B. Forney, J.T. Foster, J.R. Locke, J.T. Houghton, J. Delderfield, and J.T. Schofield. Infrared radiometer for the *Pioneer Venus Orbiter*. I: Instrument description. *Applied Optics*, **18**, 3893–3900, 1979.

3.13 Questions

1. Draw a block diagram indicating the main components required for an infrared radiometer designed to measure temperature as a function of height by viewing the limb of the atmosphere from a spacecraft.

   Indicate briefly what factors are involved in choosing (a) the spectral region, (b) the angular field of view, (c) the entrance aperture, and (d) the calibration scheme used by the radiometer.

2. Derive a formula to express the noise equivalent temperature (NET) of a radiometer in terms of its geometry, the spectral bandpass and optics transmittance, the integration time, and the detector noise equivalent power (NEP).

   A radiometer has entrance aperture 0.01 m^2, and its bandpass is from 660 to 670 cm^{-1}. The transmittance of the optics is 50% and the field of view is $0.1° \times 1°$. Estimate the integration time needed to obtain a NET of 1 K if the detector NEP is 10^{-9} W $Hz^{-1/2}$, and the target temperature is 250 K.[You may assume that the Planck function is given by the approximation

   $$B(\nu,T) = 2 \times 10^{-11}\ T^4\ \mathrm{m^{-2}ster^{-2}}\ (\mathrm{cm^{-1}})^{-1} \text{ at } \nu = 665\ \mathrm{cm^{-1}}.]$$

3. Make a single sketch, with axes labelled from 0 to 750 K and 0 to 100 km, which shows the main features of the vertical profiles of temperature versus height on Venus, Earth and Mars. Comment briefly on the fundamental reasons for the similarities and differences between them.

4. Describe the main features of an experiment on an orbiting spacecraft that could measure temperatures in the atmosphere of Venus over the range from the surface to 100 km altitude. Specify, with brief reasons for the choice, some approximate but realistic values for the following instrument parameters: operating wavelengths, spectral resolution, aperture, field of view, and dwell time.

5. Show using these numbers that a signal-to-noise ratio at least of the order 100 to 1 can be obtained for an observing wavelength of 5 μm and a typical Venus middle-atmosphere temperature of 240 K. What temperature accuracy and vertical resolution would be expected in the atmosphere above the cloud using this technique? You may assume that the detector performance is specified by a noise equivalent power of $\sim 10^{-10}$ W $s^{-1/2}$.

[The Planck function $B(\lambda,T) = 6 \times 10^{-8}$ W cm^{-1} sr^{-1} and its derivative $dB/dT = 3 \times 10^{-9}$ W cm^{-1} sr^{-1} K^{-1} at 5 μm and 240 K.]

6. The preceding experiment is to be adapted for temperature sounding with the highest possible vertical resolution in the atmosphere of Mars. Summarise briefly, and as quantitatively as possible, how the technique and the instrument used at Venus would be modified for this new application at Mars.

4 Energy balance and entropy

4.1 Bolometric and greenhouse temperatures

Venus receives almost twice as much energy per unit area from the Sun as Earth does, and nearly four times as much as Mars. However, the surface conditions on frozen Mars and baking Venus are both sustained by roughly equal amounts of *net* heating, due entirely to differences in their atmospheres that determine the albedo, the fraction of incoming radiative energy that is reflected back to space.

Significant amounts of solar energy reach the ground on all of the terrestrial planets. Even on Venus with its thick cloud cover, enough sunlight diffuses through to provide about 17 watts per cm^2 of surface insolation on the average, about 12% of the total absorbed by Venus as a whole. The opacity of the troposphere is large at long wavelengths, and the surface temperature must rise to 730 K in order to force enough infrared cooling to balance the incoming solar energy (the greenhouse effect).

An airless body with the same albedo and heliocentric distance as Venus would reach equilibrium for a mean surface temperature of only about 230 K. Convection in the troposphere carries energy upwards to the base of the stratosphere, where radiative cooling to space can occur strongly. On Venus, this level (the tropopause) occurs about 40 km above the surface. The corresponding distances for Earth and Mars are 10 km and 30 km, and on these planets the enhancements in surface temperature due to greenhouse warming are ~40 K and ~10 K, respectively. The surface and free air temperatures on Mars can be significantly higher due to airborne dust; model calculations discussed below (§5.5) show the warming due to dust can be 50 or even 100 K in the middle atmosphere.

On all planets, the temperature in the middle atmosphere or mesosphere tends to be constant with height, because the atmosphere here is optically thin. The equilibrium temperature is determined by the balance between the absorption of upwelling infrared from the surface and troposphere, and cooling to space, if no significant absorption of direct solar energy takes place. However, the basically isothermal nature of the middle atmosphere is modified on the terrestrial planets by absorption of moderate amounts of solar and thermal energy in thin dust or cloud layers, and in the near-infrared bands of minor species, such as water vapour and carbon dioxide. On Earth, the effect is greatest due to photochemical processes producing large amounts of ozone, which absorbs strongly in the ultraviolet.

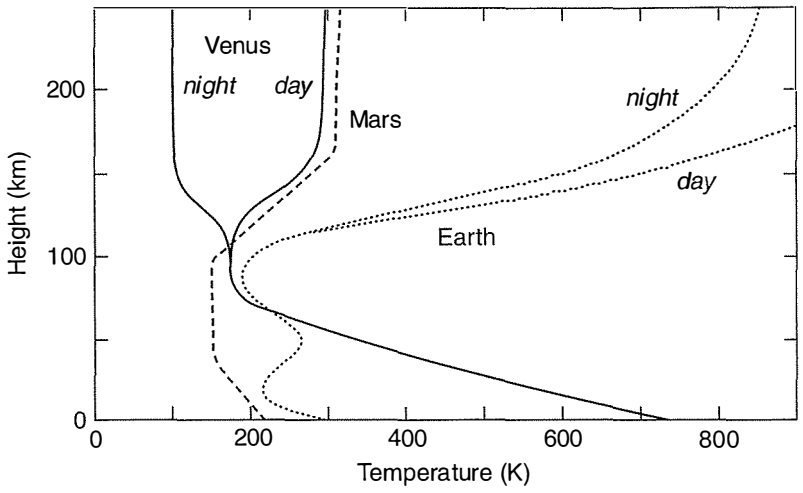

Fig. 4.1
Mean temperature profiles for the terrestrial planets, based on observations.

The *thermospheres* of Venus and Mars are cooler than Earth's because of the greater abundance of carbon dioxide, which is very efficient at radiating heat to space (Fig. 4.1). Above about 150 km, the temperature on these two planets is approximately constant with height on the day side at about 300 K. The terrestrial thermosphere is the seat of rapid winds, up to 1000 $m\,s^{-1}$ or more, which tend to redistribute energy absorbed from the Sun over the dark as well as the sunlit hemisphere. The result is a day–night difference of around 200 K about a mean temperature of 1000 K. On Venus, however, the night-time temperature in the thermosphere is very low, around 100 K, with very steep day–night gradients. Apparently the flow of air in response to the temperature gradient is inhibited by large-scale eddies. On Mars, the night-time temperature has not been measured at high altitudes.

4.2 Radiative energy balance of a planet

The energy balance of a planet can be calculated from knowledge of the incoming irradiance from the Sun or star, the albedo or reflectivity of the planet, and the distance between the two. On the gas giant planets, we also have to take account of any internal source that may be present. The result of a simple balance calculation is a value for the radiative equilibrium temperature of the planet, T_E, also known as the effective or equivalent blackbody temperature, at which the incoming and outgoing fluxes of radiative energy are the same (Fig.4.2).

For a planetary body with no atmosphere and an emissivity in the thermal infrared which is close to 1, like Mercury or the Moon, this is the geometrically weighted average physical temperature of the surface.[50] For a planet with a thick atmosphere, like Venus or Jupiter, T_E is some complex weighted mean of the vertical temperature profile. On Venus, though, the clouds are opaque over most of the infrared spectrum, and are high enough in the atmosphere that they are above most of the gaseous opacity, so the radiative equilibrium temperature is close to the physical temperature at the cloud tops (about 235–240 K).

[50] If the planet were a flat, black disc perpendicular to the planet–Sun line, then by definition its temperature would be T_E everywhere, or $1/2^{1/4}$ T_E if the dark side of the disc world is in good thermal contact with the sunlit surface of the planet.

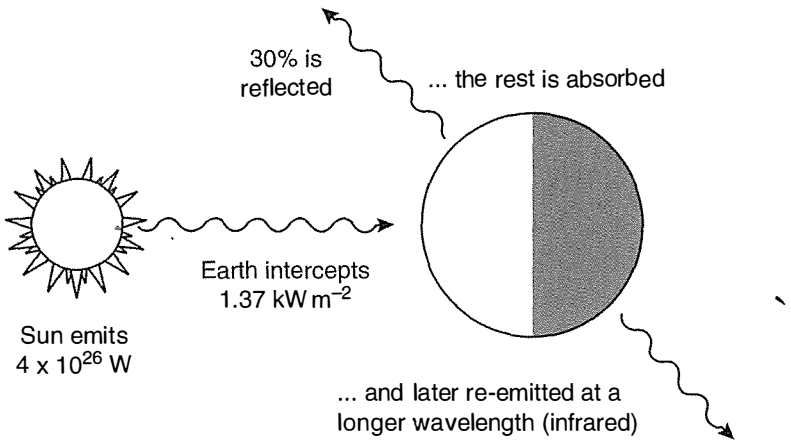

Fig. 4.2
Radiative energy balance: the Sun emits as a blackbody at temperature T_S and the planet at a temperature T, such that it emits the same amount of energy as it receives, after allowing for the fraction reflected, given by its albedo A.

This value was known long before it was realised that the temperature profile in the atmosphere below the clouds reached a temperature 500 K higher at the surface. Thus, for an elementary description of the temperature distribution in any planetary atmosphere – the most basic aspect of the climate on the planet – we must work out not only the equilibrium temperature of the whole body, but how this relates to the mean vertical temperature profile.

In order to go on and calculate how the temperature profile varies with solar zenith angle, i.e., from equator to pole and from day to night, some consideration of the dynamical transport of heat is unavoidable. Without this, Venus, for example, with its slow rotation, would have a much lower cloud-top temperature at midnight than at noon, whereas in fact they are almost the same. The radiative time constant – a measure of the time taken to cool by radiation when the source is removed – is a key factor.

4.2.1 Effective radiating temperature

The *effective radiating temperature* T_E of a planet is the temperature of a blackbody that radiates the same total energy to space, and should not be confused with the *brightness temperature* T_B we defined in the previous chapter when discussing instruments. T_B applies to a specific wavelength and bandpass, and can be wavelength dependent, whereas T_E refers to the energy contained in the entire spectrum of all wavelengths. Thus, applying the Stefan-Boltzmann law, the two are related by

$$\sigma T_E^4 = \int_0^\infty B(T_B,\lambda)\, d\lambda.$$

If the object in question is in fact a blackbody, as is often the case to a reasonable approximation, then T_B is independent of wavelength and T_B and T_E are identical.

Effective radiating temperatures of the terrestrial planets can be calculated as illustrated in Fig. 4.2, using the data in Table 4.1. The radiating temperature of the surface of the Sun is $T_S \approx 6000\,\mathrm{K}$ and its radius R_S is about 0.7 million kilometres, so we obtain for the total radiant power of the Sun:

$$E_{Sun} = 4\pi\sigma R_S^2 (T_S)^4$$

where the Stefan-Boltzmann constant σ is equal to 5.670×10^{-8} W m^{-2} K^{-4}. The solar constant S, which is defined as the power per unit area arriving at the planet at a distance D_{PS} from the Sun, is then given by

$$S = \sigma T_S^4 (R_S/D_{PS})^2$$

from which we find that S is approximately 1.37 kW m^{-2} for the Earth, and roughly twice as much at Venus, and half as much at Mars.

In order for the temperature of the planet to be in overall equilibrium, the power emitted over its whole area, E_P, must be equal to the total incoming power of the Sun that is intercepted by the projected area of the planet, less the fraction A which is reflected back to space, i.e.,

$$E_P = 4\pi\sigma R_P^2 (T_E)^4 = (1 - A) S \pi R_P^2$$

which can be solved for T_E, the effective radiating temperature of the planet, given a value for the Bond albedo A.[51] This, sometimes called the bolometric albedo, is defined as the fraction of the incident radiation of all wavelengths that is scattered in all directions. Accurate values for the Bond albedo are hard to obtain; when measuring the reflectivity of planets from the Earth, in particular the outer planets, what we see is the radiation reflected in a certain direction, and even a spacecraft orbiting the planet cannot observe all possible directions. If the observer, Sun, and planet are in the same line, the albedo measured is called the geometric albedo. If the surface of the planet is a perfect Lambertian reflector, then the Bond and geometric albedos are the same. Otherwise, they depend upon the scattering properties of the planet's surface and atmosphere.

The Earth's Bond albedo may be changing with time as part of global climate change affecting cloud and aerosol amounts. Values between 0.3 and 0.4 are usually estimated; using the higher of these, the result for the Earth is that T_E is approximately 255 K, or −18 °C. This, the average equivalent blackbody temperature of a solid sphere the same size and albedo as the Earth at the same distance from the Sun, is clearly not the same as the Earth's mean surface temperature, the difference being due to the 'greenhouse' effect of the atmosphere.

Energy from the Sun reaches the surface of the planet because the atmospheric blanket is nearly transparent at visible wavelengths in the absence of clouds. The balancing, cooling radiation, however, is in the infrared part of the spectrum because the source is so much

[51] The Bond albedo is named after the American astronomer George Bond, who introduced the concept in 1860.

Table 4.1 Radiative equilibrium temperatures of the terrestrial planets, calculated from simple energy balance models.

	Venus	Earth	Mars
Distance from Sun (Mkm)	108	150	228
Planetary Bolometric (Bond) albedo, A	0.76	0.4	0.15
Tropospheric Lapse Rate (K km^{-1})	10.7	9.8	4.5
Radiative equilibrium temperature, T_E (K)	239	255	226
Surface temperature (K)	730	290	235

cooler, a few hundred degrees instead of a few thousand. Wien's law states that the peak emission occurs at a wavenumber equal to approximately twice (actually 1.962 times) the temperature of the source, i.e., 563 cm^{-1} or 17.75 μm for the Earth, 12,000 cm^{-1} or 0.83 μm for the Sun, and about 100 cm^{-1} or 100 μm for Uranus and Neptune.

4.3 Model spectra of the planets

Figure 4.3 shows the calculated spectra for all of the planets using the same approximate model as above; viz., a perfectly black emitter at the equilibrium temperature in the thermal infrared, and a reflecting sphere of albedo A in the solar wavelength regime.[52] In reality, of course, A is a continuous function of wavelength and the actual spectra show much more structure (see the example of the spectrum of Jupiter in Fig. 3.11).

[52] Once again we note that the value of A, even for the Earth, is very hard to determine accurately, and the values for A, and hence for T_E, found in textbooks and the scientific literature can vary depending on the assumptions made.

4.4 Radiative balance on Venus

On Earth and Mars, most of the solar energy that heats the planet is deposited at the surface, driving the convection that produces an

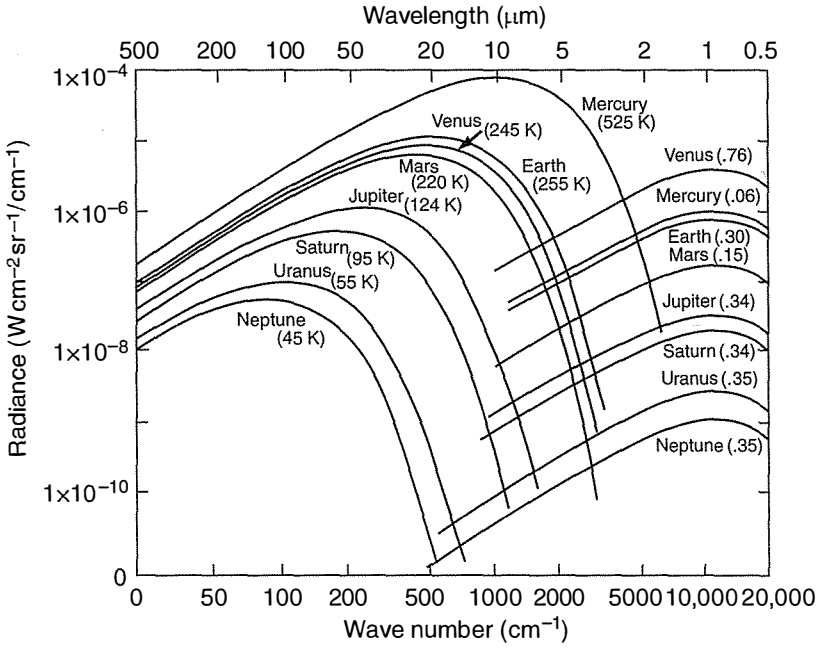

Fig. 4.3
Spectra of model planets in radiative balance, calculated assuming a perfectly black emitter at the equilibrium temperature shown in the thermal infrared, and a reflecting sphere of the albedo shown in the solar wavelength regime.

adiabatic temperature profile in the troposphere. It is less obvious what should be expected on Venus with its thick atmosphere and dense cloud layers, which make it difficult for solar radiation to penetrate to the surface. In fact, probes have found that about 12% of the fraction of the radiant energy from the Sun that is absorbed by Venus heats the surface, an average of 17 watts per square metre. Because of the high albedo of the sulphuric acid cloud droplets at short infrared wavelengths, photons are much more likely to be scattered than absorbed, allowing a significant fraction of the total energy to diffuse through the cloud layers and reach the surface, particularly at wavelengths outside the absorption bands of the main atmospheric gases. Both the clouds and the gases are much more opaque in the thermal infrared than in the visible, so the solar energy deposited at depth cannot escape directly to space as long-wave radiation. The surface temperature rises as a result, and heat is instead raised by convection along an approximately adiabatic temperature–pressure profile to a level near the cloud tops, where it can radiate to space. Venus has a deep troposphere, therefore, despite the fact that the peak heating occurs 50 km or so above the surface.

The calculation for an airless body with the same albedo and heliocentric distance as Venus finds radiative equilibrium at a mean temperature of only about 230–240 K, close to the actual temperature at the Venusian cloud tops. This is not surprising, since the clouds are opaque in the thermal infrared and, so far as long-wave radiation is concerned, they are effectively the surface of the planet. This is not inconsistent with the filtering of a fraction of the incoming short-wave radiative energy through the clouds to the real surface, and then back up to the cloud tops, which lie near the tropopause, as sensible heat carried mainly by convection.

Measurements by the *Pioneer Venus* orbiter of the angular and planetographic distribution of total reflected solar energy and emitted thermal flux were integrated over the globe of Venus (actually just the northern hemisphere, since there were few observations of the other half of the planet) to obtain the net infrared cooling and the total solar heating. The results (Schofield and Taylor, 1982) confirmed that the planet is in overall energy balance to within the accuracy of the measurements, which were limited to an estimated 15% by incomplete spectral and spatial coverage.

4.4.1 Comparing the energy budgets of Venus and Earth

On Earth, half of the radiant energy from the Sun is deposited at the surface (50%), with smaller proportions absorbed in the atmosphere (20%) or reflected back into space (30%). On Venus, however, as we have seen, the proportions are more like 3%, 21%, and 76%, respectively, with the bulk of the energy absorbed by the planet deposited well above the surface in the principal cloud layers ($21/(21 + 3) = 78\%$, see Fig. 4.4). The energy balance calculation for the planet as a whole that led to an equilibrium temperature of 230–240 K

for Venus gives 250–255 K for Earth, higher despite Earth's greater distance from the Sun.

Such comparisons depend on the values taken for the hemispherical Bond albedo in each case. To reduce the uncertainty in this number, and to monitor its variability and trends as a key component of climate research, elaborate schemes have been proposed for measuring the total energy reflected and emitted from the Earth. Despite the fact that this is a difficult measurement, requiring multiple spacecraft in different orbits to do it properly, a similar project for Venus would be very valuable. It could also settle the question of whether any significant part of the high surface temperature is attributable to the release of heat from the interior, which may be greater for Venus than for Earth, although the value is unknown. Interior heat release cannot, in any case, be the dominant influence in surface temperature because of the constraints placed by the energy balance measurements mentioned above.

Since the biggest difference between Venus and Earth in the energy balance equation is the albedo, the underlying physics centres on the composition, microstructure and optical properties of the different types of cloud. Even short-range climate change projections for the Earth depend crucially on understanding the role of different cloud types and how they may change with temperature, circulation, and pollution loading of the atmosphere. Venus probably has more than one type of cloud, as evidenced by the ultraviolet markings and suggestions of possible major variations occurring in the poorly observed deep layers, and at the poles (Chapter 7). The sulphurous nature of the clouds indicates that volcanic emissions have a major role in maintaining the cloud cover in its present state, and that evolution in the degree of volcanism may change the cloud properties, the albedo, and hence the climate of Venus in significant ways on a range of timescales.

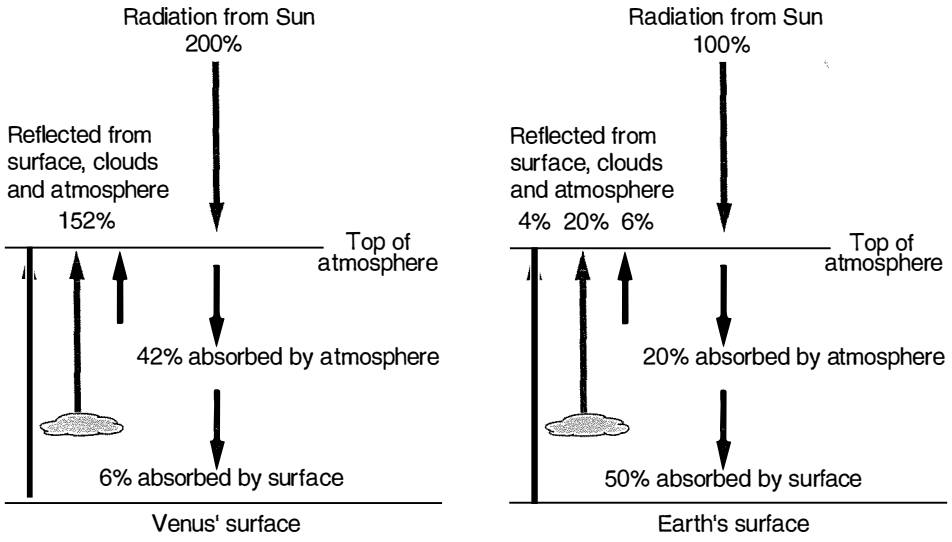

Fig. 4.4
The different components of the radiative energy budgets of Venus and Earth are shown as planet-wide averages, taking the solar irradiance at Venus as twice that at Earth. (Actually, the insolation at Earth relative to that at Venus varies between 50% and 55% when the orbital eccentricities of 0.0167 and 0.007, respectively, are taken into account).

4.4.2 Contributions of individual components to the greenhouse effect

In Chapter 9, climate models for Venus are discussed. One interesting use to which these can be put is to estimate the contribution of each component of Venus' atmosphere to the greenhouse warming at the surface by removing each from the model in turn. Such an experiment was carried out by Bullock and Grinspoon (using their Venus Evolutionary Climate model, see §9.4.5); the results are summarised in Fig. 4.5.

The largest effect on the surface temperature of removing key atmospheric constituents from the model is, not surprisingly, that due to carbon dioxide, while the number for clouds is very dependent on how they are modelled. The larger effect of water vapour relative to the smaller contributions from other trace species comes from its very rich infrared spectrum, which makes it the principal greenhouse gas on Earth and compensates for its low mixing ratio on Venus. In contrast, notwithstanding its key role in cloud formation, sulphur dioxide makes a relatively small spectral contribution on both planets, even on Venus where its abundance is relatively high, because it has few infrared bands.

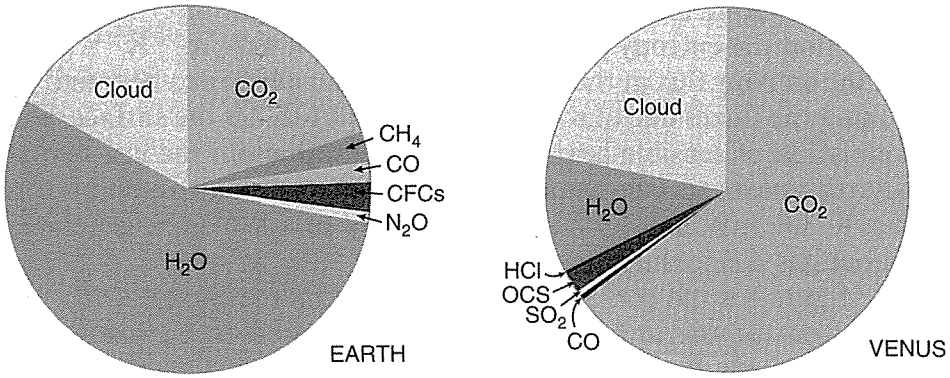

Fig. 4.5
The relative contributions of greenhouse gases and clouds to the surface temperature on Earth and Venus, according to model calculations.

4.4.3 Entropy fluxes on Earth and Venus

While the climate of a planet is determined mainly by the energy fluxes at the top and bottom of the atmosphere, the fluxes of *entropy* give clues to the processes that convert 'high grade' incoming solar radiation into the 'low grade' thermal infrared flux that delivers energy at the same rate back into cold space. These processes are irreversible and must, according to the second law of thermodynamics, result in a monotonic increase in total entropy. Entropy s is a measure of the level of availability of energy in a given system, which can also be expressed in terms of the degree of disorder of the system. When a glass of water spills, the disorder of that system increases and the availability of its energy to do work decreases; the entropy increases, and the situation cannot be reversed without the removal of entropy from the water to some external system in such a way that the total entropy of both increases. The second law can be written

$$\frac{ds}{dt} = \frac{Q}{T} \geq 0$$

where Q is the rate of diabatic heating per unit mass and T the temperature at which the heating occurs.

Many authors have used entropy budget arguments to study the relevance of the second law of thermodynamics to the climate system and to the understanding of atmospheric phenomena.[53] Energy flowing through the Earth's climate system is degraded through a series of processes to successively lower temperatures, with consequent production of entropy. Diabatic heating in the atmosphere includes radiative heating, the release of latent heat, heating by transport and conduction, and frictional dissipation. The total rate of entropy production of the Earth can be estimated from the differences in entropy flux across the boundary between the planet and space:

$$\frac{ds}{dt} = I_0(1 - A)\left(\frac{1}{T_E} - \frac{1}{T_S}\right)$$

where I_0 is the solar irradiance, A the albedo, and T_E and T_S the effective radiating temperatures of the Earth and Sun. Inserting values we find that the entropy production is about 900 mW $m^{-2} K^{-1}$. Similarly, the entropy flux at the bottom of the atmosphere can be found by summing the fluxes due to solar radiation that reaches the surface, and the emission of sensible heat and terrestrial radiation, the last two at the Earth's mean surface temperature of 288 K. In round numbers, this comes to 300 mW $m^{-2} K^{-1}$, leaving 600 mW $m^{-2} K^{-1}$ to be generated by processes inside the atmosphere.

The figure for the entropy difference between the fluxes at the top and bottom of the atmosphere can be compared to the estimated entropy budgets for the individual processes inside Earth's climate system, as illustrated in Fig. 4.6. To obtain the entropy rates shown,

[53] The specific calculations discussed here are from the work of Peixoto *et al.* (1991); Goody (2007), and Kleidon and Lorenz (2004).

Table 4.2 The entropy and energy budgets of Earth's atmosphere as calculated by Peixoto *et al.*, (1991). The entropy is estimated by dividing the energy flux by a representative temperature and plotted in Fig. 4.6 to show the overall balance.

	Energy (Wm^{-2})	Temperature (K)	Entropy ($mWm^{-2}K^{-1}$)
Sun to atmosphere	238	5760	41
Surface to space	20	288	−71
Cloud to space	88	259	−341
Atmosphere to space	129	252	−513
Sun to surface	170	5760	−29
Sensible heat to atmosphere	20	288	71
Surface to atmosphere	68	288	236
Absorbed solar radiation	68	252	258
Absorbed terrestrial radiation	48	252	24
Latent heat	79	266	298
Sensible and frictional heating	22	280	9

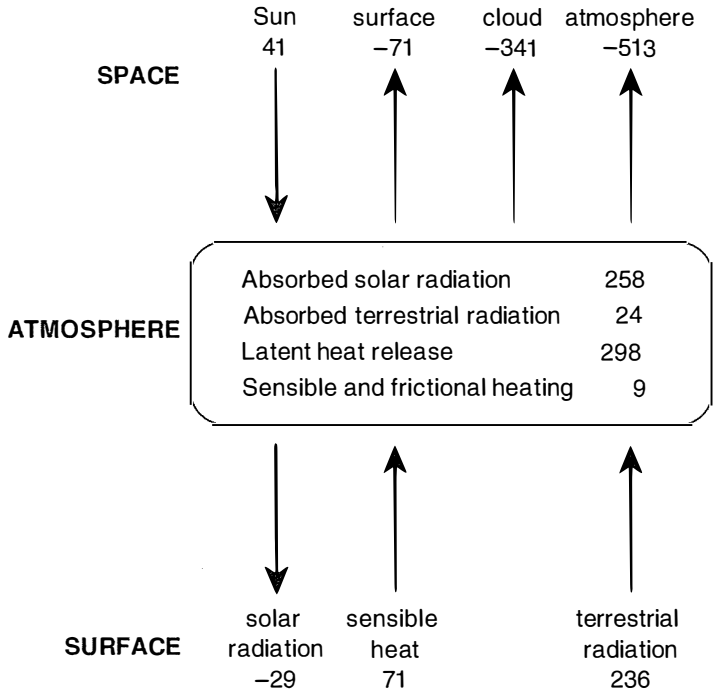

Fig. 4.6
The budget of entropy σ in the global atmosphere, as estimated by Peixoto *et al.* (1991). The flux of entropy into and out of the atmosphere is indicated by arrows; the quantities in the box are those processes that generate entropy internally. The numbers are entropy in mW $m^{-2}K^{-1}$ from Table 4.2.

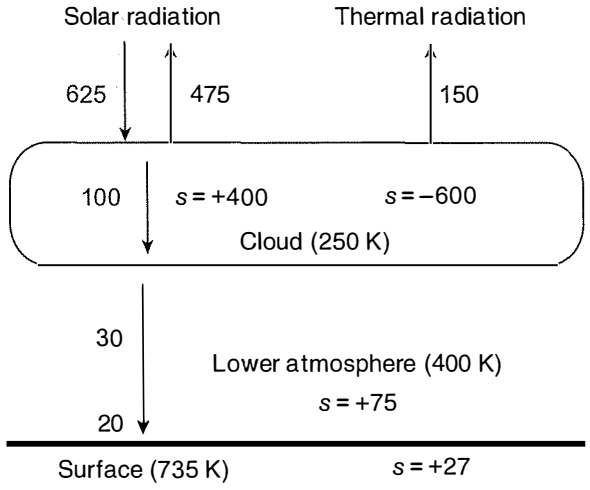

Fig. 4.7
The energy and entropy budget of the atmosphere of Venus as estimated by Titov *et al.* (2007). The unlabelled figures are energy in W m^{-2} and s is entropy in mW m^{-2} K^{-1}.

representative values for the fluxes of solar and terrestrial radiation have been assumed to be absorbed in the atmosphere at the 500 mb level, where the temperature is typically 252 K. Latent heating is calculated assuming a global net precipitation rate of 1 m yr^{-1} and a condensation temperature of 266 K; the estimated energy transfer by sensible heating and frictional dissipation are assumed to take place at a temperature of 280 K, representing the mean value in the lowest layer near the surface. Again, in round figures, these components do add up to 600 mW m^{-2} K^{-1} as expected.

An attempt has been made to carry out an analysis of this kind for Venus, as shown in Fig. 4.7. The overall situation is rather different than that for Earth, since very little sunlight penetrates to the surface of Venus. As a result, the sources of radiative entropy on the surface and in the lower atmosphere represent only about 20% of the total balance, with the largest sinks and sources of radiative entropy on Venus both located in the upper cloud deck. The fluxes of energy, and typical temperatures in each region, are reasonably well known from measurements and are also shown in Fig. 4.7. The resulting estimates of the entropy budget, however, do not add up, suggesting there must be additional important mechanisms that balance the net flux of radiative entropy on Venus.

Dissipative mechanisms associated with transport and precipitation of water are probably negligible in the dry atmosphere, while remote sensing and *in situ* measurements reveal only weak small-scale turbulence within the cloud layer, contributing entropy production estimated at less than $1\,\mathrm{mW\,m^{-2}\,K^{-1}}$. Other candidates, whose contribution is unknown and difficult to estimate without data from new experiments, include surface volcanism and the physical–chemical processes involved in cloud formation and dissipation.

4.5 Mars

The rock and dust that makes up most of the surface of Mars is a good absorber of thermal infrared radiation, and since the atmosphere is thin, with little cloud, the planet as a whole has a low Bond albedo ($A \sim 0.15$, compared to about 0.125 for the Moon). At Mars' mean distance from the Sun, this corresponds to a radiative equilibrium temperature of about 220 K, not that much less than the corresponding value of about 240 K derived above for Venus with its highly reflective clouds.

Measurements have provided a large enough sample of the surface temperatures on Mars to allow a globally and seasonally average value of around 235 K to be estimated. Mean values like this are not so meaningful on Mars as they are on Venus and Earth, since the low heat capacity of the Martian atmosphere permits diurnal and seasonal excursions of the order of 100 K, largely governed by the thermal inertia of the surface and other factors such as sublimation of frost deposits. When calculating equilibrium temperatures for the surface at particular locations and times of the year, two interesting cases can be considered: the maximum temperature at noon in summer (Sun overhead conditions), and the energy balance at the poles in midwinter (semi-permanent darkness).

4.5.1 The maximum surface temperature on Mars

Solving the energy balance equation

$$\sigma(T_E)^4 = (1 - A)S$$

using the optimum (i.e., smallest) value for the range of estimated albedos for Mars, 0.15, and the closest separation from the Sun (205 million km, compared to 249 million km at its farthest), gives a radiative equilibrium temperature of about 50 °C, well above the melting point of ice on Earth. At the pressure on Mars, if this were the surface temperature, ice would sublime to form vapour without melting (Fig.1.12). Of course, the radiative balance calculation neglects the dynamical, as well as the radiative, effects of the atmosphere, including convective cooling, and also takes no account of latent heat effects. The highest temperature actually observed on the surface of Mars so far is about 20 °C.

4.5.2 Polar night

During the polar night, in the absence of solar heating, the infrared radiative cooling is balanced primarily by the latent heat released by CO_2 condensation from the atmosphere. The relevant temperature for the cooling calculation is the temperature at which atmospheric carbon dioxide changes phase from gas to solid, which is 145 K at 4 mb. This releases latent heat of about $L_{CO_2} = 6 \times 10^5\,\mathrm{J\,kg^{-1}}$, so we can write

$$\sigma(145)^4 = mL_{CO_2}$$

where m is the mass deposited per second on one square metre of the polar cap. The length of the winter night on Mars is about 200 days, and the mean radius of the polar cap is about 1000 km, while the density of CO_2 snow, depending on how tightly it is packed under its own mass, is in round numbers about 1 kg per litre. Inserting these values gives an estimated seasonal cap thickness, over the course of the winter, of one metre. During winter, this lies on top of the perennial icecap, a much thicker layer of ice and trapped dust, and starts to vanish in the spring.

As a quick check on this calculation, we can estimate what fraction of the total mass of the Martian atmosphere this represents. The mass of the seasonal icecap works out at about 3×10^{15} kg, while that of the whole atmosphere is 3×10^{16} kg when averaged over all seasons. The swing in atmospheric pressure over a year is therefore estimated to be 10%, which compares reasonably well for a rough estimate with the values from 6.9 mb to 9 mb measured at the *Viking 1* Lander site.

4.5.3 A two-box energy balance model for Mars

Simple box models have been found to be very useful when considering the roles of temperature and salinity in the circulation of the oceans on Earth (see *Elementary Climate Physics*, Chapter 11). They can also give insights into the atmospheric circulation if the overarching regulatory principles can be written down, which is more difficult for the atmosphere than the ocean in this instance. One interesting approach is to

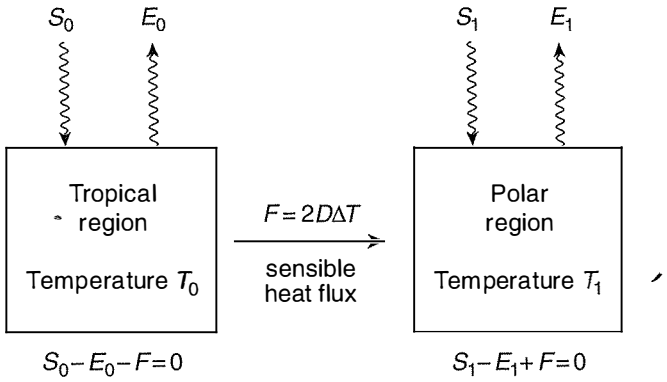

Fig. 4.8
A two-box energy balance model for Mars. Each box represents an equal surface area, so the dividing line between the equatorial and the polar box falls at 30 degrees latitude. T_0 and T_1 are characteristic mean temperatures ($T_0 > T_1$), S and E represent ingoing and outgoing radiative energy fluxes, and F is the energy transferred as sensible heat by the circulation of the atmosphere.

adopt the *principle of maximum entropy production*, an empirical extension of the second law of thermodynamics which postulates that a system not only increases its entropy with time, but also seeks to maximise the rate at which it does so.[54]

Consider the system shown in Fig. 4.8. A box representing the Martian tropics (latitudes from the equator to 30 degrees) is at a mean temperature of T_0 while a second box of equal area represents the higher-latitude regions at T_1. Each is heated and cooled by radiation from the Sun and to space, respectively, and heat flows from the warmer low latitudes to the cooler poles by atmospheric transport, with a flux F which satisfies

$$F = S_0 - E_0 = E_1 - S_1$$

where S is the incoming solar heating in each box and $E\,(=\sigma T^4)$ is the outgoing radiative cooling. For overall energy balance, we also have

$$S_0 + S_1 = E_0 + E_1$$

The rate of production of entropy s is given by

$$\dot{s} = F\left(\frac{1}{T_1} - \frac{1}{T_0}\right) = \sigma T_1^3 - \frac{S_1}{T_1} + \sigma T_0^3 - \frac{S_0}{T_0}$$

and this is a maximum when

$$\frac{d\dot{s}}{dT_0} = \frac{dT_1}{dT_0}\left(3\sigma T_1^2 + \frac{S_1}{T_1^2}\right) + 3\sigma T_0^2 + \frac{S_0}{T_0^2} = 0$$

Some manipulation of these equations gives

$$\left(\frac{E_0}{E_1}\right)^{\frac{1}{4}} = \left(\frac{S_0}{S_1}\right)\left(\frac{4 + E_1/E_0 + 3S_1/S_0}{4 + E_0/E_1 + 3S_0/S_1}\right)$$

The solar heating S is proportional to the surface area perpendicular to the equator presented by each box, since we are considering annual mean values, multiplied by $(1-A)$, where A is a representative albedo

[54] First advanced by Paltridge (1975). The treatment here follows that of Lorenz *et al.* (2001), and Goody (2007). It should be noted that the principle of maximum entropy production is not universally accepted. For a positive review see Ozawa *et al.* (2003), and for a cogent criticism, see Goody (2007).

that can be estimated from spacecraft data. The combination of the two gives a value for S_0/S_1 in the range from 2 to 4, the high uncertainty being due to the albedo values, particularly at high latitudes where the steep incidence angles, as well as the ice and haze present there, increase the albedo substantially over lower latitudes.

The simplest way to solve for E_0/E_1 is numerically, using a spreadsheet. Using the low end of the range for S_0/S_1, a solution is found for $E_0/E_1 = 1.41$, close to the value of 1.48 obtained by Goody (2007) from spacecraft data. No errors are quoted on the latter value, but these are unlikely to be less than 5% and probably rather higher, more like 20%. Also, since the ratio of temperatures T_0/T_1 has to be the fourth root of this number, the solution predicts that the temperatures differ by only about 10% (e.g., 198 K for equatorial latitudes and 180 K for the poles), which seems rather low, even allowing for the fact that this is the net emission from the surface and the atmosphere, and not the surface alone.

If, instead, S_0/S_1 is taken as the higher and probably more reasonable estimate of 4.0, the result is $E_0/E_1 = 1.85$, corresponding to a low-latitude box temperature of 215 K and a polar temperature of 175 K. These temperatures are similar to those found by Lorenz *et al.* (2001) by a different maximum entropy production analysis, and they are within the observed range of surface temperatures on the planet. It is clear that more and better data, like that being gathered by the Mars Climate Sounder described in the previous chapter (§3.9.4), is needed on temperatures, albedos and net thermal emission to refine this interesting approach to better understanding the energy budgets of the polar regions on Mars.

4.6 Internal heat sources on the outer planets

Figure 4.9 shows measurements from spacecraft of the reflected and emitted radiant energy from three of the giant planets. Clearly, Jupiter and Saturn emit more radiation than they receive, indicating the presence of an internal heat source. In fact, their atmospheres are heated from below by roughly as much as they are heated from above by the Sun. As would be expected from simple geometry, the solar heating varies approximately as the cosine of latitude on Jupiter and Saturn. However, the thermal emission profiles show almost no latitudinal variation, suggesting that some interior process is very effective at redistributing heat towards the polar regions. One possibility that has been suggested is that the internal heat source is regulated by the solar heating, in such a way that the sum of the two remains approximately constant. One way in which this could happen is if the convection of heat from the interior is partially suppressed by solar heating of the upper atmosphere, resulting in a smaller vertical temperature gradient and less vigorous vertical transport at lower altitudes.

The internal sources of heat are due most likely to slow contraction of the bodies, either in an overall sense or as a result of fractionation

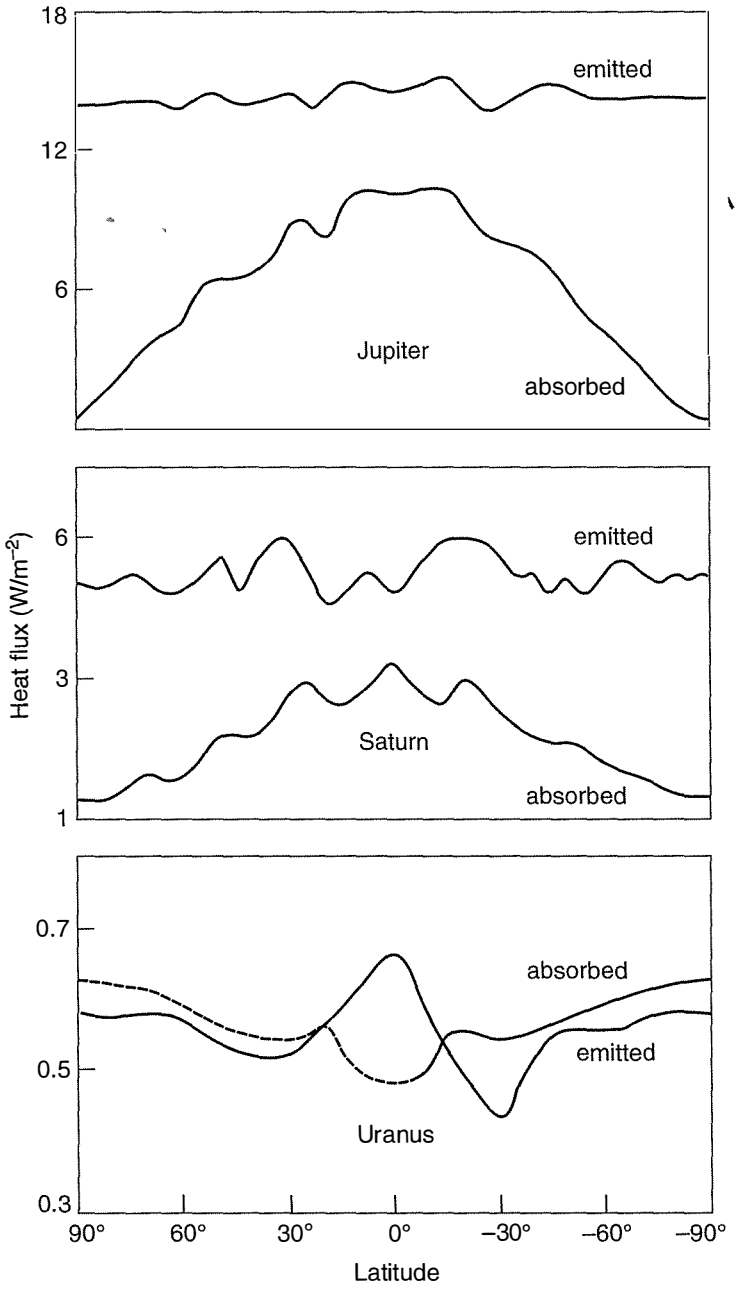

Fig. 4.9
Energy balance profiles as a function of latitude for Jupiter, Saturn, and Uranus, based on measurements by the *Pioneer* and *Voyager* spacecraft.

and phase changes in the interiors, with the consequent release of gravitational potential energy. Some models of the interiors of the giant planets predict 'rain-out' of droplets of liquid helium towards the interior in the deep atmosphere, supporting the second of these possibilities. The idea that overall shrinkage of a fluid body would produce large amounts of radiated heat was originally proposed by Kelvin and Helmholtz in the nineteenth century as a possible source for the energy of the Sun.

The Kelvin-Helmholtz process can be evaluated from the classical expression for the gravitational potential energy dU of a body

$$dU = -\frac{Gm(r)dm}{r}$$

where dm is the mass contained within a shell with mass $m(r)$ of a planet with overall radius R and total mass M. By replacing the actual density variation with the mean value, an approximate solution in the form

$$U = -\frac{3M^2G}{5R}$$

whence

$$\frac{dU}{dR} = -\frac{3M^2G}{5R^2}$$

is found. Equating dU/dR to the observed internal energy flux from Jupiter (i.e., the difference between the solar input and the infrared output, integrated over all wavelengths) of 15 $W\,m^{-2}$, we find that a contraction of the order of a centimetre per year would account for the internal source.

The data in Table 4.3 include the magnitude of the internal source for all four outer planets. It can be seen that Uranus, but not Neptune, is an exception in that the calculated radiating temperatures are not significantly smaller than the observed bolometric temperatures. Table 4.3 also demonstrates that Jupiter, Saturn and Neptune roughly fit empirical laws in which:

1. the internal flux is proportional to 1/(distance from Sun)^2, suggesting that the solar constant or the composition controls the internal flux, and
2. the internal flux is proportional to the mass of the planet, suggesting that the gravitational energy of accretion per unit mass is important.

Uranus is an enigma, and its apparent lack of any internal source may mean that more than one mechanism is at work on the four planets, or that the data on temperature and albedo is inadequate. Although models have been constructed of the interior structure of all of the gas and ice giants that could explain their different internal sources, it needs to be kept in mind that they are constrained by very little observational data, and should be regarded more as theories than explanations. The situation will improve when Uranus and Neptune have been studied with orbiters and entry probes.

4.7 A two-box model for Titan

Titan has a substantial greenhouse effect, although smaller than that of the Earth, and very small compared to Venus, since the surface temperature of 94 K is significantly higher than its overall external radiative balance temperature. The latter is about 82 K, with an error

Table 4.3 Data relating to the energy balance of the outer planets, compared to two empirical models, in which (i) the internal heat source is proportional to the inverse square of distance from the Sun, and (ii) to the mass of the planet. These 'laws' are illustrated by scaling the value for Jupiter by the relevant parameter in each case.

	Jupiter	Saturn	Uranus	Neptune
Solar flux ($W m^{-2}$)	50.8	15.2	3.76	1.52
Geometric albedo	0.274	0.242	0.215	0.215
Absorbed flux ($W m^{-2}$)	9.22	2.88	0.738	0.297
Emitted flux ($W m^{-2}$)	14.66	4.89	0.696	0.73
Internal source F_{int} ($W m^{-2}$)	5.44	2.01	0.042	0.433
Model 1: $F_{int} \propto 1/R^2$ ($W m^{-2}$)	(5.440)	1.604	0.398	0.160
Model 2: $F_{int} \propto M$ ($W m^{-2}$)	(5.440)	1.600	0.250	0.293
Radiogenic heat flux ($W m^{-2}$)	0.005	0.006	0.025	0.025
Radiative equilibrium temperature (K)	113	84	60	48
Observed bolometric temperature (K)	127	96	59	60

estimated as a few degrees, mostly due to the uncertainty in Titan's spatially and wavelength–integrated albedo. The solar constant is only about 1% of that at Earth, and of that about 10% of the incoming sunlight at the top of the atmosphere penetrates the haze layers and reaches the surface.

The maximum entropy model of Fig. 4.8 is in some ways more applicable to Titan than to Mars, because Titan has a thicker atmosphere with smaller seasonal and latitudinal variations. Furthermore, new measurements of the surface temperature of Titan are available from the Composite Infrared Spectrometer (§3.11.1) on the *Cassini* Saturn orbiter. CIRS mapped the latitudinal distribution of zonally averaged surface brightness temperatures in the thermal infrared at a wavelength of 19 μm (a wavenumber of 530 cm^{-1}). This is a spectral 'window' of low atmospheric opacity, the remainder of which could be removed by measuring the dependence of radiance on the emission angle.

From the mean of four years of data, the surface brightness temperature at equatorial latitudes was found by Jennings *et al.* (2009) to be 93.7 ± 0.6 K, in agreement with the *in situ* measurement by the *Huygens* lander. Temperature decreases toward both poles, reaching 90.5 ± 0.8 K at 87° N and 91.7 ± 0.7 K at 88° S.

Now, following the treatment by Lorenz *et al.* (2001), heat flows from a box representing the low latitudes on Titan at a mean temperature of T_0 to the higher-latitude regions at T_1 by atmospheric transport with a flux F, which is assumed to be proportional to the temperature difference ΔT. The constant of proportionality is twice the coefficient of meridional heat diffusion D, which has units of $W m^{-2} K^{-1}$. The entropy flux is zero when $D = 0$, and also when D is large, since in the latter case the temperature difference tends to vanish; at some intermediate point, the rate of temperature change with increasing transport and the overall entropy production are both at a maximum (Fig. 4.10).

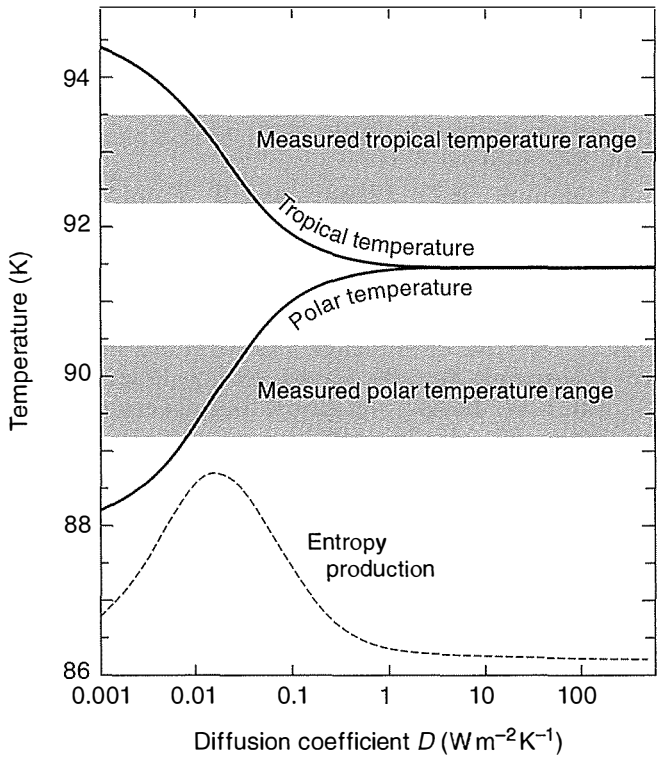

Fig. 4.10
Temperatures at low and high latitudes in a two-box model for Titan, as a function of the coefficient of meridional heat diffusion D. The dashed line shows the rate of entropy production, also as a function of D, in arbitrary units. The shaded bands are surface brightness temperatures measured by the Composite Infrared Spectrometer (CIRS) on the *Cassini* Saturn orbiter in the polar and tropical regions on Titan. Modified from Lorenz *et al.* (2001).

For the Earth, there exist good estimates of F, calculated from models that reproduce observed conditions accurately for weather forecasting and other purposes. These give $F = 20$–$40\ \mathrm{W\,m^{-2}}$ or a total flux of about $5 \times 10^{15}\,\mathrm{W}$ per hemisphere, which corresponds to $D \sim 1\ \mathrm{W\,m^{-2}\,K^{-1}}$. This can be compared to the model where, for the Earth, $T = 288\,\mathrm{K}$ and $D = \sigma T^3/2 = 0.68\ \mathrm{W\,m^{-2}\,K^{-1}}$.

Encouraged by this agreement for the familiar case of the Earth, we take $T = 90\,\mathrm{K}$ for Titan and find that $D = 0.02\,\mathrm{W\,m^{-2}\,K^{-1}}$. Thus the model predicts that Titan's atmosphere, although four times thicker than Earth's, is nearly forty times less efficient at transporting heat. However, it also predicts the correct temperature difference of $\Delta T \approx (I_0 - I_1)/8D = 3.5\,\mathrm{K}$ between low latitudes and the poles, seemingly confirming that something is suppressing latitudinal transport on Titan relative to what would be expected by simple scaling from the Earth. The processes responsible, perhaps related to surface thermal properties, condensation of atmospheric species, or large-scale organised motions, such as the polar vortex, seem to be missing from the most sophisticated models of Titan's atmosphere (§8.6).

4.8 References and further reading

Goody, R.M. Maximum entropy production in climate theory. *J. Atmos. Sci.*, **64**, 2735–2739, 2007.

Jennings, D.E. *et al.* Titan's surface brightness temperatures. *Astrophys. J.*, **691**, L10, 2009.

Kleidon, A., and R.D. Lorenz. Entropy production by Earth system processes. In *Non-Equilibrium Thermodynamics and the Production of Entropy: Life, Earth, and Beyond*. Springer Verlag, Heidelberg, 2004.

Lorenz, R.D., J.I. Lunine, P.G. Withers, and C.P. McKay. Titan, Mars and Earth: Entropy production by latitudinal heat transport. *Geophys. Res. Lett.*, **28**, 415–418, 2001.

Ozawa, H., A. Ohmura, R.D. Lorenz, and T. Pujol. The second law of thermodynamics and the global climate system: A review of the maximum entropy production principle. *Rev. Geophys.*, **41,** 1018, 2003.

Paltridge, G.W. Global dynamics and climate change: A system of minimum entropy exchange. *Q. J. Roy. Meteorol. Soc.*, **101**, 475–484, 1975.

Peixoto, J.P., A.H. Oort, M. de Almeida, and A. Tome. Entropy budget of the atmosphere. J. *Geophys. Res.*, **96**, 10981–10988, 1991.

Schofield, J.T., and F.W. Taylor. Net global thermal emission from the Venus atmosphere. *Icarus*, **52**, 245–262, 1982.

Titov, D., M.A. Bullock,, D. Crisp, N.O. Renno, F.W. Taylor, and L.V. Zasova. Radiation in the atmosphere of Venus. In *Exploring Venus as a Terrestrial Planet*, ed. by L.W. Esposito, E.R. Stofan, and T.E. Cravens. Geophysical Monograph No. 176, 1121–138, American Geophysical Union, 2007.

Vardavas, I.M., and F.W. Taylor. *Radiation and Climate*. Oxford University Press, 2007.

4.9 Questions

1. Using the information in Appendix A, estimate the following:
   (a) the power output of the Sun in watts,
   (b) the stratospheric temperature on Venus,
   (c) the mean height of the tropopause above the surface of Mars.

2. Show that the energy liberated during the collapse of a sphere of mass M and uniform density, from infinity to radius R, is given approximately by:

$$E = -\frac{GM^2}{R}$$

where G is the universal constant of gravitation. Assuming this is all converted to thermal energy, give a crude estimate for the internal temperature of Jupiter by equating this energy to the mean internal energy.

3. Jupiter is observed to be still releasing its energy of formation at a rate of approximately $5.4\,\mathrm{W\,m^{-2}}$. Using the expression from the preceding question, calculate the rate at which the radius of Jupiter shrinks, expressed in $\mathrm{mm\,yr^{-1}}$. Discuss the limitations of this calculation, and possible other sources of the internal energy being released.

4. State the principle of maximum energy production and comment briefly on its justification. Derive the expression

$$\left(\frac{E_0}{E_1}\right)^{\frac{1}{4}} = \left(\frac{S_0}{S_1}\right)\left(\frac{4 + E_1/E_0 + 3S_1/S_0}{4 + E_0/E_1 + 3S_0/S_1}\right)$$

that links the incoming solar and outgoing thermal energy, S and E, respectively, from a two-box model for a planetary atmosphere. Inserting typical values for Titan and Earth, what can you conclude about the efficiency of the circulation of Titan's atmosphere relative to Earth's?

Atmospheric temperature structure

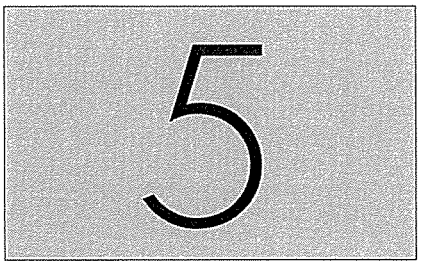

We saw in the previous chapter that about 50% of the electromagnetic radiation emitted by the Sun at wavelengths in or near the visible part of the spectrum reaches the ground on Earth, where most of it is absorbed. The lower atmosphere is then heated by the ground, and becomes unstable against convection. If the temperature gradient is too steep, lower layers will be more buoyant than those above and they will tend to rise, forcing more powerful convection. If the gradient is too shallow, the motion will stop until the temperature gradient builds up again. The net result is that the gradient is usually close to the *adiabatic lapse rate*, at which convection is just possible. Assuming that *hydrostatic equilibrium* applies, and that there is no net exchange of energy between a parcel of air and its surroundings, then the perfect gas law and some elementary thermodynamics tell us that the temperature gradient with height is just the acceleration due to gravity divided by the specific heat of the air. Thus it is constant for a given composition, and works out to be equal to approximately $10\,\mathrm{K\,km^{-1}}$ for dry terrestrial air. For moist air, it is less (about $6.5\,\mathrm{K\,km^{-1}}$ typically), and can be as small as $3\,\mathrm{K\,km^{-1}}$.

5.1 Model vertical temperature profiles for the terrestrial planets

The vertical temperature profile for an atmosphere whose composition and cloud properties are known can be calculated by solving the radiative transfer equation at each of a large number of discrete height levels, with the constraint that the emitted and absorbed energy are equal. The resulting *radiative equilibrium* profile differs from the real profile in situations where the dynamical transport of heat makes a significant contribution. This is the case in the troposphere of the Earth, where the mean thermal infrared opacity is high and convective overturning transports heat vertically with greater efficiency than radiation.[55] An analogous situation applies in the other seven substantial atmospheres in the Solar System.

A simple, approximate method of calculation provides useful insights and allows comparisons between the planets, as well as bringing out the common physics at work. This separates the atmosphere into

[55] See *Elementary Climate Physics*, Chapter 2.

two vertical regions, the lower of which (the troposphere) is optically thin at visible and near-infrared wavelengths ($\lambda < 5\,\mu$m) but optically thick in the thermal infrared ($\lambda > 5\,\mu$m). The upper layer, the stratosphere, is optically thin in a wavelength-averaged sense defined by $\bar{\tau} = \int_0^\infty \tau_\lambda d\lambda > 1$, or <1, where the optical thickness τ_λ is the product of absorption coefficient and path length. Alternatively, optically thick (or thin) can be defined to mean that a photon traversing the slab will do so with a probability of not less (or more) than $1/e$ of being absorbed or scattered.

In the troposphere, heat energy is more efficiently transferred by advection rather than by infrared radiation, despite the existence of 'windows' in the spectrum where the constituent gases are transparent or nearly so. The convective motions that transfer heat upwards tend to be adiabatic, resulting in a roughly constant vertical temperature gradient or lapse rate.

Above the tropopause, the density becomes low enough that this situation reverses, and radiative energy passes freely at most wavelengths between atmospheric layers and outwards to space. In this region, dynamics is less efficient than radiation at moving heat around and vertical motions tend to be suppressed. The resulting stably stratified stratosphere, containing in the case of the Earth about 10% of the mass of the atmosphere, is characterised to first order by a constant temperature with height.

A simple *radiative–convective model* of each Earth-like atmosphere can therefore be defined in terms of the tropospheric lapse rate $\partial T/\partial z$, the stratospheric temperature T_s, and the pressure p_t at the tropopause, where the transition between the two occurs (Fig 5.1). Alternatively, if the mean surface temperature T_0 is known, this defines the vertical temperature profile in the model without requiring knowledge of the tropopause height. The independent variables are the abundances of the principal greenhouse gases and the planetary albedo A, which is the

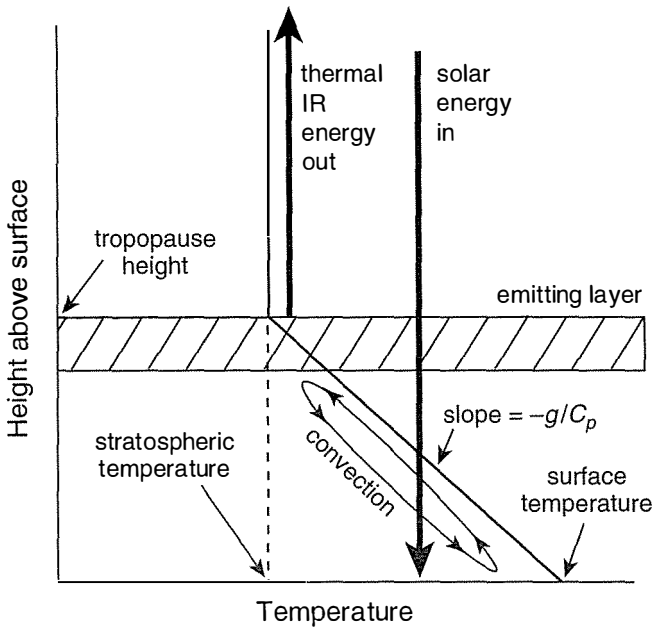

Fig. 5.1
Illustrating the basis for a simplified calculation of model vertical temperature profiles for an atmosphere like that of Mars or Earth, where most of the solar energy reaches the surface, and most re-emission of space takes place near the tropopause. Similar considerations, with modifications to allow for the different role of the surface and for internal energy sources where these exist, can be applied to Venus, Titan, and the outer planets.

fraction of the total solar energy falling on the planet that is reflected or scattered back to space.

Most of the cooling by emission to space takes place from a narrow range of altitudes near the tropopause, where the atmosphere is sufficiently optically thick to have a significant emissivity, but the overlying path is optically thin enough to allow the emitting layers to 'see' space. The energy being radiated is transported to this level from the warm surface by convection; we assume that the lower, optically thick, convectively mixed region of the atmosphere is in convective equilibrium.

The temperature gradient in the troposphere can be calculated approximately by considering a parcel of air that is raised vertically. If we assume that there is no net exchange of energy between a parcel of air and its surroundings, and that the process is reversible, then entropy s is conserved. Hence

$$\mathrm{d}s = C_p \frac{dT}{T} - \left(\frac{\partial V}{\partial T}\right)_p \mathrm{d}p = 0$$

where V is the molar volume and C_p is the specific heat capacity of one mole at constant pressure.

Assuming hydrostatic equilibrium, pressure p is related to density ρ at a given height z by $dp = -\rho g dz$, where g is the acceleration due to gravity. Assuming the ideal gas law $pV = RT$ and substituting both into the above equation and rearranging, we find

$$\frac{\partial T}{\partial z} = -\frac{g}{C_p}$$

for the dry adiabatic lapse rate.[56] Thus, the temperature gradient is constant, and, since the specific heat is equal to about 1000 J kg^{-1} K^{-1} for dry air on Earth, its value is approximately 10 K km^{-1}. The lapse rate on Venus is close to that of the Earth because the specific heat of CO_2 is nearly the same as (actually slightly less than) that for nitrogen, while the planet is slightly less massive. Mars has a significantly smaller lapse rate because of its lower mass and hence smaller value of g (Table 5.1).

For moist air, the tropospheric temperature gradient is less and can be can be calculated using the Clausius-Clapeyron equation to include

[56] In meteorology, 'lapse rate' refers to the falling off of temperature with height that is a common characteristic in the troposphere of any of the planets, and is a positive number, while dT/dz is negative.

Table 5.1 Data for calculating model temperature profiles for Venus, Earth and Mars.

Radius of the Sun (km)	700,000		
Effective temperature of Sun (K)	5780		
	Venus	Earth	Mars
Distance from Sun (Mkm)	108	150	228
Bolometric (Bond) albedo, A	0.76	0.4	0.15
Atmospheric molecular weight (g)	44	29	44
Acceleration due to gravity (m s^{-2})	8.88	9.81	3.73
Specific heat C_p (J kg^{-1} K^{-1})	830	1005	830
Tropospheric lapse rate (K km^{-1})	10.7	9.8	4.5

the important latent heat effects due to condensables such as water vapour or, on Titan, methane. The average value for $\partial T/\partial z$ on Earth is about $6.5\,\mathrm{K\,km^{-1}}$, and it can be as small as $3\,\mathrm{K\,km^{-1}}$. On Mars, the presence of airborne dust distributes solar heating throughout the troposphere, changing the lapse rate to about half of its adiabatic value. Measurements find values that are typically about $2\,\mathrm{K\,km^{-1}}$.

The lapse rate above the tropopause, where convection stops, tends to zero (i.e., constant temperature with height) because there is no longer enough absorption above the layer to stop most of the emitted photons reaching space. Then each layer is heated by radiation from the optically thick atmosphere below, and cooled by radiating to space, to the same degree; to first order, height is no longer important. This region is called the stratosphere, since it is stratified in the sense that the layers are not convectively unstable as they are in the troposphere.

The stratospheric temperature T_x may be estimated by treating the region as if it were a single slab of gas which is optically thin at all wavelengths, rather than just on average, which is the real situation. Then T_x is related to the effective radiative temperature of the Earth T_E by the expression for the energy balance of the stratosphere, treated as a slab of emissivity and absorptivity e:

$$e\sigma T_{E^4} = 2e\sigma T_{X^4}$$

whence

$$T_X = \frac{T_E}{2^{1/4}}$$

The equilibrium temperature T_E for the planet is found by using the Stefan-Boltzmann law to find the temperature at which the planet emits a total energy equal to the integrated solar irradiance S it receives (§4.2). The latter can be scaled using the inverse square law from measurements that find about $1368\,\mathrm{W\,m^{-2}}$ at the Earth's distance from the Sun, or it can be calculated from a knowledge of the effective temperature of the Sun (5780 K), the solar radius, and the planet–Sun distance.

If the model is to be completely self-contained, a method has to be found to calculate either the tropopause altitude or the surface temperature, since only the slope of the profile is known in the lower atmosphere. One way is to use a simple greenhouse model in which the atmosphere is modelled as a stack of slabs of different temperature. Consider, for simplicity, the use of a model in which the atmosphere is represented by a single slab. By definition this emits upwards and downwards at temperature T_E, the downward component adding to the solar flux heating the surface of the planet. For the example of the Earth, this additional 'greenhouse' component raises the model's surface temperature to 303 K, which may be compared to the observed mean surface temperature of about 288 K. Adding more layers improves the accuracy of this estimate, and is essential for a very thick atmosphere like Venus, although one layer works for Earth and Mars.

Table 5.2 Model-derived temperatures on the terrestrial planets.

	Venus	Earth	Mars
Radiative equilibrium temperature (K)	239	255	226
Stratospheric temperature (K)	201	214	190
Surface temperature (K)	730	290	235

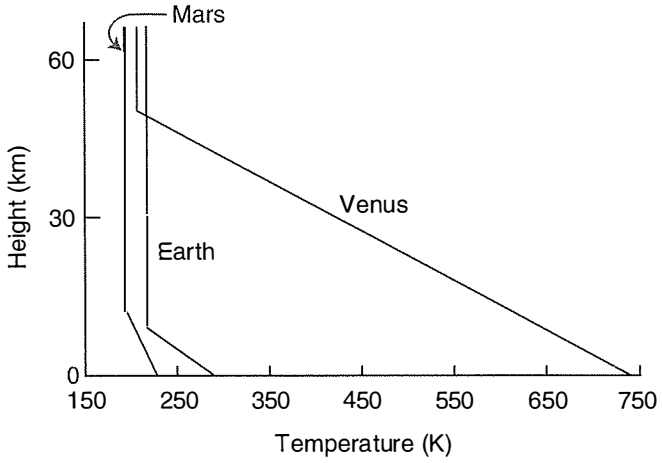

Fig. 5.2
Calculated model profiles of temperature vs. height above the surface on Venus, Earth and Mars.

With the surface temperature worked out in this way, the model is completely specified. Table 5.1 lists the input parameters for all three terrestrial planets, Table 5.2 lists the resulting model parameters, and Fig 5.2 sketches the resulting models.

5.2 Observed vs. model temperature profiles: Earth

On the Earth, the region where convection dominates vertical heat transport is known as the *troposphere* ('turning region'). The upper boundary occurs near the level where the overlying atmosphere is of such a low density that a substantial amount of radiative cooling to space can occur in the thermal infrared region of the spectrum. At the *tropopause*, radiation cools rising air so efficiently that the temperature tends to become constant with height and convection ceases. The height of the Earth's tropopause varies by about 6 km with latitude, being highest (around 16 km) in the tropics, where solar heating is greatest, but it is generally quite a distinct feature in the temperature profile everywhere, and usually occurs only slightly below the temperature minimum.

The Earth's *stratosphere* originally got its name because it is the region where convection stops and the air forms layers that tend to stay put, i.e., the atmosphere is stratified. The absence of enough absorption above the tropopause to stop emitted photons from reaching space causes the lapse rate to tend to zero (i.e., to a constant temperature with height). Each layer is heated by radiation from the optically thick atmosphere below, and cooled by radiating to space, so height is no

longer important to first order. The fact that the stratospheric temperature is soon observed to increase is a consequence of the absorption of solar ultraviolet radiation by photochemically produced ozone in the Earth's stratosphere. Ozone absorbs in the Hartley band, which forms a continuum from 0.2 to 0.3 μm. Below 70 km, virtually all of the energy absorbed is converted to heat. The ozone concentration in the stratosphere peaks near 25 km, but a calculation of the heating rate finds that this peaks at a height of about 50 km. The temperature is also a maximum at this level, which forms the *stratopause*.

Above the stratopause, the temperature declines again, reaching a minimum at the *mesopause*, where the second temperature inversion occurs, signifying the end of the *mesosphere*. The mesopause at around 50 km altitude is the coldest level anywhere in the Earth's atmosphere.

Between the tropopause, where large-scale vertical convection ceases, and the mesopause, the atmosphere remains fairly well mixed by turbulence produced by a variety of instabilities in wave motions and the mean flow. A fairly small distance up into the thermosphere, at around the 100 km altitude level on Earth, diffusion takes over as the dominant process and the atmosphere starts to separate into its lighter and heavier components. The very tenuous region above this level (the *homopause*) is often called the *exosphere*, since here light elements escape the planet's gravitational grip and are lost to space.

While the models described above are based on realistic physics, they need to be tested by comparison with observations to assess the impact of the considerable simplifications made. In addition to the assumptions relating to optical thickness in the different wavelength regimes, the model neglects any absorption that takes place in the stratosphere due to clouds, ozone etc., and also neglects all dynamical effects except convection.

Starting with the most familiar example, Fig 5.3 shows some vertical temperature profiles measured by radiosonde balloon ascents over the same location (Scandinavia) on Earth in four months of the year, chosen to represent the four seasons. Comparing these to the simple

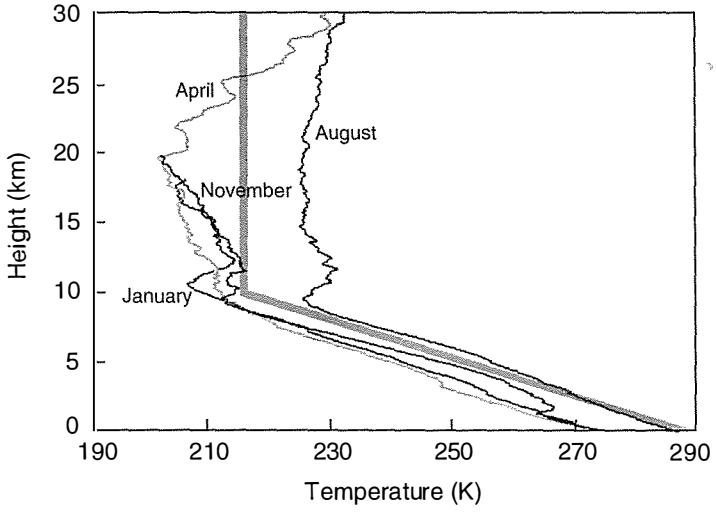

Fig. 5.3
Vertical temperature profiles measured by radiosonde balloon ascents in the months indicated, compared to a simple radiative–convective equilibrium model with a tropopause height of 10 km.

radiative–convective equilibrium model, which is meant to represent a global as well as a seasonal mean, is of course not an exact procedure, but it does give a feeling for the fact that the model representation is not too far from reality. If similar agreement is available for the less-explored planets, then we can have some confidence that (a) we understand the dominant processes at work, and (b) experiments using simple models can be used to understand the basic response of climate to changes in forcing, resulting from changes in solar flux, albedo, atmospheric composition or surface pressure. While this gives useful insights, it will always be prudent to refine any conclusions with more sophisticated models requiring large computers and complex programs to run.

5.3 Observed vs. model temperature profiles: Venus

Venus with its deep atmosphere of nearly pure CO_2 and extensive cover of sulphur-bearing clouds is in some respects an extrapolation of the current trend on Earth. The properties of the H_2SO_4 clouds on Venus contribute significantly to the high surface temperatures by scattering conservatively at short (solar) wavelengths, while strongly absorbing long-wavelength (planetary) radiation. Changes in the optical properties or depth of the cloud layers on timescales of years or longer will affect climatic variables such as surface temperature and the general circulation regime. At present, the radiative, dynamical and chemical processes appear to be in balance, but the stability of the currently observed state, which may depend on the level of active volcanism, is debatable (§9.4).

The surface of Venus is hot enough to liquefy the lower-melting-point metals, such as lead or tin, the result of an extreme case of the greenhouse effect in an atmosphere that is 96% carbon dioxide with a surface pressure of nearly 100 bars. Water vapour, sulphur compounds and the global cloud coverage also contribute to the opacity in the thermal infrared, trapping the sunlight that diffuses through the clouds to the surface at visible and near-infrared wavelengths, where the gases and particles are less absorbing.

The principal factors that maintain the present climate on Venus are probably very active volcanism, providing a steady supply of carbon dioxide, water vapour and cloud-forming sulphurous gases from the interior, and possibly chemical interactions between the surface and the atmosphere.

The assumption of an adiabatic profile with the value of the specific heat corresponding to CO_2 gives a tropospheric lapse rate of about $10\,\mathrm{K\,km^{-1}}$. The high albedo of $A = 0.76$ and the dense atmosphere, opaque at most infrared wavelengths, mean that Venus is in balance with the Sun at a radiative equilibrium temperature of only 230 K, which is less than for the Earth, while the surface temperature is a scorching 730 K. The vertical distance between the surface at 730 K and the tropopause at 230 K is then expected to be approximately 50 km, which is quite close to the observed height. Above the cloud

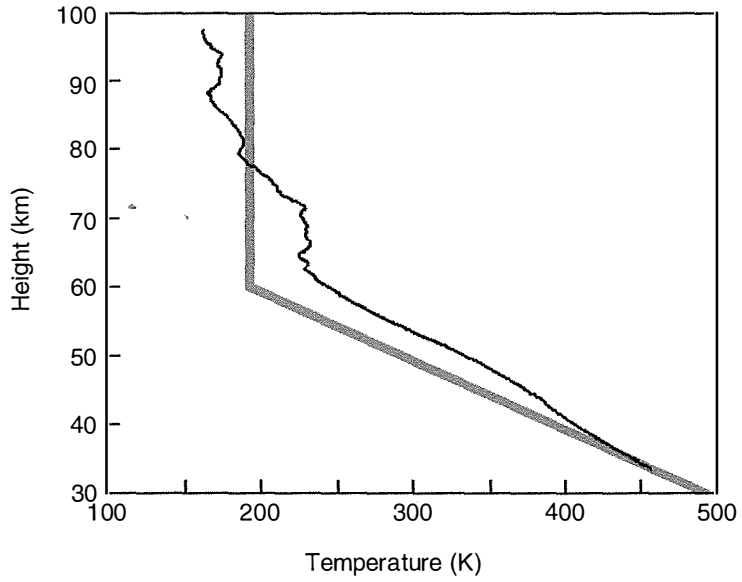

Fig. 5.4
A temperature profile from the radio occultation experiment on the NASA *Magellan* spacecraft (thin line), compared to a Venusian radiative–convective equilibrium climate model similar to that in Fig. 5.2.

tops, the atmosphere is optically thin in the thermal as well as the solar part of the spectrum; we again expect an isothermal profile like that in the terrestrial stratosphere, but here at a temperature of 193 K, cooler than the Earth. As Fig 5.4 shows, this is not far from what is observed, although there is some discrepancy, probably mainly attributable to absorption of both solar and thermal radiation in the cloud and haze layers that exist on Venus in the 40 to 70 km altitude range. The simple model, of course, makes no allowance for the effects of the clouds, except through the value of the albedo A.

5.4 The global temperature structure on Venus

The results for the diurnal variation of temperature at a given height from the *Pioneer Venus* orbiter radiometric temperature experiment (§3.8.2) show equator-to-pole gradients in the opposite sense to that expected if radiative heating dominates (Fig 5.5, left). Instead, the stratosphere is typically 15 to 20 K warmer at the pole than at the equator. This was interpreted as evidence for large-scale overturning of the atmosphere from low to high latitudes, with compressional heating in the descending branch of the circulation over the polar regions (§8.3.3). Another prominent feature linked to dynamical activity is the polar collar, a belt of cold air surrounding the polar vortex at cloud-top level, where a strong zonal jet (an isolated region of high winds) occurs.

At the equator the dependence of temperature in the stratosphere (65 to 95 km) on longitude is dominated by a wavenumber 2 solar tide with an amplitude of about 10 K (Fig 5.5, right).

Transient features, including travelling waves, are present on a wide range of scales. Night side temperatures in the mesosphere (95 to 110 km) show a local temperature maximum near the antisolar point, evidence for a subsolar-to-antisolar circulation in the low-pressure regime.

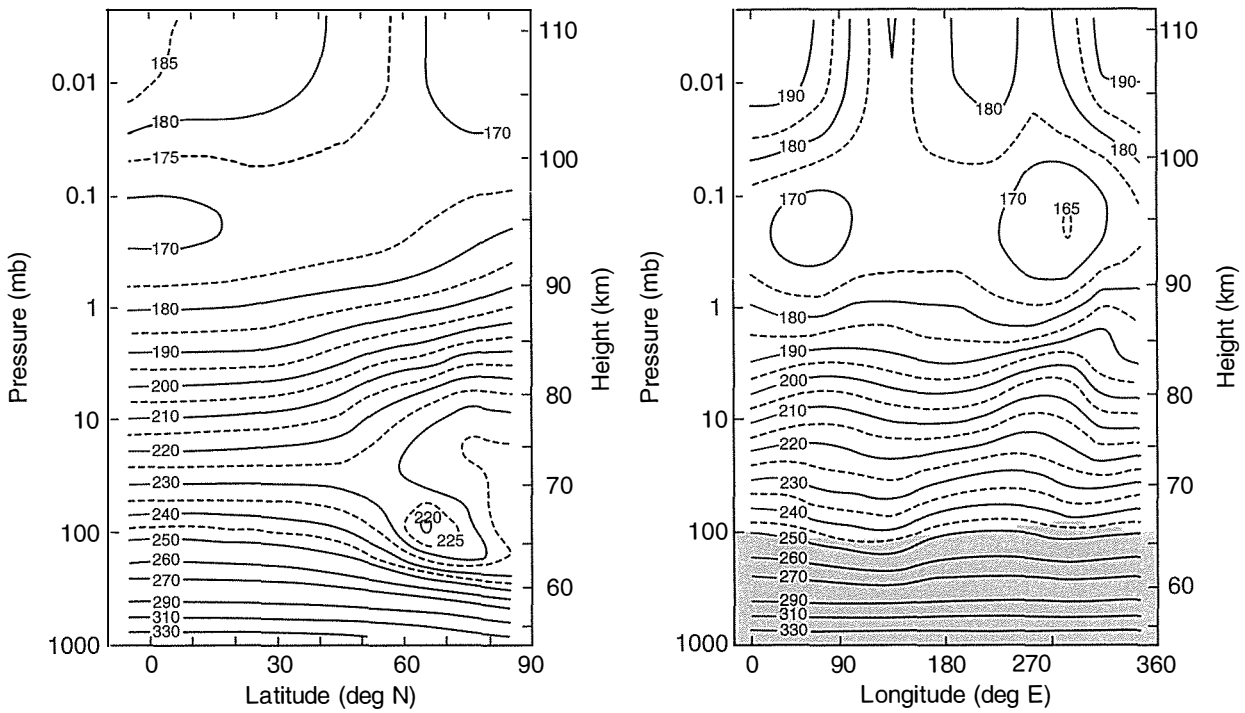

Fig. 5.5
The mean temperature field above the clouds in the northern hemisphere of Venus, retrieved from radiances measured by the *Pioneer Venus* VORTEX radiometer (§3.8.2) in 1979–80. On the left are the zonal mean temperatures (averaged over latitude), on the right are the temperatures measured within 10 degrees of the equator, as a function of longitude.

5.5 Calculated vs. measured temperature profiles: Mars

Figure 5.6 shows the profiles measured during the descent to the Martian surface of the probes *Viking 1* in 1976 and *Pathfinder* in 1997, compared to a radiative–convective equilibrium model fitted to the data by choosing a tropopause height of 50 km and a tropospheric lapse rate $\sim$2 K km^{-1}. Mars has very large global and seasonal fluctuations in temperature, so the comparison is only approximately like-with-like, and in any case it can be seen that there are large oscillations in the individual measured profiles that are generated by waves and tides in the Martian atmosphere. Nevertheless, the basic troposphere–stratosphere structure can be seen to be present.

The dry adiabatic lapse rate g/C_p is 4.5 K km^{-1} on Mars, and it might seem surprising that the observed vertical gradient in the troposphere is not closer to this in the absence of significant latent heat effects by the small amount of water vapour present. The large difference is due mainly to the absorption and emission of radiation by airborne dust. The effect of the dust loading is to modify the vertical temperature gradient by affecting the radiative balance and radically altering the lapse rate, while warming the middle atmosphere by as much as 50 or even sometimes 100 K over the predicted dust-free state.

Figure 5.7 shows global mean model temperature profiles with and without dust, assuming a solar constant of 593 Wm^{-2} and a global mean albedo of 0.25. These numbers gives 210 K for the effective

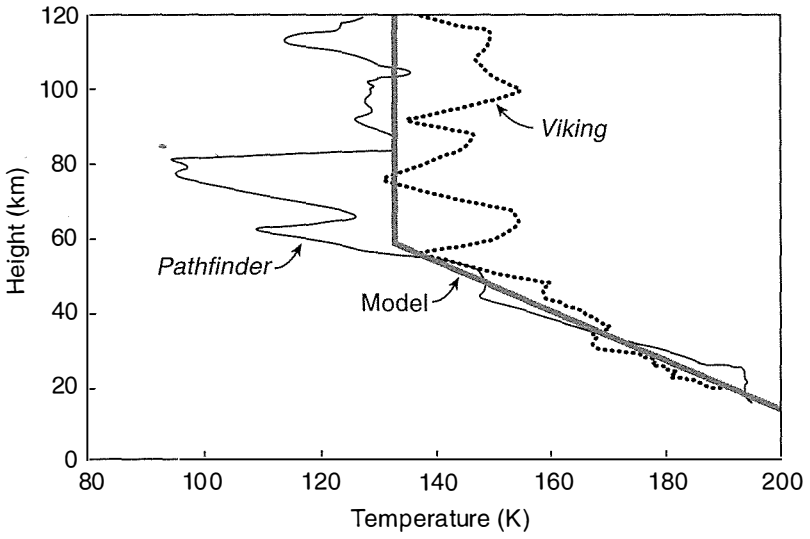

Fig. 5.6
Two measured temperature profiles in the atmosphere of Mars show large oscillations due to wave activity, but when smoothed show approximately the troposphere–stratosphere characteristics predicted by a simple radiative–convective equilibrium model, with a tropopause height of around 50 km and a dust-modified lapse rate of $\sim$2 K km^{-1}.

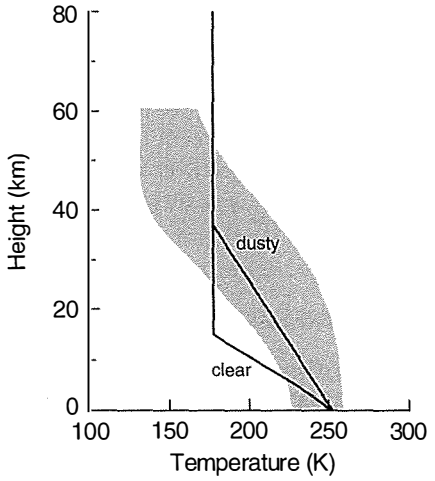

Fig. 5.7
Simple models of the mean temperature profile for present-day Mars with a clear and a dusty atmosphere, and a surface temperature of 250 K. The shaded area represents the envelope of a number of measured profiles for comparison.

radiating temperature of Mars, a predicted stratospheric temperature of 177 K, and a surface temperature, calculated from a single-slab greenhouse model, of 250 K in both cases. Using the dry adiabatic lapse rate for the dust-free case, and reducing the lapse rate to 2 K km^{-1} for the more realistic situation, raises the height of the tropopause dramatically from 16.2 km above the surface to 36.6 km. With this refinement, the simple model better fits the mean of the envelope of a set of observed temperatures on Mars, shown by the shaded area in the figure.

5.6 Calculated vs. measured temperature profiles: Jupiter

The existence of an internal energy source heats the atmosphere from below, making Jupiter's atmosphere qualitatively like Earth and Mars in this respect. The heating drives convection, which would be expected

to result in a lapse rate close to adiabatic in the troposphere. The high value of the specific heat for a hydrogen–helium mixture means that the lapse rate in Jupiter's atmosphere is only about a fifth of the corresponding terrestrial value (2 vs. $10\,K\,km^{-1}$), despite the higher gravitational field on Jupiter (Table 5.3).

The tropopause is near the cloud tops, where a transition occurs between vertical transport by convection and cooling to space by radiation. The first measurements of temperature and pressure below the clouds were made by the *Galileo* probe during its parachute descent into Jupiter's atmosphere on 7 December 1995. The thermal structure at the probe's low-latitude entry site was determined from a pressure level of 10^{-9} bars, approximately 1000 km above the 1 bar pressure level, to 132 km below the 1 bar level, where the pressure was 22 bars. The probe showed the temperature does follow the dry adiabat quite closely between 0.41 and 24 bars, consistent with the low water content found by the mass spectrometer, although the lapse rate from 5 to 15 bars was slightly sub-adiabatic, corresponding to a static stability of about $0.1\,K\,km^{-1}$.

The probe entered the atmosphere in one of the relatively cloud-free belts, which corresponds to the descending branch of the large-scale convection cells that appear to donate the circulation on Jupiter (cf. Fig 8.4). This may explain the dryness of the atmosphere, with water vapour and hence oxygen under-abundant by a factor of 10 or more relative to cosmogonical expectations (§6.12, §6.13). It could also explain the static stability, the non-zero value of which suggests that upward heat transport is not attributable to convection at this location. A second probe in one of the adjacent belts would, in this interpretation, have shown much higher levels of humidity and a super-adiabatic gradient, indicating the substantial upward transport of heat and 'moisture' (whether water, ammonia or another volatile species). Associated with this would be latent heat effects, and, especially where cloud formation occurs, the actual profile should differ substantially from the dry adiabat. New probe missions to Jupiter to see if this is indeed the case have been discussed, but so far not implemented.

If the lapse rate is known or can be inferred it can be used to construct simple models for Jupiter, like those for the terrestrial planets. Using the measured planetary albedos to calculate the stratospheric temperature,

Table 5.3 Gravitational acceleration g, specific heat C_p, and dry adiabatic lapse rates g/C_p for the eight atmospheres of the Solar System.

	g m s^{-2}	C_p J gm^{-1} K^{-1}	Adiabatic lapse rate $K\,km^{-1}$
Venus	8.89	0.8501	10.468
Earth	9.79	1.0040	9.760
Mars	3.74	0.8312	4.500
Jupiter	24.25	12.3591	1.963
Saturn	10.00	14.0129	0.714
Uranus	8.80	13.0137	0.676
Neptune	11.10	13.0137	0.853
Titan	1.35	1.0440	1.301

as before, the only missing factor is the tropopause height. In sophisticated model atmospheres, this is computed from the radiative transfer equation, using theoretical and laboratory data on the spectral properties of the atmospheric gases. Hydrogen and helium, being symmetric molecules, lack fundamental vibration–rotation bands and so tend not to interact significantly with infrared photons at moderate pressures of 1 bar or less. So, around the tropopause region and above, the main source of opacity is the minor constituents, such as ammonia and methane, analogous to the role of carbon dioxide for the Earth.

Jovian radiative transfer calculations can be complicated, however. The path lengths on such a large planet are very long, and even weak transitions, such as those responsible for the hydrogen quadrupole bands, make a significant contribution in regions where strong bands of ammonia and methane are absent. In the deep troposphere, the opacity is dominated by pressure-induced bands of hydrogen. At low pressures, hydrogen has no important absorption bands in the infrared because of the symmetry of the molecule, but at higher pressures the molecules are distorted by collisions, producing temporary, induced dipole moments and transitions between rotational states. This kind of absorption, involving N_2, CH_4, and H_2, actually dominates in the atmosphere of Titan, as will be discussed below.

Calculated radiative–dynamical equilibrium model profiles, which include the pressure-induced bands, place the Jovian tropopause at a pressure close to 1 bar, the mean surface pressure on Earth. Adopting this value, we find that the 'two straight line' model based on simple physics is a useful, although not perfect, fit to the vertical temperature profile on Jupiter (Fig 5.8). Similar results can be obtained for the

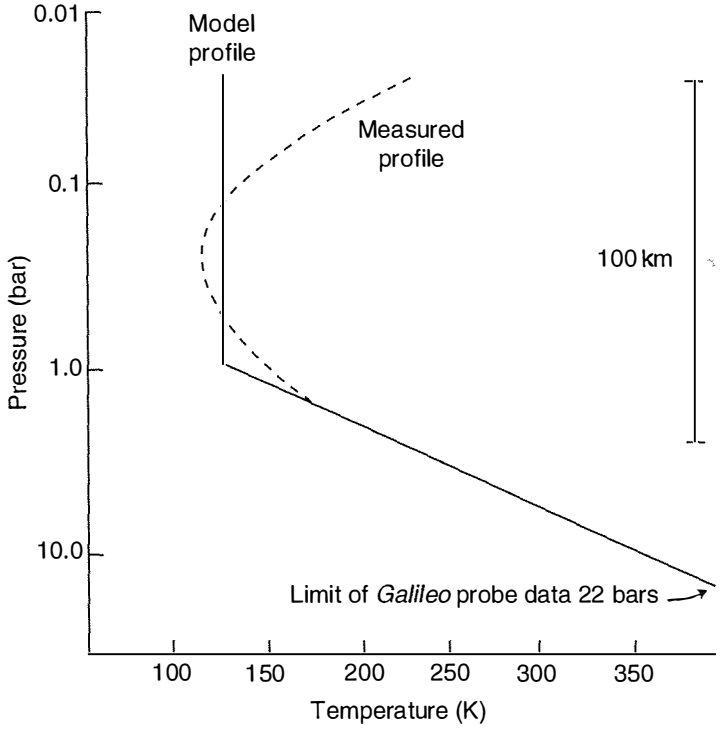

Fig. 5.8
A simple radiative–convective Jovian model temperature profile for an internal energy source equal to the solar input, compared to a curve representing the mean of measurements made by various spacecraft. In the troposphere, the measurements are direct thermometry by the *Galileo* probe; near the tropopause and above they are a smoothed combination of data from radio occultation experiments and infrared remote sensing instruments on the *Pioneer*, *Voyager*, and *Galileo* spacecraft.

other giant planets. The main deficiency is in the upper atmosphere, due (as on Earth) to a source of heating in the stratosphere producing a temperature rise that is not represented in the simple model. Jupiter has no ozone layer, of course; there, the heating is due to absorption of sunlight by hydrocarbon gases and by aerosols produced photochemically from those gases, especially methane, in the stratosphere and above. Similar processes are important on all of the outer planets, and also on Titan.

The temperature in the atmosphere at every level depends on the magnitude of the internal heat source. In the simple model, we would not expect the tropopause height, which depends on the opacity profile of the atmosphere and hence primarily on its composition, to vary much if the internal source changed by a small factor, although there is a relatively weak dependence of absorption coefficient on temperature. Thus, the tropospheric lapse rate remains almost unchanged, but the stratospheric temperature increases. Suppose the internal source changes from its present value, taken for simplicity to be equal to the solar input (Table 4.3), and increases by a factor of three, so the net output is four times the solar input rather than twice. Then the stratospheric temperature T_x increases from $T_E/2^{0.25}$ to become just equal to T_E. This model is shown, along with the case for no internal source, in Fig 5.9.

The other outer planet atmospheres can be dealt with in a similar way, using estimates of the internal heat source and the albedo from measurements by broadband radiometric instruments, and temperature sounding measurements by infrared spectrometers and radio occultation profile inversions. The resulting profiles are summarised in Fig 5.10. As would be expected, they get progressively cooler with

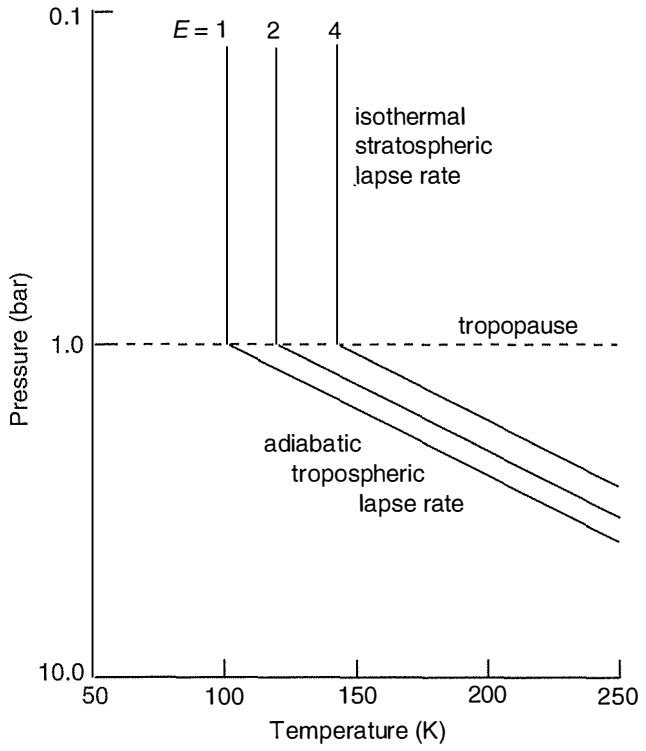

Fig. 5.9
Jovian model temperature profiles for three values of the internal energy source, zero, one, and three times the solar input, corresponding to total heat input $E = 1$, 2 and 4 times solar.

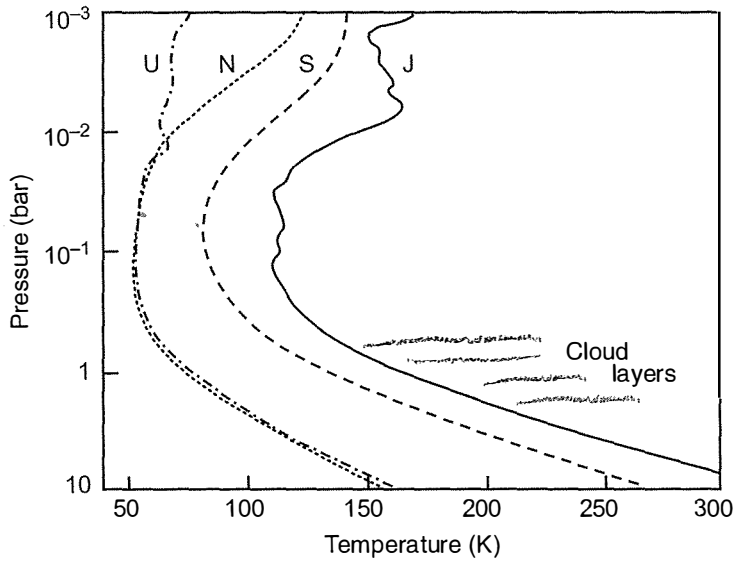

Fig. 5.10
Representative vertical temperature profiles for the atmospheres of the outer planets based on measurements and models. Neptune is as warm as Uranus despite its greater distance from the Sun because Neptune has a measurable internal source of heat, while that on Uranus appears to be negligible.

distance from the Sun and smaller internal sources; in the case of Uranus and Neptune these effects almost balance, giving very similar profiles, except in the thermosphere.

5.7 Thermal structure in Titan's atmosphere

The *Huygens* probe which landed on Titan in January 2005 obtained a profile of temperature as a function of altitude as it descended (Fig 5.11). In the upper atmosphere, from about 1400 km down to 150 km, the measured deceleration was used to infer pressures and densities, which were then converted to temperature using the equation of state for a perfect gas with an appropriate value for the atmospheric mean molecular weight. Below 150 km, measurements with higher accuracy (better than 1 K) were obtained by direct measurement, using temperature-sensitive resistors ('thermistors') exposed to the atmosphere as thermometers.

By analogy with the Earth, Titan's atmosphere is subdivided into regions defined by the way temperature varies with height above the surface. On both planetary bodies, the temperature profile is characterised by *inversions* produced by a localised region of heating, such as occurs in the middle atmosphere of the Earth due to the absorption of solar radiation by ozone, and on Titan in methane and other hydrocarbons, as well as the high haze layers. The regions between the temperature maxima and minima are given similar names in both atmospheres, but the vertical extent of each region is different, with Titan's atmosphere generally being more extensive than the Earth's due mainly to the lower gravity. In fact, the extent of Titan's atmosphere is comparable to the radius of the solid body (2575 km), while that of the Earth is sometimes likened to the skin on a grape.

About 10% of the electromagnetic radiation emitted by the Sun at wavelengths in or near the visible part of the spectrum reaches the ground on Titan, where it heats the ground sufficiently for the atmosphere to become unstable against convection. Since Titan has the same

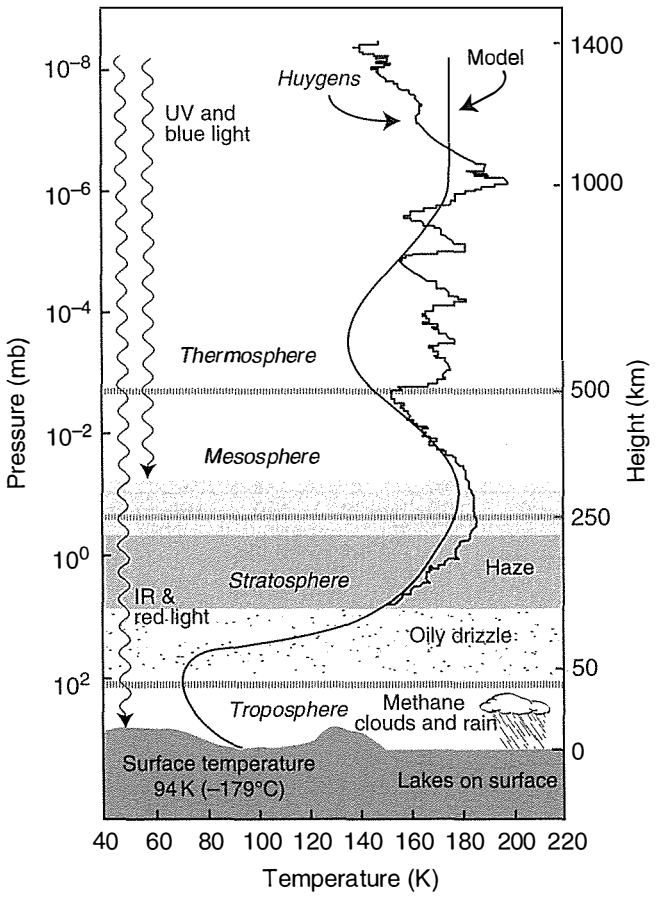

Fig. 5.11
Titan atmospheric temperature profiles from *Huygens* descent measurements and a model atmosphere based on global measurements by infrared remote sensing, showing the temperature profile, clouds and haze layers, precipitation, and surface, and some of the important radiation fluxes. The two coincide closely below the haze layers.

main atmospheric constituent as on Earth, the resulting lapse rate differs mainly due to the difference in gravity, and its value on Titan works out to be only about $1.4\,\mathrm{K\,km^{-1}}$. Again, this varies depending on the amount of condensable vapour present, mainly in the form of methane. The temperature lapse rate measured by *Huygens* is shallower (more stable) than the dry adiabatic lapse rate – the rate for the buoyancy of a dry air parcel to just balance the vertical pressure gradient – but does support moist convection.

The temperature falls with height from the surface of Titan up to about 40 km, so this level is referred to as the tropopause by analogy with Earth. At the *Huygens* entry site, the probe's sensors found that the temperature minimum, and hence the tropopause temperature, was 70.43 K at about 44 km, where the pressure was 115 ± 1 hPa. This is about 1 K colder than the earlier *Voyager* radio occultation measurements, but most of this difference can be ascribed to the assumption by *Voyager* scientists of an atmospheric composition of pure N_2. The addition of 1.5% of methane brings the two measurements into agreement, a remarkable result considering they were made at different locations on Titan, and more than twenty years apart.

By analogy with this philosophy for naming the troposphere, the lower stratosphere on Titan is then the shallow, quasi-isothermal region near 50 km, while the upper stratosphere is the much deeper region from about 50 to 300 km altitude where temperature increases

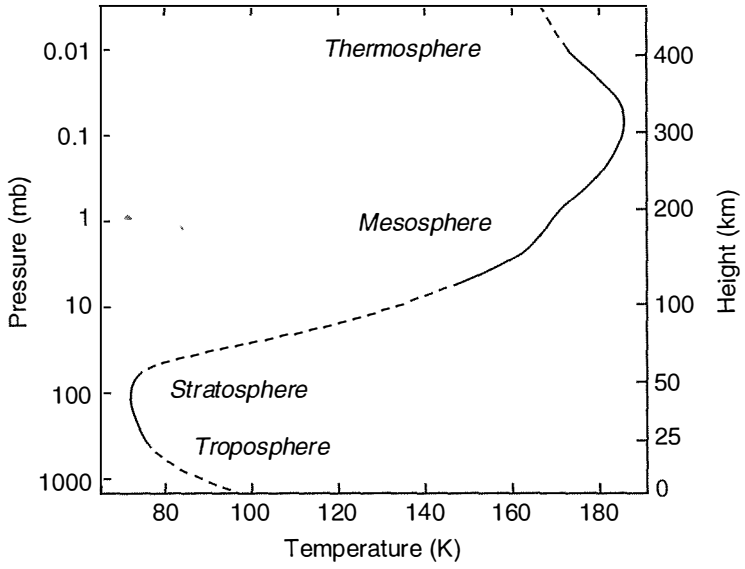

Fig. 5.12
A vertical temperature profile in Titan's atmosphere retrieved from infrared spectra obtained by the *Cassini* CIRS instrument. The dotted segments are those parts of the profile where these measurements have little information and the profile relaxes to the a-priori model, which is based on *Voyager* radio occultation profiles.

with height, i.e., the region between the first temperature minimum and the first maximum above the surface.

On Titan, the temperature increase in the upper stratosphere is due to the heating effect of the absorption of UV solar radiation by different gases and aerosols. In the measurements by *Huygens*, the temperature rises from a minimum of 70.43 K at 44 km altitude (where the first temperature inversion occurs) to 186 K at 250 km. Prior to *Huygens* entry measurements, data from the Composite Infrared Spectrometer on *Cassini* provided information on the lower and upper stratosphere from roughly 70 to 400 km in altitude. This indicated the presence of a stratopause at around 310 km altitude with the same maximum temperature of 186 K found by *Huygens* and *Voyager* (Fig 5.12).

As for the other atmospheres of the Solar System, Titan's stratosphere can be modelled as an optically thin slab and its temperature related to the effective radiative, or equivalent blackbody, temperature of the planet by the radiation laws. The stratosphere is heated from below by the infrared flux from the planet, and cooled by emitted fluxes in the upward and downward directions, each assumed proportional to the fourth power of its temperature. By balancing the two, we find that the mean stratospheric temperature is about 70 K for Titan, close to what is observed just above the tropopause before heating in the haze layers takes over. Above the stratopause, the temperature declines again, reaching a minimum at the mesopause, which on Earth is at around 80 km altitude. This is the coldest level anywhere in the Earth's atmosphere, at about 180 K. *Huygens* observed an inversion region corresponding to the mesopause on Titan at 490 km with a temperature of 152 K.

The pressure at the mesopause is only a few microbars. With such low densities of gas above, solar photons in the extreme ultraviolet and very energetic particles penetrate into the region, ionising and dissociating molecules and releasing kinetic energy, causing the temperature

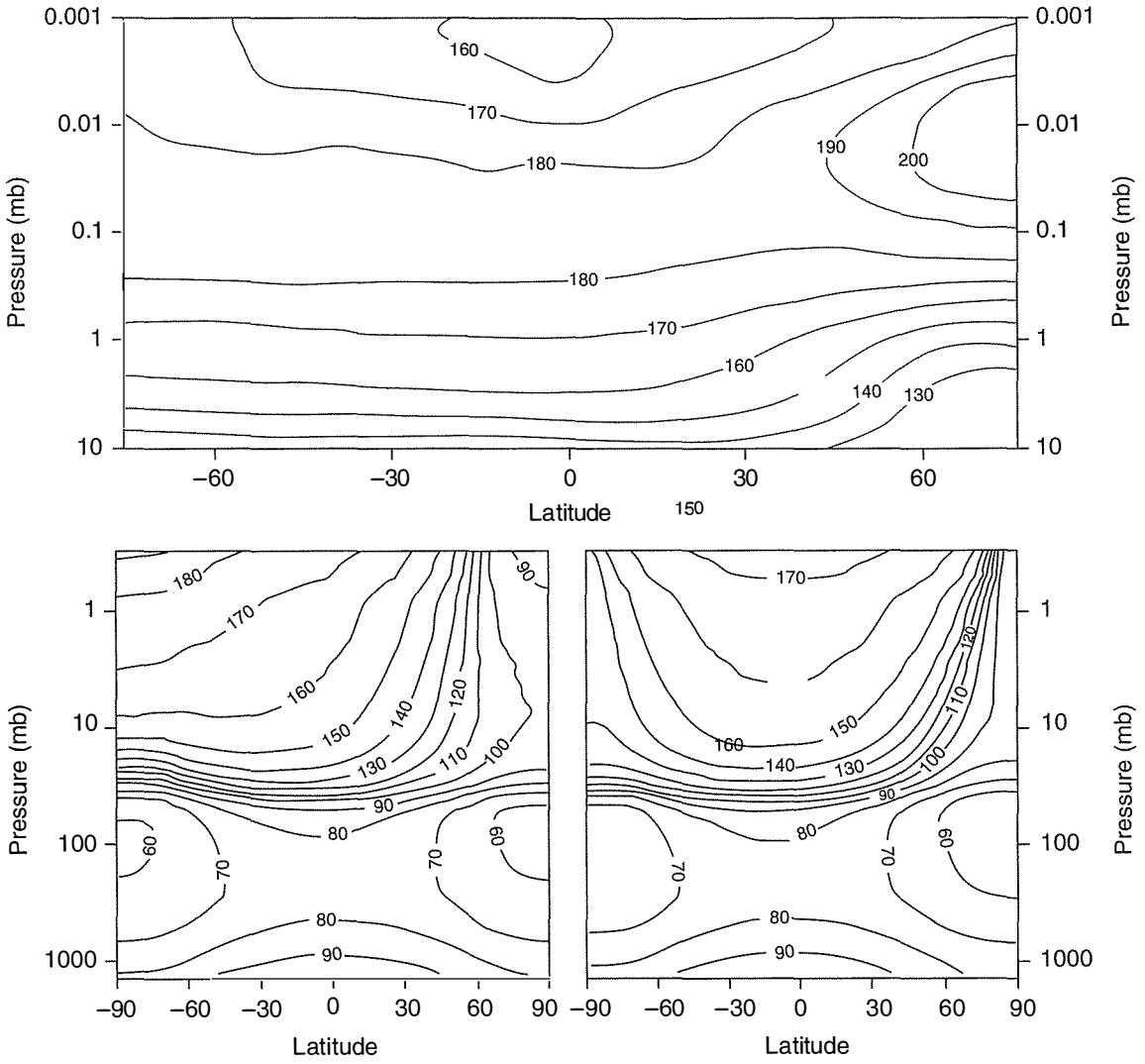

Fig. 5.13
Measured and modelled meridional cross sections of zonally averaged temperature (K) in Titan's atmosphere, from *Cassini* CIRS data (top) and computed by the 2D theoretical model of Hourdin *et al.* (1995), below. In the model output, northern winter solstice is represented on the left and spring equinox on the right; the measurements are averages over an extended period in northern winter. Note the differences in vertical scale due to limitations in the height coverage that the measurements have so far achieved.

to increase rapidly with height. The Earth's thermosphere begins at around 85 km altitude and, depending on solar activity, reaches temperatures of more than 1000 K. On Titan, the thermospheric temperatures were expected to increase steadily with altitude from about 140 K at the mesopause at around 600 km, up to around 190 K above 1200 km. *Huygens* found rather higher temperatures than the models predicted (Fig 5.11), an average temperature of 170 K with vertical oscillations 10–20 K in amplitude produced by gravity waves and tidal phenomena. Since Titan's atmosphere is generally much more extended than Earth's, the exosphere begins much higher above the surface, at an altitude of around 1200 km.

Atmospheric temperature data for Titan are still quite scarce, although radio occultation and infrared sounding data from *Cassini* are improving the situation. Figure 5.13 shows the global distribution

of temperature as predicted by a general circulation model in 1995. The *Cassini* data find similar temperatures to the model where they overlap in the upper atmosphere, but nadir observations of surface temperature by the same instrument find that the model predictions of the latitudinal temperature gradient at the surface are too high by a factor of three or four (see §4.7). Measurements and models agree that seasonal variations are greatest in the upper atmosphere (§8.6).

5.8 References and further reading

Achterberg, R.K., B.J. Conrath, P.J. Gierasch, F.M. Flasar, and C.A. Nixon. Titan's middle-atmospheric temperatures and dynamics observed by the *Cassini* Composite Infrared Spectrometer. *Icarus*, **194**, 263–277, 2008.

Bagenal, F., W. McKinnon, and T. Dowling, eds. *Jupiter: The Planet, Satellites and Magnetosphere*. Cambridge University Press, 2004.

Flasar, F.M. *et al.* Temperatures, winds, and composition in the Saturn system. *Science*, **307**, 1247–1251, 2005.

Hourdin, F., O. Talagrand, R. Sadourny, R. Courtin, D. Gautier, and C.P. McKay. Numerical simulation of the general circulation of the atmosphere of Titan. *Icarus*, **117**, 358–374, 1995.

Irwin, P.G.J. *Giant Planets of Our Solar System: Atmospheres, Composition, and Structure*, 2nd edition. Springer, 2009.

Schofield, J.T., and F.W. Taylor. Measurements of the mean solar-fixed temperature and cloud structure of the middle atmosphere of Venus. *Q. J Roy. Meteorol. Soc.*, **109**, 57–80, 1983.

5.9 Questions

1. The solar irradiance at the mean distance of Venus from the Sun is $2626\,\mathrm{Wm}^{-2}$ and the Bond albedo of the planet is 0.76. Show that the planet should be in radiative equilibrium with the Sun at a temperature of about 240 K. Explain, with the aid of a simple adiabatic model of the vertical temperature profile and a sketch, how Venus can have a surface temperature of about 740 K.

2. Assuming any reasonable value for the albedo of the planet and its mean surface temperature, and a solar constant $S = 1360\,\mathrm{Wm}^{-2}$, calculate the values describing the temperature profile in a simple model of the present-day atmosphere of the Earth, assuming a dry adiabatic lapse rate in the troposphere and an isothermal stratosphere in radiative equilibrium, given that the radiative equilibrium temperature of the Earth with respect to the Sun is 255 K. Sketch the model profile, indicating the value of key parameters on the sketch.

3. In a theory of the early Earth, all of the greenhouse gases in the atmosphere have twice their present-day abundances. Indicate approximately how the dry model temperature profile from the first part of the question would change in response to this difference in composition. (Assume the 'strong absorption limit', in which the optical depth of an atmospheric path is proportional to the square root of the number of absorbing molecules it contains, and that the Earth's albedo is the same as at present.) In a new sketch, add this profile to the one derived in the previous question, indicating the approximate values of the stratospheric and surface temperatures, and the height of the tropopause, in each case.

   A version of the 'early Earth' model further assumes that the atmosphere then was more cloudy than at present, resulting in an albedo that is twice the present-day value. Add this profile, and its defining values, to the sketch.

4. A star is losing mass at a rate of 5 million tonnes per second, all of which is converted into radiation. It is orbited by three rapidly rotating planets, A, B, and C, in circular orbits of radius 50, 100 and 150×10^6 km, respectively. These are identical except that the closest has no atmosphere, the second has a cloudy atmosphere and the third has an atmosphere without cloud. Estimate the surface temperature T_s at the equator on each planet.
   (You may make the following simplifying assumptions:
   (a) The albedo is 0.3, the emissivity is 1.0, and the obliquity is zero for all three planets.
   (b) The atmosphere, where present, may be modelled as a vertically homogeneous slab of temperature T_a, which is transparent in the near infrared but opaque at longer wavelengths.
   (c) The cloud, where present, consists of conservatively scattering particles that increase the planetary albedo to 0.8, but do not absorb photons.
   (d) Heat transfer around the globe by conduction or advection can be neglected.)

   Now consider the situation where assumption (d) no longer applies and the atmospheric circulation is so vigorous that the surface temperature is the same everywhere on planets B and C. What are their surface temperatures now?

5. In a simple global mean model of the atmosphere of Jupiter, the temperature in the stratosphere is 120 K and the lapse rate in the troposphere is $2\,\mathrm{K\,km^{-1}}$. Show that these approximate figures are consistent with the idea that Jupiter has an internal source of heat that is approximately equal to that which it receives from the Sun.
   What would the temperature in the stratosphere and the lapse rate in the troposphere in the model become if the internal source were three times as large as it actually is? Illustrate this with a sketch of temperature vs. height for both the original and the new model atmospheres.

6 Atmospheric composition and chemistry

In a first look at the compositional variations between atmospheres in the Solar System, the thing that stands out is the predominance of hydrogen and helium in the giant outer planets, gases that are rare in the terrestrial planet atmospheres. The basic reason (§2.4) is that the outer Solar System was cold enough to condense ices that led to rapid growth of protoplanets massive enough to retain large amounts of the light gases present in the primordial nebula. This also accounts for the much larger size of the outer planets compared to Earth, and for the great depth of their atmospheres.

Other contrasts that stand out are the anomalous nature of Earth's atmosphere within the inner Solar System, attributable to the equitable temperature for liquid water and the development of life, and the peculiar case of Titan, the only outer planet satellite with a thick atmosphere. More subtle differences in composition between the atmospheres of Venus, Earth, and Mars on the one hand, and Jupiter, Saturn, Uranus, and Neptune on the other, give many clues to the evolution of the planets, and are important for understanding the science of climate and meteorology.

In this chapter, we are primarily concerned with the processes that affect the composition of each atmosphere, and the extent to which they are common throughout. Some of these processes that can change the climate over long periods of time are very slow, like the loss of certain species to space or the combination of others with surface minerals. Other processes are fast, like ozone photochemistry, and these can produce seasonal or even diurnal variations. The slow processes are dealt with in the chapters on atmospheric evolution (Chapter 2) and climate change (Chapter 9), and are only considered briefly here.

6.1 Bulk compositional of terrestrial planetary atmospheres

Variations in atmospheric composition on the inner planets may be due to many factors, principally:

1. gradients in the composition of the protosolar nebula from which the planets condensed,

Table 6.1 Atmospheric composition on Venus, Earth, and Mars expressed as fractional abundances for the main components and parts per million or billion (ppm or ppb) for minor constituents. Water vapour is very variable on all three planets, as is sulphur dioxide on Venus and Earth.

	Venus	Earth	Mars
Carbon dioxide	0.96	0.0003	0.95
Nitrogen	0.035	0.770	0.027
Argon	70 ppm	0.0093	0.016
Water vapour	~10 ppm	~0.01	~0.0003
Oxygen	trace	0.21	0.0013
Sulphur dioxide	~150 ppm	~0.2 ppb	0
Carbon monoxide	40 ppm	0.12 ppm	0.0007
Neon	5 ppm	18 ppm	2.5 ppm

2. different escape rates for gases leaving the planet, as a result of the different rates of particle and photon irradiation of the upper atmosphere, and the differences in gravitational attraction,
3. physical and chemical processes, which depend directly or indirectly on distance from the Sun, and which govern the exchange of material between the surface and interior of the solid planet and the atmosphere.

The primary atmospheres of all four inner planets (i.e., those that formed with the solid bodies themselves) were lost in the distant past during the T-Tauri phase of the Sun (§2.3.5). The present atmospheres are secondary, i.e., produced by the outgassing of carbon dioxide, water vapour, nitrogen and other gases from the crust, augmented by an influx of cometary and meteoritic material. The amount of each gas, and the admixture of other gases, depends on the initial composition of each planet and its subsequent evolution, particularly its thermal history. Some gases, such as argon, are produced by the decay of radioactive materials and leak out from the crust to form a significant component of the present day atmospheres of Venus, Earth, and Mars (Table 6.1).

6.2 'Original' vs. 'derived' composition

Following the formation of the early versions of the current atmospheres, the principal gases present were primarily carbon dioxide and water vapour, with significant amounts of nitrogen and argon, and traces of other gases like neon and sulphur dioxide. Sulphur-rich gases, especially SO_2, were copiously emitted by the early volcanoes, but most of it was quickly washed out of the atmosphere because it is so soluble in water, ending up as sulphates and other compounds in the crust. Similarly, any ammonia that was not converted by photochemistry to nitrogen would dissolve and end up in sedimentary material in the regolith.

The fact that the Earth has so much water implies that all three planets must have been very wet to start with. There is no plausible

mechanism for concentrating the water on just one of a family of planets forming close together from a common supply of material. Most of the water originally on Venus and Mars has either escaped from the planet or remains hidden under the surface.

The atmospheric pressure on the early Earth was probably considerably higher than it is now, due mainly to a high abundance of carbon dioxide. If so, it would have been more like present-day Venus. Over time, however, the oceans removed CO_2 to produce carbonate rocks, a process that probably also happened on Mars and Venus, although perhaps to a lesser extent. Apparently, Venus either lost most of its water too soon for much carbonate production to occur, or else the carbonates were later recycled back into the atmosphere as CO_2. Such recycling requires the kind of high temperatures found only in the interior so, if it was important, this implies that Venus had plate tectonic activity in the past, a process that seems to be absent now. Radar images of the surface of the planet show none of the large plates normally associated with crustal overturning on Earth.

Carbonate production on Mars would have declined when the liquid water on the surface froze three or four million years ago. Only fairly small amounts of carbonate rock or dust have been found on Mars to date, and none on Venus, although this may not mean much, since it is not easy to look, and there have been almost no analyses of the regolith, especially on Venus. It is possible that large carbonate deposits await discovery underground on both planets, covered by windblown deposits or lava flows over the eons since they were laid down.

A significant amount of the early atmosphere on Mars, including much of the original water, could have been lost, along with CO_2 and nitrogen, during massive impacts at the time when the Solar System contained much more randomly circulating debris. The cratering record on the Moon and Mars speaks of a period of heavy bombardment some four billion years ago. Venus would also have been bombarded, but is more massive and could retain more of its atmospheric CO_2. In addition, Venus seems to have remained volcanically active much longer than Mars, so its atmosphere has been replenished by volcanoes right up to the present epoch.

On the other hand, being closer to the Sun, Venus lost (and continues to lose, see §6.7) water by dissociation in the upper atmosphere, followed by escape of hydrogen and oxygen, while at least a large fraction of the early water on Mars is still there as ice and buried permafrost. The lower temperature and vapour pressure of water on Mars reduces but does not eliminate the loss of water by processes such as solar wind sputtering.

To explain the gross characteristics of the present-day atmospheres, these events need to be quantified, along with factors such as the roles of atmospheric and heterogeneous chemistry, and of phase changes, such as cloud and ice formation. The history of water on each planet, and the other information that can be gleaned from relative abundances and isotopic ratios within individual elements, involve both the common reactive species (H, He, C, O, N, S) and their products, and the rare and noble gases (Ar, Kr, Xe, Ne, etc.).

6.3 Processes causing compositional variations

Following the overview above, we look more closely at individual processes and their relative importance on each planet.

1. The gravitational separation of species in the exosphere, where the density is very low and there are few collisions, affects the availability of species for removal from the atmosphere to space, for example, by thermal escape or solar wind erosion (§2.5), and affects the long-term evolution of the atmosphere.
2. The evaporation and condensation of volatile species onto and out of the polar caps, as occurs with water and carbon dioxide on Mars, affects the spatial distribution of important sources. The effects are greatest at high latitudes, but tend to propagate across the hemisphere. They could lead to the long-term migration of water from one pole to the other if the seasonal reversal, in which dry ice and water ice in each polar cap evaporates in the spring while the other becomes a sink for both species in the autumn, and vice versa, is not symmetrical.
3. Volcanic sources produce plumes of sulphur dioxide and other gases on Venus, and methane is believed to escape from cryovolcanoes on Titan. Even continuously erupting volcanoes vary in intensity, so these again are likely to be time-dependent sources, both individually and in a globally averaged sense.
4. Chemical reactions in the gas phase, for instance, those that involve H_2SO_4 on Venus, ozone on Earth, and carbon monoxide on Mars, may be cyclical or permanent.
5. Condensation to form clouds removes gases from the atmosphere. On Jupiter, the visible cloud tops seen over most of the disc consist mostly of frozen ammonia, with NH_3 gas greatly depleted in the cold atmosphere above relative to its abundance in the warmer atmosphere below.
6. Photochemical destruction, for instance, of methane and certain other hydrocarbons on Earth and Titan, reduces the abundance at higher altitudes and lower latitudes until they are replenished by sources on the surface.
7. Chemical removals by reaction with the surface, for instance, carbonate formation from CO_2 and sulphate formation from SO_2, in the atmospheres of the terrestrial planets.
8. Catalytic reactions on cloud droplets, as in the Antarctic ozone 'hole' on Earth, where heterogeneous chemistry on ice clouds accelerates catalytic reactions between ozone and trace species, including compounds of chlorine and other halogens.
9. Dynamical transport from source regions or to sinks can greatly affect composition, for instance, ozone amounts at low latitudes on Earth tend to be lowest where the production is greatest because of the way the stratospheric circulation behaves. Ozone production by solar UV radiation occurs principally in the tropical upper stratosphere, but most of the ozone is found in the mid-to-high latitudes of the northern and southern hemispheres. The circulation (§8.2)

transports ozone from the tropics polewards, and down into the lower stratosphere at high latitudes.

6.4 Key chemical cycles

Investigations of the composition of the terrestrial planetary atmospheres have revealed some key chemical cycles that have important effects on the abundances of the major and minor atmospheric constituents. Among the most important are those that involve H_2SO_4 on Venus, ozone on Earth, and carbon monoxide on Mars. It is important to emphasise, however, that the chemistry, like the physics, is the same for all atmospheres; all interactions go on everywhere, just not necessarily to the same degree, since the boundary conditions are different.

On Venus, and Earth, and probably early although not present-day Mars, sulphuric acid aerosols are a key component of the climate system. These form when volcanically produced SO_2 reacts with atomic oxygen, produced by photolysis of water vapour, to produce SO_3, which then combines with more water, thus:

$$SO_2 + O + M = SO_3 + M$$

where M is any molecule, followed by:

$$SO_3 + H_2O = H_2SO_4$$

This sequence is shown as part of a larger family of reactions in Fig. 6.1. Also shown is a summary of the factors controlling ozone in Earth's middle atmosphere, in this case including the important effects of transport and catalytic reactions. The basic chemical scheme consists of a set of four reactions, two representing the production:

$$O_2 + h\nu_1 \rightarrow O + O,$$
$$O + O_2 + M \rightarrow O_3 + M$$

and two representing possible paths for the destruction of ozone:

$$O_3 + h\nu_2 \rightarrow O + O_2$$
$$O + O_3 \rightarrow 2O_2$$

where $h\nu_1$ represents a photon in the spectral range that dissociates oxygen (about 0.1 to 0.2 μm), and $h\nu_2$ a photon in the range that dissociates ozone (about 0.2 to 0.3 μm).

The bottom part of Fig. 6.1 shows the CO_2–CO–CO_2 cycle on Mars, which is believed to provide the answer to a long-standing mystery. Solar ultraviolet radiation can penetrate right down to the surface on Mars, thus easily dissociating large amounts of carbon dioxide to form the monoxide, which is much more stable against the effects of UV photons:

$$CO_2 + h\nu \rightarrow CO + O \quad (\lambda < 224\ \text{nm})$$

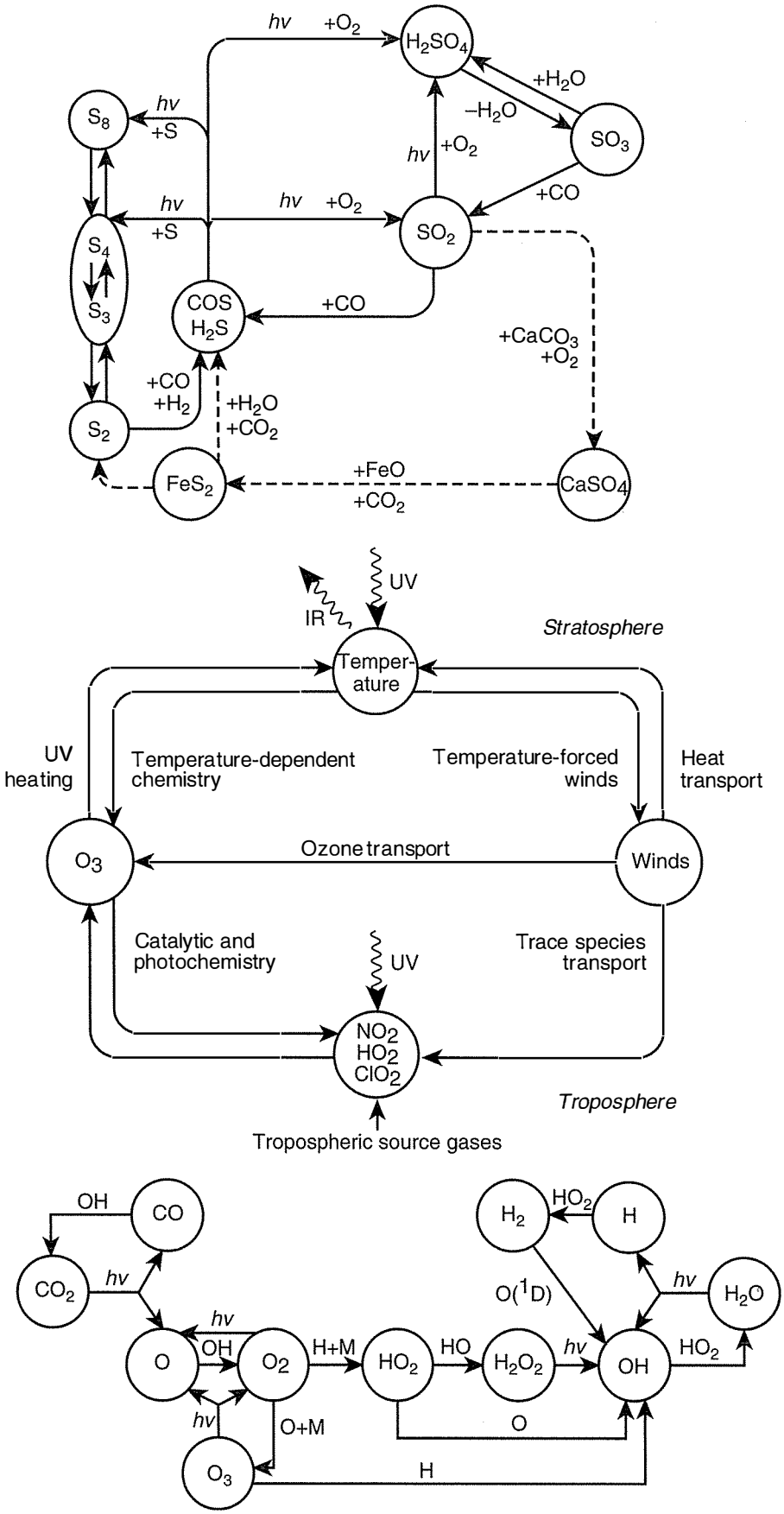

Fig. 6.1
Three key atmospheric photochemistry cycles. (Top) sulphuric acid production, as it is thought to occur on Venus; (centre) ozone production in Earth's stratosphere; (bottom) the cycle involving H_2O and OH that recycles carbon monoxide back into carbon dioxide on Mars. Versions of all of these are found on all three planets but with different degrees of dominance due to the boundary conditions, factors such as oxygen abundance and volcanic activity.

This proceeds rapidly enough that the atmospheres of Mars and Venus would have been entirely converted to CO long ago, were there not other reactions that convert CO back into CO_2. Measurements show that the dissociation products, CO and O_2, are present only in quite small amounts (Table 6.1), and it is necessary to postulate some extremely efficient recombination mechanism for CO_2.

It is now thought that this is achieved by efficient vertical mixing, coupled with a rapid recombination rate. The reaction is enhanced by catalysis involving hydrogen peroxide and the hydroxyl radical OH, produced by the action of solar UV on water vapour:

$$H_2O + h\nu \rightarrow OH + O \quad (\lambda < 190 \text{ nm})$$

followed by:

$$CO + 2OH \rightarrow CO_2 + H_2O$$

Since the H_2O is continuously regenerated, quite small amounts of water vapour are sufficient to maintain a predominance of CO_2 on Mars and Venus.

Carbon dioxide is, of course, not only the main atmospheric constituent on Mars and Venus, but also an important 'greenhouse' molecule on the Earth. On all three planets, the regeneration process is assisted by other reactions, including some involving ozone especially on Earth, or heterogeneous processes, for example, between the atmosphere and the surface on Venus.

The case of CO on Venus is worth studying in more detail, since the finite lifetime of that gas there means it has a variable distribution as it is transported between sources and sinks. The tropospheric CO abundance has been mapped from space, and the latitudinal gradient, in particular, is found to have important implications for understanding the circulation of the global atmosphere (§8.3.3).

6.5 Volatile behaviour of carbon dioxide on Mars

Volatiles are substances that occur in more than one phase in, or in contact with, the atmosphere. Important examples are water on Venus, Earth, and Mars, carbon dioxide on Mars, ammonia on the Jovian planets, and methane on Neptune and Titan. Because of the low prevailing temperatures on Mars, at one end of a large temperature cycle, carbon dioxide as well as water is involved in the seasonal cycles involving condensation and evaporation at the poles. Since carbon dioxide is the main constituent of Mars' atmosphere, the fact that it condenses in the polar night during the long period of perpetual darkness that occurs each winter results in a significant seasonal variation of the atmospheric pressure all over the planet. The global swing of around 30% in the mean surface pressure is a defining characteristic of the present climate on Mars. Figure 6.2 compares measurements made by *Viking* landers with theoretical model predictions and shows good agreement between the two.

To quantify the surface pressure cycle, and understand its asymmetry between northern and southern winter, requires a detailed understanding of the heat balance in the polar regions. During the winter, the high latitudes are in permanent darkness for approximately twice as long as on the Earth, due to the longer year on Mars. Without direct solar heating, and with only a thin atmosphere to transport heat into the region, the temperature rapidly falls below the condensation point for CO_2. This is a phenomenon that, except for some very cold regions in the upper atmosphere where thin carbon-dioxide 'cirrus' clouds can condense at any latitude or time of the year, only occurs in the polar night. The average temperature on Mars is about −60 °C; at the *Pathfinder* landing site, about −76 °C (197 K) was measured just before dawn. These and other typical non-polar temperatures are well above the CO_2 freezing point of −123 °C (150 K).

At the poles, radiative cooling would produce extremely low temperatures, were it not for the trillions of tons of CO_2 that precipitate as snow, releasing latent heat and tending to keep the temperature close to the freezing point. If the winter were long enough, all of the CO_2 would condense eventually, leaving the planet with an even thinner atmosphere consisting mainly of argon and nitrogen. As it is, the sunlight returns to the region and begins to reverse the process before it reaches this stage. The global pressure increases throughout Martian spring, and then starts to fall again as the opposite pole goes into its long winter night. When the pressure is highest, the north polar cap has lost most or all of its frozen CO_2, exposing a surface of water ice. At the south pole, however, the residual cap exhibits much lower surface temperatures, showing that frozen CO_2 is still present, even at the end of the summer. There is also a lot of water ice there, too; a recent estimate based on surface-penetrating radar measurements placed the amount in the south polar cap alone at the equivalent of a global ocean of water 11 m deep.

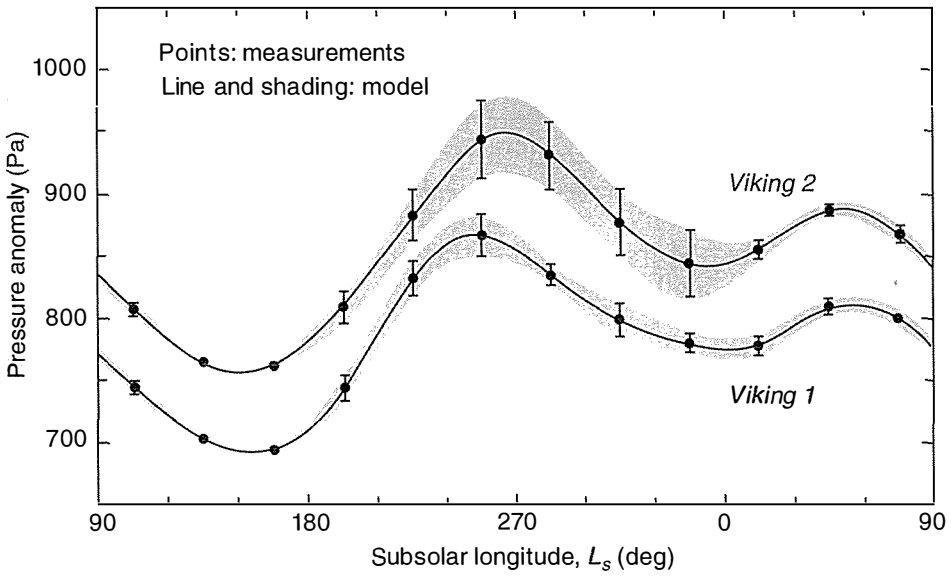

Fig. 6.2
Pressure at the *Viking* landing sites (22 °N, 48 °W and 48 °N, 226 °W) as simulated by the European Mars model (http://www-mars.lmd.jussieu.fr/mars.html), compared to the measurements made by the landers themselves. The shaded bands are the model results; the widths of these, and the bars on the measurements, show the variability due to weather patterns. These are mainly fronts like those we experience on the Earth, and are more active in the northern winter. The vertical displacement of the two curves is simply due to the fact that the *Viking 2* site is lower than *Viking 1*, so the mean pressure is higher.

Calculations using models of the seasonal expansion and contraction of the north polar cap also match observations, showing that the expected rates of deposition of CO_2 ice, allowing for the release of latent heat, radiation of heat to space, and heat transport by dynamics, can be quite well represented in the model (Fig. 6.2). To explain the different behaviour of the south polar cap, the radiative energy balance must be different, and this has proved harder to reproduce in models, suggesting that additional processes are involved. A fit can be achieved by adjusting the amount of dust that is mixed into, or lies on top of, the two polar caps as a result of the different circulation patterns and dust storm activity levels. The amount of dust determines the reflectivity and the infrared emissivity of the ice, affecting the time it takes to sublime away in the springtime. Another possibility is that poorly understood dynamical factors cause more carbon-dioxide ice to be deposited on the south pole in the first place, making a thicker covering that takes longer to vanish, so that in fact it never does.

Whatever the reason for the persistence of CO_2 ice at the south pole, it has to overcome the effect of the bias in heating due to Mars' orbital eccentricity. This might have provided a convenient explanation for the north–south irregularity, except that it works in the wrong direction because the planet is closer to the Sun in the southern spring. The asymmetry in the annual pressure cycle – the pressure minimum during late northern winter is less deep than the corresponding minimum during late southern winter – is also related to the different behaviour of the two poles with regard to condensation and release of carbon dioxide. Here, however, the behaviour is at least in line with simple intuition, since the higher pressures occur near perihelion.

6.6 Water on Mars

The amount, distribution and physical state of water on Mars have long been major research topics. A hundred years ago, many believed the theory popularised by Percival Lowell that canals could be seen on the surface of the planet, presumed to be built by intelligent inhabitants for purposes of irrigation. Mars' north polar cap had been observed as early as 1666 by Giovanni Cassini, and the southern equivalent in 1672 by Christiaan Huygens; in 1781 William Herschel observed both and wrote that he believed they were ice sheets like those on the Earth, leading him to conclude that 'Mars has a considerable but modest atmosphere... in many respects similar to ours'.

The belief that Mars resembled the Earth in having water existing near the surface in all three phases, including liquid, suffered a setback when early space missions observed what seemed to be a desert world, albeit one that does have water ice in the polar caps and below the surface soil at other latitudes. Most of the latter is 'permafrost', meaning it stays frozen all year round, although water adsorbed in the top metre or so of soil can be released in summer and reabsorbed in the winter. While it is true that the pressures and temperatures on Mars are too low for liquid water, some of the subsurface water may be present

as liquid in regions of geothermal activity, low-level remnants of the active volcanoes that clearly erupted in the early years of the planet's history. These regions will be prime targets in the search for life on Mars, if or when they are found.

Spectrometers on the two *Viking* spacecraft that orbited Mars beginning in 1976 made detailed maps of the column abundance of atmospheric water vapour (Fig. 6.3) to address its role in the present-day climate. Even the maximum amounts, seen in the northern summer, are very small, although this not due to an overall shortage of water on the planet, but rather because the temperatures are so low that even saturated air has a low absolute humidity. Evidently, the most important source of water vapour in the entire Martian atmosphere is the north residual polar cap, from which large quantities of water vapour sublime during late spring and early summer, producing a maximum in the humidity of the air. The southern polar cap, by contrast, produces only about half as much, because, although the north polar cap is mostly water ice, the south polar cap has a permanent component of frozen CO_2 as well as H_2O under the seasonal veneer of CO_2 ice. This does not explain whether there is a net transfer between the poles during the seasonal cycle as a result of there being more water vapour in the northern hemisphere than the south. It is not even clear what sign it has, i.e., whether the north pole is collecting water by whatever process makes it more abundant there, or whether water is being cryopumped towards the south pole along the concentration gradient.

Questions like these can be addressed by studying the climate with a computerised general circulation model, in which the fluxes of water, carbon dioxide and dust can be followed in response to the changing seasons, and their regular, annual exchange between the atmosphere, surface and subsurface quantified. While Fig. 6.3 shows how the amount of water vapour in the atmosphere was observed to vary during a Martian year, Fig. 6.4 shows the total quantity of water in each hemisphere and in the global atmosphere that corresponds to this,

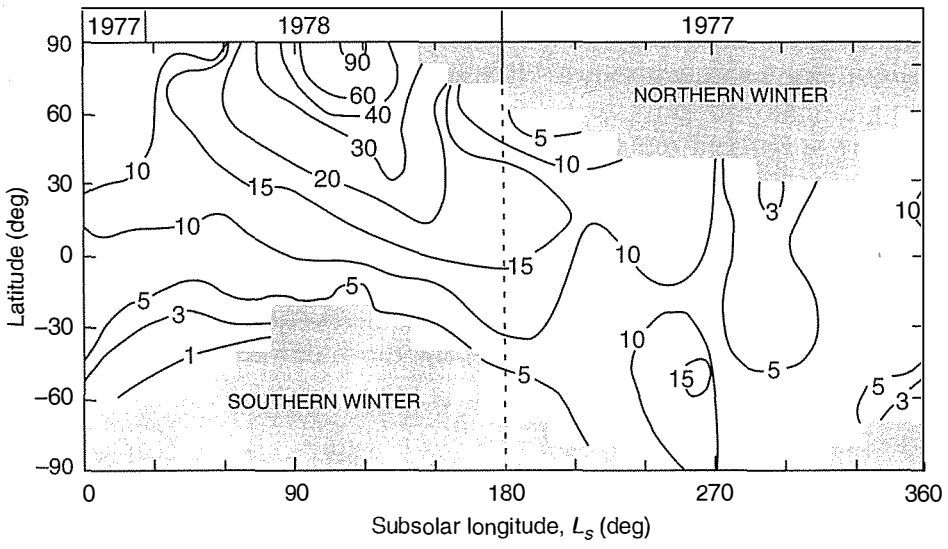

Fig. 6.3
The water content of the atmosphere, over one Mars year, as observed by the Mars Atmospheric Water Detector on the *Viking* orbiters. Note the much higher concentrations in the northern summer (near $L_S = 90$ deg), relative to the south. The unit is precipitable micrometres, the thickness of the liquid layer that would result if all of the water in the atmosphere condensed on the surface. Earth's atmosphere typically holds about one thousand precipitable micrometres.

according to a model that matches the observations. About three billion tons of water vapour is released from the polar caps in the northern Martian summer, enough to cover the planet to a depth of less than a millimetre if it were condensed to form liquid water. This is far less than on Earth, again because the lower temperatures and densities on Mars mean that the atmosphere can hold and transport much less water, even if it is in contact with a plentiful supply on or underneath the surface. The degree of interhemispheric 'pumping' that takes place each year is small, so its role in the climate remains uncertain, but could be significant on long timescales.

The amount of water vapour in the atmosphere varies with latitude as well as season, with four times as much in a vertical column at 60° N as at 30° N in northern summer, for instance. Comparisons between observations and models of the smaller variations in the annual cycle of water in the tropics suggest that there must be another significant reservoir of water on Mars besides the polar caps and the atmosphere. Water vapour increases in the spring near 30° N long before the permanent water ice cap receives enough heating to supply a significant amount of vapour at this latitude, which would seem to confirm that it comes from a source on or just below the surface. It has been estimated that the amount of water that is adsorbed in the top few centimetres of the Martian soil is ten times the total load in the atmosphere, in which case it must contribute to any mass of water that transfers permanently between the hemispheres during the course of the Martian year.

In addition to water adsorbed in the soil or regolith, there are likely to be subsurface deposits of more or less pure ice as well. Some of this ice may be seasonal, melting and contributing vapour to the atmosphere in the summer; but most of it is probably permanently frozen and so lost to the modern climate system. Calculations show that ground ice is stable a metre or so below the surface everywhere

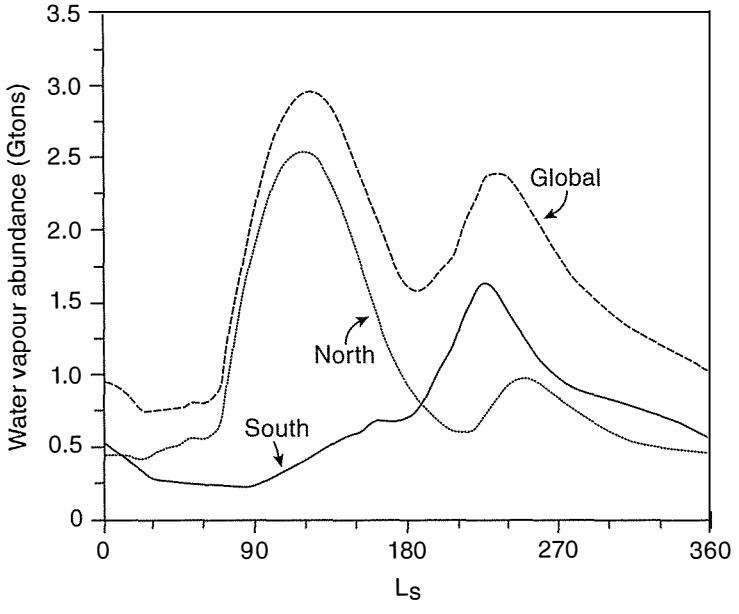

Fig. 6.4
These curves show how the amount of water present in the atmosphere, as vapour or clouds, varies as a function of subsolar longitude, according to the Mars general circulation model developed at NASA Ames Research Center. The maximum, in northern summer, for the whole planet, is three billion tons of water, nearly all of it in the northern hemisphere. The southern maximum is smaller, but again the bulk of the water is in the summer hemisphere, as would be expected. The asymmetry between the hemispheres is something that probably varies with the long-term climate cycles driven by cyclical changes in Mars' orbit.

polewards of about 40° latitude. The models that predict this depend strongly on the nature of the soil, however, especially its thermal inertia, the quantity that measures how rapidly a material tends to heat and cool when exposed to or removed from heating by the Sun. If the Martian subsurface has a low thermal inertia, corresponding, for example, to a fairly loose aggregate soil, then ice is stable just below the surface at all except tropical latitudes in the models.

The first experimental data to test these theoretical expectations were *Viking* observations of splashy deposits around certain impact craters, and of glacier-like flows in some shallow valleys. This constitutes good evidence for substantial subsurface ice deposits, in non-polar as well as polar regions, but does not provide enough information when it comes to estimating the total amount on the planet. In 2008, the *Phoenix* lander did not have to dig very far to uncover ice very near to the surface at its high-latitude landing site (68° N), although it could not address the important question of how far down it extends, nor provide any information about the local variations that must exist.

There is further evidence for large amounts of ice in the southern hemisphere of Mars from three different instruments on board the 2001 *Mars Odyssey* spacecraft. These experiments, measuring gamma radiation and energetic neutrons, are sensitive, not to water itself, but to the effect of hydrogen in any form in the soil slowing down or absorbing the emission produced when cosmic rays impact the Martian surface. Some of the neutrons are absorbed and then emit a gamma ray of a specific and characteristic energy, which is detected by the spacecraft. H_2O must be by far the most common hydrogen-bearing molecule on Mars, so the lack of specificity in any detection of large amounts of hydrogen is not too much of a problem.

The gamma-ray results pertain principally to the top metre or two of the subsurface. The data imply that the Martian soil is relatively dry near the surface, with large quantities of hydrogen, presumed to be H_2O in the form of ice, present below a depth that varies from pole to equator. To match the data, the water-rich layer contains a fifth to a half of ice by mass, and since ice is less dense than soil the material is mostly ice by volume. It is found close to the surface near the pole, with its upper boundary moving progressively deeper towards midlatitudes. By latitude 40 °S, the ice-rich layer is still present, but the overlying ice-free layer is more than a metre deep. It remains to be shown whether there is enough frozen water on Mars to have filled the oceans that seem to have existed on the surface around four billion years ago.

6.7 Water on Venus

Venus has between ten thousand and one hundred thousand times less water in its atmosphere than exists in the oceans and atmosphere of the Earth. The surface and lower atmosphere of Venus may always have been too hot for liquid water or ice, but large amounts of water could have outgassed from the interior and resided as vapour in the

atmosphere until it was dissociated and lost to space. Today, the atmosphere contains only very small amounts of water as vapour, about 30 parts per million. Further (probably larger) amounts of H_2O are incorporated in the clouds as liquid droplets of sulphuric acid containing 5–25% water, and possibly other hydrated material as yet undetected. Below the clouds, water vapour is found to be remarkable constant with latitude and with height, the abundance being close to 0.003% everywhere. Above the cloud tops, at around 66 km, maximum values in the water vapour mean mixing ratios of about 0.01% have been observed in the early afternoon, while minimum values of less than 0.0006% were found at night. The region of anomalously high values is highly localised, with a sharp transition to lower values on the rest of the day side, and may be a region of localised upwelling, driven by the Sun, carrying moisture from below. Alternatively, solar heating might be driving H_2O out of the cloud droplets near noon that gets re-absorbed at night.

Although water is scarce on Venus by terrestrial standards, the ratio of deuterium to hydrogen is over one hundred times more on Venus than Earth, supporting the idea that Venus had much more water initially, but that most of it has been lost since. The loss processes involve dissociation to form hydrogen and oxygen, followed by escape of hydrogen from the planet, a process that depends strongly on the abundance of water vapour in the middle and upper atmosphere. According to calculations, Venus could have lost an ocean of present-day terrestrial proportions in less than five hundred million years.

The disposal of the oxygen produced by water vapour dissociation in the upper atmosphere is a key issue: it must either have escaped from the planet along with the hydrogen, or else have ended up bound chemically in the crust. Most of the weathering processes that remove atmospheric oxygen on Earth involve liquid water or water vapour, but recent measurements suggest that oxygen atoms escape more easily from Venus. This may be because Earth has a shield against solar wind ablation provided by its relatively strong magnetic field. Even the current rate of loss of water from Venus, as estimated from spacecraft measurements of escaping hydrogen and oxygen ions, is enough to remove the entire current, relatively small, water inventory in only about two hundred million years. Unless we are observing the planet just as it finishes drying out completely, there must be a source of water at the present time. This replacement water could come from cometary impacts, but most likely it is being vented from the same volcanoes that keep the sulphur dioxide content of Venus' atmosphere high, despite its short chemical lifetime (§6.9).

6.8 Carbon monoxide chemistry on Venus

The principal source of carbon monoxide in the atmospheres of both Venus and Mars is the dissociation of CO_2 by solar ultraviolet radiation, which occurs primarily at high levels since the energetic photons required do not penetrate very deep into the atmosphere. The principal

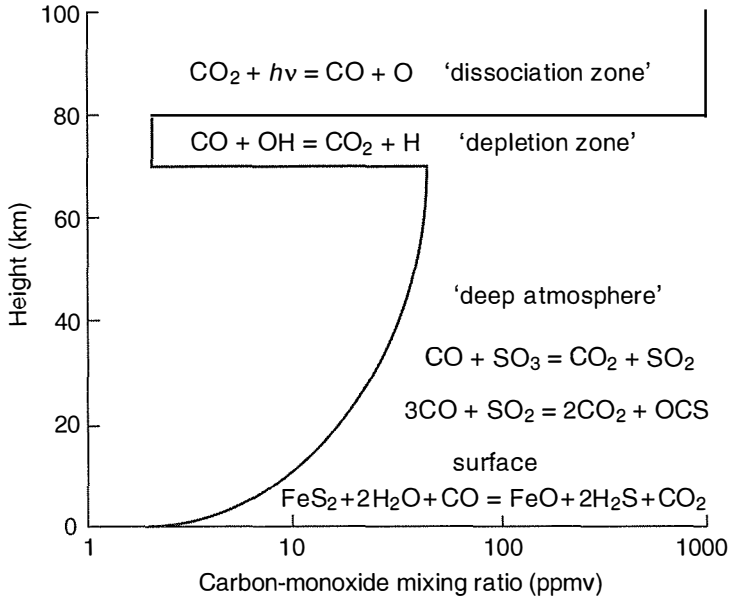

Fig. 6.5
A summary of observations of the carbon-monoxide profile in the atmosphere of Venus, showing the reactions that produce CO in the upper atmospheric dissociation zone, as well as those that remove it in the depletion layer in the clouds, in the hot troposphere, and at the surface.

sinks for CO on both planets are reactions at and near the surface, although on Venus there is another 'depletion zone' near the cloud tops, probably the result of hydroxyl production, followed by a reaction of the OH with CO (Fig. 6.5). The mystery then is why the CO abundance rises again below the clouds, where there is no known source. Indeed, we might ask why there is any significant amount of carbon monoxide in the lower atmosphere at all.

During its encounter with Venus in February 1990, the NIMS instrument (§3.10.3) on the *Galileo* spacecraft used spectroscopy of the CO 2-0 vibration–rotation band in the 2.3 μm spectral region to observe the concentration of CO in the deep atmosphere, around 30 km above the surface. These data indicated relatively high concentrations of CO at high northern latitudes, as shown in Fig. 6.6. Because of the geometry of the trajectory, the *Galileo* observations did not extend so far south as they did north, so it was not possible to say from these data whether the increase of CO with latitude also occurs in the other hemisphere until symmetric behaviour was confirmed in observations by *Venus Express* in 2006.

What is the source of the lower-atmospheric CO, and why should its proportion in the well-mixed lower atmosphere increase systematically from equator to pole in both hemispheres? Vertical diffusion from the upper atmosphere seems an unlikely candidate because of the very short chemical lifetime of CO, probably only a few days or less in the cloud-top depletion zone. Chemical sources are also unlikely, because current understanding of atmospheric chemistry on Venus suggests *depletion* at all levels in the lower atmosphere. In addition, it is difficult to come up with an explanation based on chemistry for the horizontal gradient observed by *Galileo* and *Venus Express*.

Volcanoes are sources of carbon monoxide on the Earth, and this is likely to be the case on Venus as well. The highest mountain region on

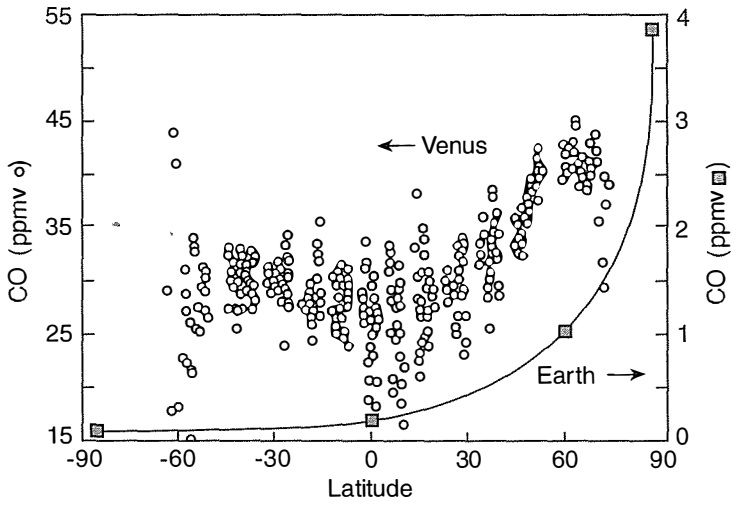

Fig. 6.6
The points in the upper frame are the measured carbon-monoxide mixing ratio in the troposphere on Venus as a function of latitude (after Collard *et al.*, 1993); the curved line is approximately the corresponding distribution of CO in the Earth's stratosphere in northern winter. See also the more recent measurements in Fig. 8.13.

Venus, Maxwell Montes, is approximately below the northern CO maximum, which could explain the horizontal gradient if it is also the biggest volcanic source. We have yet to observe any volcano, including Maxwell, in the process of erupting on Venus. However, the indirect evidence for volcanism from radar and infrared images of the surface is compelling, and improved observational techniques will probably eventually confirm that volcanic activity is still widespread.

This still does not mean that volcanism produces the observed latitudinal gradient, unless the complex that includes Maxwell is the major contributor to tropospheric carbon monoxide in the northern hemisphere, and a correspondingly large source can be identified at the same latitude in the south. In fact, the concentration of volcanic constructs, active or not, identified in radar images, is considerably higher in the equatorial regions on Venus, another argument against this particular hypothesis. To evaluate the case most favourable to a volcanic origin for the latitudinal gradient, suppose we represent all volcanoes by a single source of CO at the latitude of Maxwell (about 65° N). The mean volcanic flux of carbonic gases into Earth's atmosphere is estimated as about $2.4 \times 10^{11}\,\mathrm{kg\,yr^{-1}}$. Nearly all of this is carbon dioxide, with a relatively small and variable amount of the monoxide. Again looking for an upper limit estimate, suppose that *all* of the carbonic gases emitted on Venus are in the form of CO for some reason.

The total mass of Venus' atmosphere is $\approx 4.8 \times 10^{20}\,\mathrm{kg}$. For a mean mixing ratio of 3×10^{-5} (30 ppmv), the total mass of CO is $\approx 10^{16}\,\mathrm{kg}$. The enhancement seen in the data is about a third of the mean value, and is present over ~10% of the surface area of Venus (i.e., that polewards of 65° latitude). This requires an additional $\sim 3 \times 10^{14}\,\mathrm{kg}$ of CO. Even with the above extreme and unlikely assumptions, it would take about 10^3 years to emit enough CO to account for the observed anomaly – much longer (by about five orders of magnitude) than the chemical lifetime.

Volcanism never was a very likely explanation for the observed distribution of carbon monoxide on Venus, and this simple calculation

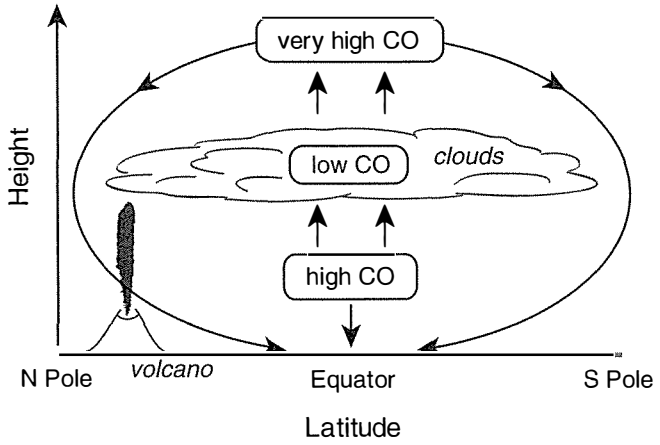

Fig. 6.7
Carbon-monoxide circulation on Venus, showing the transport of CO from the source in the upper atmosphere to the surface at the polar limit of the Hadley circulation, where rapid downwelling is expected. The depletion of CO in the cloud layers is minimal at the poles, not only because of the short time available, but also because of the limited amount of solar UV radiation available to drive photochemistry.

rules it out with near certainty. If that were not enough, the north–south symmetry recently observed by *Venus Express* is another reason to look elsewhere, since there is no Maxwell-type complex at 60 °S latitude. An explanation based on the general circulation of Venus' atmosphere offers much more promise than any of the preceding three hypotheses (Fig. 6.7).

As on Earth and Mars, mass transfer from the upper to lower atmosphere occurs on Venus with downward motion in the polar region. The air transported to high latitudes by the 'Hadley cell' circulation is recycled at the edge of, and inside, the polar vortices (§8.3). On Venus, these are larger and more permanent than the terrestrial equivalents, so downward advection of CO, which is observed to occur on a large scale on Earth, probably does so to an even greater extent on Venus. The observations give us reasonable estimates of the area over which descending motion takes place, but little clue as to the mean downward velocity or, therefore, the rate of mass flow, but we can estimate what would be required, as follows. The descending part of the polar vortex occupies roughly one tenth of the surface area of the 'cap' of enhanced CO (assuming that this extends all of the way to the pole). Thus, a process in which high-CO air is transferred efficiently to lower levels, where it then mixes with low-CO air, quickly enough to avoid loss, should give a mixing ratio of $\sim 1000/10 = \sim 100$ ppmv, which is the right order of magnitude. The fact that the enhanced CO region has a reasonably steep boundary implies that the loss processes are fairly efficient compared with equatorward transport, as expected.

6.9 Sulphur dioxide on Venus and Earth

The importance of sulphur dioxide on Venus stems from its role:

1. as an indicator of very active volcanism at the surface,
2. as part of the processes which form and maintain the sulphuric acid cloud layers,
3. as part of a chemical system involving a non-uniform distribution of SO_2, elemental sulphur, and probably other compounds, that give

rise to the ultraviolet markings in the clouds that form the visible face of Venus, and

4. as a 'greenhouse' gas contributing to the hot climate on Venus.

The high sulphur content of the atmosphere on Venus, including the H_2SO_4 clouds, is a powerful indicator of recent volcanic activity, since gases like sulphur dioxide have a short lifetime in the atmosphere before they are removed by interaction with the surface. The measured abundance of SO_2 in the deep atmosphere is about 180 ppm, which is more than one hundred times too high to be in equilibrium with the surface. The time constant for the decline of the sulphur abundance in the atmosphere if the source were removed is a few million years, indicating that the atmospheric sulphur must be of recent origin. *Pioneer Venus* ultraviolet spectra showed a decline by more than a factor of ten in sulphur dioxide abundance at the cloud tops over a five-year period, and more recently, *Venus Express* has also detected large, short-term variations in SO_2 near the 100 km altitude level.

Because of the difficulties associated with observing through the clouds, it has not been possible to associate these large changes in SO_2 above the clouds with specific eruptions on the surface. However, similar SO_2 variations are seen in the terrestrial upper atmosphere following large volcanic events on the Earth. For instance, the injection of an estimated 20 million tons of SO_2 into the stratosphere by the eruption of Mount Pinatubo in the Philippines in 1991 left localised contrasts of more than ten times the mean abundance, even 100 days after the event. The mean volcanic flux of carbonic gases, mostly CO_2, into the Earth's atmosphere is estimated to be 2.4×10^{11} kg each year, while the mass of sulphur compounds is 20 times less, 1.2×10^{10} kg per year.

The injection of sulphur compounds, primarily SO_2 gas, into Venus' atmosphere may be related to the rate at which heat is released from the interior if the latter is primarily due to volcanism. On Earth, the main mechanism is convective overturning of the crust associated with plate tectonics, but this process seems to be absent on present-day Venus. Volcanoes on the Earth produced about 4×10^{10} W on average, about 0.1% of the total heat flux from the Earth's interior. If Venus released energy from the interior at the same overall rate, but it is all accounted for by volcanoes, then we would expect 1000 times as much gas, in particular, sulphur dioxide, to be released. In fact, the concentration of SO_2 in Venus' atmosphere is approximately 100,000 times that in Earth's.

A large part of this difference could be explained by the difference in the way SO_2 is removed from the atmosphere on the two planets. SO_2 gas probably has a similar lifetime in the stratospheres of Earth and Venus, since both are very dry, and the main loss process is conversion to sulphuric acid. However, most of the SO_2 on Earth never makes it beyond the troposphere, where a very efficient rain-out mechanism operates. This could easily account for the missing factor of 100 in the estimate above.

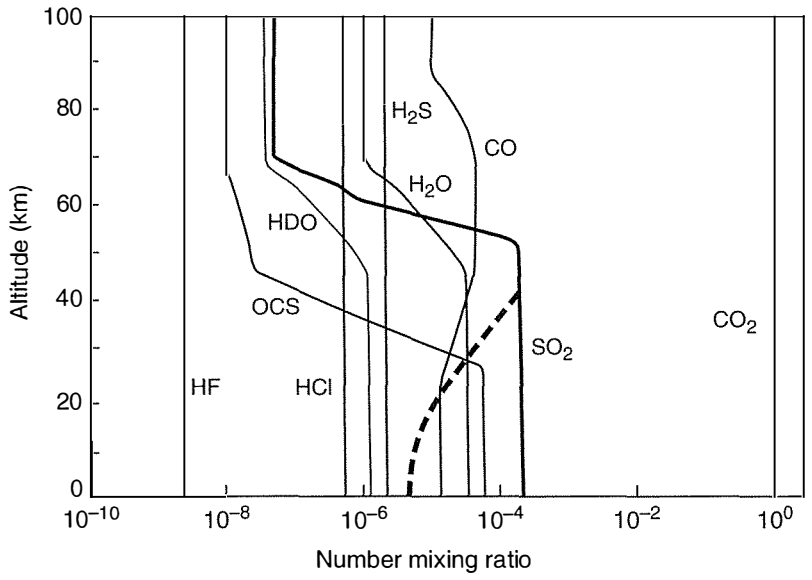

Fig. 6.8
Mixing ratios assumed in the baseline models of Bullock and Grinspoon (2001) shown as a function of altitude. The dashed line is the SO_2 mixing ratio profile derived by Bertaux *et al.* (1996) from *VEGA 1* and *2* entry probe data.

Two other approaches to estimating the level of volcanic activity on Venus have been tried. Measurements from spectroscopic instruments on orbiters like *Venus Express* can search for evidence of plumes from active vents containing high concentrations of sulphur dioxide, water vapour, carbon monoxide and other volcanic gases. However, the combination of high spatial resolution and high spectral resolution required makes this a more promising approach for an instrument on a long-lived floating balloon platform, deployed just below the cloud layers. Both NASA and ESA are considering flying such missions, but probably not before 2020.

Another approach involves searching for hot spots that might be fresh lava fields by mapping the thermal emission in the infrared at wavelengths that probe down to the surface. Suppose an instrument of aperture A on a satellite orbiting D km above Venus has a spatial resolution at the surface of d km and makes observations with resolution $\Delta\lambda$ in the spectral window near $\lambda = 1.05\,\mu$m, where the atmosphere is nearly transparent and most of the emission reaching the instrument is from the surface. The cloud particles scatter almost elastically at this wavelength, giving a high throughput with a fraction a of the radiance attenuated by the clouds. The scattering diffuses the radiation so that the spatial resolution attainable is limited to about 50 to 100 km.

To detect the presence of a lava field at temperature T_1, where the surrounding temperature is T_0, we must have

$$\frac{[e_1 B(T_1,\lambda) - e_0 B(T_0,\lambda)](d/D)^2 A(1-a)\Delta\lambda\sqrt{t}}{\text{NEP}} > 1$$

where e refers to surface emissivity and t is the duration of the measurement in seconds. Again, this is easier from a platform flying below the clouds, but in principle is possible from an orbiter if the lava field is

extensive enough and a lot hotter than its already scorching surroundings. Even then, any thermal anomalies due to lava have to be carefully distinguished from atmospheric opacity variations, due mainly to structure in the cloud layer, which is a large effect (§7.1). The instrument also observes temperature differences due to surface relief, since a mountain top 10 km above the plain below is about 100 degrees cooler than its surroundings. Further complications arise because variations in surface composition give rise to patterns of different emissivity e, making some features look brighter in the infrared, even when they are at the same temperature as nearby regions. Finally, of course, the lava flow has to be observed when it is fresh because it soon starts to cool to the temperature of its surroundings as it flows and spreads out. It is perhaps not surprising that the definite identification of erupting volcanoes is difficult.

6.10 Isotopic ratios in atmospheric gases

The isotopic ratios within the abundance for a given chemical element can give important clues about the early history of the Solar System, the formation of the planets, and the evolution of their atmospheres. Particularly interesting cases are the deuterium to hydrogen ratio (^{2}H/^{1}H or D/H), and the isotopic ratios of helium (^{2}He/^{3}He), nitrogen (^{15}N/^{14}N), carbon (^{12}C/^{13}C/^{14}C), and oxygen (^{16}O/^{18}O). The noble gases, argon (^{36}A/^{38}A/^{40}A), krypton, neon, and xenon are all both heavy (hence not prone to escape) and inert (hence not prone to removal by chemical reactions with the crust), and so the ratios of their abundances on different planets should be a strict test of any model or theory.

The isotopic abundances among these and other elements contain a record of the history of the materials from which they derive. The following origins are characterised by distinctive isotopic ratios:

1. capture from the solar nebula in the early Solar System,
2. capture from the solar wind at a later stage,
3. the collision of volatile-rich bodies such as comets with the planet,
4. radioactive decay in the interior, followed by release into the atmosphere.

Argon, for instance, has three common isotopes, of which ^{40}Ar is primordial and ^{36}Ar and ^{38}Ar are produced by radioactive decay of potassium ^{40}K. Primordial argon and neon are more than an order of magnitude less abundant on Earth than on Venus, and less common on Mars than Earth by a similar large factor. These observations strongly suggest that the present atmospheres accreted along with the planetary bodies and were later outgassed. The differences in argon abundance can then be explained in terms of differences in the density of the solar nebula at the time of formation, as can the ratios of the rare gases to carbon and nitrogen.

The isotopic ratios of carbon and oxygen are approximately the same on Venus, Mars, and Earth, but those of nitrogen are different. ^{15}N/^{14}N in the Martian atmosphere is about 1.7 times greater than

that on Earth. If it is assumed that the ratio of two isotopes of similar mass and identical chemical properties was approximately the same in all of the planets at formation, then models which calculate the preferential loss of the lighter isotope from the exosphere of Mars require that nitrogen was initially much more abundant on Mars than it is now, by a factor which different estimates place between 20 and 300.

Deuterium in water on Mars is enriched by a factor of five over the same ratio in water on Earth. Studies of how this could have been achieved by fractionation (the faster loss of the lighter isotope) during the loss of large amounts of water from the upper atmosphere have estimated (with considerable uncertainty) that the initial supply of water was enough to produce a layer several tens of metres deep over the entire globe of Mars. This is of the order of ten times too small to account for the water that seems to have been present, according to the geological evidence (§6.6). Of course, as we have seen, most of the original water may not have been lost but may still be present as ice and permafrost. Alternatively, or additionally, large amounts of water may have been removed by the impact of large meteors, which would not discriminate between isotopes. It is therefore not difficult in principle to reconcile the measurements.

6.11 Composition and chemistry in outer planet atmospheres

Originally, the elemental abundances in Jupiter were thought to be the same as in the Sun, as would be expected if the star and its planets formed from the same mass, and Jupiter retained all of its original material by virtue of its low temperatures and strong gravitational field. Although that is now known not to be the case, all of the gas giant planets were large enough and cold enough to retain large proportions of the lighter elements, predominantly hydrogen and helium, which were present in the primordial cloud from which the Solar System formed. These are, in consequence, mostly atmosphere, increasing in density and temperature with depth to very high values, and with the heaviest elements concentrated near the core. In Jupiter, the internal heat source (§4.6) raises temperatures to at least 10,000 K, at pressures well in excess of a million bars. Under these conditions even the hydrogen liquefies and becomes highly conducting, generating Jupiter's strong magnetic field.

The energy being released near the centre of the planet drives rising motions in air parcels that eventually radiate heat to space from the upper reaches of the atmosphere. The deep part of the convective cycle exposes the gases to high temperatures and pressures, where chemical reactions can proceed that would be inhibited in the cooler outer layers. If equilibrium is reached under such conditions, all common elements will combined with hydrogen to form the most stable compound, usually the fully hydrogenated form. Thus:

- Carbon $\rightarrow$ CH_4 (methane)
- Nitrogen $\rightarrow$ NH_3 (ammonia)

- Oxygen → H_2O (water)
- Sulphur → H_2S (hydrogen sulphide)
- Germanium → GeH_4 (germane)
- Arsenic → AsH_3 (arsine)
- Silicon → SiH_4 (silane)
- Phosphorus → PH_3 (phosphine)

This is consistent with what we observe: all of these species have been detected and measured in some or all of the outer planet atmospheres. The composition of Jupiter is the best studied, because it is larger, closer, and warmer than the others, but even there, the uncertainties in the abundances obtained using spectroscopy are quite large. The main problem is the multiply-layered cloud system, which interferes with remote spectroscopic measurements and is associated with a variable distribution of condensing species. The major constituents, hydrogen and helium, and the important noble gases, are hard to measure using spectroscopy in any case, since they have no spectral lines in the infrared except very broad pressure-induced features that blend into the continuum. Their only characteristic sharp spectral lines are at short wavelengths, in relatively inaccessible parts of the ultraviolet spectrum, and these originate in the very low density outer layers of the atmosphere. Dissociation and gravitational separation occur at these levels, so the measured mixing ratio cannot be taken to be representative of the atmosphere as a whole. The best information we have on the major constituents in Jupiter's atmosphere is from mass spectrometers on the *Galileo* entry probe.[57]

Galileo confirmed that the composition of Jupiter's atmosphere is mostly hydrogen (about 86%) with the remainder mostly helium. The hydrides, especially methane and ammonia, are, as expected, the principal minor constituents, although their relative abundances are significantly different from the mix in the Sun (typically by factors in the range from 2 to 4; see Table 6.2). Many other species, in particular

[57] The probe was released by the *Galileo* orbiter spacecraft in July 1995, following a six-year flight from the Earth. On 7 December, the probe entered Jupiter's atmosphere at over 100,000 miles per hour, slowed using a heat shield and parachute, and descended through 150 km of the top layers of the atmosphere in 58 minutes. The last signals were received from a depth where the pressure was 22 bars.

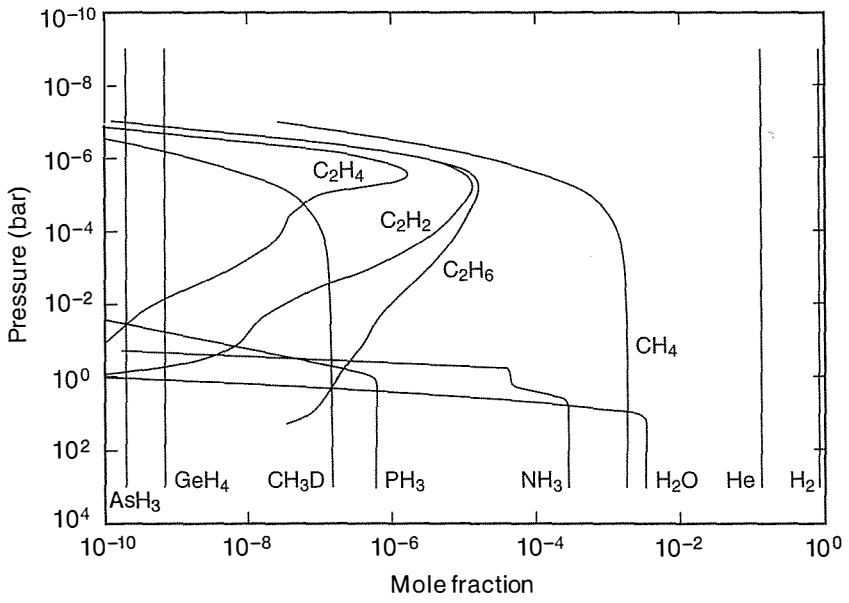

Fig. 6.9
Vertical profiles of composition on Jupiter (Irwin, 1999). Three categories of behaviour are evident: (i) species that do not condense and are well mixed throughout, like hydrogen, helium and germane (GeH_4); species that are well mixed in the lower atmosphere but freeze out in the colder upper atmosphere, like water vapour, ammonia and phosphine (PH_3); and finally the hydrocarbons, principally methane (CH_4), which dissociates and produces ethylene (C_2H_4), acetylene (C_2H_2), ethane (C_2H_6) etc at high levels where photochemistry can occur.

Table 6.2 Composition data for the outer planets, shown relative to the abundance of hydrogen in Jupiter and in the Sun. The fraction of helium molecules in Jupiter's atmosphere is $\frac{f_{He}}{\sum_n f_n}$; 13.6%, that of methane 0.18%, and ammonia is 0.061%. Water vapour is variable and neither the total nor the mean amount is very well known, but is of the order of 0.05% in the mixed part of the atmosphere below the condensation level.

	Solar fraction f	Jupiter fraction f	f solar	Saturn fraction f	f solar	Uranus fraction f	f solar	Neptune fraction f	f solar
H_2	1.0	1.0	1	1.0	1.0	1.0	1.0	1	1
He	0.1954	0.157	0.8	0.13	0.67	0.18	0.92	0.18	0.92
H_2O	1.352×10^{-3}	$\sim 6 \times 10^{-4}$	~0.44	2×10^{-7}	0.00	?	?	?	?
CH_4	6.623×10^{-4}	2.1×10^{-3}	3.17	4.5×10^{-3}	6.8	0.019	29	0.027	40
Ne	2.405×10^{-4}	2.46×10^{-3}	0.1	?	?	?	?	?	?
NH_3	1.664×10^{-4}	7.1×10^{-4}	4.27	$> 1.1 \times 10^{-4}$	> 0.66	?	?	?	?
H_2S	3.170×10^{-3}	8.1×10^{-3}	2.56	?	?	?	?	?	?
Ar	5.024×10^{-6}	1.81×10^{-3}	3.6	?	?	?	?	?	?
PH_3	7.262×10^{-7}	6.94×10^{-7}	0.96	7.94×10^{-6}	10.9	?	?	?	?
GeH_4	8.532×10^{-9}	8.1×10^{-10}	0.1	2×10^{-9}	0.23	?	?	?	?
Kr	4.083×10^{-9}	8.69×10^{-9}	2.13	?	?	?	?	?	?
Xe	2.958×10^{-10}	8.74×10^{-10}	2.95	?	?	?	?	?	?
AsH_3	4.688×10^{-10}	8.1×10^{-10}	1.73	2.3×10^{-9}	4.27	?	?	?	?

more complex hydrocarbons, including C_2H_2, C_2H_4, C_3H_4, and C_3H_8, are present in the thinner upper atmosphere where enough solar radiation penetrates to drive photochemical reactions. Methane is dissociated and the fragments reassemble as a range of heavier hydrocarbons. Some of these condense to form a thin haze of oily droplets that contributes to the yellowish colour of the disk, particularly in the cases of Jupiter and Saturn (and Titan).

The rising motions from the interior bring gases rich in volatile species, such as water and ammonia, up to cooler levels where they condense to form cloud layers. From simple equilibrium cloud condensation models, Jupiter is expected to have at least three layers of cloud in the region visible to the outside observer, and more below that. In models, the top layer is composed of ammonia ice, the one below that of hydrogen sulphide in combination with ammonia as ammonium hydrosulphide, NH_4SH, and the lowest of the three of water. The very uppermost clouds have been observationally verified to be ammonia ice crystals, but the composition of the lower main cloud deck is proving more difficult to verify. It may not be NH_4SH, but is probably composed of some combination of ammonia and hydrogen sulphide. There is also direct evidence for a deeper cloud consisting predominantly of water, as expected, but probably with ammonia and other soluble compounds in solution (§7.3).

6.12 Elemental abundances in Jupiter's atmosphere

The *Galileo* probe composition measurements obtained in the deep troposphere, where vertical mixing is occurring and below the levels where condensation of ammonia takes place, can be assumed to represent bulk values for Jupiter in most cases. Exceptions may have to be made for the cases of helium, which models predict may liquefy and 'rain out' at depth, for neon, which is soluble in the helium drops and thus suffers the same fate, and for oxygen, which is present mainly as H_2O. As on Earth, water vapour is very variable on Jupiter due to the meteorological effects discussed in the next section, and a representative estimate for the total water and hence oxygen in Jupiter has yet to be obtained. It remains to explain the enrichment with respect to the solar value in carbon, sulphur, nitrogen and the noble gases by factors between two and four shown in Table 6.2. These enrichments would not be present if Jupiter formed from a simple condensation of the solar nebula.

What seems to have happened instead is that C, N and S all accreted as ices, probably principally those of NH_3, CH_4 and H_2S, along with water ice, until a nucleus formed that had sufficient mass to attract the lighter gases. Once the nucleus reached about 10 Earth masses it was heavy enough to cause a runaway gravitational collapse of the nearby nebula gas and trap massive amounts of hydrogen and helium. The heavier elements were enriched, since the light gases were not trapped in significant amounts until the core exceeded this minimum size.

There is a problem with this theory, however. Table 6.2 shows that the heavy noble gases are also enriched over the expected solar nebular values by about the same factor as carbon, sulphur and nitrogen. Although they would all have been present in solar proportions in the protosolar cloud, argon, krypton, and xenon would not have contributed much to the mass of the icy planetesimals involved in Jupiter's formation, because the temperatures were too high for these gases to be trapped effectively as ices, and of course they do not form compounds that might freeze more easily.

In models of Solar System formation, water ice condenses in the circumstellar disk at temperatures around 150 K. Argon requires temperatures below 30 K to be trapped and would be depleted by many orders of magnitude in icy planetesimals formed at much higher temperatures. The noble gases would then have had to have been trapped gravitationally along with the hydrogen and helium, and would not be enriched.

There are two main schools of thought on how to explain this dilemma. The first is that the uniform enrichment of heavy elements that is observed on Jupiter must mean that these elements were in fact trapped in very cold icy planetesimals. These must have formed much further from the Sun than Jupiter's present orbit, perhaps in the local interstellar medium on the outer edge of the cloud that formed the original solar nebula. Alternatively, the solar nebula may have been much colder at Jupiter's distance from the Sun than current models have deduced.

The second possible solution is if the water in the proto-Jovian planetesimals froze, not as amorphous ice, but in the crystalline form, trapping the volatile compounds of the heavy elements as clathrates in the ice lattice. These are complexes in which molecules of one substance are completely enclosed within the crystal structure of another. For instance, a gas like argon might be trapped in the lattice formed by frozen water. However, argon clathrate is only stable at temperatures below 38 K, hence the requirement for low temperatures persists in this interpretation. Also, the formation of clathrates requires much more water per trapped molecule than does trapping as ordinary ice, so the O/H ratio in Jupiter would need to be larger than the solar ratio, not just by three or four times, but by at least an order of magnitude more than that. This makes it even more essential to obtain data on this crucial quantity.

6.13 Water on Jupiter

The mixing ratio of water in the atmosphere of Jupiter has been measured many times by spectroscopic instruments on spacecraft and at observatories on the Earth. The values they find are generally low, of the order of a part per million, and variable with time and location. This is, of course, not surprising in view of the vapour pressures expected at the low temperatures in the upper troposphere and above, which is the part of the atmosphere observable at most wavelengths from outside the planet. As noted above and further discussed in Chapter 7, the deepest level that can be sounded in the infrared is the top of the water cloud, at a pressure of about 3 bars and a temperature close to 273 K.

Even this relatively modest depth of penetration is achievable by optical instruments only in 'hot spots', regions in the dark belts where

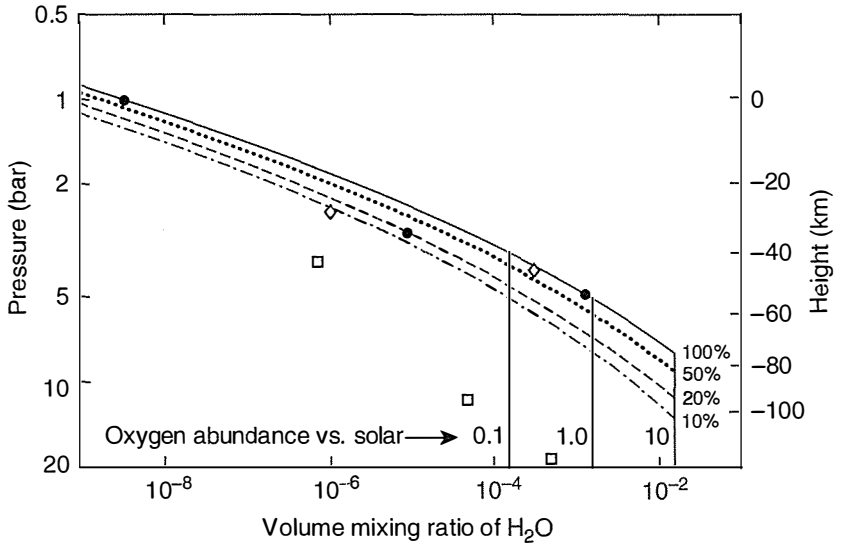

Fig. 6.10
Models of the vertical profile of the water vapour volume mixing ratio in Jupiter's atmosphere (Irwin, 1999). The solid curve is the saturation vapour pressure, and the vertical solid lines show the cut-off value if the oxygen abundance in Jupiter, relative to hydrogen, is 0.1, 1 or 10 times the 'solar' value of 1.5×10^{-3}. The parallel curves are for 50, 20, and 10% relative humidity. The points mark various estimates that have been made using data from the *Voyager* and *Galileo* spectrometers and the *Galileo* entry probe instruments; the inconsistency between these is due at least in part to variability within the atmosphere, between belts and zones, for instance.

the upper ammonia and ammonium hydrosulphide clouds are thin or absent. These form when air that has been 'freeze dried' in ascending, cloud-forming regions, corresponding roughly to the bright, cloudy zones in visible light, cools and sinks to complete the circuit in a planetary-scale convection cell. In this interpretation, the locations and times when observations of water vapour amount are possible are always the relatively dry regions; just how dry can vary, depending on local meteorological conditions on Jupiter.

It was hoped that the *Galileo* probe, penetrating well below the water cloud, would operate deep enough to get a measurement of the O/H ratio that can be taken as representative of Jupiter as a whole. The values measured by the probe mass spectrometer found an upper limit for water vapour of 6.9×10^{-7} at pressures less than 3.8 bars, rising to $(4.8\pm2.2)\times10^{-5}$ at 11.7 bars, and possibly to an order of magnitude larger at 18.7 bars. These data are consistent with the estimates from the infrared flux measurements also made from the probe, as well as with the earlier *Voyager* IRIS spectroscopic measurements (Fig. 6.10). All imply that the atmosphere is severely sub-saturated at pressures greater than approximately 1.5 bars, but the fact that the mixing ratio is still increasing steadily at the depth where the probe ceased transmitting suggests that the region of dry descending air extends well below the 20 bar level. A new mission to Jupiter, called *Juno*,[58] plans to use microwave spectroscopy from orbit to probe the deep atmosphere and sound the water content below the 100 bar level at all latitudes, hopefully penetrating into the well-mixed region and determining the elusive O/H ratio at last.

[58] *Juno* is scheduled to launch in August 2011, and to arrive at Jupiter in 2016.

6.14 Atmospheric composition on Titan

Table 6.3 shows the molecular abundances in Titan's atmosphere, including recent measurements by the *Cassini* Saturn orbiter and the *Huygens* Titan probe. The main constituent is nitrogen, like the Earth, at about 97%. Argon is abundant throughout the Solar System and was expected to be a major constituent on Titan, perhaps as much as 10% of the atmosphere according to some estimates. However, when it was finally measured by the *Huygens* mass spectrometer, the abundance was found to be very low, less than a part per million (actually 0.28 ppm) for the primordial form ^{36}Ar, and 43.2 ppm for the radiogenic isotope ^{40}Ar. The other noble gases are so scarce they were not detected at all. The low abundance of primordial noble gases probably means that the nitrogen that makes up most of the atmosphere we see today was originally captured as NH_3, and then converted to N_2 by photolysis due to the action of solar UV radiation on the early atmosphere. Ammonia freezes easily, and as ice it is a significant component of most comets, which are remnants of the swarm of planetesimals that formed the planets and their satellites. Had the conditions during Titan's formation allowed the capture of N_2, they would have also

been conducive to the capture of argon and the other inert gases in something like the proportions known to have existed in the primordial mixture.

The *Huygens* measurements confirm that the second most abundant molecule on Titan is methane, CH_4. Its mole fraction is 1.41×10^{-2} in the stratosphere, increasing below 32 km until it reaches a plateau of about 4.9×10^{-2} at about 8 km. These data are in good agreement with the stratospheric CH_4 value inferred by CIRS on the *Cassini* orbiter ($1.6 \pm 0.5 \times 10^{-2}$) in the lower atmosphere, and the estimate from *Huygens* radiometry of about 5% at the surface. The mass spectrometer witnessed a spike in the methane signal after landing, which suggests a surface saturated in liquid methane. Other organic species, including cyanogen, benzene, and ethane, were also detected in very small amounts. Molecular hydrogen occurs in the 0.1–0.2% range, along with trace amounts of various nitriles, including hydrogen

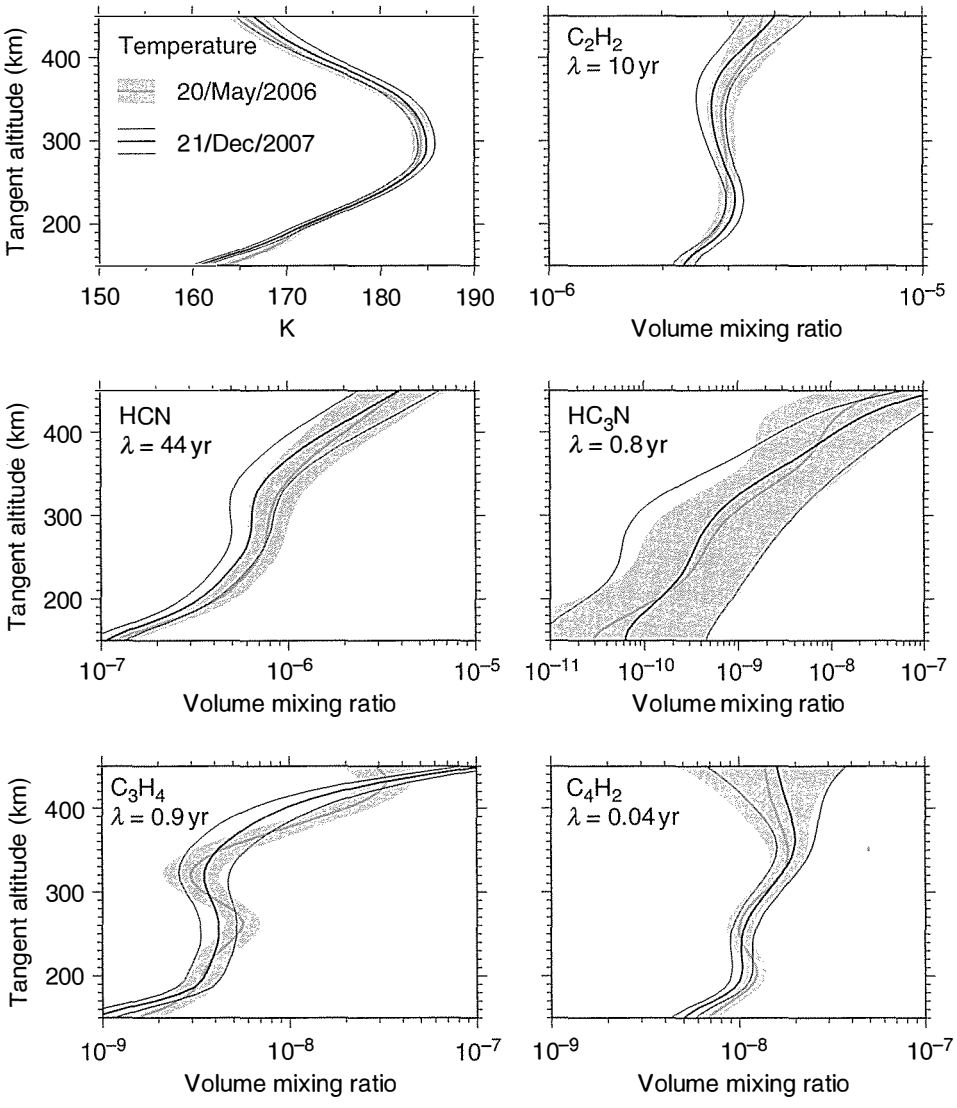

Fig. 6.11
Temperature and composition profiles in the upper atmosphere of Titan measured by the *Cassini* composite infrared spectrometer, obtained at 34° S and 46 °S on 20 May 2006 and 21 December 2007, respectively (Teanby *et al.*, 2008), The profiles show good consistency over this time, implying a stable balance between production and loss mechanisms. λ is the photochemical lifetime of the species at 300 km.

cyanide (HCN), and oxygen species, including carbon dioxide, carbon monoxide, and water vapour. Most of the water on Titan is frozen, of course; the crust and the topographical features seen on it are probably made mainly of water ice, as hard and rigid as steel at temperatures of less than 100 K.

Spectrometers like the CIRS instrument (§3.11.1) on *Cassini* have measured profiles of short-lived trace species in Titan's atmosphere all over the globe, and over an extended period of time (Fig. 6.11). The implications of these for the circulation of Titan's atmosphere are discussed in §8.6.

Table 6.3 Chemical composition of Titan's neutral atmosphere, from a combination of Earth-based observations and *Cassini–Huygens* measurements. From Coustenis and Taylor (2008).

Gas		Mole fraction	
Major components			
Nitrogen	N_2	0.97	
Methane	CH_4	1.4×10^{-2}	Stratosphere
		4.9×10^{-2}	Surface
Monodeuterated methane	CH_3D	8×10^{-6}	
Hydrogen	H_2	0.0011	
Argon	^{36}Ar	2.8×10^{-7}	
	^{40}Ar	4.32×10^{-5}	
Hydrocarbons		Equator	North pole
Ethane	C_2H_6	7×10^{-6}	1.1×10^{-5}
Acetylene	C_2H_2	2.5×10^{-6}	3×10^{-6}
Monodeuterated acetylene	C_2HD	6×10^{-10}	2×10^{-9}
Propane	C_3H_8	3.5×10^{-7}	6×10^{-7}
Ethylene	C_2H_4	1.5×10^{-7}	5×10^{-7}
Methylacetylene	C_3H_4	5.2×10^{-9}	2×10^{-8}
Diacetylene	C_4H_2	1.1×10^{-9}	2×10^{-8}
Benzene	C_6H_6	2.0×10^{-10}	3.8×10^{-9}
Nitriles			
Hydrogen cyanide	HCN	7.7×10^{-8}	7.8×10^{-7}
Cyanoacetylene	HC_3N	3.0×10^{-10}	4.4×10^{-8}
Cyanogen	C_2N_2	5×10^{-10}	9×10^{-10}
Dicyanogen	C_4N_2		
Acetonitrile	CH_3CN	1.5×10^{-9}	
Oxygen compounds			
Water vapour	H_2O	8×10^{-9}	
Carbon dioxide	CO_2	1.1×10^{-8}	1.3×10^{-8}
Carbon monoxide	CO	$(2–4) \times 10^{-5}$	
		$(2–6) \times 10^{-5}$	
Isotopic ratios			
$^{13}C/^{14}C$		82.3 ± 1	
$^{14}N/^{15}N$ in HCN		67	
in N_2		183 ± 5	
D/H in CH_3D		1.2×10^{-4}	
in HD		2.3×10^{-4}	
in C_2HD		$1–3 \times 10^{-4}$	

6.15 The methane problem on Titan

The high abundance of methane in Titan's atmosphere is mysterious because the lifetime of the gas in an atmosphere exposed to solar radiation is quite short. Methane is continuously dissociated by UV photons, to produce first higher hydrocarbons and nitriles. These diffuse to the cooler part of the atmosphere and condense, producing haze, which eventually precipitates out as surface deposits (§7.4). Some of the latter, including methane itself, can evaporate and return to the atmosphere, but the denser materials are removed permanently. Calculations show that the amount of methane seen in the atmosphere at present should be removed after a lifetime of the order of 100,000 years, very short compared to the age of the Solar System.

In the years before anyone knew what lay beneath Titan's shroud of haze, planetary scientists leaned towards the concept of a liquid methane ocean, with an admixture of higher hydrocarbons, such as C_2H_6, which continually replenished the atmosphere. This, too, would be depleted eventually, of course, but it might have been massive enough to persist to the present epoch. Now, however, ground-based and *Cassini* radar measurements and images have ruled this out by showing most of Titan's surface to be solid, with only localised, relatively small lakes that are probably the result of recent rainfall and could dry up seasonally. The long-term methane supply must be mostly below ground, soaked into a porous regolith, which may have large 'aquifers' in contact with the atmosphere through cracks or channels in the icy crust. Some recent *Cassini* images of the surface have shown features that look like cryovolcanoes, probably driven by methane escaping from the interior and expelling water-rich lava, which soon freezes.

6.16 References and further reading

Bertaux, J.–L., T. Widemann, A. Hauchecorne, V.I. Moroz, and A.P. Ekonomov. VEGA 1 and VEGA 2 entry probes: An investigation of local UV absorption (220–400 nm) in the atmosphere of Venus (SO_2 aerosols, cloud structure). J. *Geophys. Res.*, **101**(E5), 12 709–12 745, 1996.

Bullock, M.A., and D.H. Grinspoon. The recent evolution of climate on Venus. *Icarus*, **150**, 19–37, 2001.

Collard, A.D., F.W. Taylor, S.B. Calcutt, R.W. Carlson, L. Kamp, K. Baines, Th. Encrenaz, P. Drossart, E. Lellouch, and B. Bézard. Latitudinal distribution of carbon monoxide in the deep atmosphere of Venus. *Planet. Space Sci.*, **41**, 7, 487– 494, 1993.

Coustenis, A., and F.W. Taylor. *Titan: Exploring an Earthlike World.* 330pp. World Scientific Publishing, July 2008.

Irwin, P.G.J. Cloud structure and composition of Jupiter's atmosphere. *Surveys in Geophysics*, **20**, 505–535, 1999.

Owen, T.C., P. Mahaffy, H.B. Niemann, S. Atreya, T. Donahue, A. Bar-Nun, and I. de Pater. A low-temperature origin for the planetesimals that formed Jupiter. *Nature*, **402**, 269–270, 1999.

Read, P.L., and S.R. Lewis. *The Martian Climate Revisited: Atmosphere and Environment of a Desert Planet.* Springer-Praxis Books, 2004.

Taylor, F.W., S.K. Atreya, Th. Encrenaz, D.M. Hunten, P.G.J. Irwin, and T.C. Owen. The composition of the atmosphere of Jupiter. In *Jupiter: The Planet, Satellites and Magnetosphere*, ed. by F. Bagenal, W. McKinnon, and T. Dowling, Cambridge University Press, pp. 59–78, 2004.

Teanby, N.A., *et al.* Titan's winter polar vortex structure revealed by chemical tracers. J. *Geophys. Res.*, **113**, E12003, 2008.

6.17 Questions

1. Venus has about the same total mass of nitrogen in its atmosphere as the Earth, but much more atmospheric carbon dioxide, and much less atmospheric water vapour. Describe briefly a plausible evolutionary scenario that could account for these facts.

2. Describe, in outline only, the processes and chemical cycles responsible for (a) the ozone layer on Earth, (b) the production of the principal cloud layers on Venus, and (c) the production and loss of carbon monoxide on Mars. Discuss briefly the relevance or otherwise of each mechanism on the other two inner terrestrial planets.

3. Explain in general terms the basic evolutionary processes that give rise to the observed composition of the atmosphere of Jupiter. How might these have differed on the other three gas giant planets? How do the gaseous abundances relate to the composition of the observed cloud layers on Jupiter?

4. Outline a plausible scenario for the processes that led to, and currently support, the observed composition of the atmosphere of Titan. In particular, suggest why it is mainly nitrogen, like the Earth, and discuss the anomalous abundance of methane. How do the gaseous abundances relate to the composition of the observed cloud layers on Titan?

Clouds, haze, aerosols, and dust

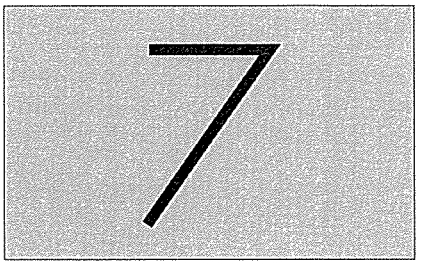

All planetary atmospheres contain small, airborne particles of solid or liquid material. If the concentration of particles is large, and forms layers or clumps that are optically thick, we tend to call them clouds. A less spatially well-defined distribution of particles that is more transparent, so that a person or instrument can see (not necessarily at visible wavelengths) long distances while still being able to detect optically that the particles are present, would be called a haze. Finally, we have the ubiquitous distribution of very small particles that is present everywhere, even under nominally clear conditions; we usually refer to these just as *aerosols*.[59]

Clouds are usually an important part of the hydrological cycle of a planet, in the broader sense of involving ammonia on Jupiter and methane on Titan, as well as water on Earth. Hazes are less so, but they are an important source of opacity in radiative balance calculations. Diffuse aerosol layers can also affect radiation transfer significantly, especially over long path lengths, and are often a key component in important reactions in atmospheric chemistry (the ozone cycle on Earth, the sulphur cycle on Venus, the production of organics on Titan).

The formation and distribution of clouds in all their variants depend on the composition, temperature, and dynamics of the atmosphere. Most clouds in the Solar System are of liquid or ice particles produced by condensation. They are prone to re-evaporation, often in cycles that transfer large amounts of latent heat. On Mars, however, the largest component of the atmospheric greenhouse effect is airborne mineral dust, lifted from the surface by winds and *dust devils*. Mars also has clouds of frozen water and carbon-dioxide ice, especially near the poles.

[59] Strictly, cloud and haze particles are aerosols as well because they meet the definition of 'a dispersion of solid and liquid particles suspended in gas'. However, we usually save the term for a dispersion that is nearly, or actually, invisible, except under special observing conditions.

7.1 Cloud structure on Venus

The bright and nearly featureless appearance of Venus when viewed through a telescope led early observers to conclude that the planet had a cloudy atmosphere.[60] The clouds were naturally assumed to be water, with the surface hidden beneath often pictured as water-rich with steaming, tropical forests. Some later suggestions, driven by the fact that the sunfall on Venus is twice that on the Earth,[61] and noting that the clouds have a yellow tinge, fancied a desert planet with the air full of wind-blown dust.

[60] The first scientific report of the atmosphere of Venus is generally attributed to Lomonosov, who saw the disc of the planet surrounded by a halo while observing the solar transit of Venus from St Petersburg in 1761.

[61] Although, as discussed in Chapter 4, the albedo of Venus is more than twice that of the Earth (0.76 vs. 0.30), so Venus absorbs considerably *less* solar energy than Earth.

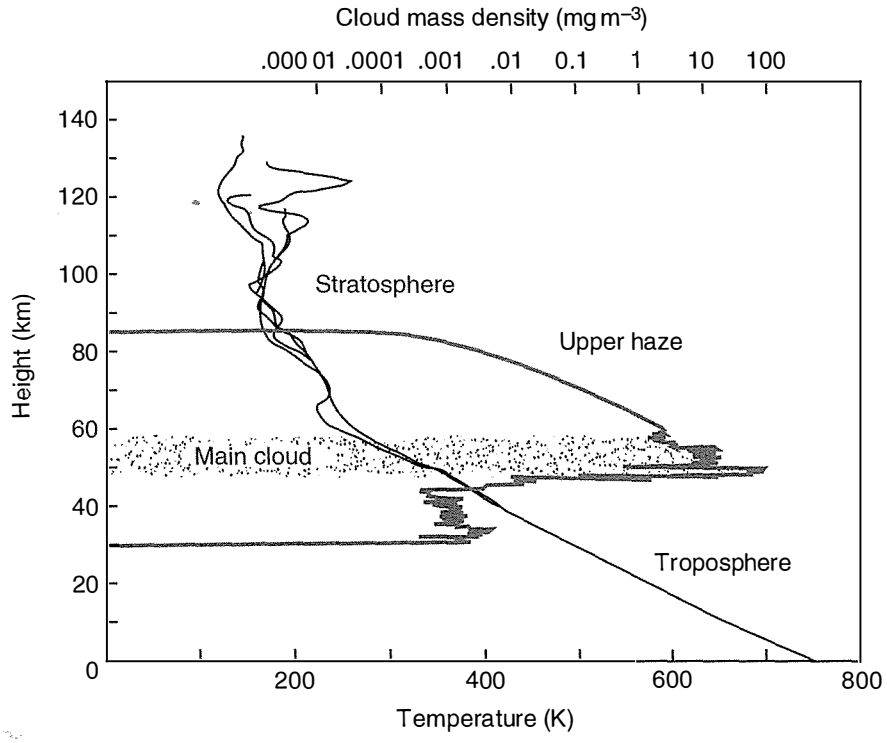

Fig. 7.1
Vertical profile of the total mass density of cloud particles on Venus (note log scale) from entry probe data, superposed on temperature profiles, also measured by probes. The cloud profile relies heavily on data from the *Pioneer Venus* large probe nephelometer instrument, so it is probably not typical of the whole planet, especially since data from orbit shows a high degree of global and temporal variability.

7.1.1 Particle size and composition from photopolarimetry

It was not until the 1970s that studies of the spectrum and polarisation of reflected sunlight from Venus showed the primary cloud constituent, in the uppermost cloud layers at least, is a strong aqueous solution of sulphuric acid. H_2SO_4 is formed when H_2O and SO_2 of volcanic origin combine photochemically near the cloud top level. This remains the only positively identified constituent of the clouds, although there is some evidence from remote sensing and entry probe data for additional large, irregularly shaped particles that may be solid rather than liquid. Also, the disc of the planet shows dark markings when photographed through an ultraviolet filter; these are due to absorption by a secondary, variable constituent of the clouds that has yet to be definitively identified. Finally, the clouds over the polar regions have been found to have different optical properties from those at lower latitudes, indicating differences in particle composition, size, or shape. The *in situ* measurements that might clarify this have yet to be obtained, due to the technical difficulties of deploying entry probes at high latitudes. A floating probe in the polar clouds may be needed before the answer is found.

7.1.2 Vertical structure

The main cloud deck enshrouds the planet completely in a layer that extends from about 45 to about 65 km above the surface, with haze layers above and below (Fig. 7.1). Below the cloud deck, the H_2SO_4 is

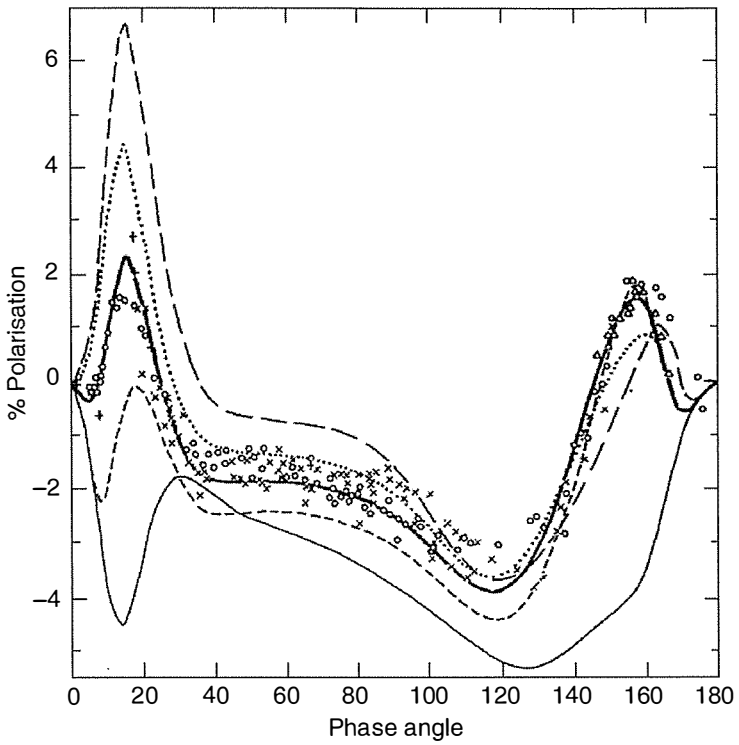

Fig. 7.2
A determination of the droplet size in the clouds of Venus[62] in which measurements (shown as points) of the polarisation of sunlight at 0.55 μm wavelength are compared to models of the multiple scattering process in the clouds for five values of the particle radius a from 0.6 to 1.5 μm. This plot shows that $a = 1.05 \pm 0.1$ μm fits the data, while simultaneous fits at several other wavelengths allow the refractive index of the cloud material to be determined as well, identifying the composition as sulphuric acid.

thermally decomposed to SO_3 and H_2O, leaving the lower atmosphere relatively clear. The particles range in diameter from less than 1 to possibly over 30 microns and tend to a trimodal distribution in the lower layers. The uppermost layer covers most of the planet and has a single particle size of 1.05 microns, with a very narrow range, as revealed by polarisation studies (Fig. 7.2). The process that determines this value, and keeps it within such tight limits, has not been identified. Similar fits at several other wavelengths allow the refractive index of the cloud material to be determined as well; it provides a good match with concentrated sulphuric acid in the proportion $3H_2SO_4 \cdot H_20$, which identified the composition as concentrated sulphuric acid, 75% H_2SO_4 and 25% H_2O. More recent measurements indicate the proportion of water in the cloud droplets may vary with height or from place to place.

Entry probes have studied the vertical profile of cloud properties using nephelometers, instruments that illuminate the cloud as they pass through in order to estimate particle density and other parameters from the backscattered intensity at various angles and wavelengths. These found that the clouds on Venus are really extensive layers of haze, with lower particle densities than most terrestrial water ice or vapour clouds. If so, visibilities of many kilometres would be possible. However, recent remote sensing studies of the deepest cloud layers has shown that the generally bland and uniform appearance of the clouds as seen through telescopes from Earth is deceptive, and there are large variations in the deep cloud layers, with some dense, cumulus-type concentrations in places. The *Pioneer Venus* large probe, which carried a sophisticated nephelometer, evidently passed through one of the less dense regions. The sketch in Fig. 7.3 shows the general scheme of the clouds as they are now understood, and the approximate levels at

[62] James E. Hansen and J.E. Hovenier, 'Interpretation of the polarization of Venus', *Journal of the Atmospheric Sciences*, Vol. 31, pages 1137–1160, 1974. This is the same James Hansen who is now a well-known expert on climate change modelling and pundit for the perils of global warming.

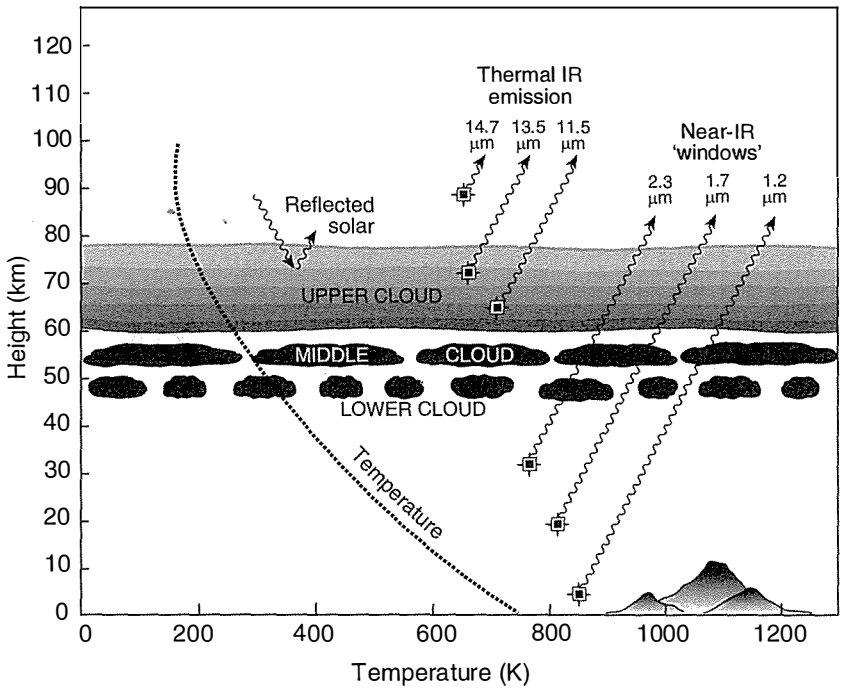

Fig. 7.3
A schematic diagram of the cloud layers on Venus and the levels to which the atmosphere is probed by observations at different wavelengths. Long-wave infrared emission originates in and above the clouds, while the hot lower atmosphere is the source in the near-infrared spectral 'windows'. After Baines *et al.* (2006).

which radiation detected at various near and thermal infrared wavelengths is emitted.

This, and other findings about the deep cloud properties, followed the discovery of the near-infrared spectral 'windows' in the 1980s (§1.2.2). In spite of their physical thickness, the clouds of Venus are not completely opaque at all wavelengths. They are highly efficient scatterers at visible and near-infrared wavelengths, and the hot surface and lower atmosphere of Venus can be seen from outside the atmosphere in emission at wavelengths where the CO_2 and H_2O absorptions are low. Maps of this emission revealed the large horizontal variations in the density of the cloud deck, and winds and other meteorological processes at depths where the temperature and pressure have Earth-like values, at around 1 bar and 300 K (§8.3).

7.1.3 Production schemes

Figure 7.4 shows a plausible chemical scheme for the production of the cloud layers on Venus, as a cycle fed by SO_2 and H_2O from volcanoes on the surface (see also Fig. 6.1). This is obviously oversimplified, however, since it does not explain several observed features, including:

1. The ultraviolet markings. Figure 7.5 shows the disc of Venus with the dynamical behaviour near the cloud tops delineated by dark markings, apparently produced by an unknown absorbing material that is mixed non-uniformly in the clouds. A combination of sulphur dioxide gas and traces of elemental sulphur reproduces the observed spectral behaviour of the dark cloud features, and the former is certainly present while the latter is probably part of the chemical cycle that produces the H_2SO_4 in the cloud droplets.

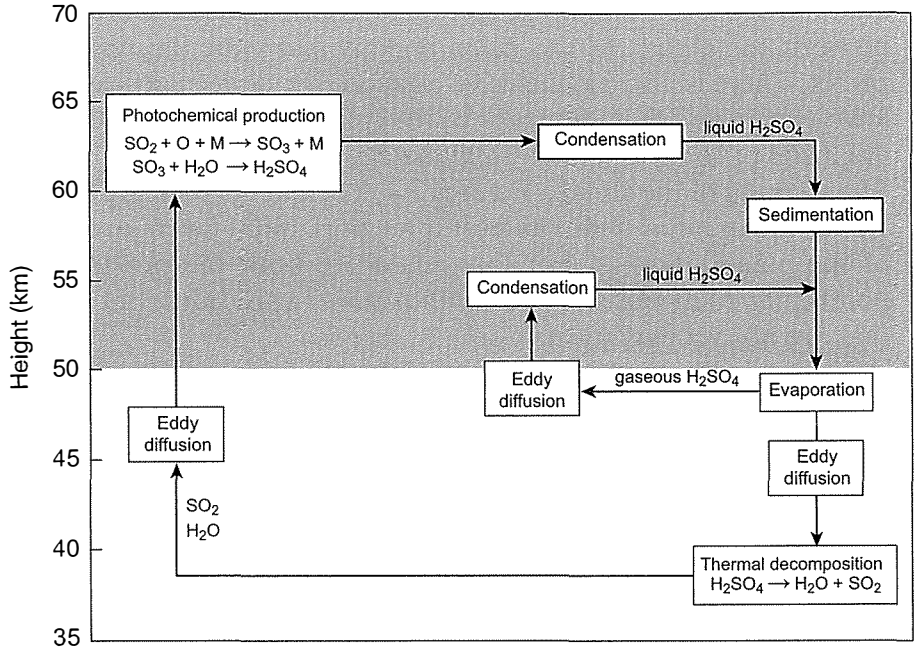

Fig. 7.4
A simple model of cloud chemistry on Venus that explains the main features of the observed cloud cover, although many of the details, such as vertical and horizontal structure and compositional variations, remain to be explained.

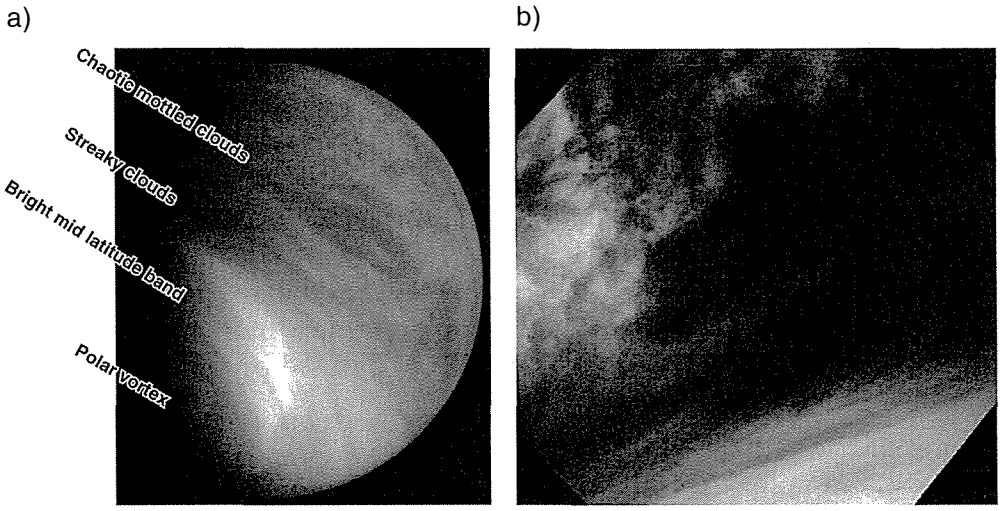

Fig. 7.5
The cloud tops on Venus imaged in reflected sunlight through an ultraviolet filter (left), selecting wavelengths around 0.365 μm. The labels refer to the way the clouds are organised in qualitatively different patterns in distinct latitude zones by the dynamical regimes which dominate there. On the right is a closer view of cloud structure near the transition between the equatorial area dominated by convection and the midlatitude area populated by streaky clouds, with the edge of the southern polar hood at the bottom.

2. The global cloud structure. Figure 7.5 shows how markings seen in the UV are organised differently in different latitude zones on the planet. Like the clouds on Earth, the patterns reflect the circulation and dynamical behaviour of the atmosphere, as discussed in Chapter 8.
3. The evidence for varying particle size and composition. Spectra taken in the clouds from probes and from satellites orbiting above both indicate variations in the cloud properties from place to place. In

addition to the UV markings, there are various systematic differences between the clouds in the polar regions and over the rest of the planet. There is also inconclusive evidence for larger particles in the lowest layer, and that these may be irregular in shape, suggesting they are made of some unknown solid material.

4. The layering of the clouds. Figures 7.1, 7.3, and 7.5 indicate how the clouds are organised into at least three horizontal layers over much of the planet. This is probably related to both the previous two points, i.e., to dynamical and compositional variations, but in ways that are not yet explained.

7.1.4 Lightning

Another long-standing debate is whether lightning is present in the Venusian clouds. The standard view used to be that they are too tenuous, although we now know that localised dense clouds, storms, and clouds of volcanic ejecta could provide the right conditions. Impulsive radio frequency signals in the 100 kHz to 5.6 MHz range, for which lightning is the only known source, have been detected by spacecraft. The orbiting *Venus Express* has detected strong, low-frequency 'whistler' mode discharges[63] that have been interpreted as due to a level of lightning activity that is similar to that on the Earth, but probably cloud to cloud, rather than cloud to ground. Despite evidence like this, there are some who still do not believe lightning occurs on Venus, and who point out that no flashes have been detected optically, despite scans of the dark side of the planet from orbiting spacecraft designed to search for such evidence. When this was done for Jupiter, many flashes were quickly detected. However, flashes are expected to be rarer and less energetic on Venus than on Jupiter, more like the level of activity on Earth, but more obscured and diffused by the clouds.

[63] 'Whistlers' are pulses of electromagnetic waves that occur at descending frequencies around 100 Hz, lasting about one second in duration. The name comes from the whistling sound of descending pitch that they produce in radio receivers.

7.2 Clouds and airborne dust on Mars

7.2.1 CO_2 clouds

On Mars, clouds occur much less frequently than on Earth, and the mean coverage on the visible disc is only a few per cent. The cloudiest regions are the winter poles, in the seasonal darkness where carbon dioxide freezes and forms clouds that snow out onto the polar cap. CO_2 clouds are also found at lower latitudes, but they tend to be very tenuous and at great heights where the atmosphere is extremely cold. High hazes and wispy cirrus clouds of CO_2 ice crystals are found mainly at night and typically 80 to 100 km above the surface. They are most easily seen from orbiting spacecraft in images of the atmosphere at the limb of Mars, especially in the early morning, after which they usually vanish as the Sun rises. More persistent examples are seen occasionally and have been photographed from landers on the surface.

7.2.2 Water clouds

Since CO_2 clouds tend to form in the dark, especially at the winter pole, most of the Martian clouds seen in visible images are made of water ice (Fig. 7.6). Analogues to most of the common terrestrial types occur on occasion. Convective clouds tend to occur near local noon over high ground, where the surface is strongly heated. The atmosphere near the surface then becomes unstable; the resulting rising air column saturates and produces clouds that are generally observed at heights from 4 to 6 km above the surface.

Extensive hazes of water ice crystals are seen high above the Martian poles in autumn and spring. The effect is greatest in the northern autumn, when the 'polar hood', as it is known, extends as far south as 50° N. It tends to disperse in the early winter, probably because the ice crystals making up the hood grow larger and precipitate out of the atmosphere.

Orographic clouds, which form as a result of air flowing over elevated features on the surface, are seen both as extensive layers over large-scale topography and as lee clouds behind tall structures, such as the giant volcanoes. They can extend for hundreds of kilometres.

Dense ground hazes of condensed water vapour are common, especially at dawn and dusk and over low areas. The thin atmosphere of Mars means that the surface cools rapidly as the solar heating drops off towards nightfall, and the air becomes saturated with water vapour. The resulting fog can persist all night and into the morning, often precipitating onto the surface to form a thin, bright layer of frost that lasts for several hours.

Fig. 7.6
A relatively rare sight: an overcast sky on Mars. This picture was taken by the camera on the *Mars Pathfinder* lander in 1997, about an hour before sunrise. The Earth was near the centre of the frame at the time, but is hidden by the clouds of water ice crystals floating about 15 km above the surface.

7.2.3 Airborne dust

On Mars, unlike Venus and Earth, the suspended material that has the greatest effect on energy balance and hence climate is not condensate clouds but, rather, airborne mineral dust. The surface of Mars experiences high winds and temperature excursions that lead to high rates of erosion of rock and soil, and there is neither rain nor open bodies of water to trap this as sediment. It is not surprising, therefore, that large amounts of fine material are present on the surface, and the atmosphere nearly always appears to contain a considerable load of reddish dust. This is quite well mixed through the lower 20 or 30 km, and can extend up to altitudes of 50 km or more during storms.

The lowest value of the vertical optical depth at visible wavelengths observed by either of the *Viking* landers during their first year of operation was 0.18 at one site and 0.36 at the other, and the maximum was about 5; more recently, the *Mars Exploration Rovers, Spirit* and *Opportunity*, have observed similar values (Fig. 7.7). Even the smaller values are large enough to absorb substantial amounts of solar energy that would otherwise reach the ground. When models of the dust are used to extrapolate these measurements to calculate the optical depth

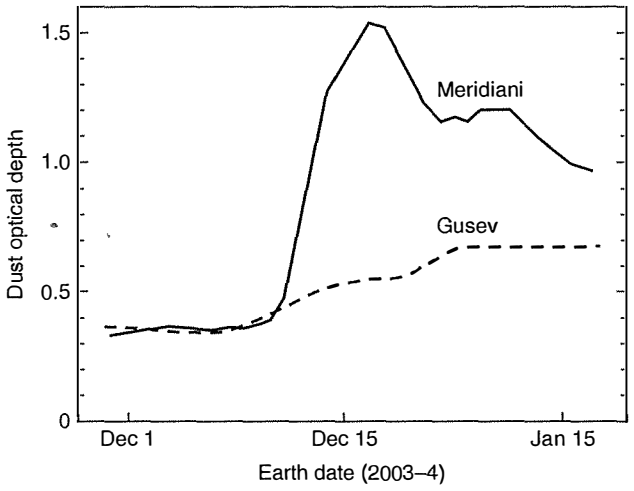

Fig. 7.7
The optical depth of the dust in a vertical column from December 2003 to early January 2004 at the two *Mars Exploration Rover* landing sites, Gusev Crater (lower curve) and Meridiani Planum (upper curve). A large regional dust storm occurred in mid December near Meridiani. For comparison, an optical depth value of 1.0 would correspond to a very smoggy day, and a value of 0.1 to a clear day, in Los Angeles.

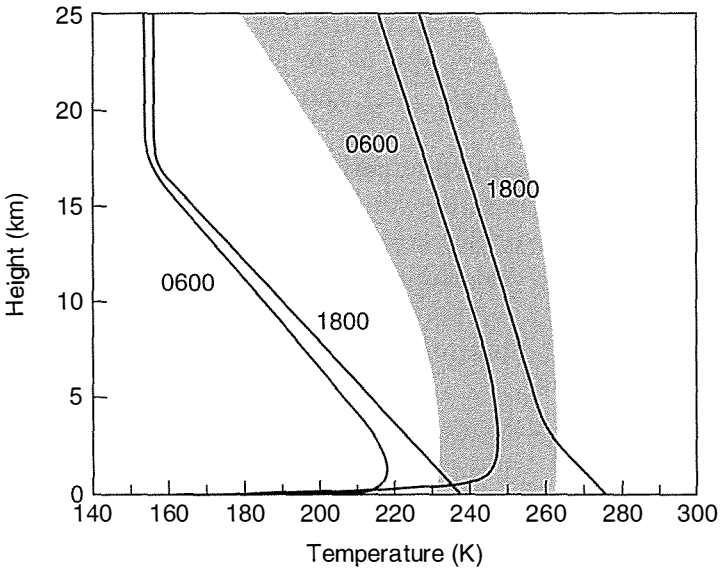

Fig. 7.8
Temperature profiles for Mars showing the effect of solar heating due to dust absorption. The left-hand profiles are for a clear atmosphere, at the local times shown, and the right-hand pair for a dusty atmosphere. The shaded area shows the envelope of the temperature profile measurements made by the *Mariner 6* and *7* spacecraft. After Gierasch and Goody (1972); see also Fig. 5.7.

at infrared wavelengths, it is found to also be enough to modify the temperature profile substantially, and hence to affect the surface temperature and the atmospheric dynamics (§5.5).

Numerical climate models developed from those used for forecasting on Earth can be used to apply known theory and boundary conditions to explain the observed conditions on Mars. This requires dealing with temperatures that are very variable, with season, time of day, and location on the planet. The goal is to extend or refine the model until a fit is achieved; sometimes this leads to important breakthroughs in understanding, or the identification of previously unknown or neglected processes. A classic example of this is the sequence of events that first revealed the important effect of airborne dust on radiative transfer in Mars' atmosphere.

Early modellers were not aware of the size of the dust effect, and omitted it, producing initially very puzzling results, which bore little resemblance to the real behaviour of Mars as observed by the early

space probes. For instance, calculations of the atmospheric temperature profile were coming out much too cold, as Fig. 7.8 illustrates. They soon recognised and fixed the problem, initially using crude estimates of dust amounts and assumptions about the size and optical properties (such as refractive index) of the individual grains, to achieve the improved profiles also shown in the figure. The difference is enormous, nearly 100 K, even in the global mean. Given the variability in dust amount on a local scale, we begin to understand how small amounts of dust raised by local gusts and dust devils can lead to thermal contrasts that result in global storms.

Improved calculations of the effect of airborne dust in models of the Martian climate require better knowledge or assumptions about the properties of the particles. Estimates have been made of the particle size distributions, concentrations and optical properties of the material in the atmosphere under various conditions of dust loading using data from cameras, spectrometers, and other instruments on the *Mariner, Viking* and *Phobos* spacecraft. The refractive index and the absorption coefficient describe the way in which dust scatters and absorbs the incoming sunlight and outgoing planetary infrared radiation. These depend on the composition of the material which, unlike clouds and hazes, is not expected to have a simple composition, nor a spherical shape, which introduces further complexities.

From the way the dust is produced, it must consist of a variety of minerals eroded from different geological units on Mars over the ages. It must also have been thoroughly mixed by the dust storms, so that the same mixture is found everywhere on the planet, as with the sand, soil, and other fine material on the surface. The evidence so far is consistent with such a heterogeneous mixture. Magnesium carbonate and magnesium sulphate have been identified, although their formation processes tend not to be mutually compatible, suggesting the dust was produced by mixing material originally laid down in different regions or layers. Geological arguments, along with measurements of the optical and magnetic properties of the dust, have been interpreted as showing that it contains smectites, which are clays rich in iron oxide, and palagonite, a glassy mineral that could have been formed either in volcanoes or during meteoritic impacts. The observed tendency of the Martian soil to form clumps is indirect evidence for traces of additional 'cement'-like material, such as magnesium sulphate, to provide adhesion between particles.

The size distribution of the airborne particles is a key parameter when calculating their effect on the transfer of solar and infrared radiation in the atmosphere. This not easy to determine, and in any case it must vary a lot in space and time. Not surprisingly, sample particles that have been studied, including some recent images of captured dust grains under the microscope on board the *Phoenix* lander, are found to be very fine, typically about one or two microns across, just a little larger than the wavelength of visible light. However, larger particles than this would be expected to become airborne under windy conditions, with some around ten times larger (a thousand times

more massive) contributing to the dust cloud for shorter periods during vigorous storms.

7.2.4 Dust dynamics and storms

Extending models of the Martian environment from one-dimensional energy balance calculations to a full three-dimensional, time-dependent global circulation model or GCM obviously requires an understanding of how the dust is lifted, transported, and removed from the atmosphere. The dust on Mars is extremely mobile because, despite the large amounts of frozen water present in the polar caps and buried in the crust, and the near-saturated state of the atmosphere, the surface environment is mostly very dry. In an attempt to find out what wind speed was required under simulated Martian conditions, particularly of low pressure, to raise dust from a loose particulate surface, experiments were carried out in a large wind tunnel at the NASA Ames Research Center in California, beginning in the 1970s.

In simple theory, the minimum velocity v^* required to move a grain of diameter D and density ρ is given by equating the horizontal wind stress to the force of gravity on the particle, which gives

$$v^* = A\sqrt{\frac{\rho g D}{\rho'}}$$

where ρ' is the density of the air and A is a coefficient that has to be determined experimentally. Since A has to include the effects of local deviations from a spherical monodispersion on a flat open plain, as well as any effects of inter-particle forces due to electrostatics and cohesion, or of particle spinning and saltation (bouncing and knock-on motions), this is a gross approximation at best. However, it has been found useful for dust lifting studies on Earth and makes a starting point for Mars.

Experiments were carried out on silica microspheres, natural silt, and ground walnut shells, to provide a range of material types, without prejudice as to whether any of these, especially the last, would be found on Mars. The results showed that particles around 100 μm across, corresponding to fine sand rather than dust, were the easiest to move, with both larger and smaller particles requiring higher winds. The free-air wind speeds required to lift fine dust particles from a flat layer came out to be over 100 m s^{-1}, larger than would be expected on Mars under any normal set of conditions. Later experiments with fine clay particles reduced this estimate considerably for dust lying on an irregular surface, such as a bed of pebbles, although several times 10 m s^{-1} still seemed to be required. Winds as high as 30 m s^{-1} are certainly found on Mars, although not very frequently.

Matching findings like these to the observed dustiness of the Martian atmosphere depends, of course, on the efficiency of the dominant

removal mechanisms. The processes by which particles leave the atmosphere depend on their size; the very small particles could stay airborne for a long time if left alone. However, they have to contend with the plunging temperatures at night, when the settling rate is augmented by water and CO_2 freezing onto the airborne dust particles. This not only adds to their mass, it also increases their cohesiveness, so they are more likely to cluster together and precipitate out faster.

The fact that the Martian atmosphere seems to maintain a substantial level of airborne dust at all times, despite these losses in the diurnal cycle, indicates that the background wind field and local disturbances are energetic enough to raise dust into the air more or less continuously. The authors of the wind tunnel studies described above, which found dust quite difficult to lift under simulated Martian conditions with reasonable wind speeds, also noted that a swirling or vortex motion could be more effective than laminar winds. The small tornadoes known as dust devils occur in desert regions of the Earth, and are now known to be extremely common on Mars. They have belatedly been recognised as a key factor in maintaining a high level of airborne dust, even when the atmosphere is otherwise relatively quiescent. One can be seen at work in Fig. 7.9.

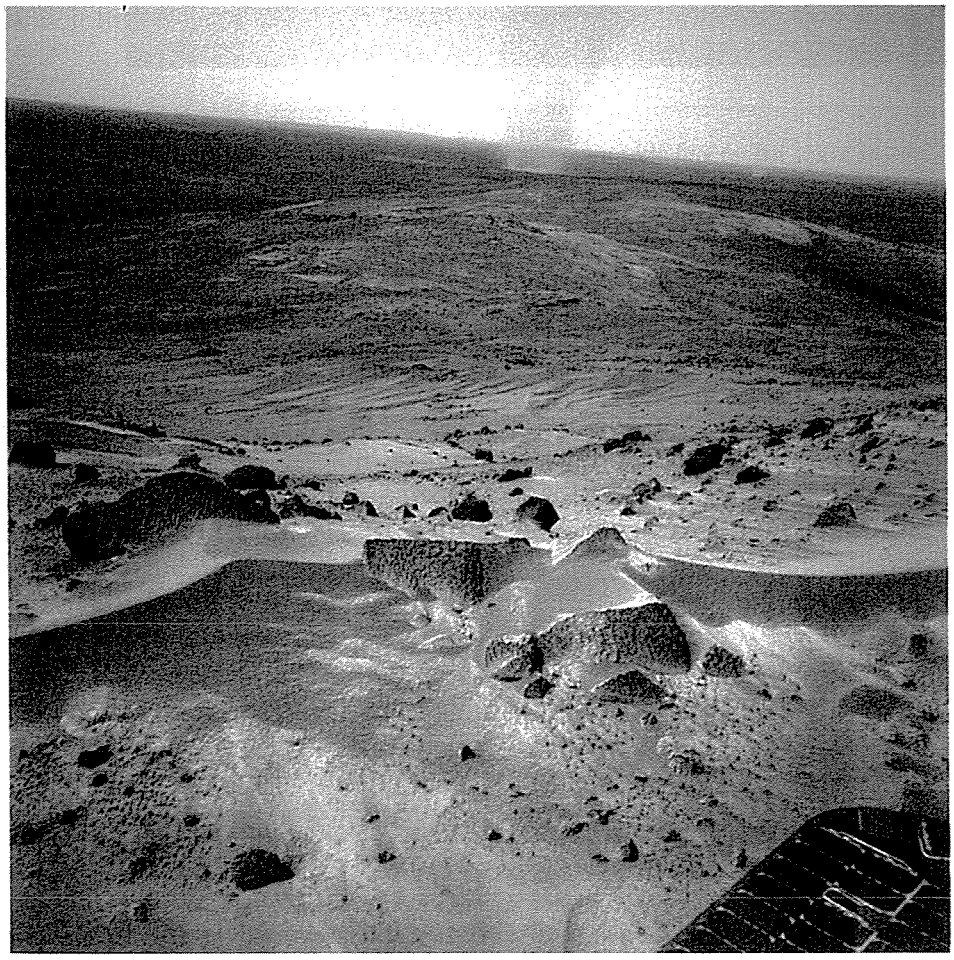

Fig. 7.9
A large dust devil, approximately one kilometre in height, one of many observed by the *Mars Exploration Rovers*. The dust they contain is opaque enough to cast a shadow, and their passage across the surface leaves a trail of disturbed material that has been observed from orbit by the camera on *Mars Global Surveyor*.

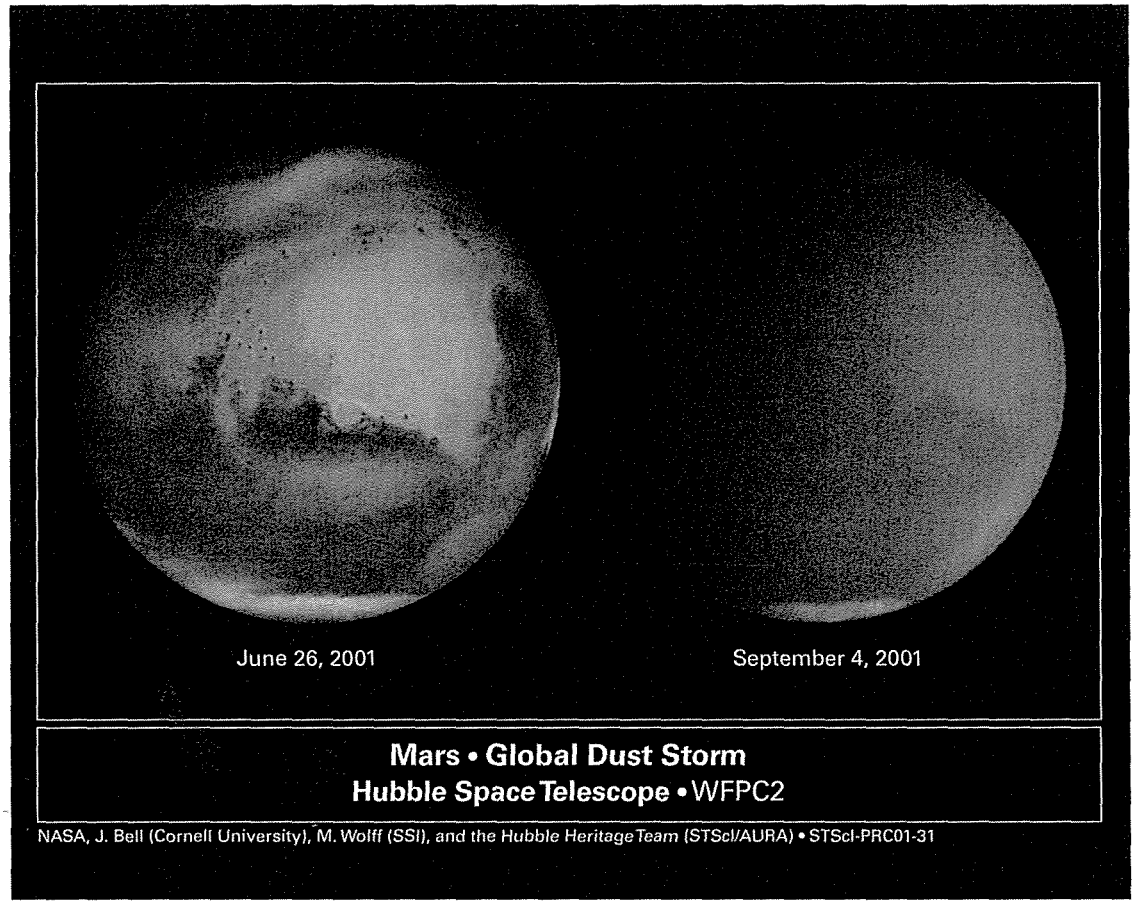

Fig. 7.10
Two *Hubble Space Telescope* views of Mars, before and after the onset of a global dust storm in 2001.

During stormy conditions, dust is raised everywhere that strong winds and turbulence scour the surface. Before the dust amount is enhanced by a storm, it helps to start and maintain the process by local winds produced through its affect on atmospheric heating. By absorbing and scattering solar and thermal radiation, dust heats both the atmosphere and the surface, as can be seen by comparing the dusty and dust-free profiles in Fig. 7.8. This makes the atmosphere more stable with respect to convection in the regions with large amounts of airborne dust, and also reduces horizontal temperature gradients and winds inside the dust cloud. However, the winds, especially near the surface, are likely to be strong near the edge of a dust cloud due to the large temperature gradients there. The net effect is to increase the extent of the disturbance, helping to explain why it sometimes spreads at great speed. The enhanced winds whip up additional and larger particles from the dusty plains, producing an opaque blanket that can cover the entire planet (Fig. 7.10).

Nothing like this happens on Earth, despite surface wind stresses that are generally larger than those on Mars, mainly because the dust is more quickly removed from the atmosphere by coagulation in wet environments, or by forming condensation nuclei for clouds and precipitation. Even if all of the land on Earth were as dry and dusty as

Mars, the oceans would make it difficult for Martian-style global dust storms to propagate. Global storms do not occur every year on Mars, but when they do it tends to be in the same season of the year, when the planet is close to perihelion, and the solar heating is about 40% greater then than it is when Mars is furthest from the Sun (at aphelion). They also tend always to originate in approximately the same part of the southern hemisphere.

7.3 Cloud formation, composition and mass density on Jupiter

We have already seen how the fully hydrogenated versions of common elements (NH_3, CH_4, etc.) form in Jupiter's atmosphere, and how some of these form clouds at temperatures that fall as low as 100 K at the tropopause. The highly convective atmosphere, driven by the internal release of heat, brings moist air up from great depths, cooling as it rises, and depositing a layer of each volatile in turn as a cloud at the appropriate condensation level (Fig. 7.11).

If the abundance of each species is known, or is assumed from 'solar composition' models where measurements do not exist, it is straightforward to calculate the level of cloud formation for each species. The density of the condensed material in the cloud can be estimated as well, with the assumption that dynamics can be neglected in the calculation, which of course is very simplistic. In practice, condensable material is

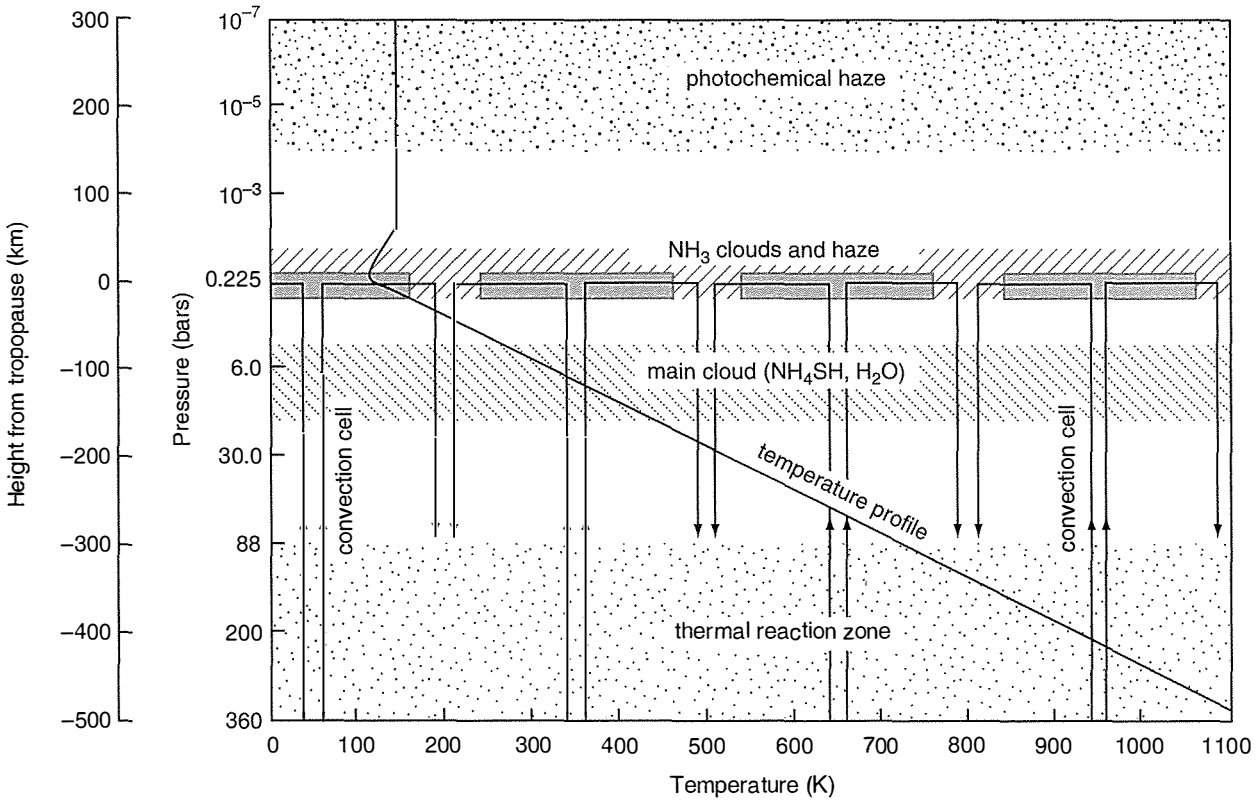

Fig. 7.11
Cloud diagram for Jupiter showing rising and falling regions, and multiple cloud layers, from Beer and Taylor (1972).

being supplied from below in upwelling regions, and cloud formation tends to be suppressed in downwelling regions where the air has been freeze-dried at high levels before it arrives. Coalescence and rain-out will also have a major effect on the cloud density in any particular region, making the actual cloud density a function of the local meteorology in a way analogous to the familiar situation on the Earth.

For simple liquid/vapour and solid/vapour transitions, the condensation levels of clouds may be estimated from simple thermodynamics.

The Clausius-Clapeyron equation is:

$$\frac{dp}{dT} = \frac{Lp}{RT^2}$$

where L is the latent heat of vaporisation per mole. If L is assumed to be constant with temperature then:

$$\ln\left(\frac{p}{p_1}\right) = -\frac{L}{R}\left(\frac{1}{T} - \frac{1}{T_1}\right)$$

Condensation occurs when the partial pressure of vapour (xp, where x = mole fraction, and p is the total atmospheric pressure) is equal to the saturated vapour pressure defined by the phase boundary curve. For example, for the ammonia ice to vapour phase transition, the following relationship is found:

$$\ln(p) = 15.56 - \frac{3643.6}{T}$$

where p is measured in atmospheres, and T in K.

We can calculate the height range over which clouds form and estimate the mass of condensate by comparing the partial pressure of each species with the saturated vapour pressure at each height level, obtaining the latter from the Clausius-Clapeyron equation, as discussed above. Some species react together first, e.g.

$$NH_3 + H_2S \rightarrow NH_4SH(\text{solid})$$

Then the thermodynamics are more complicated, but may be adequately approximated by a similar equlibrium constant equation of the form:

$$\ln(p_{NH_3}) + \ln(p_{H_2S}) = 34.12 - \frac{10833.6}{T}$$

where p_{NH_3} and p_{H_2S} are the partial pressures (in atm.) of NH_3 and H_2S, respectively. Here, condensation will occur in an atmosphere when:

$$\ln(x_{NH_3} \times p) + \ln(x_{H_2S} \times p) \geq 34.12 - \frac{10833.6}{T}$$

where the x's are the volume mixing ratios of NH_3 and H_2S, respectively, and p is the total pressure.

For Jupiter, clouds of water ice, ammonium hydrosulphide, and ammonia ice are expected at the levels shown in Fig. 7.12. Extending a similar treatment to Saturn and Uranus predicts layers of the same material, but at greater depths since condensation tends to occur at about the same temperature for a given species (Fig. 7.13). This treatment neglects basic processes, such as vertical motions, which feed moist air up to the condensation level, and must affect the cloud density, as well as photochemistry and rain-out, but does nevertheless seem to give a reasonable zeroth-order prediction of the clouds that actually occur.

Pure condensates are usually white, so how can we explain the 'bright' coloration of the Jovian clouds? Firstly, it should be remembered that the images we are all familiar with have been considerably colour-stretched and enhanced. Anyone who has actually observed Jupiter through a telescope will know that in reality the dominant colour is a yellowish brown. Even the Great Red Spot has only a faint brick-red tinge and not all observers agree that it is red (although an analysis of the intensity in different wavelength filters on spacecraft cameras show that there is a blue absorber present that is not found in the surrounding clouds). The colours that are present, technically known as 'chromophores', are probably due to impurities in the condensates. Various forms of elemental sulphur may contribute to the reds, yellows and browns, while it is also possible that the red spot

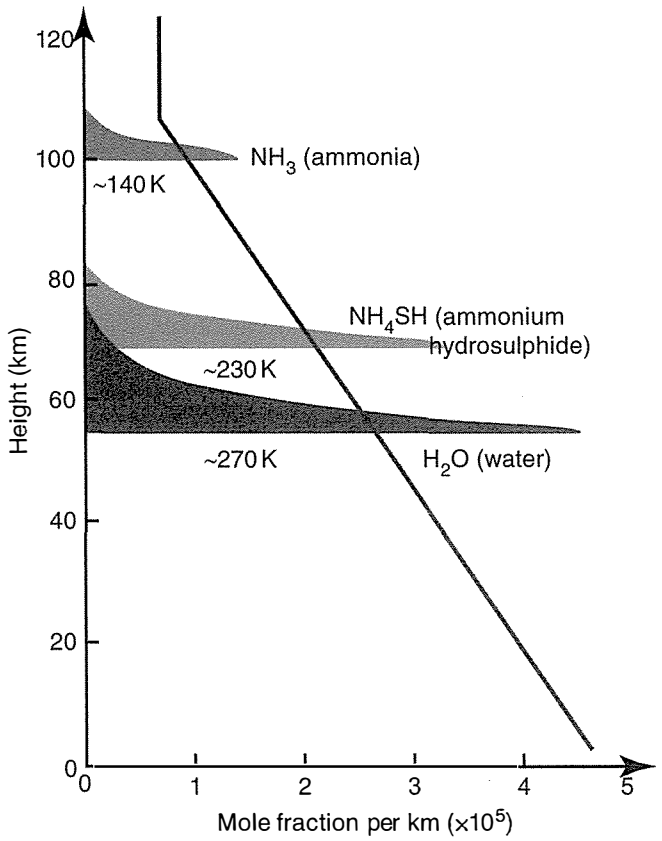

Fig. 7.12
A cloud condensation model for Jupiter, showing the predicted levels of the three uppermost layers relative to a model temperature profile. The pressure at the base of the water cloud is about 3 bars, and near the top of the ammonia cloud, near the tropopause, it is about 0.3 bars. Most of the coloration of the visible face of Jupiter seems to be due to the ammonium hydrosulphide layer, produced by combination of hydrogen sulphide and ammonia ($H_2S.NH_3$). Although this compound is white, it probably contains other sulphur compounds as impurities, and these are often yellow or brown.

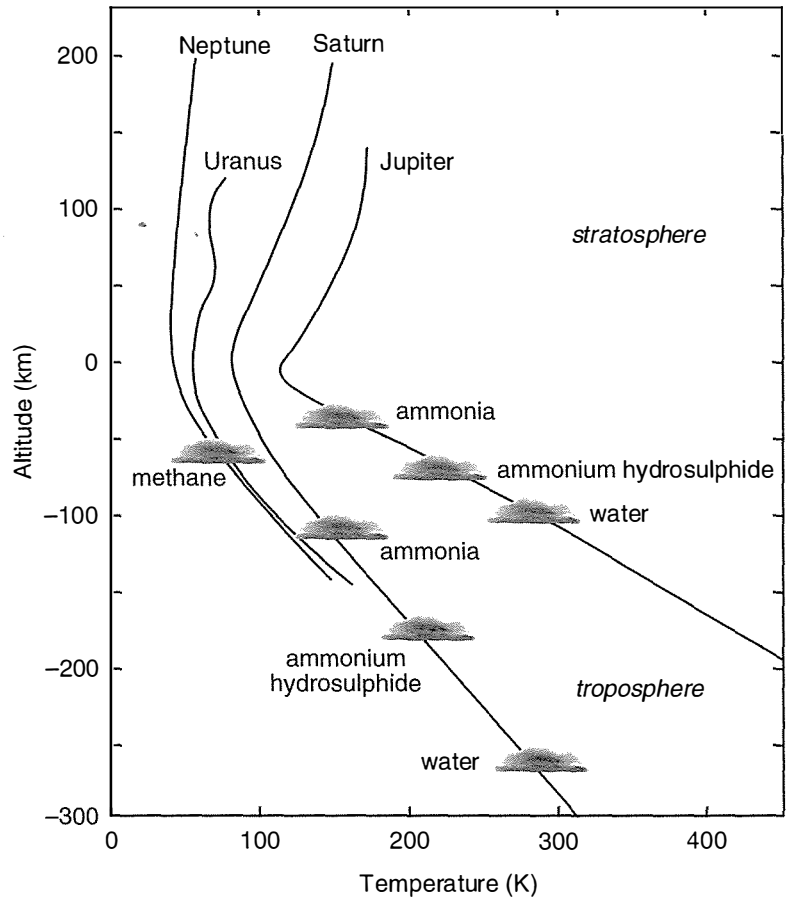

Fig. 7.13
Predicted levels for cloud layers to form on Saturn, Uranus and Neptune, compared to Jupiter, and calculated from similar cloud condensation models. The clouds of a given composition occur at about the same temperature on each planet, but only Uranus and Neptune are cold enough for the condensation of methane; on Jupiter and Saturn it stays gaseous.

may be coloured by phosphorus produced by reactions in the deep atmosphere involving phosphine.

7.4 Clouds, haze and rain on Titan

Various types of cloud and haze exist on Titan, dominated by two types:

1. the yellow-orange tinted photochemical hazes at high levels, around 200 km above the surface, that are responsible for the appearance of the satellite from Earth and space; and
2. sporadic, cumuliform methane clouds, localised in space and time, at altitudes between 15 and 18 km at tropical latitudes, and more frequently and higher, but still below 30 km altitude, at both poles.

It is also possible that there is a near-global layer of methane ice cirrus, below the hydrocarbon haze layers. The profiles measured by *Huygens* show that the methane relative humidity, with respect to pure methane condensation, is around 80% at altitudes from 8–16 km, but 100% between 20 and 30 km. These conditions correspond to the condensation of methane ice over the higher range, a condition that may apply over much of Titan. The growth of the crystals would eventually lead to some of them precipitating out, in which case (as on Earth) heavy ice particles falling through the relatively warm lower atmosphere would

melt or evaporate before reaching the surface. The quantities are likely to be such that this normally amounts to not more than a moderate drizzle (Fig. 7.14).

In addition to photochemical hazes at high levels and methane clouds in the troposphere, a variety of condensate zones for other species could exist at intermediate levels in the stratosphere, leading to cloud or haze formation, especially if suitable seed nuclei are present to facilitate condensation. Infrared spectra of Titan include broad emission features that have been attributed to condensates like C_4N_2, C_2H_2, HCN, and perhaps C_2H_5CN. Ethane, C_2H_6, can also condense at Titan atmospheric temperatures, but is less abundant than methane. Ethane clouds have been detected at polar latitudes, where it is thought that they are formed as a result of stratospheric subsidence and the particularly cool conditions near the north pole, where winter conditions prevailed at the time.

Despite the variety of energetic cloud activity seen on Titan, less than 1% of the globe has tropospheric cloud cover at any given time, although the coverage of high-level haze is virtually 100% at all times.

7.4.1 The haze layers in the upper atmosphere

The photochemically produced haze on Titan is often described as smog, since it is produced in a way that is analogous to the familiar urban pollution on Earth. The products of photodissociation of nitrogen and methane recombine and produce larger molecules, which mix downwards into cooler regions where they condense and form the stratospheric haze layers. These lie high in the atmosphere and increase the apparent size of the disc seen through a telescope from the Earth by several hundred kilometres, which is why Titan used to be thought the largest moon in the Solar System, whereas in fact it is slightly smaller than Ganymede.

The interpretation of photopolarimetry data on the haze acquired by the *Pioneer* spacecraft constrained the particle radius to about 0.1 μm, assuming the aerosols are made up of spherical particles. However, the high phase angle brightness measurements made from *Voyager* some years later required the particle sizes to be nearer 0.5 μm. Attempts to reconcile the two included the suggestion of a multimodal distribution for the particle sizes, and the possibility that the particles are irregularly shaped, possibly aggregates constructed from smaller units. In any case, a model in which the particles are all spherical and of nearly the same size, which works quite well for the upper cloud layers on Venus, seems to be too simplistic for Titan.

The refractive index of the haze particles is an important parameter that can be estimated from measurements of candidate materials produced in the laboratory by passing electrical discharges though a mixture of methane and nitrogen. The optical properties of the organic matter (sometimes called 'tholin', a general term derived from the Greek word for 'muddy', without implications for the chemical composition) produced in these experiments provide a reasonable match to

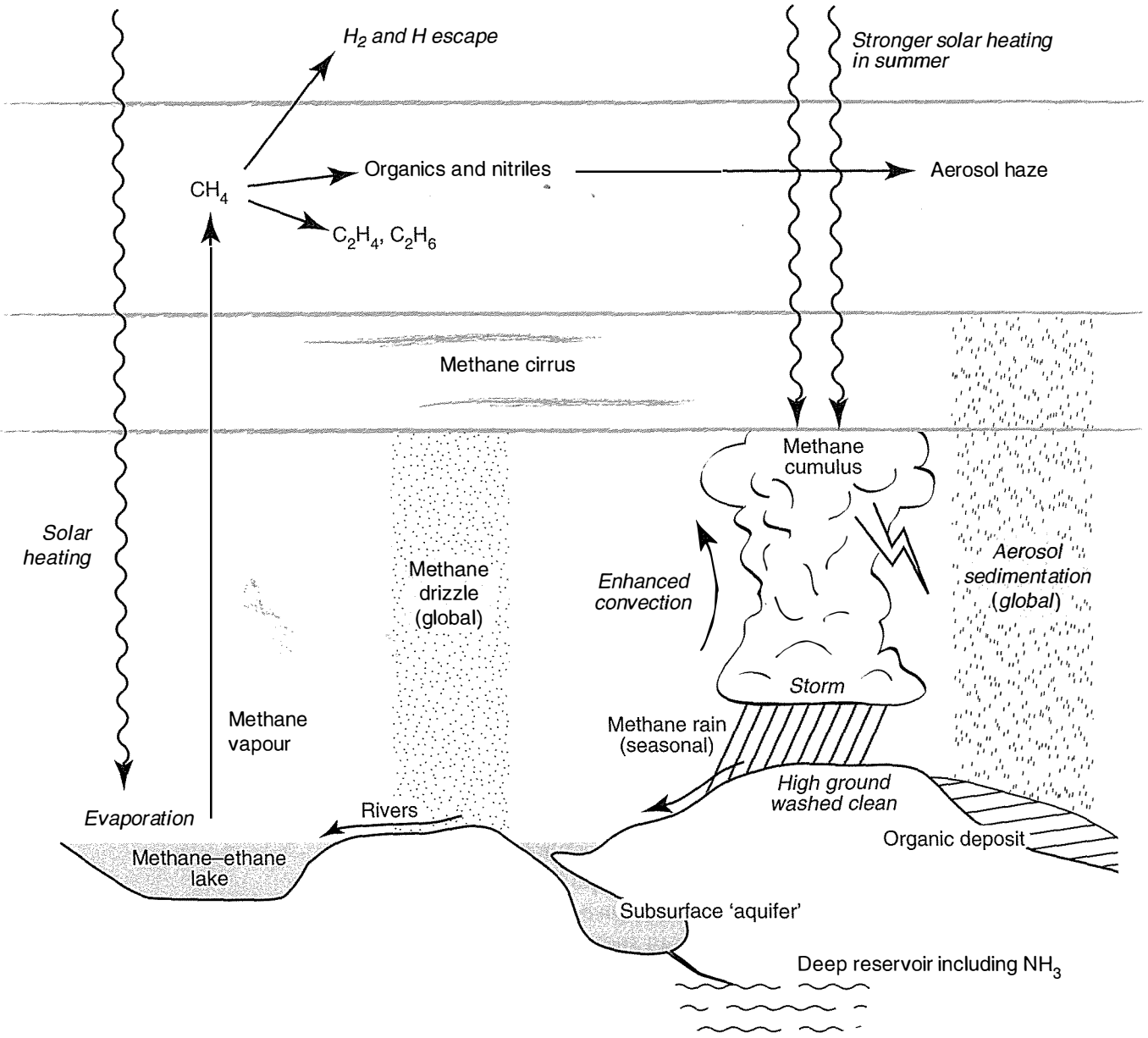

Fig. 7.14
A summary of the key observed and inferred features of Titan's meteorology strikes some unique parallels with the Earth: haze, cirrus and cumulus clouds; convective storms, lightning, and precipitation; rivers and lakes; subsurface reservoirs of liquid and gas in contact with the atmosphere.

the general features of the observed spectrum of Titan, supporting the inference that the haze is composed of organic molecules of photochemical origin.

If the haze production process continues for long enough, some of the higher-order products will become sufficiently abundant that sooner or later they are bound to form larger particles that fall out of the stratosphere. At least some of these consist of refractory materials, that is, oily or solid substances which, once formed, do not evaporate under the conditions that prevail on Titan. Once in the troposphere, they drizzle down to the surface, and apparently contribute to the level of atmospheric turbidity detected there by the *Huygens* probe.

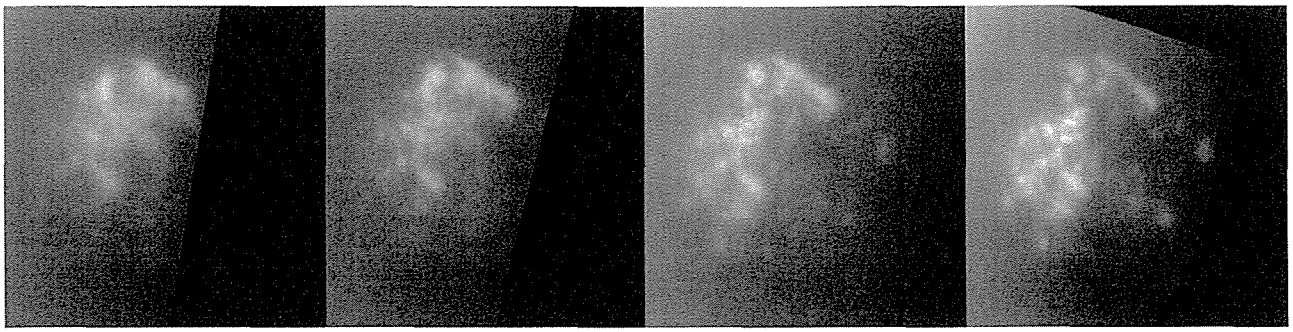

Fig. 7.15
Methane clouds near the south pole of Titan, observed from *Cassini*. The first and last pictures are about 5 hours apart, showing how the cloud evolved in that time.

7.4.2 Clouds in the troposphere

In addition to the hazes covering Titan, relatively dense, localised, cumulus-type clouds form in the lower atmosphere (Fig. 7.15). The evidence that these are composed primarily of methane follows since this very abundant species will condense and evaporate at the temperatures in Titan's troposphere where the clouds are seen to form, much as water does on Earth. Particles from the high-altitude hazes may provide nucleation sites for the growth of larger methane droplets as they drizzle down to the surface. Where the conditions of temperature and relative humidity are right, these composite particles will grow and rain out, accelerating the rate at which both haze and cloud particles are removed from the atmosphere. The methane clouds appear sporadically, are very dense, and capable of producing methane rain in large quantities at times, suggesting that Titan meteorology is as complicated as Earth's (§8.6).

The dry river valleys and coastlines seen on Titan are evidence for fluid flows on the surface, which implies that heavy precipitation comparable to terrestrial monsoons must occur at times. *Cassini* visible and infrared images revealed that the horizontal structure, height, and optical depth of Titan's clouds are highly dynamic. Vigorous cloud centres have been seen to evolve convectively, rising from the middle to the upper troposphere within 30 minutes and dissipating within the next hour, probably through rain. They occur, like the monsoons, at the end of the warmest part of the year when the atmosphere is saturated and beginning to cool. Phenomena like circulation-induced convergence, forcing associated with Saturn's tides, and variations in surface topography and volatile composition, must all have a role in Titan's stormy, wet weather.

7.5 References and further reading

Baines, K.H., S. Atreya, R.W. Carlson, D. Crisp, P. Drossart, V. Formisano, S.S. Limaye, W.J. Markiewicz, and G. Piccioni. To the depths of Venus: Exploring the deep atmosphere and surface of our sister world with *Venus Express*. *Planet.Space Sci.*, **54**, 1263–1278, 2006.

Beer, R., and F.W. Taylor. The abundance of CH_3D and the deuterium-hydrogen ratio in Jupiter. *Astrophys. J.*, **179**, 309–327, 1973.

Gierasch, P.J., and R.M. Goody. The effect of dust on the temperature of the Martian atmosphere. J. *Atmos. Sci.*, **29**, 400–402, 1972.
Neumann, G.A., D.E. Smith, and M.T. Zuber. Two Mars years of clouds detected by the Mars Orbiter Laser Altimeter. J. *Geophys. Res.*, **108**(E4), 5023, 2003.
Titov, D.V., F.W. Taylor, H. Svedhem, N.I. Ignatiev, W.J. Markiewicz, G. Piccioni, and P. Drossart. Atmospheric structure and dynamics as the cause of ultraviolet markings in the clouds of Venus. *Nature*, **456**, 620–623, 2008.
West, R.A., K.H. Baines, D. Banfield, A.J. Friedson, B. Ragent, and F.W. Taylor. Jovian clouds and hazes. In *Jupiter: The Planet, Satellites and Magnetosphere*, ed. by F. Bagenal, W. McKinnon, and T. Dowling, Cambridge University Press, 79–104, 2004.

7.6 Questions

1. The Clausius-Clapeyron equation for the pressure–temperature relationship between liquid and vapour is

$$\frac{\mathrm{d}p}{\mathrm{d}T} - \frac{Lp}{RT^2}$$

where L is the latent heat of vaporisation per mole and R is the universal gas constant. If at some point on the phase boundary $p = p_1$ and $T = T_1$, and assuming that L does not vary with temperature, show that:

$$\ln\left(\frac{p}{p_1}\right) = -\frac{L}{R}\left(\frac{1}{T} - \frac{1}{T_1}\right).$$

2. In the region of Jupiter's atmosphere where water and ammonia clouds are expected to form, the temperature structure is approximately represented by a dry adiabatic lapse rate Γ. Hence

$$T = T_0 - \Gamma z$$

where z is the height above a reference level where $T = T_0$ and $p = p_0$. Derive the hydrostatic equation for such a level and show that:

$$\frac{p}{p_0} = \left(\frac{T}{T_0}\right)^{\frac{Mg}{RT}} = \left(\frac{T}{T_0}\right)^{\frac{Mc_p}{R}} = \left(\frac{T}{T_0}\right)^{\frac{C_p}{R}}$$

where M is the mean molecular weight of the atmosphere, c_p is the heat capacity per unit mass at constant pressure and C_p is the heat capacity per mole at constant pressure.

3. Consider a parcel of air rising from the deep atmosphere of Jupiter that has a volume mixing ratio x of water vapour. The partial pressure of water at any point will then be

$$p_{\mathrm{H_2O}} = xp = xp_0\left(\frac{T}{T_0}\right)^{\frac{C_p}{R}}$$

This water will start to condense at the level where its partial pressure exceeds the saturated vapour pressure. Show that the condensation level occurs where:

$$p_{H_2O} = p_1 \exp\left(-\frac{L}{R}\left(\frac{1}{T} - \frac{1}{T_1}\right)\right)$$

4. Given that the latent heat of condensation for water vapour is $L = 2.5 \times 10^6\,\mathrm{J\,kg^{-1}}$ and that its saturated vapour pressure is 610 Pa at 273 K, solve the above equation for T. (Hint: take the log of each side of the equation and use a graphical method of solution.) Calculate the corresponding atmospheric pressure and the height relative to the level at pressure p_0.

(The following data is provided: the temperature at $p = 10^5$ Pa is 273 K, the volume mixing ratio of water in the deep atmosphere is approximately 10^{-3}, the acceleration due to gravity on Jupiter is $26.2\,\mathrm{m\,s^{-2}}$, the heat capacity per mole at constant pressure is $C_p = 3.5R$, and the mean molecular weight of Jupiter's atmosphere is $0.002\,27\,\mathrm{kg\,mol^{-1}}$).

8 Dynamics of planetary atmospheres

8.1 Introduction

Every planetary atmosphere is in a state of almost constant motion. In considering the nature of these motions, it is convenient to think in terms of three related components:

1. the general circulation;
2. waves, eddies and turbulence; and
3. transient phenomena.

By the *general circulation* we mean the mean, permanent, global-scale patterns, such as the familiar westerlies and trade winds on the Earth, or the zonal superrotation on Venus. *Waves, eddies and turbulence* are all departures from the mean state, the first periodic and the last chaotic, with eddies somewhere in-between. The quasi-permanent giant eddies, of which the Great Red Spot on Jupiter is the best-known example, are important in the atmospheres of the giant gas and ice planets of the outer Solar System. *Transient phenomena* are localised, but not necessarily small, weather systems that grow, travel and eventually dissipate, like the familiar depressions and anticyclones on terrestrial weather maps, and the giant dust storms on Mars.

8.1.1 General circulation regimes

Certain features are common to all general circulation regimes. The air in the region of the globe that is most strongly heated by the Sun will tend to be less dense than parts where there is little or no radiative heating but cooling to space still goes on. The simplest example, not found in our Solar System, although Venus comes close, would be a planet that does not rotate at all, or which rotates at the same rate as its orbit so it keeps the same face towards the Sun at all times. Then, if the sunlight penetrates deep into the atmosphere and warms the surface, the air will rise, and migrate at higher levels to the antisolar point, where the difference between cooling and heating is greatest, and subsidence takes place (Fig. 8.1).

All of the planets in the Solar System rotate fast enough to reduce the temperature contrast between day and night at the surface to a

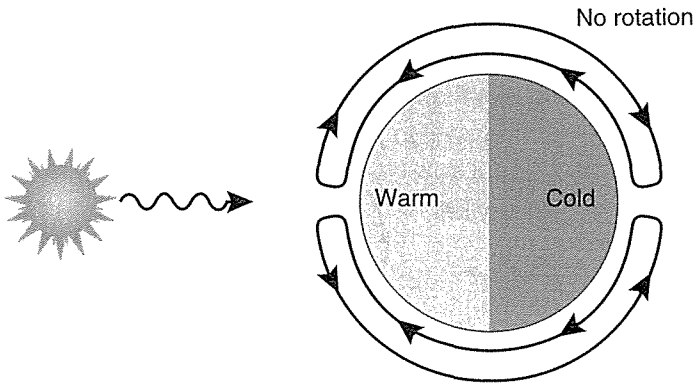

Fig. 8.1
A subsolar to antisolar circulation regime, such as would exist, in principle, on a smooth planet that kept one face towards the Sun at all times. Such a regime is found on Venus above about 100 km altitude, where the slow overall zonal rotation rate of the upper atmosphere appears to be not very different to that of the solid planet, i.e., about once every 243 Earth days.

value that is less than the difference ΔT between the mean equatorial temperature and that at the poles. That is, the length of the day t_{day} satisfies an expression of the form

$$\frac{\partial T}{\partial t} = -\frac{1}{\rho C_p}\frac{\mathrm{d}}{\mathrm{d}z}\Delta F < \frac{\Delta T}{t_{day}}$$

at levels in the atmosphere where ΔF is the net radiative cooling, the density is ρ, and the specific heat is C_p. On Venus, this is the case in the lower atmosphere, although the 'day' that is relevant is not the time for the solid planet to rotate – about 243 Earth days – but rather the time for the super-rotating atmosphere to travel around the planet, closer to 4 days. Then, the coldest, descending air is at the poles and the circulation regime is from equator to pole, forming a *Hadley cell* (Fig. 8.2).

If the planet rotates rapidly, a single Hadley cell extending from equator to pole is not stable, and multiple cells form (Fig. 8.3). The instability results primarily from the *Coriolis force*, which changes the direction of flow on a rotating platform relative to a stationary one. The effect on the Earth, for instance, is to gradually divert the polewards flow to the east in each hemisphere, closing the cell before it reaches the pole. Secondary and tertiary cells (the Ferrel and Polar cells) are needed to complete the circuit from equator to pole.

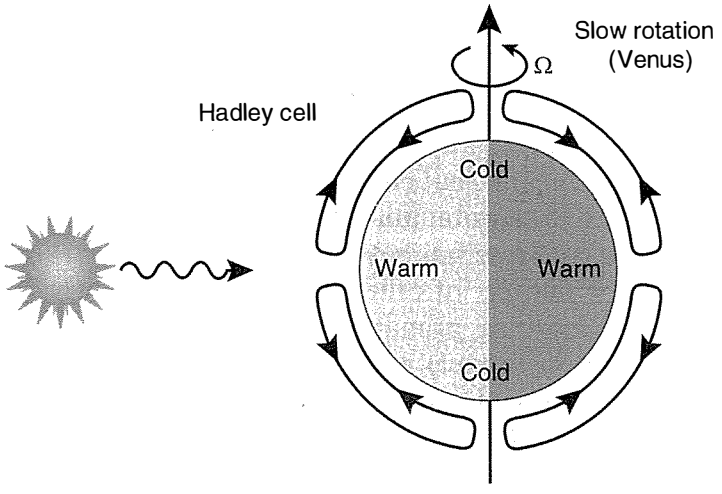

Fig. 8.2
An equator-to-pole circulation regime, such as would exist, in principle, on a planet that rotates fast enough to reduce the temperature contrast around the equator so that it is less than that from equator to pole. The hemispherical cells are named after George Hadley, who postulated such behaviour for the Earth as long ago as the eighteenth century. In reality, the regime most similar to this is found in the middle atmosphere of Venus, which rotates much faster than the solid planet, efficiently redistributing heat from the day to the night side.

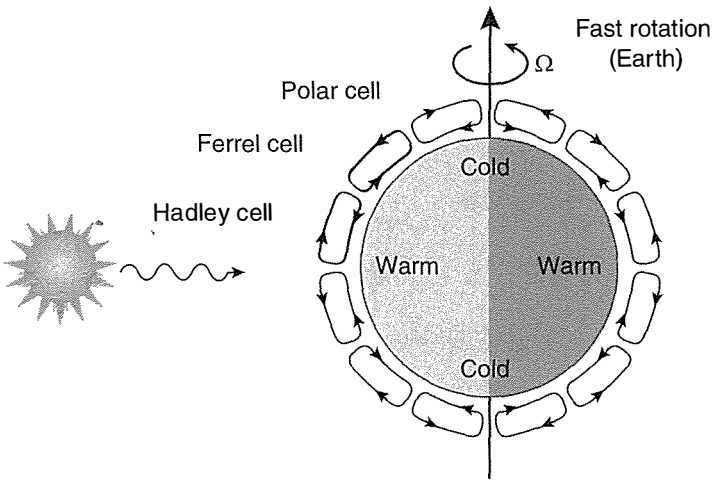

Fig. 8.3
A multiple cell regime, expected to exist on a rapidly rotating planet where the lowest mean temperatures are at the poles but equator-to-pole cells are unstable. Such a regime is found on the Earth, and commonly described in terms of three circulation cells, the Hadley, Ferrel (after a nineteenth-century American meteorologist), and Polar cells.

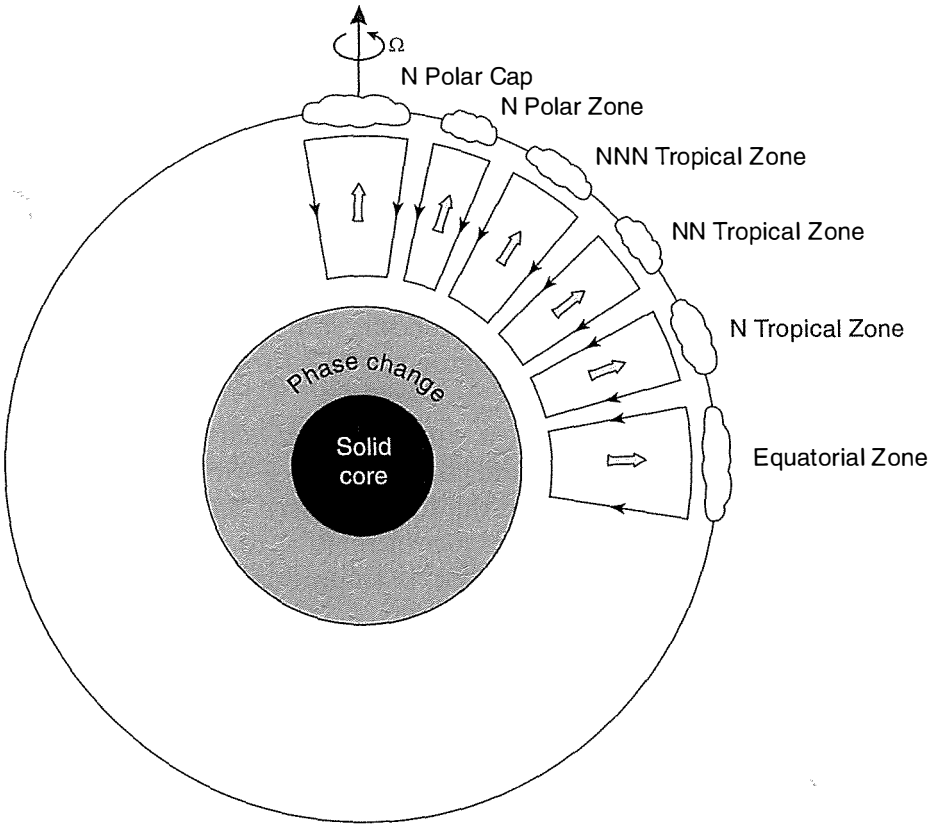

Fig. 8.4
A possible concept for the general circulation on Jupiter, with six cells in each hemisphere corresponding to the dominant belt–zone structure observed in the clouds. The large arrows represent the transfer of heat from the interior by the cells. The absence of a solid surface and the existence of an internal heat source mean the cells extend to a considerable, but unknown, depth. (For a different and more modern concept, see Fig. 8.25.)

On Venus, the Coriolis effect is smaller than on Earth, and the Hadley cells extend nearer, but not all the way, to the poles. On Jupiter, on the other hand, the combination of its large radius, rapid rotation, deep atmosphere, and internal heat source, combine to transport heat globally in a large number of cells. The upwelling branch of each cell carries moisture (meaning primarily ammonia, rather than water, at the cloud top level on Jupiter), which condenses to form cloud, giving the planet its characteristic banded appearance. Figure 8.4 shows an early concept for this behaviour, which could relate to Saturn and possibly the smaller giants as well. More recent thinking, based on

models that take detailed account of the very rapid spin of Jupiter, and of the latitudinal variation of the heat release from the interior of the planet, tend to favour an alternative concept in which the convection cells form cylinders around the axis of rotation. This is discussed below as part of a broader assessment of Jovian atmospheric dynamics, and pictured in Fig. 8.25.

8.1.2 Waves, eddies and turbulence

The principal categories of wave motion in planetary atmospheres can be categorised as

- acoustic or sound waves,
- gravity waves,
- Rossby waves, and
- atmospheric tides.

Acoustic waves are longitudinal, that is, they consist of a series of compressions and expansions of the air along the direction of propagation. Although they are common in nature (speech, thunder, wind-related noises), they carry relatively little energy and are unimportant except on very local scales.

Gravity waves occur when the restoring force, acting against gravity, is due primarily to the vertical density gradient in the atmosphere. A given sample or 'parcel' of air can then oscillate as it exchanges potential energy for kinetic energy and vice versa, the motion being perpendicular to the direction of propagation. A classic example is to imagine a parcel of dense air being carried up the side of a hill by the wind, and then falling on the other side. Its inertia will carry it below the level with the same density, so it becomes buoyant and experiences an upwards force which eventually prevails. It overshoots once more, and starts to descend, and so on, producing a vertically transverse wave (usually called an 'internal' gravity wave, to distinguish it from 'external' waves that occur on the surface or boundary of a fluid, like the ocean waves seen from the shore). The process that produces gravity waves does not need a solid obstacle: winds can interact with a variety of flow or density anomalies (a rising plume in a cloud formation, for instance, or some other kind of weather system) to produce the initial displacement that forces the waves. There is ample evidence for gravity waves on Earth, Mars, and Venus and it would be surprising if they do not occur on Titan also, produced by flow over surface features and flow around weather systems in the atmosphere.

Large-scale *horizontally* transverse waves are found in rotating atmospheres due to the variation with latitude of the Coriolis effect, which exerts a restoring force on an eastward flow that is perturbed, for any reason, away from the purely east–west direction. If this pushes the air mass across the equator, the restoring force is in the other direction (i.e., still towards the equator) and a long-wavelength oscillation, called

a *Rossby wave*, results. Their large scale, and the fact that they owe their origin to the curvature and rotation rate of the planet, gives them the alternative name of *planetary waves*. The force on a westward flow is away from the original direction, so the air mass cannot oscillate, and westward-propagating Rossby waves do not occur. This explains the absence of planetary wave activity in Earth's stratosphere in the summer, when the mean flow is predominantly to the west. The nature of planetary waves on the Earth was first explained by Carl-Gustav Rossby in the 1940s; we now know that they feature strongly on Venus and Mars as well.

Any cyclical motion that has a period that is a sub-multiple of the solar day is termed a *tide*. All atmospheres experience a *gravitational tide*, induced by the apparent daily motion of the Sun, and of the planet's satellites, if any, in the sky. This is the origin of the familiar tide in the Earth's oceans, which is due primarily to the gravitational attraction of the Moon on the water as the surface of the planet rotates through the Earth–Moon line. The Sun also exerts a gravitational tide, which is about half as strong as that of the Moon. However, in the atmosphere the gravitational effect of both bodies is so small as to be negligible when compared to the cycle in temperature, pressure, and winds induced by the diurnal heating effect of the Sun. This, the *thermal tide*, is also the only important tide on the other planets (although Titan is an interesting exception, due to the large distance from the Sun and the proximity of massive Saturn), so the prefix 'thermal' is often dropped.

Tides in the atmosphere contain a range of Fourier components, because the forcing is non-sinusoidal and the atmospheric response is non-linear. However, the semi-diurnal component tends to dominate the observed tidal behaviour of all three terrestrial planets, a counter-intuitive result that is, however, explained by classical tidal theory. The theory, which has occupied the minds of many great scientists from Newton onwards, including Euler, Laplace, and Kelvin, is complicated, and the outcome depends on many factors, including the mean wind and the interference between the various components. It shows that the diurnal tide cannot propagate vertically, leaving the next most strongly forced, the semi-diurnal component, to dominate in the free atmosphere if not at the surface itself.

Tidal oscillations, and other forms of travelling gravity waves, are seen to grow in amplitude as they propagate upwards. The kinetic energy they carry is proportional to the density times the amplitude of the wave squared, i.e., ρA^2, so in order to conserve energy the amplitude grows vertically as $\rho^{-1/2}$. Eventually the wave becomes unstable and 'breaks', dissipating as the chaotic motion known as turbulence. This is difficult to treat quantitatively, except by statistical methods or very simplified parameterisations. Turbulent flow can be treated as composed of a range of 'eddies' – rotating air parcels – of various sizes, sometimes very large and long-lived, as in the atmosphere of Jupiter. Theories of eddy diffusion and eddy viscosity can then be developed that treat the eddies as individuals, with a power

spectrum that tends to smaller and smaller scales through viscous interactions until the energy is dissipated as heat.

8.1.3 Transient phenomena

Fluctuations in the steady state are commonly termed *weather* when relatively short term, apparently chaotic, changes are being considered. Large, travelling disturbances – fronts, cyclones, and storm systems – are of particular interest. These can be recognised in the cloud patterns on Mars and Venus, and the related winds inferred from tracking their motions in visible and infrared images. On the Earth, processes with periods of seconds are sometimes important (in thunderstorms, for example), ranging up to oscillations in the ocean circulation which might have periods of decades or longer. Jupiter's Great Red Spot is a giant eddy, and so might be regarded as an extreme example of atmospheric turbulence, although it is more usually considered to be a long-lived anticyclonic storm system. In any case, it will not last indefinitely, although it was first observed more than 300 years ago.

On rapidly rotating planets, including Earth and Mars but not Venus or Titan, most transient weather systems are the result of *baroclinic* instabilities. These occur where temperature contrasts produce deviations from the linear relationship between pressure and density in a fluid sufficient to generate a disturbance, typically at the edge of a strong airflow like a jet stream. Latent heat release during convective cloud-formation processes can also be important, as for example in thunderstorm genesis on the Earth or Jupiter. Radiative–dynamical feedbacks involving large amounts of airborne dust play a somewhat similar role on Mars in producing the great global dust storms.

8.2 Earth atmospheric circulation

Without trying to cover the whole topic in depth, it is useful to discuss some aspects of the atmospheric circulation on Earth that are relevant to planetary atmospheres in general.

8.2.1 Geostrophic balance

In the vertical direction, gravity is approximately balanced by the force due to the pressure gradient as expressed by the hydrostatic equation relating the fields of pressure, p, and density, ρ:

$$\frac{\partial p}{\partial z} = -\rho g \qquad \text{(hydrostatic equation)}$$

where g is the acceleration due to gravity and z is the height measured from the ground upwards. Strictly speaking, additional terms are

required when the atmosphere is in motion, but these can usually be ignored as long as the scale of the motion is larger than the depth of the system.

In the horizontal direction, a parcel with unit mass and a zonal velocity u experiences a *Coriolis acceleration* fu where $f = 2\Omega \sin\Phi$, Ω is the planetary rotation rate, and Φ is latitude. Consider motions whose horizontal scale is L and whose magnitude is of order U. As long as $U << fL$ and if the frequency of the time dependence is much less than f, the horizontal force due to the pressure gradient and the Coriolis force must balance. This is termed *geostrophic* balance. For the zonal wind u, it gives

$$f\rho u + \frac{\partial p}{\partial y} = 0 \qquad \text{(geostrophic balance equation)}$$

where y measures the northward direction. Friction has been neglected.

8.2.2 The thermal wind equation

The thermal wind equation is a relationship between the vertical derivative of the horizontal wind and the horizontal temperature gradient. Here we shall derive it for the zonal wind only, i.e., the component parallel to the equator.

A few manipulations of the hydrostatic and geostrophic balance equations yield the thermal wind equation. First, divide the former by the latter after moving the Coriolis force term to the right-hand side. The ratio of the two derivatives becomes $\partial z/\partial y$ taken at constant pressure. This intermediate result states that on surfaces of constant pressure, which ripple up and down in the real atmosphere, the downhill accelerations due to gravity are balanced by Coriolis accelerations. If we now take the derivative with respect to z, use the ideal gas relationship $p = \rho RT$, and rearrange, the result is

$$\frac{\partial u}{\partial z} = -\left(\frac{g}{fT}\right)\frac{\partial T}{\partial y} \qquad \text{(thermal wind equation)}$$

where the partial derivative with respect to y is at constant p, and that with respect to z is at constant y.

A familiar example of the application of the thermal wind equation is the increase of eastward wind with height, which occurs in the Earth's troposphere at midlatitudes, and which is associated with the decrease in temperature towards the poles.

8.2.3 Cyclostrophic balance

On a slowly rotating planet like Venus, the Coriolis term is negligible, and in order to convert temperatures to winds we need to calculate the

equation of *cyclostrophic* balance, which represents the balance between pressure gradients and the centripetal force associated with the zonal wind motion.

Starting with the hydrostatic primitive equations[64] for a shallow atmosphere in which $a + z \approx a$, where z is altitude and a is the planetary radius:

[64] See, for instance, *Introduction to Circulating Atmospheres* by I.N. James, Cambridge University Press, 1994, for a detailed derivation of these equations.

$$\frac{du}{dt} - \frac{uv \tan\phi}{a} - 2\Omega v \sin\phi + \frac{1}{\rho a \cos\phi}\frac{\partial p}{\partial \lambda} = F_\lambda$$

$$\frac{dv}{dt} - \frac{u^2 \tan\phi}{a} + 2\Omega v \sin\phi + \frac{1}{\rho g}\frac{\partial p}{\partial \phi} = F_\phi$$

$$g + \frac{1}{\rho}\frac{\partial p}{\partial \xi} = F_\lambda$$

For a slowly rotating planet like Venus, the terms in the rotation rate Ω drop out and some manipulation gives the cyclostrophic thermal wind equation:

$$2u\frac{\partial u}{\partial \xi} = \frac{R}{\tan\phi}\left(\frac{\partial T}{\partial \phi}\right) \qquad \text{(cyclostrophic thermal wind equation)}$$

where λ and ϕ are latitude and longitude, u and v the zonal and meridional winds, R the gas constant ($191.4\,\mathrm{J\,kg^{-1}\,K^{-1}}$ for Venus) and ξ is a height-like variable defined by:

$$\xi = -\ln\left(\frac{p}{p_0}\right).$$

8.2.4 The Rossby number

The geostrophic approximation is so useful that it is valuable to have a simple test to show when it can be applied: this is the purpose of the Rossby number R_0. An expression for this is found by observing that, if there are fluctuations present, there will be an acceleration term in the momentum balance, so that the geostrophic balance equation becomes

$$f\rho u + \frac{\partial p}{\partial y} = \rho\frac{\partial u}{\partial t}$$

For geostrophy to apply, the new term on the right must be small compared to the Coriolis term. Taking the ratio of the characteristic scales of the two terms we find

$$R_0 = \frac{U/t^*}{fU} = \frac{U}{fL} \approx \frac{10^3 \text{cm s}^{-1}}{10^{-4}\,\text{s}^{-1} 10^8\ \text{cm}} = 0.1 \quad \text{(Rossby number equation)}$$

where U, t^* are characteristic zonal velocity and timescales, respectively, and L a characteristic length. The representative values ($v = 10$ m s^{-1}, $L = 1000$ km) show that geostrophic balance is often a good approximation on the Earth for large-scale atmospheric motions.

8.2.5 The deformation radius

Another useful concept is the Rossby radius of deformation, a horizontal length which emerges as a natural scale of motion in stably stratified atmospheres on rotating planets. A familiar example is given by the large-scale waves that dominate the weather at midlatitudes on the Earth; these are instabilities that emerge spontaneously with this length scale. To see how this arises, consider a flow of characteristic depth D and horizontal scale L, illustrated in Fig. 8.5. As discussed above, the thermal wind equation will determine a relationship between temperature fluctuation and wind shears. Dimensionally,

$$U' = \left(\frac{D}{fL}\right) g \left(\frac{T'}{T}\right)$$

where T' is the temperature contrast associated with the flow, T is the full temperature, and L is the horizontal scale of the temperature variations. Now consider time-dependent fluctuations in place of spatial variations in temperature, and their effect on the evolution of the flow. As long as viscosity is negligible, the angular momentum of rings of moving fluid, dominated by the general rotation of the fluid with angular velocity f, will be conserved. Upward motion leads to convergence and hence spin-up near the bottom of the layer (Fig. 8.5) and U increases to U', given by

$$\frac{U'}{L} \approx f\left(\frac{\delta z}{D}\right)$$

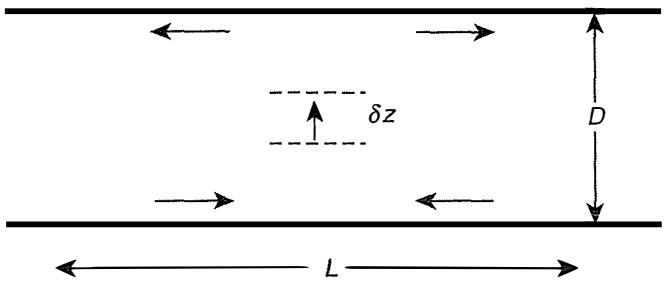

Fig. 8.5
Illustrating the deformation radius L in a layer of depth D.

But in a stratified atmosphere, temperature variations will also be proportional to the vertical displacement (assuming the motion is fast enough to be adiabatic), and

$$T' = \delta z\left(\frac{\partial T}{\partial z} + \frac{g}{C_p}\right)$$

Combining these two equations gives a relation between U' and T':

$$U' = \frac{fLT}{D\left(\frac{\partial T}{\partial z} + \frac{g}{C_p}\right)}$$

which must be satisfied at the same time as the thermal wind equation. To achieve this, a constraint on the horizontal scale must be satisfied, namely

$$f^2L^2 \approx D^2 g\left(\frac{\partial T}{\partial z} + \frac{g}{C_p}\right) \qquad \text{(deformation radius equation)}$$

which defines the deformation radius L. Its size is typically 1000 km in Earth's atmosphere; where motions of this scale are present on other planets, it indicates that the processes invoked above are acting together there, too.

8.2.6 Zonal superrotation

The tendency for the axial component of absolute angular momentum to be conserved following the motion of individual parcels of air can result in important constraints on the kind of circulation a planetary atmosphere can exhibit. There are, however, cases where the zonal (east–west) flow of the atmosphere is observed to be more rapid on average than that of the surface beneath. This is the phenomenon of *superrotation*, and it is found in the atmospheres of Earth, Venus, and Titan, with related phenomena on the outer planets where high winds are seen but are not related to a solid surface.

To understand superrotation, we must consider the processes that may be responsible for departures from perfect angular-momentum conservation. Our first task is therefore to measure superrotation quantitatively. For simplicity, we will only consider flow that is symmetric about the rotation axis of the planet (axisymmetric flow). If we consider a parcel of air moving around the planet with a zonal velocity u at a perpendicular distance a from the rotation axis, the specific angular momentum of the flow is

$$m = a\cos\phi\ (\Omega a\cos\phi + u)$$

where ϕ is latitude. Now we define local superrotation s as:

$$s = \frac{m}{\Omega a^2} - 1 \qquad \text{(local superrotation equation)}$$

so that $s = 0$ for solid-body rotation, and any observations of positive values of s imply that there must be non-conservative forces at work. In considering the whole planet, we integrate $\Omega \rho r^2$ over the entire atmosphere to obtain the total axisymmetric component of absolute angular momentum for an atmosphere at rest with respect to the surface. We then define the global superrotation S as

$$= \frac{\iint \rho m \, \mathrm{d}A}{\iint \rho \Omega a^2 \cos^2 \phi \, \mathrm{d}A} - 1 \qquad \text{(global superrotation equation)}$$

with similar properties to s. In particular, values of S greater than zero imply non-conservative torques on the atmosphere, produced for example, by friction with the surface or some non-axisymmetric effect. For the Earth, S is positive, but small (about 0.015), while for Venus S is of order 10. Titan superficially resembles Venus in many ways (slowly rotating, completely cloud-covered, atmosphere driven by differential heating of the upper layers, greenhouse heating of the lower atmosphere, small influence of surface topography) and also has a high value of S, but apparently about ten times smaller than Venus (§8.6.1).

8.2.7 Meridional circulation

On the Earth, the circulation is towards the pole at the equator, but deflected towards the east in the northern hemisphere by the Coriolis force. The latter dominates by midlatitudes, closing the Hadley cell and allowing the Ferrel cell to take over at higher latitudes. On slowly rotating Venus, the Coriolis force is very small and the Hadley

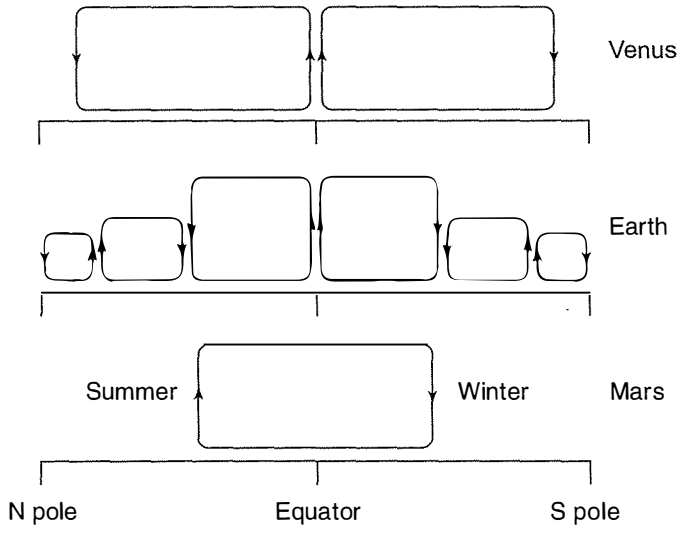

Fig. 8.6
Very simplified schematics of the general circulation of the atmospheres of the terrestrial planets Venus, Earth, and Mars (at equinox).

circulation extends nearly all the way to the pole. On Mars, the circulation has a larger seasonal dependence than on the other two terrestrial planets, but for part of each year it appears to have a modified Hadley circulation in which a single cell spans both hemispheres (Fig. 8.6).

8.2.8 Waves

Terrestrial meteorologists classify atmospheric waves into many different types, but the most important, especially in a large-scale comparative planetology context, are the Rossby and gravity waves defined above (§8.1.2). Most of the large-scale periodic features that are seen, for example, in satellite maps of atmospheric temperature fields on the Earth and Mars, are Rossby waves. Midlatitude Rossby waves are involved in the formation of the large horizontal Y-shaped feature that dominates the appearance of Venus when it is imaged at ultraviolet wavelengths (Fig. 8.7). In that case, a similar feature might be expected to occur on Titan, although the different composition of the clouds makes it more difficult to observe. There is indirect evidence for Rossby wave activity on Titan in the behaviour of the trace atmospheric gases that are variable across the globe, and of the methane condensate clouds that have been seen moving with the wind near the surface.

Gravity waves arise when parcels of air of different density to their surroundings oscillate under the control of buoyancy forces, as in the lee waves which form behind a mountain, as a result of relatively dense air being forced to ascend to cross the obstruction, and then falling freely on the other side. The rising and falling motion, which is principally in the vertical direction along the gravity gradient, can result in a significant restoring force due to compression of the air in the direction of motion of the parcel. When this effect is important, the resulting periodic motion is sometimes called an acoustic gravity wave. In general, the importance of gravity g relative to the inertial force due to motion with speed U can be measured by a quantity called the *Froude*[65] *number* F, defined by $F = \frac{U}{\sqrt{gH}}$, where H is the pressure scale height. Then, for gravity waves $F \ll 1$, and for acoustic gravity waves $F \approx 1$. The situation where $F \gg 1$ corresponds to the familiar case of ordinary acoustic waves, i.e., pressure waves that propagate without reference to the force of gravity.

[65] After William Froude (1810–1879), who became famous for his studies of the flow of water around the ships of different hull shapes.

A particular kind of gravity wave, known as a *Kelvin wave*, is a prominent feature of the dynamics of the atmospheres of Earth, Mars, and Venus. These are large-scale, low-frequency gravity waves that propagate around the equator with no polewards velocity component. They tend to occur where solar forcing interacts with surface features, for example, large-scale variations in surface relief (such as massive mountain ranges) or in albedo (affecting the distribution of solar

energy absorbed). The phase of the oscillation then depends more on the topography than on the relative motion of the Sun and is a kind of non-migrating tide.

They can be described using a standard set of dynamical equations called the linearised 'shallow water' equations on an equatorial β-plane.[66] In this approximation, the disturbances h to a fluid of depth h_0 are expressed by:

$$\frac{\partial u}{\partial t} - \beta y v = -g\frac{\partial h}{\partial x}$$

$$\frac{\partial v}{\partial t} - \beta y v = -g\frac{\partial h}{\partial y}$$

$$\frac{\partial h}{\partial t} = -h_0 \nabla \cdot u \qquad \text{(shallow water equations on a } \beta\text{–plane)}$$

We look for the simplest solution of the form $u = U(y)f(x-ct)$; $h = \alpha U(y)f(x-ct)$, whence

$$c = \pm\sqrt{gh_0\alpha} = \sqrt{\frac{h_0}{g}}$$

and

$$\frac{\partial u}{\partial y} = \frac{\beta y}{c}U \text{ so } U = U_0 e^{\frac{\beta y^2}{2c}} e^{i(kx-\omega t)} \qquad \text{(Kelvin wave equation)}$$

This is the equatorial Kelvin mode, a wave trapped symmetrically about the equator with a scale factor in latitude of $\sqrt{\frac{2c}{\beta}}$. Taking the example of Venus, where $\beta \approx 6\times10^{-12}\,\mathrm{m^{-1}\,s^{-1}}$ and $c \approx 16\,\mathrm{m\,s^{-1}}$ are typical values, its meridional extent is $\approx$2300 km, equivalent to about 25° of latitude, which is approximately as observed (cf. Fig. 8.7).

[66] See page 211 in *Introduction to Circulating Atmospheres* by I.N. James, Cambridge University Press, 1994. The β-plane approximation involves setting the Coriolis parameter $f = 2\Omega \sin\phi$ equal to βy where $\beta = 2\Omega/a$. Then the atmospheric variables change only in the vertical direction, allowing a simplified solution. This is however valid only near the equator, where the Coriolis effect is small.

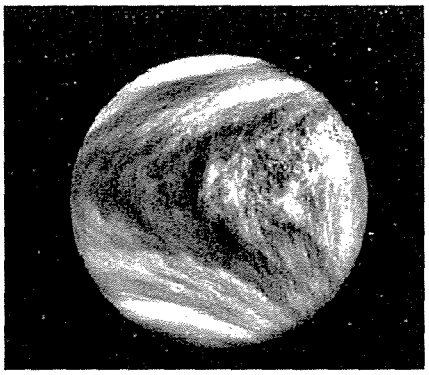

Fig. 8.7
The 'sideways Y-shaped' feature always seen on Venus, observed here by the camera on the *Mariner 10* spacecraft through an ultraviolet filter ($\lambda \approx 0.36$ μm), is probably produced by midlatitude Rossby waves enclosing a trapped equatorial Kelvin wave. The contrast is produced by variable amounts of unidentified absorber, probably sulphur compounds, in the upper cloud and haze layers. These absorb strongly at wavelengths shorter than about 0.38 μm, and act as tracers for the motions.

8.3 Venus dynamics and meteorology

8.3.1 Measurements and key phenomena

Most of our present knowledge of the dynamics of Venus' atmosphere comes from five types of measurements:

1. Entry probes: especially wind profiles obtained by tracking the descent of instrumented probes through the atmosphere, or by monitoring the trajectories of floating balloons.

2. Cloud feature tracking: contrasts seen in the clouds, especially at ultraviolet and near-infrared wavelengths, can be tracked over time to build up a pattern of the winds at the level where the features form. Recently, the use of multi-wavelength techniques has made tracking possible at several levels (from about 40 to 65 km altitude) simultaneously, by looking at different cloud layers.
3. Temperature measurements: infrared remote sounding and radio occultation measurements of the temperature field can be interpreted as wind fields using theoretical relationships, such as the cyclostrophic thermal wind relation.
4. Tracer measurements: minor constituents, such as carbon monoxide, that have variable distributions in the atmosphere can be used as tracers of the motions in the atmosphere, even in the troposphere below the clouds (using the near-infrared spectral 'windows').
5. Doppler wind measurements: made by observing the small shift in wavelength of a spectral line due to the line-of-sight motion of the atmospheric gas emitting the line.

Based on these data, the principal dynamical characteristics of Venus' atmosphere that are discussed in the following sections are:

1. The processes producing and maintaining the zonal superrotation of the atmosphere, its vertical extent, and its variability.
2. The characteristics of the equator-to-pole 'Hadley' circulation, and its behaviour with regard to angular momentum conservation and cyclostrophic balance.
3. The large-scale wave motions seen in the ultraviolet markings, including the equatorial 'sideways Y-shaped' pattern generated by planetary waves, the thermal tides, and travelling (gravity) waves.
4. The complex, rotating 'polar dipole' structure, and its links to the warm polar stratosphere and the cold polar collar.

For some important dynamical behaviour, there is not yet sufficient data of the right kind to obtain much of an understanding. This includes the range of organised regimes and chaotic weather systems seen in the cloud structure at all levels (§7.1, Fig. 7.5). Topographical effects, like those caused by the flow of the atmosphere over structure on the surface, are important on Earth and Mars. On Venus, they may be negligible as far as the general circulation is concerned, although this is uncertain due to the difficulties of observing the behaviour of the deep atmosphere of Venus below the clouds.

8.3.2 The zonal superrotation

The cloud contrasts seen in ultraviolet images (at wavelengths near 0.38 μm) show features travelling rapidly around the equator in 4 to 5 days, corresponding to speeds near 100 m s^{-1} at the cloud top height, i.e., at a pressure of order 100 mb. Features at this level travel around the planet at speeds that are more than 50 times faster than at the surface, 65 km below.

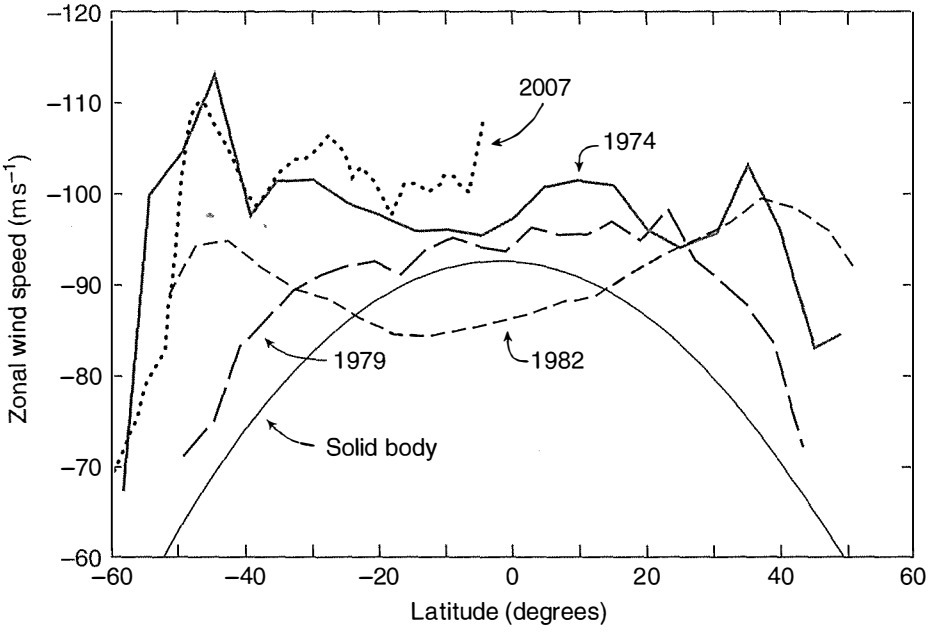

Fig. 8.8
Cloud-tracked zonal wind speeds on Venus from *Mariner 10, Pioneer Venus*, and *Venus Express*, spanning a period of more than 30 years. The strong zonal jet at latitudes near 60° seems to be a particularly variable feature. The lower solid line represents solid body rotation for comparison.

There appears to be considerable variability in time; for instance, a comparison of the *Mariner 10* and *Pioneer Venus* data seem to show (Fig. 8.8) that there are compact regions of relatively high winds (jets) in the midlatitude zones that were present in 1974 but did not exist 8 years later. This is not necessarily entirely due to a real change over time in the wind speed itself, however. The cloud structure, including the distribution of the UV markings whose origin is not well understood, could be varying within a more-or-less constant wind profile in the presence of a vertical gradient (shear). On Earth, jets tend to be quite compact, with strong gradients in latitude and height, and shear in the relevant region on Venus has been demonstrated by multispectral cloud tracking and by measurements of the vertical wind profile (Fig. 8.9). A relatively small change in cloud height could then correspond to a fairly large change in the observed propagation speed of cloud features, even if the wind field remained constant. Probably, the variations with time seen in the data in Fig. 8.8 are the result of changes in both cloud structure and wind profile, and it will be necessary eventually to separate the two to identify the causes, and the underlying meteorological behaviour.

In addition to tracking cloud motions and entry probe trajectories, the global wind field above the clouds, including the jets, can be profiled by converting temperature field measurements using the thermal wind equation or a more sophisticated diagnostic circulation model. Venus is a particularly simple case to treat, since its slow rotation means that the cyclostrophic equation, which represents the balance between pressure gradients and the centrifugal force due to the zonal wind motion, can be used. The winds forced by the temperature field measured by the *Pioneer Venus* infrared radiometer (§3.8.2) show the '4-day' zonal wind decreasing rapidly with height above the clouds and becoming very small by 80 or 90 km altitude

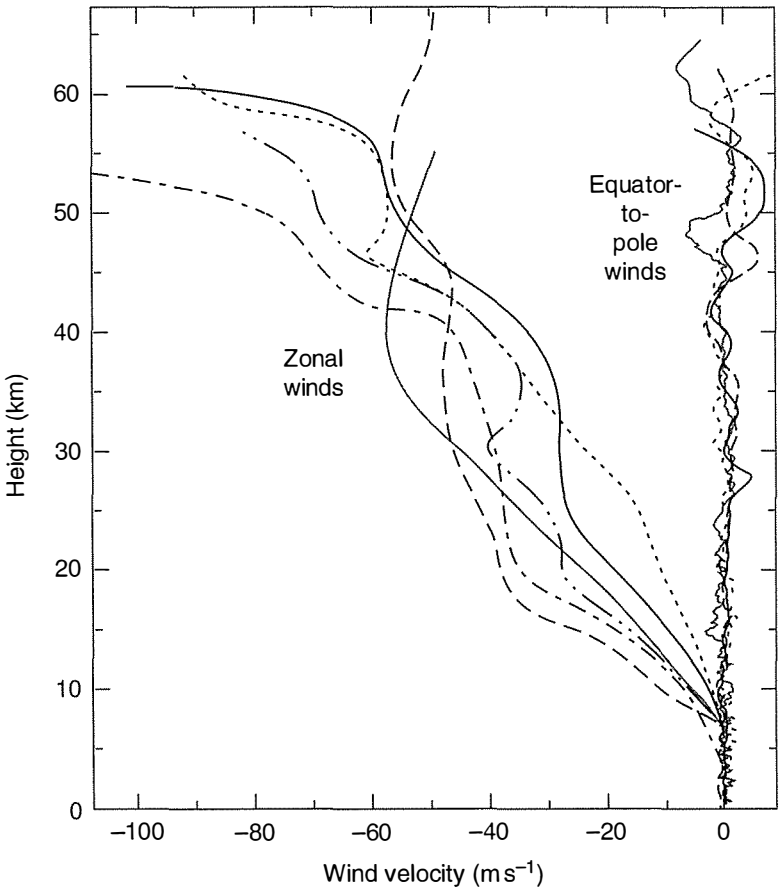

Fig. 8.9
Zonal and meridional wind velocity profiles obtained by tracking the sideways displacement of the *Pioneer Venus* probes during their descent through the atmosphere.

(Fig. 8.10). The zonal jet speed derived in this way is in reasonable agreement with the cloud-tracked winds shown in Fig. 8.8, and supports the interpretation given for their long-term variability. The height of the jet, at or just above the cloud tops, and its compactness are such that the tracer could easily appear to change speed if the height of the jet or the clouds changed by a few kilometres, without the jet itself necessarily changing speed.

Applying the global superrotation equation to Venus, using the approach outlined above in §8.2.6, yields $S \sim 10$, in contrast to the Earth, for which $S \sim 0.015$. The superrotation must be produced by the internal redistribution and storage of angular momentum. In some theories, this originates with the thermal tides due to the Sun, as the profile of solar heating moves within the atmosphere. Others, less convincingly, have suggested a persistent influx of meteorites might be responsible. Current thinking favours an internal process of the kind illustrated in Fig. 8.11, where both bulk motions (advection) and eddy processes have a role in transferring angular momentum from the surface of the planet to the cloud top region where the zonal velocities are greatest, thus producing and maintaining superrotation.

The essential feature of the model is the transfer of fluid from the pole to the equator by the lower branch of a zonally symmetric convection cell in each hemisphere. These are driven by solar heating in a 'thermally direct' sense (warm air rising near the equator); this is essentially the Hadley circulation discussed in detail previously. The

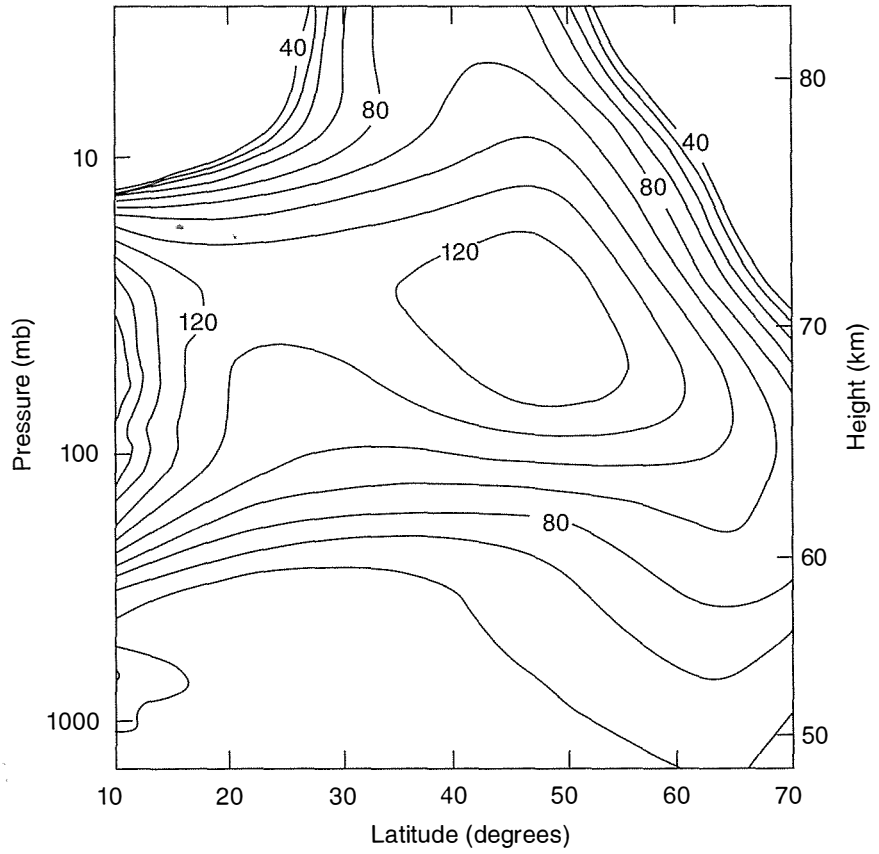

Fig. 8.10
Cyclostrophic winds on Venus, computed from infrared temperature-sounding data obtained from an instrument on an orbiting spacecraft, in this case *Pioneer Venus*.

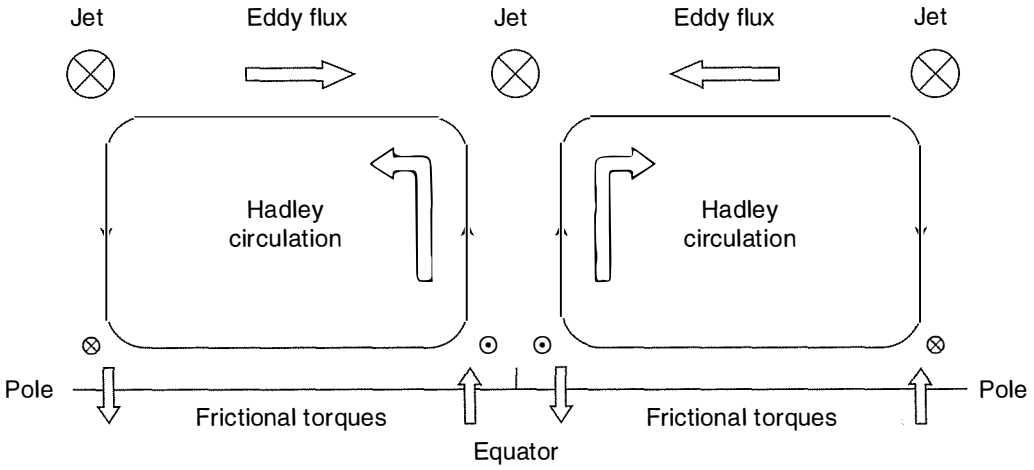

Fig. 8.11
A model for explaining the zonal superrotation on Venus, showing the zonal circulation between equator and pole and the associated transfer of angular momentum associated with this. The arrows at high altitudes show the direction of diffusive (eddy) transfer of angular momentum against the angular momentum gradient, increasing the zonal wind speed near the equator. The small arrows near the bottom of the figure show the exchange of angular momentum with the surface.

fluid initially has low angular momentum, because of the small distance from the rotation axis, but is accelerated at lower latitudes by friction between the air and the surface. The air then rises and begins to travel back towards the pole. As it does so, its angular velocity will

increase, because the radius around which it is circulating is reducing, reaching a maximum at high altitudes and high latitudes. This is the forcing for the zonal jets seen in the observed wind field (Figs. 8.8 and 8.10).

In order to reach a balanced steady state, it is necessary to suppose that angular momentum m is transferred by eddy diffusion away from the maximum in angular velocity, back towards the equator and vertically towards the ground. The local balance is expressed by

$$\nabla\cdot(\rho m u) = -\nabla\cdot F \qquad \text{(angular momentum balance equation)}$$

where F is the diffusive flux of angular momentum due to eddy viscosity. The net effect is to build up the velocity at most latitudes, ending up with maximum absolute angular momentum at the equator, and maximum absolute angular velocity at high latitudes.

This balance requires the counterintuitive result that eddy diffusion must transport angular momentum at some locations from regions of low to regions of relatively high angular momentum, against the mean gradient of m. To see how this might occur, consider a local maximum value in latitude and height, m_0, and integrate both sides of the angular momentum balance equation over a toroidal volume enclosed by a contour defined by $m = m - \delta m$. Now we use the divergence theorem[67] to write

$$\int\int\int \nabla\cdot(\rho m u)\,\mathrm{d}\tau = (m_0 - \delta m)\int\int \rho u\cdot\mathbf{n}\,\mathrm{d}S$$

For conservation of mass, $\int\int \rho u\cdot\mathbf{n}\,\mathrm{d}S$ must be zero, so we must also have

$$\int\int F\cdot\mathbf{n}\,\mathrm{d}S = 0.$$

Since $\mathbf{n}$ is defined to be anti-parallel to the gradient of m, eddy viscosity F must act down the gradient of m in some cases, but up the gradient in others, regardless of the detailed form of F.

Eddy viscosity is a complicated phenomenon and the details of the transfer mechanisms are not clear. Candidates include planetary waves of various types (Kelvin, Rossby, mixed), thermal tides, and gravity waves. The model simplifies the problem by treating it simply as a viscous frictional term, which only acts when adjacent air parcels are in relative motion; then angular momentum is transferred against the gradient of angular velocity. Provided eddy diffusion acts more efficiently in the horizontal than in the vertical, requiring anisotropic diffusion, strong superrotation can be maintained at all latitudes, including the equator.

Some indication as to whether this simplified concept can operate in a real fluid has been obtained from simulations of laboratory experiments (Read, 1986) in which superrotation was induced in tanks of rotating fluid. These showed that when a temperature gradient was applied, and allowance made for the sinks of angular momentum at the

[67] Sometimes known as Gauss' law, the divergence theorem relates the integral of the flow through a surface with the integral over the volume enclosed by the same surface. Its general form is $\int\int\int \nabla\cdot F\,\mathrm{d}V = \int\int F\cdot\mathrm{d}S$, where the left-hand side of the equation represents the total of the sources in the volume V, and the right-hand side represents the total flow across the boundary enclosed by the surface S, where $\mathbf{n}$ is the unit vector normal to the surface element $\mathrm{d}S$.

cylindrical sidewalls, values of S as large as 10, comparable to Venus, could be achieved without the need to apply external torques. On Venus the mechanism must, of course, be different in detail, but the experiment does at least demonstrate that advection and eddies can work together in the way required.

8.3.3 Meridional circulation

The mean meridional component of the cloud-tracked wind is quite slow, only a few metres per second, and the errors in the data are such that it is just possible to say that the overall direction is polewards at the cloud top, and possibly in the other direction near the cloud base (Fig. 8.12). This would be consistent with the Hadley type of circulation discussed earlier, with rising air at low latitudes and descent near both poles. Both sophisticated and simplified dynamical models, like those discussed in more detail below in connection with Mars, predict that the Hadley circulation will extend polewards for a distance of about 2000 km from the equator on the Earth and a similar distance for Mars, close to what is observed in both cases. For Venus, however, the model predicts an extent for the Hadley cell that is greater than the radius of the planet for Venus, consistent with the intuitive idea that the cell will extend all the way to the pole on a slowly rotating planet.

Then we would expect that the downward branch of the Hadley cell in each hemisphere corresponds to the region of rapid downwelling in the

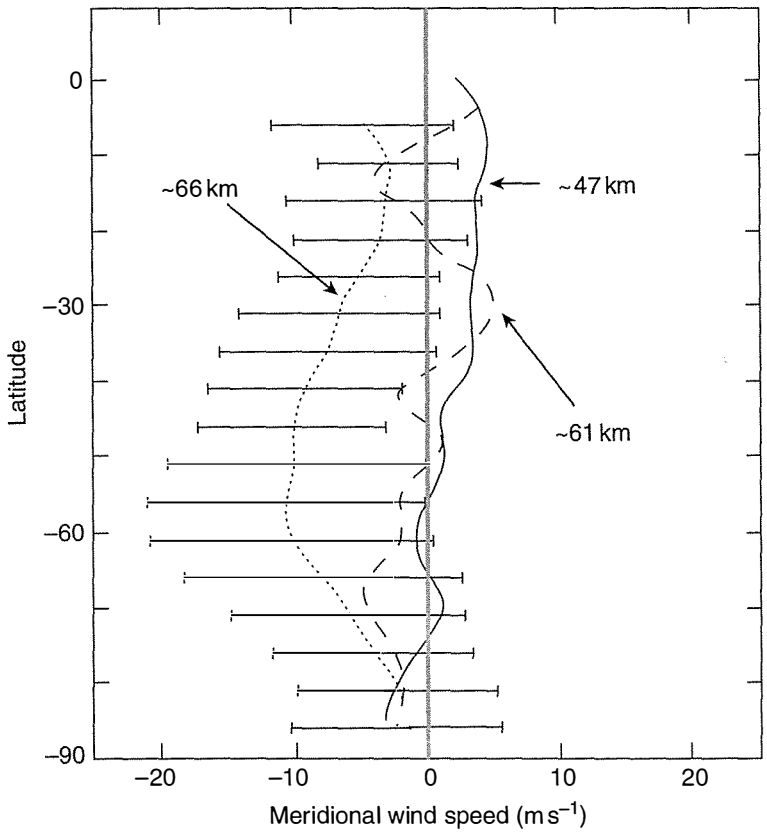

Fig. 8.12
Meridional wind speeds on Venus obtained by tracking features in the clouds from an orbiting spacecraft (*Venus Express*). The three curves are obtained at different wavelengths, corresponding to the heights in the cloud layers shown. The error bars on the curve for the winds at 66 km altitude are typical of those on the other two, which are omitted for clarity. After Sanchez-Lavega et al., (2008).

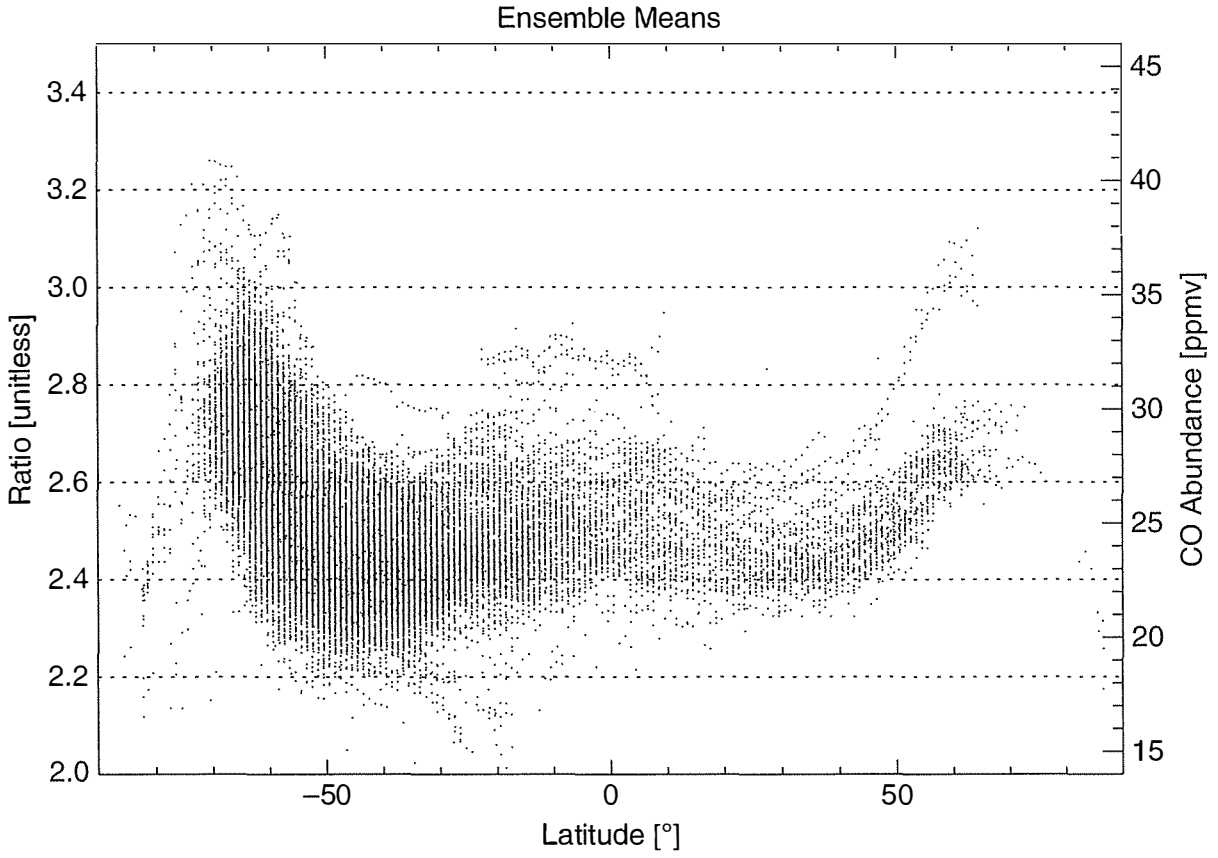

Fig. 8.13
Carbon-monoxide abundance in parts per million in the lower atmosphere of Venus, measured by *Venus Express* (Tsang *et al.*, 2009). The maxima near 65 degrees latitude in both hemispheres correspond to strong downwelling from the CO-rich upper atmosphere (see §6.8).

'eye' of the polar vortex. However, the most recent investigations by the *Venus Express* mission show a more complicated situation. The different cloud patterns seen in the images in Fig. 7.5 suggest at least four dynamical regimes in each hemisphere, and carbon-monoxide tracer measurements, like those in Fig. 8.13, imply strongly descending motions around the edge of the polar vortex, rather than at its centre. This in turn implies that the vortex is a separate dynamical system connected to, but not part of, the Hadley circulation. The existence of the polar collar and of complex, time-dependent structure inside the vortex 'eye' tends to support this finding, as discussed below.

8.3.4 Polar vortex

We have seen that there is evidence based on theory, analogy with the Earth, and the observational data, for Hadley-type equator-to-pole circulations in each hemisphere. When combined with rapid rotation in the zonal direction, these must transport large amounts of angular momentum to the poles on Venus, something that happens to a greater or lesser extent in all planetary atmospheres. It is not surprising,

therefore, that extensive vortices form over the polar regions, with rapid downwelling combined with rapid rotation. These recycle mass and angular momentum back to the equatorial regions as a permanent feature of the general circulation regime on Venus, as represented in models like that in Fig. 8.11.

Similar, but less persistent (in particular, seasonally variable) vortex phenomena are found on Earth, Mars, and Titan. Jupiter, Saturn, and presumably the other giant planets also have polar vortices, although details are limited because only oblique views of the poles have been possible from Earth or from the spacecraft that have visited the outer Solar System so far. (The small spacecraft *Pioneer 11* flew over the south pole of Jupiter in April 1973, but was not equipped to make detailed observations.) The Juno mission, planned by NASA to arrive at Jupiter in 2016, will be the first polar orbiter of any outer planet. *Galileo*, the only other mission to Jupiter to go into orbit, was confined close to the equatorial plane in order to be able to make multiple passes of the planet's large family of moons.

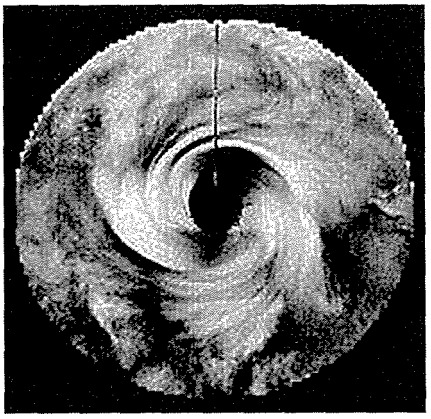

Fig. 8.14
The north polar vortex on Venus in ultraviolet light, in a mosaic of images from the *Pioneer Venus* orbiter.

Observations of the polar regions on Venus at visible or ultraviolet wavelengths clearly show vortex activity (Fig. 8.14), but few details of the interior or 'eye' of the vortex can be discerned because of the opacity at these short wavelengths of the high cloud cover that forms a quasi-permanent polar 'hood'. The hood is transparent at infrared 'window' wavelengths and a lot of additional structure can be seen in the vortex below (Fig. 8.15). In the infrared windows, the feature is observed in transmission rather than reflection, using thermally emitted radiation from the hot lower atmosphere that passes through all of the cloud layers. The opacity is less where the clouds are thinner and therefore the contrasts are generated by the cloud morphology over the pole.

The polar clouds clearly consist of multiple layers, although these have not been probed *in situ* as they have at non-polar latitudes by landers. The vertical complexity of the cloud structure, and the fact that the observed radiation has passed through all of the layers so the observations have little intrinsic height discrimination, make it hard to separate features that are produced by dynamical patterns present at different heights. As a result, only simple models or interpretations of the basic structure of the vortex are possible at present.

The outer part of the vortex is dominated by a dark crescent-shaped 'collar' region, consisting of anomalous and variable temperature and cloud structure, surrounding the pole at about 70 °N latitude and rising perhaps 15 km above the mean cloud top elevation. This has a solar-fixed component (i.e., the thickest part of the crescent shape occurs at about the same local solar time) and sometimes contains spiral streaks. The latter resemble those seen in the UV images (Fig. 8.14) but arise in cloud layers at greater depths, potentially providing some information about the vertical structure of the vortex. In time-averaged infrared images, the collar can be seen as a ribbon of cold air with a radius of about 1000 km roughly centred on the pole, the temperature of which is at least 40 K cooler than outside the feature. Its overall appearance generally suggests a predominantly wavenumber-1 disturbance

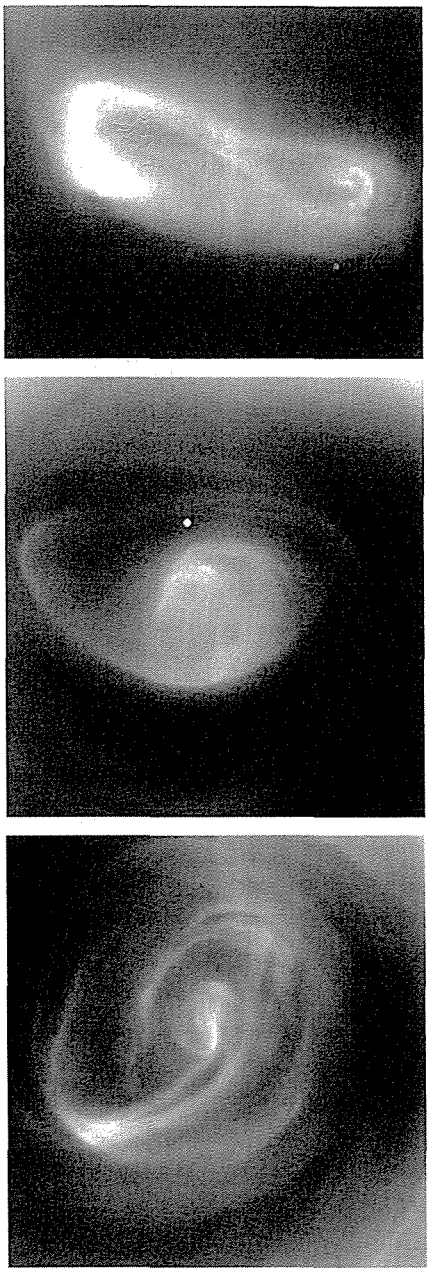

Fig. 8.15
Three infrared images, each about 2000 km across, of the south polar vortex on Venus obtained on different days in 2006 by *Venus Express* at a wavelength near 5 μm. The images show emission from the hot lower atmosphere passing through the cloud structure surrounding the pole, so bright regions are regions of lesser cloud opacity. Several layers of cloud are superimposed, making it difficult to interpret the structure in terms of detailed dynamical behaviour at any particular level in the atmosphere. The bright dot marks the rotational pole of Venus.

wrapped around the edge of the vortex, possibly also associated with the midlatitude jet since this lies just equatorwards of the collar.

Polewards of the inner edge of the collar lies the polar 'dipole', a predominantly wavenumber-2 feature, often (particularly when observed with low spatial resolution) consisting of two warm regions circulating around the pole with a variable period typically about 2.9 days. At higher resolution, these sometimes have the appearance of linked vortices, as shown in the top frame of Fig. 8.15. This beautiful structure also takes on a variety of more complex shapes, however, as the rest of the figure illustrates. Clearly many disturbances and instabilities are present in addition to the basic dipole characteristic.

If many images of the vortex, spanning several weeks of observations, are averaged together in a coordinate frame that follows its

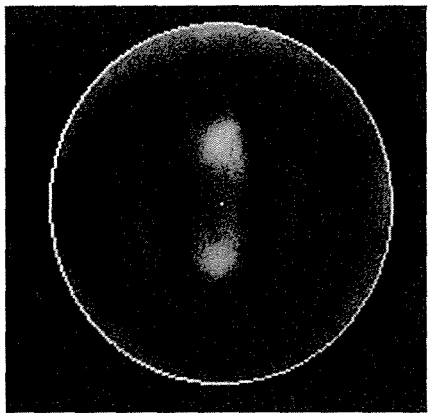

Fig. 8.16
Pioneer Venus infrared (11.5 μm) images of the north polar vortex over a 72-day period, averaged together in a rotating coordinate system matched to the rotation speed of the dipole (about 1 rotation in 2.7 Earth days). This smears out the detailed structure, but clearly shows the double character of the vortex 'eye' centred on the rotation pole, and the surrounding cold collar.

rotation, the mean appearance that emerges suggests it consists in essence of two clearings in the cloud, at locations straddling the pole and rotating around it (Fig. 8.16). The most likely interpretation is that the clearings are individual linked vortices in which most of the subsidence of the atmosphere occurs, depleting the cloud cover and allowing more radiation to escape from below. The corresponding evidence for descending motions around the edge of the vortex suggests that the idea that a single large circulation cell may fill each hemisphere, at levels near the cloud tops, needs updating to include a secondary cell near the pole. Earlier, it was been shown by calculations using a baroclinic instability model (Elson, 1982) that the geometry and temperature contrasts in the cold polar collar create conditions in which disturbances with two maxima (wavenumber 2) in longitude and periods of around 3 days (similar to the dipole's 2.9 days) have the greatest rate of growth. (The second greatest is wave 3, and indeed the south polar vortex on Venus has been observed on occasion to develop a 'tripole' appearance, or to have an overall triangular shape, as in the lower pictures in Fig. 8.15).

Thus a broad picture of the main circulation patterns on Venus has emerged (Fig. 8.17). The Hadley cell dominates low latitudes, but becomes unstable before it reaches the pole, at about 60 °N or S. The angular momentum transport by this cell gives rise to a strong

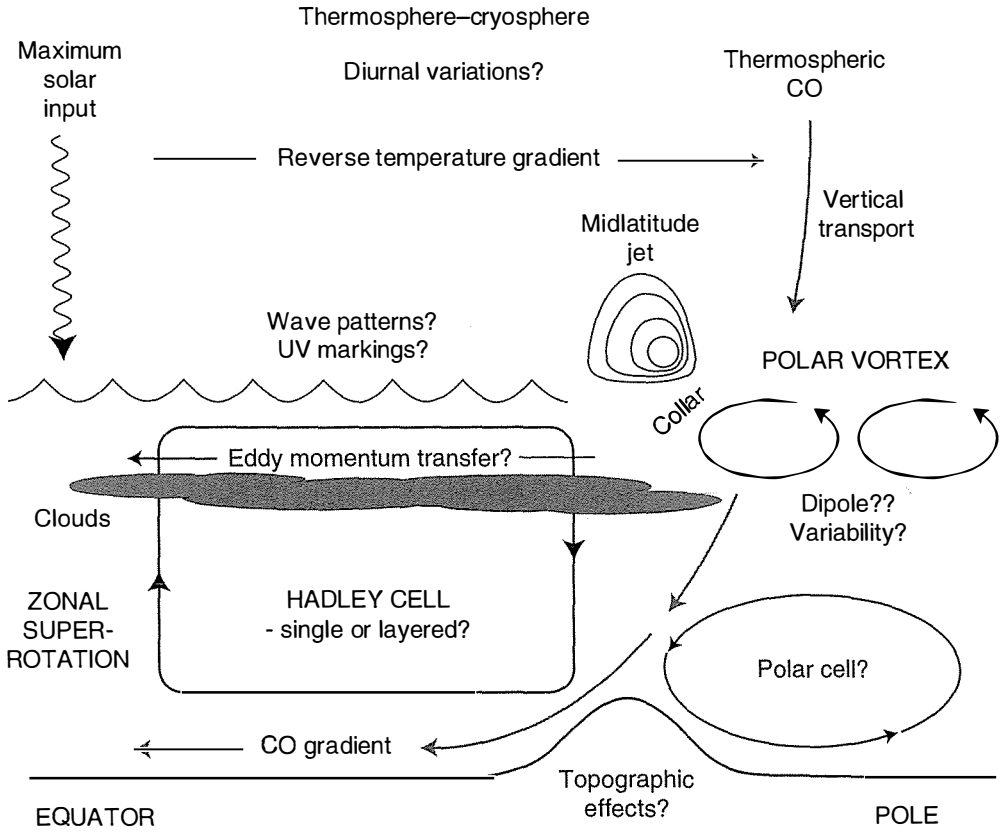

Fig. 8.17
A summary of the main features of the atmospheric circulation observed and inferred on Venus. The observations include the nature of the polar vortex and the extent of the Hadley cell circulation. The inferred properties include how it may be balanced by a counter-rotating polar cell and eddy momentum transfer, the drive for the zonal superrotation by solar heating and its balance via the reverse temperature gradient in the stratosphere.

midlatitude jet with which a cold feature, the polar collar, is associated. The wavenumber-1, solar-fixed character of the collar might be associated with the driving of the zonal superrotation at lower latitudes by the solar-induced thermal tides. In any case, it provides the conditions in which baroclinic disturbances with the basic double characteristics of the polar vortex can develop, along with much more detailed structure presumably produced by the superposition of other instabilities.

8.3.5 Subsolar-to-antisolar circulation

The previous discussion of the general circulation on Venus applies to the atmosphere up to about 80 km altitude. Above that, there is evidence that both equator to pole and subsolar-to-antisolar regimes are present together. The latter, which as already noted is the expected characteristic of a slowly rotating planet, becomes dominant above about 95–100 km altitude where the zonal superrotation, which is strongest at the cloud tops, has dropped off to a very low speed. In the deep Venusian atmosphere, the time constant for radiative cooling (i.e., the characteristic time in which the atmosphere would cool down if the Sun were removed) is several thousand times the length of even the long Venusian day. Hence the Sun appears to the atmosphere to move rapidly overhead, and the predominant gradients are equator to pole. This is the case also on Earth and Mars, where the time constants are shorter, but so also is the length of the day.

Figure 8.18 illustrates some of the evidence for the subsolar-to-antisolar regime, from Doppler wind measurements using a radio telescope on the Earth. This technique is sensitive enough to actually determine the wind speed relative to the solid planet at several locations and heights. Below 90 km altitude the winds are seen to be still predominantly zonal, but above 100 km they converge on the antisolar point.

Other evidence comes from spacecraft measurements of airglow emission from atomic oxygen and other species that are relatively abundant at high levels, due to dissociation by solar ultraviolet radiation.

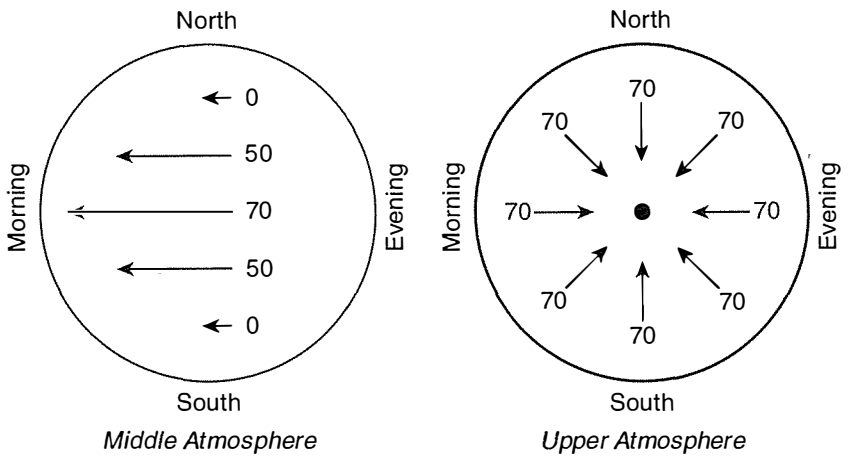

Fig. 8.18
Doppler measurements of the wind on Venus obtained by Clancy *et al.* (2007) using a radio telescope on the Earth. The diagram on the left shows the superrotation (in metres per second) in the zonal direction at a height of about 85 km above the surface of Venus; the one on the right shows how subsolar-to-antisolar flow sets in above about 100 km. The black dot marks local midnight at the equator on Venus.

The excited atoms and molecules are created on the day side, but are long-lived enough to migrate to the night side before they relax to their ground states with emission of a photon at a characteristic visible or near-infrared wavelength. The observed emission, which comes mainly from altitudes around 110–120 km, is strongly concentrated near the antisolar point, confirming the result from the Doppler measurements that show the transport at that level is towards local midnight.

8.4 Mars dynamics and meteorology

8.4.1 Key features

The atmosphere of Mars has many similarities to that of Earth. The two planets have roughly the same size, axial tilt, and rotation rate, and on both the surface receives the bulk of the incoming solar energy directly. The main differences are that the atmosphere of Mars is thin (about 0.7% of that of Earth by surface pressure) and, like that of Venus, consists almost entirely of CO_2. Even at its low surface pressure, the Martian atmosphere is thick enough to display a wide range of analogues to Earthly dynamical phenomena, including cloud formation, fronts and storms. The atmosphere shows a penchant for large-scale overturning from low to high latitudes, although (in part because of the tendency for surface temperatures to follow the Sun), the Hadley cell on Mars has a larger seasonal variation than on Earth or Venus, and near the solstices extends from the summer to the winter hemisphere, straddling the equator.

As on Earth, wave motions are an important part of the Martian circulation, with a major contribution to the excitation of various modes by the topography of the surface, which is more extreme than on other planets. Mountains up to 25 km tall and valleys down to 7 km deep are more than twice the extremes on Earth on a smaller, rapidly rotating planet, where the pressure scale height is about 8 km. The topography affects the circulation in two main ways: firstly by interfering mechanically with the flow, and secondly by enhancing the temperature contrasts at the base of the atmosphere which drive the winds in the first place. The global distribution of topography and albedo differences determine which periodicities will be driven, and those that grow fastest form the natural wave modes of the atmosphere.

The very thin atmosphere of Mars means there is little opacity to prevent nearly all of the solar heating taking place at the surface, unlike Earth where it is about half, and Venus where it is only 1% or so. This and the low thermal capacity of the air for transporting heat between regions of different temperature leads to large day/night temperature variations on Mars (Fig. 8.19). The accompanying diurnal (day–night) pressure variation is modest, but on the timescale of a Martian year the mean pressure varies by around 30%, due to the CO_2 atmosphere freezing onto the polar caps.

Frequent dust storms appear and grow in regions of massive winds, such as retreating polar cap edges. Those formed in certain regions and

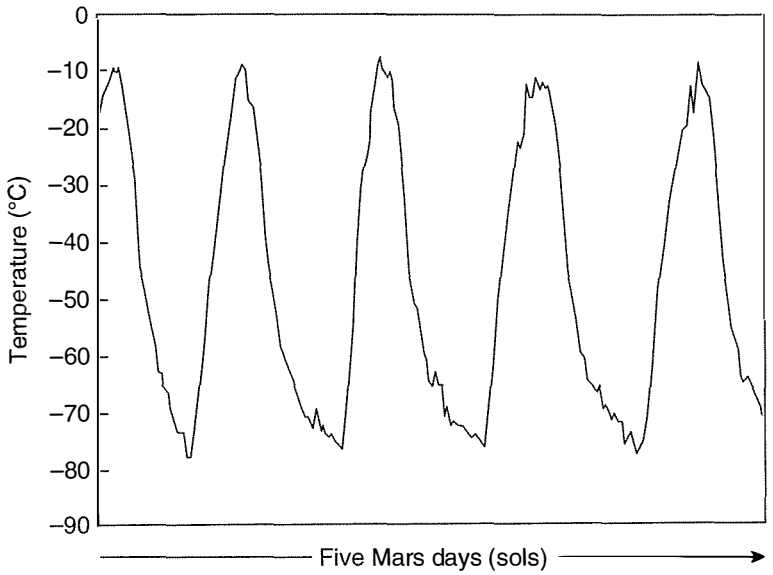

Fig. 8.19
The diurnal temperature cycle of the air 25 cm above the surface during a 5-day period on Mars, as measured by the *Pathfinder* lander in July 1997, when it was late summer at the landing site. Note (a) the large diurnal swing of nearly 70 °C, compared to only about 10 °C on Earth, and (b) the small day-to-day differences produced by weather systems travelling across the vicinity of the landing site.

times of year can grow to cover the planet, when they can easily be seen from Earth as a yellowish haze of airborne dust that obscures the disc. Global dust storms do not occur every year, but approximately biannually, due to some poorly understood aspect of the triggering and growth mechanism (possibly connected with the need to recharge the supply of dust in regions scoured by the storm). Even without storms, there is dust in the atmosphere virtually all the time, and the sky, as seen from the surface, is more red than blue, especially near the horizon. Some of the dust particles are very small, and remain airborne for a long time. The principal removal mechanism for all but the largest particles is freezing of water or carbon dioxide onto the grains, especially at night or over the dark winter pole. However, background dust levels are nearly always quite high, and small storms and localised phenomena such as dust devils have a role in maintaining this.

8.4.2 Simple circulation models

Simple dynamical models provide useful insights into atmospheric behaviour. The one developed by Held and Hou (1980; see also Read and Lewis, 2004) represents the whole atmosphere as just two layers. The lower of these layers is connected to the ground by friction, so the zonal velocity is held close to zero and is assumed to be negligible. The angular momentum per unit mass in the upper layer is assumed to be conserved within the Hadley cell, which consists of meridional flows that are polewards in the upper layer and (slowly, so not much affected by friction) equatorwards in the lower layer. The zonal flow U_M in the upper layer is then given by

$$u = U_M = \frac{\Omega y^2}{a} \qquad \text{(angular momentum equation)}$$

where Ω is the rotation rate of the planet and sin Φ (ϕ = latitude) has been approximated by y/a, where y is the northward coordinate and a is the radius of Mars. The zonal flow in the upper layer is further assumed to be in thermal wind balance with the latitudinal gradient of potential temperature θ at the interface between the two layers, so that

$$\frac{\partial u}{\partial z} = -\frac{ga}{2\Omega\theta_0 y}\frac{\partial \theta}{\partial y} \qquad \text{(thermal balance equation)}$$

Substituting for u and taking

$$\frac{\partial u}{\partial z} \cong \frac{U_M}{H} = \frac{\Omega y^2}{aH}$$

where H is the height of the two-layer stack, we have

$$\frac{\partial \theta}{\partial y} \cong -\frac{2\Omega^2\theta_0}{a^2 gH} y^3$$

which can be integrated in y to obtain

$$\theta_M = \theta_0 - \frac{\Omega^2\theta_0}{2a^2 gH} y^4$$

where θ_0 is the constant of integration.

Now we assume that the Hadley circulation is driven by the difference between this temperature θ_M and that which would apply in radiative equilibrium, θ_E. The latter is assumed to have the simple form

$$\theta_E = \bar{\theta}_E - \frac{\Delta\theta}{a^2} y^2$$

where $\bar{\theta}_E$ is the global mean value of potential temperature at this level, and $\Delta\theta$ is the equilibrium equator-to-pole difference. The value of y at which the curves for θ_M and θ_E cross closest to the pole, Y, represents the polewards extent of the Hadley cell, since it is where net heating effectively switches to net cooling. Assuming potential temperature is conserved within the Hadley circulation itself, we have

$$\int_0^Y \theta_E \, \mathrm{d}y = \int_0^Y \theta_M \, \mathrm{d}y$$

and can solve for Y to find

$$Y = \sqrt{\frac{5\Delta\theta gH}{3\Omega^2\theta_0}} \qquad \text{(latitudinal extent of the Hadley cell)}$$

Then, using the angular momentum equation above, the zonal wind in the upper branch of the Hadley cell is

$$U_M = \frac{\Omega}{a}\frac{5\,\Delta\theta\; gH}{3\Omega^2\theta_0} \qquad \text{(zonal wind in the Hadley cell)}$$

Suitable values can be inserted for the parameters in this expression to find the predicted extent of the Hadley cell in the polewards direction from the equator. Using $\theta_0 = 255\,\text{K}$ and 210 K, and $\Delta\theta = 40\,\text{K}$ and 65 K, for Earth and Mars, respectively, $Y \approx 2000\,\text{km}$ or about 18° of latitude for Earth. This is somewhat too small when compared to the observed value, which is closer to 30°. For Mars, Y is nearly the same at 2060 km, but this is about 35° of latitude and compares quite well to values determined from more sophisticated models. As noted earlier, the estimate for Venus is larger than the radius of the planet. The upper-atmosphere zonal wind speed near the equator on Mars works out to be $U_M \approx 85\,\text{m s}^{-1}$, which is also reasonable when compared to general circulation models and to the few measurements we have.

8.4.3 General circulation models and remote sensing data

Of all the other planets, Mars lends itself most readily to the use of modified terrestrial general circulation models to study atmospheric motions and their role in maintaining the climate. These solve the time-dependent equations of motion and as much as possible of the other relevant physics on a large computer to predict the temperature and wind fields and the distribution of key species, especially water vapour. The basic code of most Mars GCMs is derived from that originally developed for weather forecasting and climate studies on Earth. When all of the relevant physics is correctly incorporated in a model with an accurate radiative transfer code, the temperature and wind fields in the atmosphere can be computed for comparison with measurements. When these give good agreement, various 'what if' experiments can be performed by cautiously varying factors such as obliquity, orbital eccentricity, and surface pressure, to investigate the stability of the climate and possible past climate regimes.

All sorts of data can be used to initialise GCMs and to test the results, but the most useful are vertical temperature profiles at as many local times and locations across the planet as possible. Remote sensing instruments on satellites in polar orbits around Mars, like Mars Climate Sounder (§3.9.4), are designed to provide this sort of data but inevitably, with a single spacecraft, coverage of the planet is limited in both time and space. Even incomplete coverage results in so much data (MCS produces one profile each of temperature, dust and water vapour approximately every second) that an automated means is needed to use the data to constrain the model, or alternatively to use the model to make intelligent extrapolations and predictions for regions or times that have not yet been observed. This can be achieved by an assimilation technique, where the data is continuously incorporated into a

physically consistent set of atmospheric fields generated by the model. The combination of model and observation can then be subjected to detailed diagnosis, in order to test hypotheses in ways that would not be possible with either alone.

Data assimilation can use information from past as well as quasi-real-time observations and, in principle, all of the available knowledge of the physics of the problem can be embodied in the numerical model. Once combined, they produce an optimal analysis of the current state and long- and short-term behaviour of the climate system. The assimilation of data directly into a model is also an attractive method for the study of time-dependent phenomena using data taken asynchronously. Straightforward gridding of observations from a single satellite can lead to ambiguities in their interpretation when studying synoptic-scale phenomena which change significantly over the course of a day or two. Assimilation is also valuable when it is desirable to produce a full, physically consistent analysis of all atmospheric fields, including those not directly observed. The examination of deviations of observations from model forecasts also helps to identify deficiencies in the model, which feeds back into an understanding of the physics at work, possibly with benefits for terrestrial as well as Martian models.

As an example of a GCM with assimilation capabilities, and its applications, consider the 'EuroMars' model, developed principally in Paris, Oxford, and Granada.[68] Like most GCMs this has two main parts, a hydrodynamical code that computes the large-scale atmospheric motions, and parameterisation schemes that model the physical processes which force the general circulation. These include the radiative heating and cooling of the surface and atmosphere, including dust effects, turbulent atmospheric motions, convection, topographical drag, gravity waves, and the condensation of CO_2 in the polar regions. Figure 8.20 shows some typical output: the seasonal variation of zonal mean temperature and wind fields for the northern winter season over the whole of Mars. Runs for equinox and northern summer show, as would be expected, considerable but not perfect symmetry between the seasons over the period of half a Martian year. Some small differences occur that are mostly attributable to the large differences in surface topography between hemispheres.

In Fig. 8.21, EuroMars model temperatures are compared to the measured values derived from data obtained by the Planetary Fourier Spectrometer infrared remote sounding instrument on the *Mars Express* spacecraft (§3.9.3). These comparisons were made specifically to match, as closely as possible, the date of the landing of the *Beagle 2* probe on Christmas Day, 2003. The lander, carried to Mars by *Mars Express* and released six days earlier, made no measurements during its descent, as planned, but failed to respond afterwards. It was widely reported that the prime suspect for the failure was unusually warm atmospheric conditions that the models failed to forecast. This, however, was the result of a misapprehension based on some errors present in the processing of the first stellar occultation obtained by SPICAM (Spectroscopy for Investigation of Characteristics of the Atmosphere of Mars), another atmospheric sounder aboard *Mars*

[68] http://www-mars.lmd.jussieu.fr/

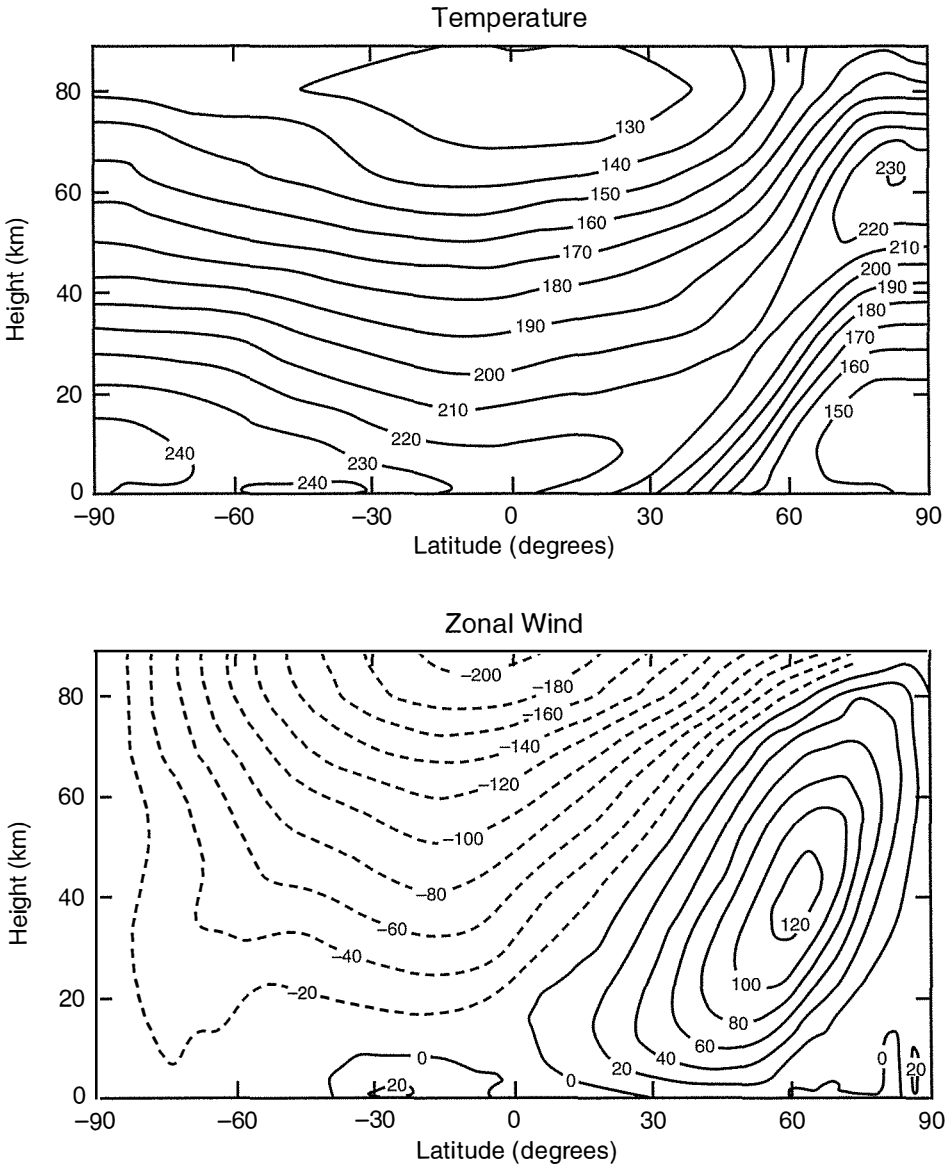

Fig. 8.20
Model results for zonal mean temperature (top) and zonal wind during early northern winter on Mars.

Express. These preliminary data were presented at a conference but rapidly revised as the correct interpretation emerged from the detailed data processing. The correctly processed SPICAM data fell well within the envelope of model predictions available before the launch of *Mars Express*.

The temperature fields in Fig. 8.21 are those observed by PFS during *Mars Express*' twentieth orbit of Mars, compared to the predictions by the EuroMars model for 'baseline' and 'warm' scenarios corresponding to the same time of year. The baseline scenario corresponds to the atmospheric dust level usually expected, while cold and warm scenarios bracket the range of conditions found on Mars at any time in the absence of major dust storms. The model also runs two dust-storm scenarios, classified as moderate and severe. At the time of the *Beagle* landing, comparison to measurements shows that the atmosphere was somewhat dustier and warmer than the baseline scenario, but that it

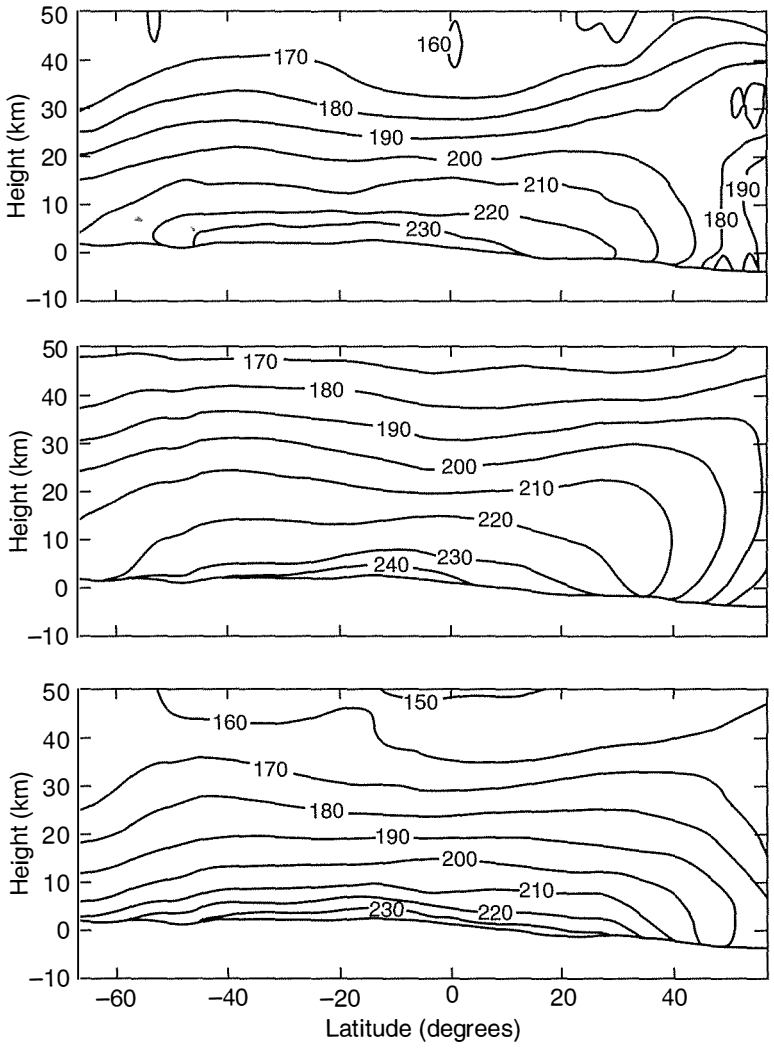

Fig. 8.21
Martian atmospheric temperatures a few days after *Beagle 2* landed. Top: Planetary Fourier Spectrometer measurements, compared to EuroMars model predictions for 'warm' (centre) and 'baseline' (bottom) scenarios, respectively.

was still colder (and therefore denser) than the warm scenario, and much colder than either of the dust-storm scenarios.

8.4.4 Dynamics of the seasonal CO_2 cycle

At the pressures found on present-day Mars, CO_2 condenses and sublimes at a temperature of around 150 K, absorbing or releasing latent heat $L = 5.9 \times 10^5\,\mathrm{J\,kg^{-1}}$. The temperature regularly falls this low during winter near the poles, so that a substantial mass of CO_2 is deposited and released during the course of the seasonal cycle. Given enough time, all of the CO_2 in the atmosphere would be involved; in fact, observations of the pressure cycle (Fig. 6.2) show that ~1/3 of the atmospheric mass condenses onto the pole each winter.

The speed v of the wind generated near the pole by this condensation can be estimated from a simple energy balance model. Equating the radiative heat loss to the latent heat release in time t for unit area of emissivity e at the condensation temperature T_C, we have

$$e\sigma T_c = L\frac{\partial M_c}{\partial t}$$

where M_c is the mass of condensate per unit area and L the latent heat per unit mass. The mass flowing across a vertical cylindrical surface surrounding the pole at radius r_0 is given by

$$\int_0^{r_0} \frac{\partial M_c}{\partial t} 2\pi r dr = 2\pi r_0 v \int_0^{\infty} \rho dz$$

so

$$2\pi r_0 H v \rho_0 = \pi r_0^2 \frac{e\sigma T_c^4}{L}$$

Rearranging and inserting values, we find that the vertically averaged velocity v is $\sim 1\,\mathrm{m\,s^{-1}}$; not a high wind but still a substantial breeze.

8.4.5 Seasonal dust cycle

The principal effects of airborne dust on global atmospheric dynamics have already been discussed and here are just briefly recapped. Dust warms the lower atmosphere and reduces the lapse rate (§5.5), making the troposphere more stable than otherwise, with a smaller vertical temperature gradient, which reduces convection and affects the development of waves and other disturbances. Gradients in the amount of dust tend to increase the near-surface winds, raising more dust that can lead to dust storms, which may remain localised or may spread across the planet (§7.2.4). Major research topics and high priorities for new missions and studies in the near-term exploration of Mars are the processes that start and end major dust storms, and determine their frequency of occurrence; the wind fields and the atmospheric distribution of dust during their development and propagation; and the surface sources, sinks and fluxes of dust. These will seek to understand why global storms occur in some years and not others, and to be able to forecast their occurrence well before humans step on Mars.

8.5 Atmospheric dynamics of the Jovian planets

Jupiter is the largest and closest, and hence the best-observed and least poorly understood, of the family of four giant planets of the outer Solar System. However, comparisons between Jupiter and Earth are less straightforward than for Mars and Venus for several reasons, principally:

1. the difference in atmospheric composition (hydrogen, helium, methane and ammonia compared to nitrogen, oxygen and carbon dioxide);
2. the large internal heat source on Jupiter: this heats the visible atmosphere from below at a rate similar to the solar input;

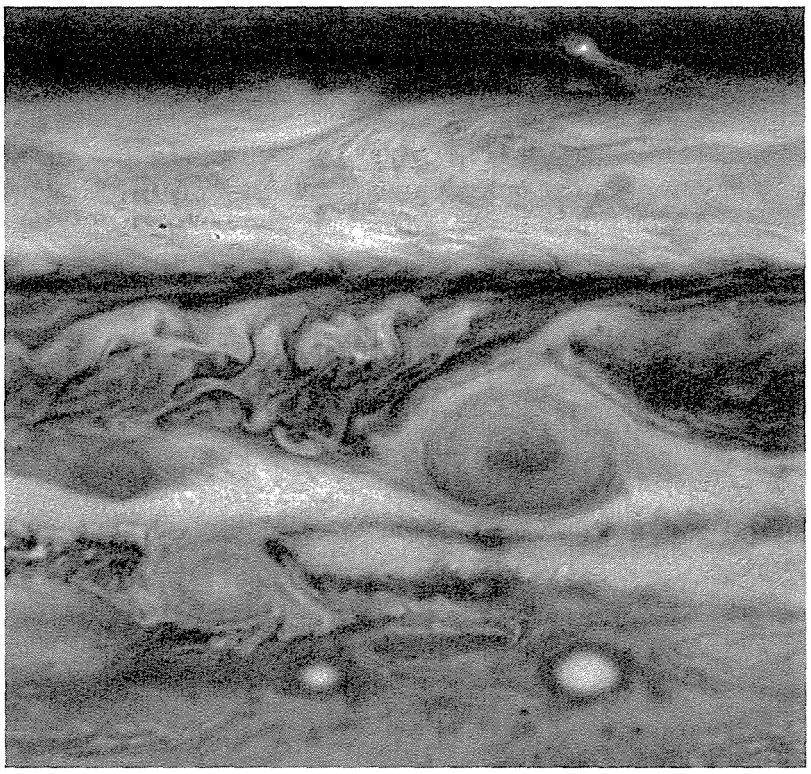

Fig. 8.22
The highly dynamic character of Jupiter's atmosphere can be appreciated from this image from the *Galileo* orbiter spacecraft of the cloud patterns in the vicinity of the Great Red Spot, showing part of the belt–zone structure, several giant eddies, and wave and turbulent activity on various scales.

3. the essentially infinite depth of the Jovian atmosphere: which means that there is no solid lower boundary to constrain vertical motions or introduce frictional drag;
4. the difference in size and rotation rates: Jupiter is more than ten times the linear size of Earth, and rotates more than twice as quickly, so Coriolis forces are much greater.

Most of the dominant dynamical characteristics of Jupiter's atmosphere can be seen in the image in Fig. 8.22 from the *Galileo* orbiter spacecraft. It shows the cloud patterns in the vicinity of the Great Red Spot, which appears near the centre of the picture; at the top is a dark belt, with a light zone below. The region of strong shear between this zone and the narrow belt below can be seen where the two meet, with wave motions being generated and large-scale turbulence below. Streamlined bands of cloud flow below and around the GRS; smaller red spots appear to the left and below, and two white ovals can be seen near the bottom of the picture.

The appearance of Jupiter is dominated by three types of global features of fundamentally dynamical origin (Fig. 8.22):

1. banded cloud structure, forming bright *zones* and relatively dark *belts*, and variations in the zonal winds at the cloud top level related to these bands;
2. giant eddies, large long-lived storm-like vortices of various colours and characteristics, including red spots, white ovals and brown barges;
3. vertically layered clouds of different compositions, primarily photochemically produced haze at the highest level, solid ammonia ice near the tropopause, solid ammonium hydrosulphide ($NH_3 \cdot H_2S$)

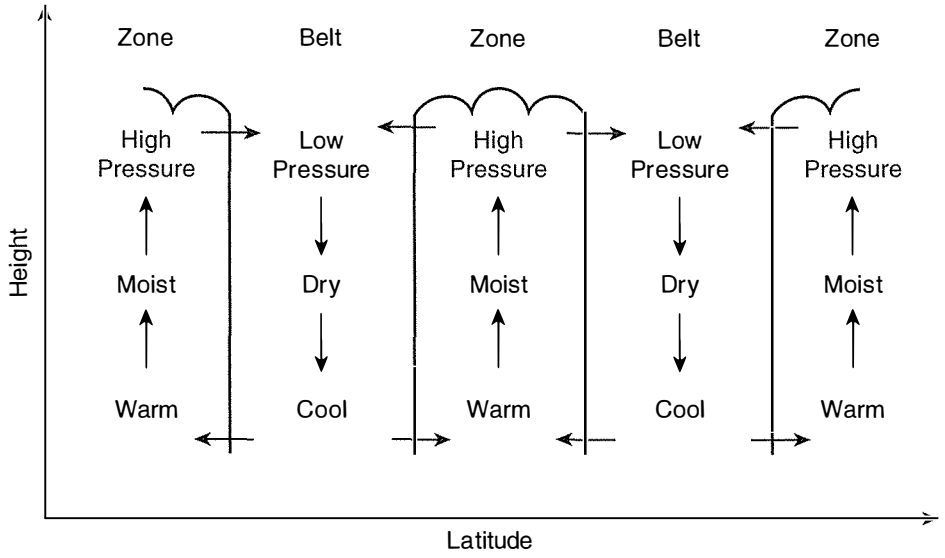

Fig. 8.23
A concept for the meridional circulation on Jupiter or Saturn, showing the formation of cloudy zones and relatively clear belts in the large-scale convective motions driven by internal heating.

below that, and water ice at the deepest level penetrated by observations so far.

Explaining even these overall characteristics, especially the first two, is not possible in simple terms, and advanced studies do not yield definitive answers either, primarily because of the limited amount of suitable data available to develop, test and discriminate between models. Simple deductions and conjectures are the most that can be made until the outer planet atmospheres are better explored.

8.5.1 The banded structure

The principal forcing mechanisms for winds in the atmospheres of all of the gas giant planets are (i) their internal heat sources and (ii) gradients in the solar heating. Clearly, there are also internal processes like latent heat exchange, sensible heat transport, Coriolis forces, etc., that are equivalent to those found on Earth, Mars, and Venus. Except apparently on Uranus, the internal heat sources in the outer planets are comparable to the energy arriving from the Sun, so they are large enough to drive measurable amounts of heat out from the interior at all latitudes, giving rise to convective overturning of the atmospheres on a planetary scale. This, and the rapid rotation rates of these large objects, apparently dominates the general circulation, which takes the form of elongated convection cells stretched around the planet in the equatorial direction.

The rising branches of the cell are richer in condensates like water and ammonia, and have denser, higher clouds than the descending branches, which have been 'freeze-dried 'in the cold upper atmosphere (Fig. 8.23). The resulting cloud contrasts give the planets their banded appearance, most prominent on Jupiter, where the uppermost cloud layers form highest in the atmosphere and have the most contrast. As we saw in Chapter 7, these high, bright clouds consist mainly of

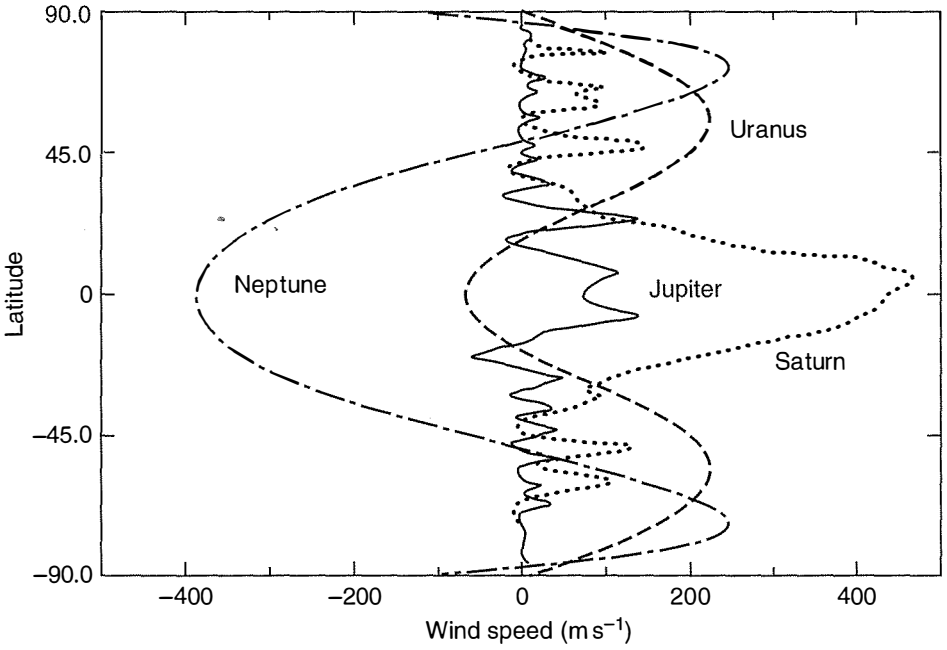

Fig. 8.24
Mean wind speeds vs. latitude on the outer planets. These were determined by tracking cloud motions at the cloud top and are therefore not all at the same pressure level, even on a given planet, requiring caution in their interpretation.

condensed ammonia. They lie close to the level at which the top of the convection cells is expected, as the lapse rate changes from near-adiabatic to near-isothermal due to cooling by radiation to space. If the belt–zone structure does indeed mark out the convection cells, it ought to be possible to use dynamical arguments to estimate the widths of the different cloud bands, as discussed below.

A Jovian GCM can also provide the strengths of the associated zonal winds, which alternate between eastward (in the direction of rotation) and westward in a way that correlates with the cloud bands (Fig. 8.24). The wind speeds at the cloud top show no obvious correlation with the amount of energy available overall to drive them; Jupiter has five or six eastward and westward jet streams in each hemisphere, moving at $\sim 100\,\mathrm{m\,s^{-1}}$, while Saturn has fewer but they are stronger. The highest wind yet seen on one of the outer planets was actually on Neptune, where some small high clouds were clocked at a remarkable $500\,\mathrm{m\,s^{-1}}$. Of course, the available data for each planet are at the level where the cloud tops can be observed, which is different for each and not necessarily the height where the wind is greatest.

Processes internal to the fluid must cause the selection of a particular length scale for the convection cells, particularly in latitude, where it determines the width of the cloud bands. Given the importance of the Coriolis force on rapidly rotating Jupiter, a likely candidate is its gradient with latitude, β. For currents in the zonal direction to be stable on a rotating planet, this must be greater than the gradient in the zonal wind shear, i.e., we must have

$$\beta - \frac{\mathrm{d}^2 u}{\mathrm{d}y^2} > 0 \qquad \text{(stability criterion)}$$

where u is the zonal wind speed and y is the meridional direction from equator to pole. If the planet rotates slowly, then β tends to zero and the gradient in wind shear must as well, so a set of alternating jets like that seen on Jupiter cannot occur. With rapid rotation, however, experiments[69] with numerical models of a homogeneous fluid on a sphere found that zonal jets that approximately satisfy the above criterion developed spontaneously.

Another experiment[70] used real wind measurements on Jupiter and Saturn obtained from successive timed photographs or movies using the *Voyager, Galileo* and *Cassini* spacecraft to calculate U, the maximum zonal wind in each of the jets, and L, the separation between these maxima. In a classic paper,[71] Rhines (1975) showed that non-linear turbulence gives way to linear Rossby waves at a certain spatial scale, characterised by $L_R = \sqrt{\frac{2U}{\beta}}$. L must be greater than L_R to satisfy the stability criterion; if L is somewhat arbitrarily taken to be π times the Rhines scale, then it follows that the ratio $2U \,/\, \beta\pi^2 L^2$ should be of order unity and approximately constant across each planet, which is indeed found to be the case, except near the equator where the dynamical regime is apparently different. Similar consistency is obtained if L is taken to be proportional to another characteristic length for large-scale flow, the deformation radius (§8.2.5).

A further relationship can be derived if it is assumed that the winds fall off to zero at some depth D not too far beneath the visible cloud tops, in which case the thermal wind equation (§8.2.4) relates this depth to the temperature contrast between zones. The measurements of the winds and temperatures that exist do not seem to be consistent with values for D, which remain roughly constant from equator to pole, as we might have expected. Jupiter has only a small axial tilt (3°), so the Sun always heats the equatorial regions more than it does the polar regions. However, the temperature difference between the equator and the poles is surprisingly small, only about 3 K, consistent with the fact that Jupiter was observed by the *Pioneer* spacecraft to emit about the same flux of infrared radiant energy at high latitudes as it does near the equator (see Fig. 4.9). There is no evidence (such as persistent meridional cloud motions) of heat being transported polewards in significant amounts. Perhaps the convection cells bringing interior heat upwards are partially inhibited by solar heating of the upper reaches at the equator, resulting in more efficient vertical transport of heat from the interior in the polar regions. Such a natural thermostat might reduce the temperature difference, and affect the depth of the dynamical features seen in the observable part of the atmosphere.

A mechanism whereby solar heating regulates the heat loss from the interior could apply whether or not the observed motions on Jupiter are confined to, and driven within, a relatively thin, meteorologically active layer at the top of the atmosphere. The features we observe may be at the boundaries of a circulation system that extends to great

[69] G.P. Williams, 'Planetary circulation. I: Barotropic representation of jovian and terrestrial turbulence', *J. Atmos. Sci.*, **35**, 1399–1426, 1978.

[70] For details, see F.W. Taylor, P.J. Gierasch, P.L. Read, and R. Hide, 'Dynamics of planetary atmospheres', *Science Progress*, **72**, 421–450, 1988.

[71] P.B. Rhines, 'Waves and turbulence on a beta-plane', *J. Fluid Mech.*, **69**, 417–443, 1975.

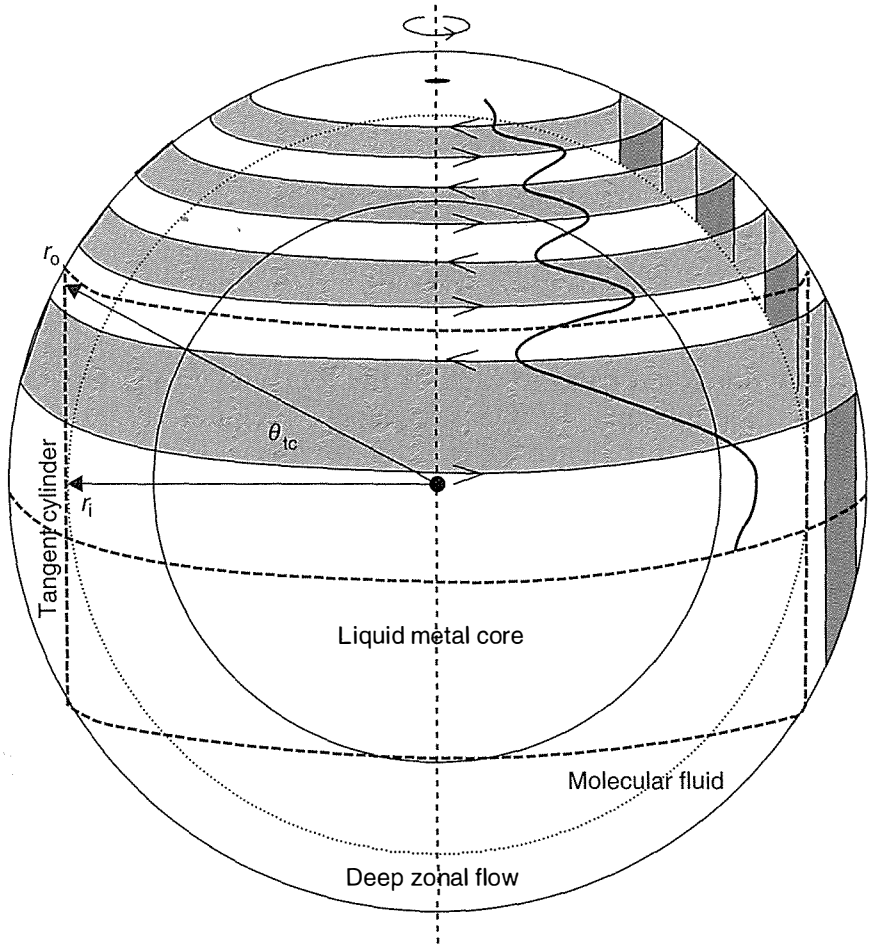

Fig. 8.25
A rotating convective model of Jupiter's atmosphere that may explain the scale of the cloud bands and the alternating jets in the wind profile with latitude (Heimpel *et al.*, 2005).

depth, perhaps right through the planet if it is fluid throughout. Certainly, the size of the internal source means that a large flux of heat has to be transported dynamically at every level. Magnetic field measurements show that the interior of the planet has a strong dynamo action, and theory predicts it must be electrically conducting at high pressures, so the circulation at depth becomes a problem in complicated magneto-hydro-thermodynamics in which many more unknowns are introduced.

Until the vertical wind profile has been measured to considerable depths inside the Jovian atmosphere it is going to be difficult to characterise the circulation there with any certainty. Deep sounding missions like Juno (§6.13) should shed some light, but at present even the qualitative nature of the dynamical regime deep in Jupiter's atmosphere is obscure. Figure 8.4 showed the simplest concept, which has convection cells extending radially from the hot core to the cloud tops, where the heat from the interior is radiated to space. In fact, there may be multiple cells stacked on top of each other or some more complicated arrangement altogether.

Recent theoretical work and modelling has led to the concept shown in Fig. 8.25, in which the deep circulation has cylindrical rather than radial symmetry. The zonal jets and the associated cloud bands would then be the surface manifestation of differentially

rotating cylinders concentric with the planet's axis of rotation. Proponents of such a scheme have pointed out that it predicts (i) different dynamical regimes to occur in the polar and equatorial regions, and (ii) motions in equatorial regions to be symmetric around the equator. The first of these follows because a limit can be placed on the depth of the atmosphere, estimated to be about 10% of the radius of the planet for Jupiter and 30% for Saturn, before forces associated with the high density and flow of large currents through metallic hydrogen take control over geostrophic balance (Fig. 8.25). The observed behaviour near the top of the atmosphere is consistent with this model, although of course this does not constitute unique proof that such a regime exists.

8.5.2 Vertical velocity estimate for Jupiter

It is possible to obtain an estimate of the vertical velocity required in Jupiter's atmosphere to transport the heat from the interior to the upper tropopause region using Prandtl's mixing length theory.[72] In this model, the effective viscosity is taken as being proportional to the square of a quantity called mixing length, notionally the distance a parcel of air travels before mixing with its surroundings, multiplied by the absolute value of the local velocity gradient. If the mixing length is taken to be the scale height of the atmosphere, it can be shown[73] that the vertical velocity w required to carry a flux of heat F is approximately proportional to $[F/\rho]^{1/3}$ in the optically thick part of the atmosphere. The value for w_0 of $\sim 1\ \mathrm{m\,s^{-1}}$ near 1 bar produced by estimates based on this formula is high by standards for the Earth, where values two or three orders of magnitude smaller are found, but not unreasonable for rising air in Jupiter's cloudy zones. Of course, mass must be conserved overall by a corresponding descending motion in the relatively cloud free belts that stretch around the planet between the zones.

[72] Ludwig Prandtl (1875–1953) worked in Hanover and Göttingen on the theory of aerodynamic flows. He developed the mixing-length model in 1925, providing an approximate way of dealing with the complex topic of turbulent flows.

[73] See *Jupiter*, loc.cit., Chapter 3.

8.5.3 The long-lived giant eddies

After the bands, the most striking characteristics of outer planet cloud markings are the various spots associated with the giant rotating air masses known as eddies. These come in a variety of colours, sizes and patterns of behaviour, have no direct analogue in the terrestrial planet atmospheres, and in general are fairly mysterious. The most conspicuous is the oval-shaped Great Red Spot in Jupiter's southern hemisphere, which measures $\sim 12{,}000 \times 20{,}000$ km, much larger than the entire Earth. Although the current GRS has been present since at least 1831, and probably much longer,[74] it does vary both in size and intensity, and appears to be steadily shrinking in the longitudinal direction. Its sense of circulation, and that in other ovals in the southern hemisphere, is counterclock-

[74] Robert Hooke reported seeing a spot on Jupiter, presumably the GRS, as long ago as 1664.

wise (anticyclonic). The eddy velocities are typically a few tens of metres per second.

Saturn also has oval-shaped circulation cells in its atmosphere, but they are fewer and less conspicuous than those on Jupiter. On Neptune, a small number of large spots have been observed, including the Great Dark Spot seen during the *Voyager 2* fly-by in 1989. This resembles its Jovian counterpart superficially, although not in detailed behaviour. However, as with the convection cells and the cloud bands, it is not known how deep these phenomena extend on any of the planets. We do know from the *Galileo* probe, which reached pressure levels of more than 20 bars and delivered the only *in situ* data so far on any of the outer planets, that high zonal velocities persist to depths of around 100 km below the cloud tops on Jupiter.

Some early theories of the origin of the large eddies assumed a surface with topography must lie below the clouds. For instance, the GRS might be a disturbance caused by flow over a very large mountain on a hypothetical surface hidden below the Jovian clouds. We now know that there is no such surface, and believe the GRS and other large oval features must originate in an instability in the mean zonal flow on Jupiter, achieving their remarkable longevity by virtue of their great size and the evident vigorous windy and turbulent nature of the atmosphere.

The instability could be baroclinic (buoyancy driven), even without a solid obstacle, but is more likely to be barotropic (mechanically driven by horizontal shear forces). The energetic jet streams that abound on Jupiter have strong shear regions at their edges and it is clear that these give rise to waves and turbulence of various kinds. A range of phenomena that possibly are important on Jupiter can produce stable solutions in models, and in laboratory simulations using rotating tanks of fluid, that resemble the GRS and other large oval features in appearance, superficially at least.

One of these is the solitary Rossby wave or 'soliton', a free mode[75] that has a single maximum, and which therefore presents as an isolated feature in models, with conditions that resemble those found in regions of zonal shear on Jupiter. It has also been shown using shallow-atmosphere models[76] that closed eddies could coexist in a stable state between two barotropic zonal jets, and that small eddies could coalesce with larger ones to form an even larger feature. In the real atmosphere, it is possible that this process, where large eddies 'feed' on smaller ones, finds an equilibrium between dissipative processes and the steady input of fresh vorticity. This is a possible explanation for the persistence of all of the large eddies, and in particular the great longevity of the GRS.

Isolated eddies can also be produced in the laboratory, under conditions that have some aspects in common with Jupiter, and the results extended to planetary conditions using theory and models. In the laboratory, the eddies may be maintained through thermal forcing by applying a temperature gradient across fluid in a rotating annulus. The

[75] Free modes are those that are not systematically driven by tidal forcing or some other sustained stress.

[76] A.P. Ingersoll and P.G. Cuong, 'Numerical model of long-lived Jovian vortices', *J. Atmos. Sci.*, **38**, 2067–2076, 1981.

forcing can be varied, along with the size, depth, and rotation rate of the fluid, in order to probe the parameter space in which such features form and discover the conditions that lead to their growth and stability.

The greatest difficulty in discriminating between simulations and models remains the lack of detailed data on the properties of the observed planetary eddies, and the processes producing forcing and those responsible for dissipation on the real planet. Most of what is known is essentially two-dimensional: movies of cloud motions in and around the GRS show it is an anticyclonic vortex with a spiral of clouds with a pale red tint circulating around a quiescent centre. The spot is higher at the centre than the edge, and tipped, with the leading (eastward) edge about 10 km higher than the trailing one; not much compared to the width along the long axis, which is over 15,000 km, but probably of some, as yet uncertain, dynamical significance. The vortex circulation falls off rapidly above the visible surface of the GRS, which is at a pressure of about 0.7 bars, but there are no measurements of the dynamical behaviour below it. High-resolution infrared imaging data has shown that the cloud cap is thin compared to its horizontal extent, and that gaps exist between the spiral-arm structure of the clouds in the vortex. The possibility of remote sounding below and inside the Spot, or of inserting an entry probe, remains a possibility for a future mission.

Much of the above discussion assumes implicitly that the Great Red Spot is the just the largest example of the variety of vortex features seen on Jupiter and the other outer planets, but this is not certain. Differences in size, colour, lifetime, and even direction of rotation, are seen. White ovals sometimes originate when elongated cloud zones break up, forming trains of roughly equally spaced features that start out looking nearly identical but may then merge. Sometimes cloud-filled eddies form in what appear to be updrafts; some have a distinct red colouration, like the GRS, which may indicate that they contain more exotic material, dredged from greater depths, than the white ovals.

8.6 Titan atmospheric dynamics

In terms of its general circulation, Titan resembles Venus, since both are slowly rotating bodies with a dense atmosphere containing a deep cloud layer. There is evidence from imaging, temperature, and composition field measurements, supported by oblateness measurements using stellar occultation data, that Titan has a superrotating atmosphere and an equator-to-pole Hadley circulation like that of Venus. An important difference from Venus is the strong seasonal cycle due to its obliquity of 26.7°, more like Earth's. Titan's atmosphere has a number of other Earth-like characteristics: in addition to having the same major constituent, nitrogen, and nearly the same surface pressure, data from the *Cassini* spacecraft which has made many close fly-bys of Titan while orbiting Saturn, have revealed storms, features formed by precipitation, and tentative evidence for lightning.

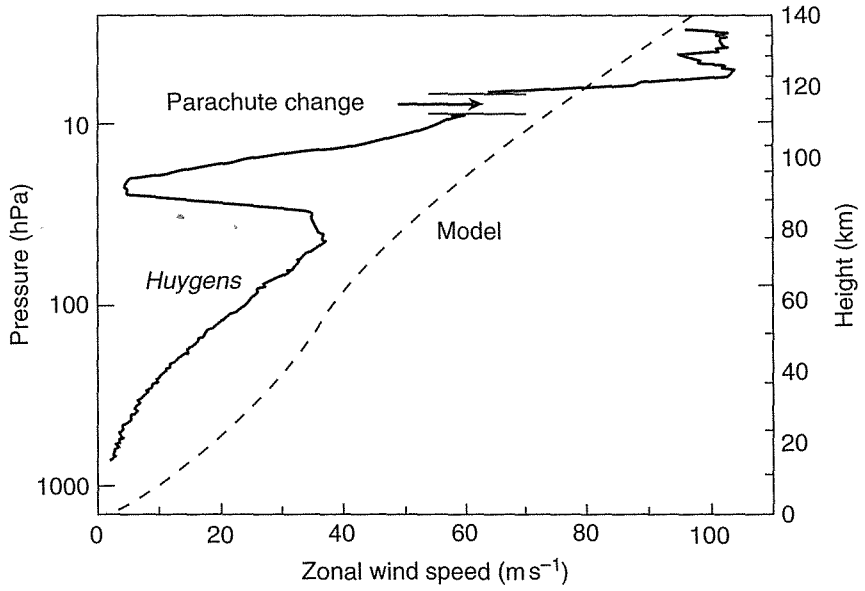

Fig. 8.26
The zonal wind versus profile[77] measured by the *Huygens* entry probe during its descent, compared to model prediction based on earlier measurements of temperature by *Voyager*. The units on the pressure scale are hectopascals, which are interchangeable with millibars (1 hPa = 1 mb)

[77] M.K. Bird et al., The vertical profile of winds on Titan. *Nature*, **438**, 800–202, 2005.

8.6.1 Zonal motions

Titan's haze cover shows faint bands parallel to the equator, suggesting rapid zonal winds. Continuing the analogy with Venus, we would expect rapid zonal winds in the same sense as the rotation of the solid body, driven by thermally induced pressure gradients in balance with the centrifugal forces arising from the rapid rotation of the atmosphere (i.e., cyclostrophic balance). Since the cyclostrophic form of the thermal wind equation is quadratic in the zonal wind, it can be integrated to yield the wind magnitude, but does not identify whether it has an east–west or west–east direction.

The latitudinal temperature contrasts first seen during the Titan encounter by the *Voyager* spacecraft in 1980 indicated zonal winds of the order of 80 m s^{-1} at 0.4 mb, comparable with those measured on Venus. From *Cassini* fly-bys in July and December 2004, the temperatures at the 1 mb level were found to be lower by around 20 K at 60° N compared to those at the equator, whereas the equator-to-pole difference is only 4–5 K in the southern hemisphere. The mean zonal winds inferred from this temperature field are weakest at high southern latitudes and increase towards the north, with maximum values at mid-northern latitudes (20–40° N) as high as 160 m s^{-1}.

Titan's disc is slightly oblate, an effect which may be attributed to the superrotation of the atmosphere. Accurate measurements along one chord can be made when a star passes behind the disc of Titan, as seen through a telescope from the Earth. The results show that, if the corresponding non- circularity is entirely due to zonal winds, their velocity is about 180 m s^{-1} at 0.25 mb. This is again much faster than the surface rotation speed of 12 m s^{-1}, and presumably, although this measurement is also ambiguous with regard to direction, in the same sense. At this level the superrotation factor is about 15.

During its descent onto the surface of Titan in 2005, the *Huygens* probe measured a wind profile using Doppler tracking (Fig. 8.26). This

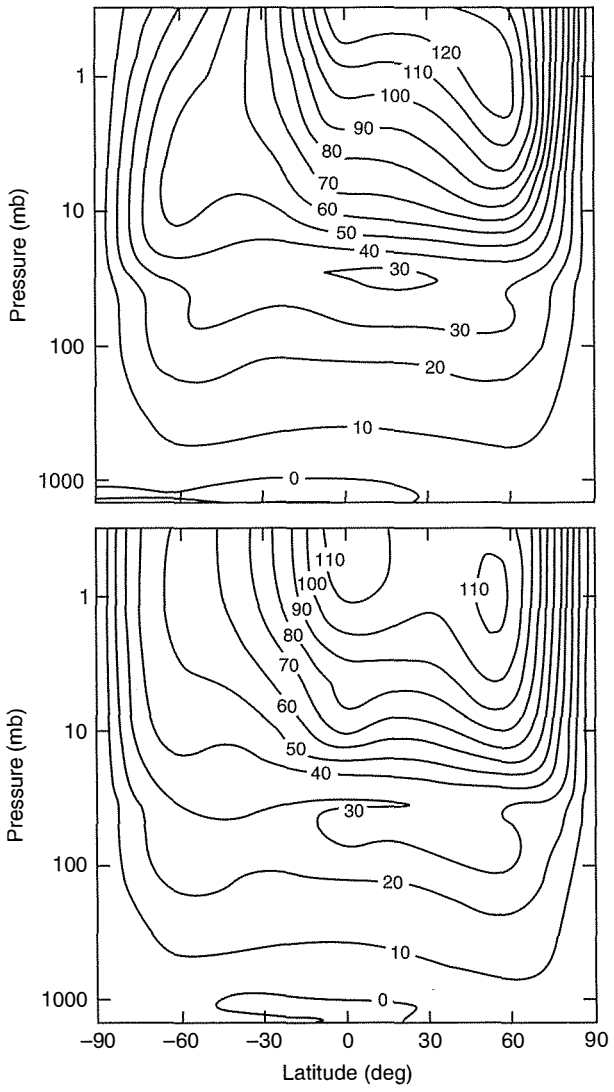

Fig. 8.27
Zonal winds ($m\,s^{-1}$) computed by a Titan general circulation model, showing superrotation and a midlatitude jet. The top frame shows the northern winter solstice and the lower frame the spring equinox. (Hourdin *et al.*, 1995.)

confirmed that the prevailing wind direction is prograde (in the same sense as the rotation of the surface), as had been inferred earlier from Earth by using infrared heterodyne spectroscopy to measure the Doppler shift of spectral lines emitted by traces of ethane in Titan's atmosphere. Similar results were obtained with nitrile lines observed at millimetre wavelengths, and high-resolution spectroscopy of Fraunhofer solar absorption lines in the visible. Wind speed and direction have also been inferred by tracking tropospheric clouds in images from *Cassini*, and even using Earth-based telescopes. These confirm that the clouds occur at around 25 km altitude and have slow, eastward motions. An attempt to track faint features in the higher-level haze led to inferred wind speeds of 28 to 99 $m\,s^{-1}$ in the 1–100 mb region, which would correspond to air circulating around the equator in about 2 to 5 days. This may be contrasted with Titan's solid-body rotation rate of 16 days, an equatorial superrotation factor of 3 to 8 (compared to between 50 and 60 on Venus).

The results from tracking the descent of *Huygens* found winds of about 5 $m\,s^{-1}$ at 25 km altitude at the entry location at about 10 °S

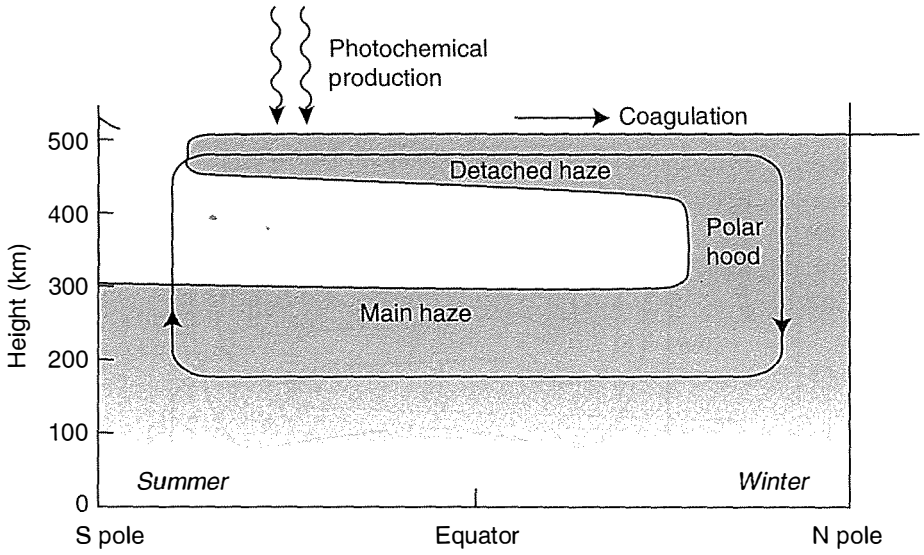

Fig. 8.28
A schematic of the circulation on Titan and its relationship to the production of polar hood hazes and a seasonal contrast in brightness between the hemispheres.

latitude. The winds decreased with altitude from 100 m s^{-1} at 140 km down to almost zero at 80 km, then increased up to 40 m s^{-1} at 60 km, before decreasing again to negligible zonal velocity at the surface. The winds measured by *Huygens* are generally smaller than expectations from models, and the sharp dip in the wind velocity in the height range between 60 and beyond 100 km was a complete surprise, although a possible explanation in terms of atmospheric tidal effects has recently been advanced.

As for Venus, dynamical models of Titan's atmosphere have been produced based on general circulation models of the Earth. The dynamical code is based on the primitive equations of meteorology, modified for Titan's radius of 2575 km, obliquity of 26°, and rotation rate of 16 days, as well as other factors, including of course the composition, cloud and temperature structure. The models obligingly produce a wind field featuring strong zonal superrotation, with winds of the same order as the observed ones, and a midlatitude jet (a compact region of high wind) at midlatitudes with about the same wind speed, around 120 m s^{-1}, as that seen on Venus. In the model, the jet is located close to 60° in the winter hemisphere, while the summer zonal circulation is much less energetic, closer to solid-body rotation (Fig. 8.27).

8.6.2 The meridional circulation

The gradients and contrasts in minor constituent composition, haze density, and temperature, all provide confirmation for the existence of an underlying Hadley (equator-to-pole) circulation on Titan, with upwelling at the equator and downwelling near the poles. For instance, the small thermal gradients of 2–3 K between equator and pole must be the result of the efficient heat redistribution achieved by this circulation. Unlike the hemispheric cells on Venus and Earth, the observational evidence suggests a pole-to-pole Hadley cell on Titan, reversing after the equinox when the Sun moves to the opposite hemisphere

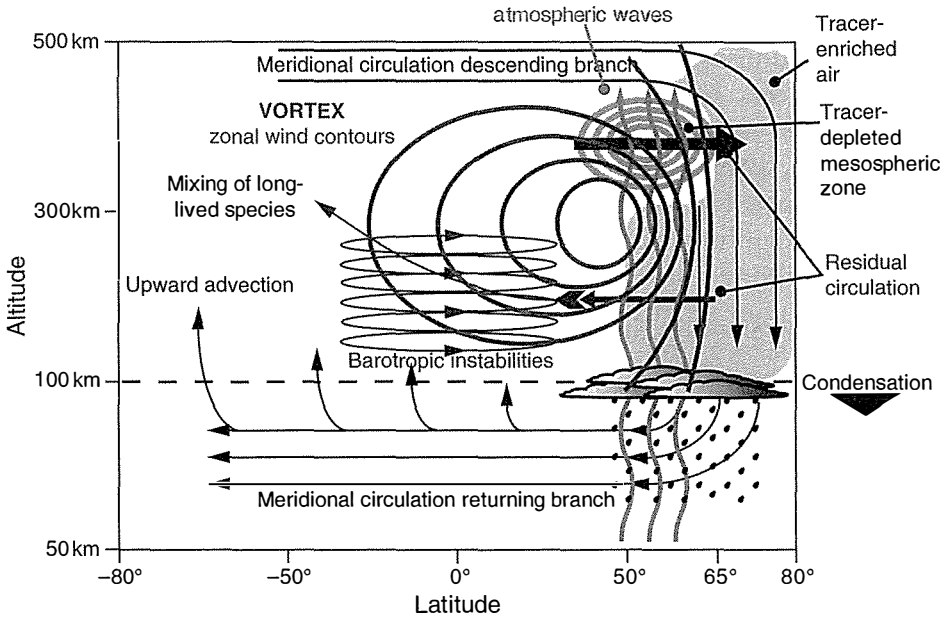

Fig. 8.29
A schematic of the dynamical processes occurring in Titan's midwinter stratosphere and mesosphere. A middle atmosphere mixing barrier associated with a vortex jet occurs around 60° N, with a polewards circulation at high levels bringing tracer-enriched air to polar latitudes and a return branch below. From Teanby *et al.* (2008).

(Fig. 8.28). Models of the seasonally varying circulation confirm this, and show the mean transport in the upper atmosphere from the summer pole to the winter pole is a consequence of the high inclination of the rotation axis, with equator-to-pole Hadley cells in each hemisphere only during the changeover from one summer to the other.

Voyager 1 in 1980 observed a darker northern hemisphere in visible light, a situation which has since been observed to reverse, with the northern hemisphere becoming brighter than the south, as Titan's season shifts from northern spring to northern winter. At near-infrared wavelengths the asymmetry is reversed, due to variations of the atmospheric and haze brightness with wavelength. The atmosphere is bright at short wavelengths due to Rayleigh scattering and dark in the near infrared due to methane absorption, whereas the haze appears to be dark in blue, and bright at red and longer wavelengths.

As on Venus and Earth, a consequence of the polewards transport of angular momentum in the meridional circulation is the formation of a polar vortex. Titan's atmosphere is rich in traces of relatively short-lived gases that are carried around by the winds and so act as tracers of the motions. The vortex, which is the major dynamical feature of Titan's polar stratosphere and mesosphere in the northern midwinter season, is delineated strongly in observations of the five chemical tracers shown in Fig. 6.11, namely hydrogen cyanide (HCN), acetylene (C_2H_2), methylacetylene (C_3H_4), cyanoacetylene (HC_3N), and diacetylene (C_4H_2). The molecular abundances measured by *Cassini* indicate an enhancement for some species in the northern stratosphere at high latitudes, produced by downwelling over the winter pole, which brings enriched air from the production zone to the stratosphere. Short-lived species are more sensitive to the downwelling due to steeper vertical composition gradients, and these exhibit higher contrasts. They show that the vortex acts as a strong mixing barrier in the stratosphere and mesosphere, effectively separating a tracer-enriched

air mass over the pole from air at lower latitudes (Fig. 8.29). Titan's strong circumpolar winds tend to inhibit mixing of the enhanced concentrations back to lower latitudes, a process similar to that which in the case of the Earth leads to the formation of the Antarctic ozone hole, although of course the chemistry inside the containment zone is different on Titan.

8.6.3 Weather, waves, tides and turbulence

Weather phenomena, in the form of precipitation and storm activity, appear to be plentiful on Titan, further reinforcing the terrestrial analogy. There seem to be at least two distinct kinds of precipitation. The first is the slow drizzle of hydrocarbons, possibly including heavy, relatively complex molecules, from the planet-wide haze layers. The second is precipitation, apparently very voluminous sometimes, from the cumulus-type clouds of methane and ethane that form in convective updrafts where local meteorological conditions are right (Fig. 7.14).

Titan has a convective troposphere about 40 km deep. Here, the atmosphere is optically thick, favouring heat transfer by vertical transport and suppressing loss to space directly by radiation. As on all planets under such conditions, the temperature falls with height at approximately the adiabatic lapse rate, given by the need for the buoyancy of an air parcel to just balance the vertical pressure gradient. On Titan, this is about $1.4\,\mathrm{K\,km^{-1}}$ for dry air, compared to $\sim 10\,\mathrm{K\,km^{-1}}$ for the Earth, the difference being due mainly to the smaller acceleration due to gravity on Titan, since the other main parameter upon which lapse rate depends, namely the bulk atmospheric composition, is nearly the same.

Direct evidence for wave processes in Titan's atmosphere remains scarce, despite the expected importance, by analogy with Venus, of barotropic waves as the principal carrier of momentum from high to low latitudes in the maintenance of the zonal superrotation. Modelling predicts predominantly wavenumber-2 activity, with an amplitude for the zonal component of about 10% of the mean wind speed, large enough in principle to be detected in horizontal maps of temperature and trace species.

As a moon rather than a planet, Titan experiences a unique phenomenon among Earth-like planets, which is the strong gravitational tide exerted by Saturn. The eccentric orbit of Titan around Saturn results in periodical oscillation in the atmospheric pressure and wind with a period of a Titan day (16 Earth days), among which the most notable effect is the periodical reversal of the north–south component of the wind. In the lower atmosphere, the effect of this tide is expected to produce a maximum temperature amplitude of about 0.3 K and winds of $\sim 2\,\mathrm{m\,s^{-1}}$, probably superimposed on the global circulation driven by the Sun. A surface wind of a few metres per second is predicted by Titan general circulation models and, indeed, drag between the air movement and the surface is an essential component of the momentum balance equation. It may be modulation by the Sat-

urnian tide that produces the periodic structure seen in wind-blown dune fields in *Cassini* images of the surface of Titan.

At times, regions on Titan experience storms and serious rainfall. Apparently, the lower atmosphere is unstable with regard to convection under conditions of relatively strong heating. The rising air can then bring large amounts of moisture up to form dense clouds that are locally thick but patchy in coverage, occurring mainly in middle and high latitudes in the summer. Thus, locally high surface temperatures, combined with a source of methane on or in the surface, lead to the rapid growth of convective storms analogous to thunderstorms and monsoons on the Earth, and accompanied by the same kind of torrential rain. The cloudy, stormy region migrates from one hemisphere to another with the seasons, producing local flooding for a short time each year in the summer. The surface accumulations of contaminated liquid methane soon drain below ground or evaporate. This inferred behaviour explains why the landscape viewed by the *Huygens* probe features river valleys and other features apparently produced by copious amounts of running liquid, although the surface was dry at the time of its landing.

8.7 References and further reading

Chapman, S., and R.S. Lindzen. *Atmospheric Tides*. D. Reidel Publishing Co., 1970.

Clancy, R.T., B.J. Sandor, and G.H. Moriarty-Schieven. Dynamics of the Venus upper atmosphere: Global-temporal distribution of winds, temperature, and CO at the Venus mesopause. *Bull. Am. Astron. Soc.*, **39**, p. 61.07, 2007.

Coustenis, A., and F.W. Taylor. *Titan: Exploring an Earthlike World*. 330pp. World Scientific Publishing, 2008.

Elson, L.S. Wave instability in the polar region of Venus. *J. Atmos. Sci.*, **39**, 2356–2362, 1982.

Flasar, F.M. *et al.* Titan's atmospheric temperatures, winds, and composition. *Science*, **308**, 975–978, 2005.

Gierasch, P.J. Meridional circulation and the maintenance of the Venus atmospheric rotation. *J. Atmos. Sci.*, **32**, 1038, 1975.

Gierasch, P.J., R.M. Goody, R.E. Young, D. Crisp, C. Edwards, R. Kahn, D. Rider, A. del Genio, R. Greeley, A. Hou, C.B. Leovy, D. McCleese, and M. Newman. The general circulation of the Venus atmosphere: An assessment. In *Venus II: Geology, Geophysics, Atmosphere, and Solar Wind Environment*, ed. by S.W. Bougher, D.M. Hunten, and R.J. Philips. University of Arizona Press, 1997.

Heimpel, M., J. Aurnou, and J. Wicht. Simulation of equatorial and high-latitude jets on Jupiter in a deep convection model. *Nature*, **438**, 193–196, 2005.

Held, I.M., and A.Y. Hou. Nonlinear axially symmetric circulations in a nearly inviscid atmosphere. *J. Atmos. Sci.*, **37**, 515–533, 1980.

Hourdin. F., O. Talagrand, R. Sadourny, R. Courtin, D. Gautier, and C.P. McKay. Numerical simulation of the general circulation of the atmosphere of Titan. *Icarus*, **117**, 358–374, 1995. Ingersoll, A.P., T.E. Dowling, P.J. Gierasch, G.S. Orton, P.L. Read, A. Sanchez-Lavega, A.P. Showman, A.A. Simon-Miller, and A.R. Vasavada. Dynamics of Jupiter's atmosphere. In *Jupiter: The Planet, Satellites, and Magnetosphere*, ed. by F. Bagenal, W. McKinnon, and T.E. Dowling, Cambridge University Press, 2006.

Lorenz, R.D., C.A. Griffith, J.I. Lunine, C.P. McKay, and N.O. Rennò. Convective plumes and the scarcity of Titan's clouds. *Geophys. Res. Lett.*, **32**, Issue 1, Cite ID L01201, 2005.

Maxworthy, T., and L.G. Redekopp. A solitary wave theory of the Great Red Spot and other observed features in the Jovian atmosphere. *Icarus*, **29**, 261–271,1976.

Read, P.L. Superrotation and diffusion of axial angular momentum. I: Speed limits for axisymmetric flow in a rotating cylindrical fluid annulus. *Q. J. Roy. Meteorol. Soc.*, **112**, 231–251, 1986.

Read, P.L., and S.R. Lewis. *The Martian Climate Revisited: Atmosphere and Environment of a Desert Planet*. Springer-Praxis, 2004.

Read, P.L., P.J. Gierasch, B.J. Conrath, A. Simon-Miller, T. Fouchet, and Y.H. Yamazaki. Mapping potential-vorticity dynamics on Jupiter. I: Zonal-mean circulation from *Cassini* and *Voyager 1* data. *Q. J.Roy. Meteorol. Soc.*, **132**, 618, 1577–1603, 2006.

Read, P.L., P.J. Gierasch, and B.J. Conrath. Mapping potential-vorticity dynamics on Jupiter. II: The Great Red Spot from *Voyager 1* and *2* data. *Q. J. Roy. Meteorol. Soc.*, **132**, 618, 1605–1625, 2006.

Sánchez-Lavega, A., *et al.* Variable winds on Venus mapped in three dimensions. *Geophys. Res. Lett.*, **35**, L13204, doi:10.1029/2008GL033817, 2008.

Taylor, F.W., P.J. Gierasch, P.L. Read, and R. Hide. Dynamics of planetary atmospheres. *Sci. Progress*, **72**, 421–450, 1988.

Teanby, N.A., *et al.* Titan's winter polar vortex structure revealed by chemical tracers. *J. Geophys. Res.*, **113**, E12003, doi:10.1029/2008JE003218, 2008.

Tsang, C.C.C., S.J. Liddell, C.F. Wilson, G. Piccioni, P. Drossart, P.G.J. Irwin, F.W. Taylor, S.B. Calcutt and the *Venus Express*/VIRTIS Team. Dynamic variability of CO concentrations in the Venus troposphere from *Venus Express*/VIRTIS-M using a band ratio technique. *Icarus*, **201**, 432–443, 2009.

8.8 Questions

1. The meridional component of the equation of motion on a spherical planet of radius a and rotational angular velocity Ω is

$$\frac{Dv}{Dt} + \frac{u^2 \tan\phi}{a} + \frac{uv}{a} + 2\Omega u \sin\phi = -\frac{1}{\rho a}\frac{\partial p}{\partial \phi}$$

where ø is latitude, p is pressure, ρ is density, and u, v, w are the components of velocity. What balance of terms in the above equation represent cyclostrophic balance?

2. Titan, the principal satellite of Saturn, rotates very slowly about its axis with a period of 16 Earth days. Assuming therefore that the Coriolis acceleration can be neglected, and further that hydrostatic balance applies and vertical variations in temperature can be neglected, show that the thermal wind equation on Titan is approximately

$$2u\frac{\partial u}{\partial z} = -\frac{g}{T\tan\phi}\frac{\partial T}{\partial \phi}$$

3. Measurements in Titan's atmosphere indicate a temperature difference between equator and high latitudes of 10 K, independent of height up to 60 km altitude. Estimate the maximum zonal wind speed, given that the atmosphere is at a mean temperature of 90 K and that $g = 1.35\,\mathrm{m\,s^{-2}}$.

4. The steady-state equations for an incompressible fluid flowing over topography are

$$u\frac{\partial u}{\partial z} + v\frac{\partial u}{\partial y} - fv = -\frac{1}{\rho v}\frac{\partial p}{\partial z}$$

$$u\frac{\partial v}{\partial z}+v\frac{\partial v}{\partial y}+fu=-\frac{1}{\rho v}\frac{\partial p}{\partial y}$$

$$\frac{\partial}{\partial z}(hu)+\frac{\partial}{\partial y}(hv)=0$$

where h is the depth of the fluid, u, v are the zonal and meridional velocities, f is the Coriolis parameter $2\Omega\sin\phi$, where ϕ is the latitude, ρ_0 the density (taken to be constant), and p the pressure. Taking the curl of the first two equations, show that they imply the conservation of potential vorticity q following the horizontal motion, where

$$q=\frac{1}{h}\left(\frac{\partial v}{\partial z}-\frac{\partial u}{\partial y}+f\right)$$

5. Using the previous result, show that q-conservation can be written as

$$\phi(\psi,q)\equiv\frac{\partial\psi}{\partial z}\frac{\partial q}{\partial y}-\frac{\partial\psi}{\partial y}\frac{\partial q}{\partial x}=0$$

where ø is a stable stream function. Hence show that weak flow will occur parallel to contours of f/h. Find the form of the weak flow which would occur on a smooth plane $(h-h_0)$, for which $\psi=Kf$ where K and h_0 are constants, and $f=2\Omega\sin\phi$, where ϕ is the latitude.

6. Take the non-linear free-surface equations for non-divergent flow:

$$\begin{aligned}Du-fv+gh_z&=0\\Dv-fu+gh_y&=0\\u_x+v_y&=0\end{aligned}$$

where

$$D=\frac{\partial}{\partial t}+u\frac{\partial}{\partial z}+v\frac{\partial}{\partial y}$$

is the horizontal advective derivative. Retaining the β-effect, show that

$$D(\xi+f)=0$$

What is the physical interpretation of this equation?

7. Consider small, non-divergent disturbances to a steady, uniform zonal flow $(U, 0)$. Put $u=U+u'$, $v=v'$, introduce a disturbance stream function ψ and show that

$$\left(\frac{\partial}{\partial t}+U\frac{\partial}{\partial x}\right)(\psi'_{xx}+\psi'_{yy})+\beta\psi'_x=0$$

when quadratic terms in ψ' are neglected. Hence, derive the dispersion relation for non-divergent Rossby waves in the presence of the basic zonal flow. Under what conditions is the phase speed (ω/k, where k is the zonal wavenumber) eastwards? Show that stationary waves (with $\omega=0$) can only exist if U is eastwards and less than βk^{-2} in magnitude.

8. The surface topography in the northern hemisphere of Mars consists of a pair of ridges oriented north–south and 180° apart in longitude. One corresponds to the Tharsis plateau centred at longitude 100° W, the other to Syrtis at about 80° E. Consider a latitude circle of length $L\approx 10\,000$ km, where $\beta\approx 2\times10^{-11}\,\mathrm{m^{-1}\,s^{-1}}$. For what range of values of U, a uniform

westerly zonal flow, might you expect to see a stationary atmospheric response excited by this topography?

9. Outline the main assumptions behind Held and Hou's simple model of a nearly inviscid, axisymmetric Hadley circulation.

Consider this model on an equatorial β-plane, so that $f=\beta y$. For a radiative equilibrium temperature profile with latitude given by

$$\Theta_E - \Theta_{E0} - \frac{\Delta\theta}{a^2}y^2$$

where Θ_{E0} is a constant and a is the planetary radius, define a suitable form for m, angular momentum per unit mass, and verify that the conservation of absolute angular momentum in (geostrophic) thermal wind balance leads to

$$\frac{\partial\theta}{\partial y} = \frac{2\Omega^2\theta_0}{a^2 g H}y^3$$

where Ω is the planetary rotation rate, g the acceleration due to gravity, and H and θ_0 are constants. Hence obtain an expression for the horizontal profile of temperature Θ_M consistent with angular momentum conservation.

10. By assuming that the Hadley circulation extends between $y = \pm Y$ in a channel with boundaries at $y = \pm L$, where $L > Y$ and $\Theta = \Theta_E$ for $|y| \geq Y$, and that there is no net heating or cooling of air parcels, show that Y is given by

$$Y = L\sqrt{\frac{5R}{3}}$$

where

$$R = \frac{g\Delta\theta H}{\Omega^2 L^2 \theta_0}$$

11. Using the approximate values in the following table for equator–pole temperature difference ΔT and a representative atmospheric temperature T in order to estimate $\Delta\theta/\theta_0$, calculate Y with the values given for each planet. Determine the extent of the Hadley circulation in latitude using the planetary radius a. How do they compare with the observed circulations?

	ΔT (K)	T (K)	a (10^6 m)	Ω (10^{-5} s^{-1})	g (m s^{-2})	H (10^3 m)
Venus	20	240	6.1	0.03	8.6	5
Earth	40	255	6.4	7.29	9.8	8
Mars	40	225	3.4	7.09	3.7	11
Jupiter	20	125	71.4	17.6	22.9	20
Titan	10	90	2.6	0.46	1.4	18

Climate and global change

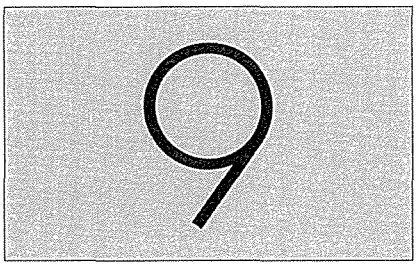

In Chapter 2, we considered how planetary atmospheres originated, and how they evolved over more than 4 billion years to those we see in the Solar System today. In subsequent chapters, we looked at the properties and behaviour of current atmospheres. In this final chapter, we focus on how atmospheric evolution affects surface conditions, on both long timescales (thousands to billions of years) and in the shorter term (decades to centuries). The physics involved is the basis for understanding climate and global change, one of the biggest problems facing life on Earth.

9.1 Definition of climate

The climate is the mean state of the atmosphere on timescales that are long compared to the diurnal cycles and the seasons. The principal parameters that define climate are:

1. The global mean surface temperature on the planet. Generally, on the Earth and by analogy on the other Earth-like planets,[78] this is the proxy for 'climate' when a single parameter is used.
2. The mean surface pressure. While not a major factor for contemporary, short-term climate change on Earth, it is very important on all planets when early evolution or long-term change is being considered.
3. The atmospheric composition, including the amount and type of cloud and proportion of greenhouse gases.
4. The albedo of the planet, determined mainly by cloud and ice cover, and surface mineralogical composition and physical state (roughness).
5. Spatial variations in the above, for example, changes in the size of icecaps, in the vertical distribution of clouds, or in the equator-to-pole temperature gradient.
6. Dynamics, since all of the above interact with each other, for instance, through the global circulation of the atmosphere, and the ocean if there is one, making the basic dynamical state another key factor in determining climate.

A simplified diagram like that in Fig. 9.1 can summarise the complex interactions between the key components of the physical climate system on the Earth. It will make an interesting exercise to modify it for

[78] Again including Titan, which matches the definition of an Earth-like planetary body as one with (a) an accessible solid surface, and (b) an optically thick lower atmosphere where vertical transfer of heat is primarily by convection (i.e., a troposphere).

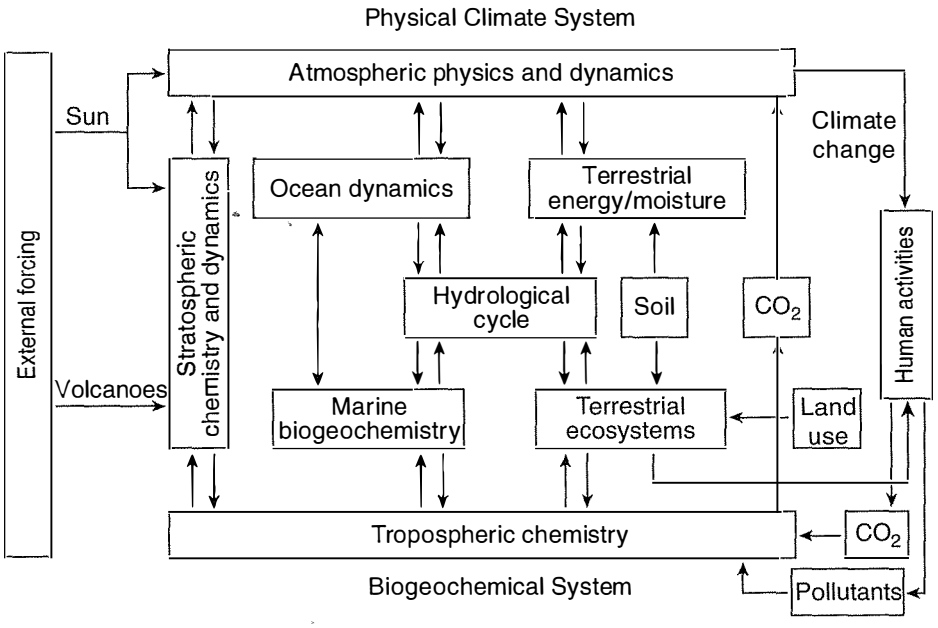

Fig. 9.1
A 'Bretherton' diagram,[79] which summarises the complex interactions between the key components of the physical climate system. On the Earth, it is impossible not to include biology as well; a simpler version should apply to planets without extant life.

[79] Named after Professor F.P. Bretherton who was chairman of the Earth System Sciences Committee of NASA's Advisory Council in 1986 when the diagram was first formulated.

planets without extant life after discussing the individual processes and models in more detail.

9.2 Climate change

Secular changes in climate have certainly occurred in the past on the Earth and Mars, and probably also on Venus and Titan, although there is limited hard evidence for the last two as yet. Major changes in climate for which there are quite firm foundations of evidence include:

1. The terrestrial ice ages, the latest of which ended about 10,000 years ago.
2. The flooding of the surface of Mars in its earliest epoch, probably more than 3.5 billion years ago.
3. The Martian polar layered deposits, which have been laid down over an extended period and continue to form right up to the present day.
4. The inferred existence of an ocean of water on Venus when the planet was young.
5. The dependence of Titan's current climate on a high proportion of atmospheric methane, a compound with a relatively short atmospheric lifetime whose abundance probably has varied on long timescales.

Many of the factors driving these and other forms of climate change are known and have been extensively studied, although because of the complex interconnections between them cause and effect has not yet been clearly established. Key climate drivers include:

1. Long-term cyclic changes in orbital parameters, such as eccentricity and obliquity, due to gravitational interactions of each planet with other members of the Solar System (the Milanković cycles).[80]

[80] Milutin Milanković worked on the effects of orbital variations on climate in the 1930s when he was Professor of Applied Mathematics at the University of Belgrade. Much more sophisticated calculations are possible now with modern computers and better data about the Solar System, but the problem is so complex that there are still many uncertainties.

2. Changes in solar output, as the Sun evolves, or due to cycles or disturbances on or inside the Sun. Familiar examples are the sunspots, which can affect solar output, although recently this particular effect has been quite small in terms of the energy radiated to the planets.
3. Changes in the planetary magnetic field, due to secular or cyclical variations in internal activity. On Mars, for example, the internally generated magnetic field appears to have gone from something stronger than the current terrestrial field to virtually zero over the life of the planet, probably due to progressive cooling of the interior. Venus is generally presumed to have similar interior processes and conditions to Earth, but its slightly smaller size, slower planetary rotation rate, and possibly somewhat different core composition, may be key factors for explaining why Earth has a significant field while Venus currently does not.
4. Changes in volcanic outgassing, again due in the long term to declining internal temperatures and volatile inventories, with episodic behaviour superimposed. Part of the reason for the current high atmospheric pressure on Venus may be a sustained high level of volcanic activity. The high methane content of Titan's atmosphere seems to be sustained by exhalation from icy vents connecting the surface to the interior ('cryovolcanoes').
5. Collisions of comets and asteroids with the planets. Obviously, a major impact can dramatically alter climate by disrupting part of the surface and modifying the atmosphere, for instance, filling it with long-lived clouds of fine debris.[81] More subtly, the ongoing flux of large numbers of much smaller, mostly undetectable rocky and icy bodies can affect the volatile inventory of a planet in the long term, although what this flux is, even for the Earth, is not well known.

These and other processes and phenomena can be incorporated into models to see how well they account for observations of the present climate and of the (still incomplete, even for Earth) record of climate change over time. They can also be used to examine the stability of the atmospheres of the planets, particularly their current states.

Climate modellers recognise that change is not a linear response to forcing, and that instabilities in a complex system with feedbacks can lead to large changes in climate as the result of relatively small changes in external factors. These are the 'tipping points' of present-day concern in the current epoch on Earth, where the best-known example is the risk of large-scale changes in the thermohaline circulation of the ocean. This is the density-driven flow that responds to temperature and salinity gradients to produce an equator-to-pole flow that plays a large part in the zonal redistribution of the energy from the Sun that reaches the Earth's surface. In models, factors such as the injection into polar waters of relatively fresh water from the partial melting of the icecaps can affect this flow, slowing or even reversing it. Evidence has been found for such behaviour at the end of the last ice age, when temperatures in the North Atlantic changed extremely rapidly. The possibility

[81] A similar effect can be produced by atomic weapons, the so-called 'nuclear winter' scenario popularised in the 1980s by Carl Sagan and his colleagues. See 'Nuclear winter: global consequences of multiple nuclear explosions', R.P. Turco, O.B. Toon, T.P. Ackerman, J.B. Pollack, and C. Sagan, *Science*, **222**, 1283–1292, 1983.

that something similar may occur again in the current epoch is being seriously considered, particularly if a general warming due to greenhouse gas increases provides a trigger.

Large, abrupt changes are very hard to predict, however, and difficult to distinguish from purely numerical instabilities in complex models, and indeed the smoothing inherent in gridded representations of the global ocean and atmosphere tends to suppress 'real' events in most cases. If the Earth's climate is at risk from rapid climate change originating in the ocean circulation we are not very likely to know about it until it happens. Methane trapped in sub-Arctic permafrost, where it could be rapidly released in a warmer climate, leading to rapid positive feedback through its 'greenhouse' contribution, could be another threat. Analogous behaviour on the other planets does not seem to be an issue so far as we can tell at present, although there may be analogous instabilities on Mars, Venus, or Titan that will be seen to be relevant when the planets are better explored.

9.3 Models of climate change on the Earth

Studies of climate and global change on the Earth include 'paleoclimatology' – the evolution of the atmosphere and conditions on the surface over the history of the planet – and forecasting of short-term global change in the next fifty to a hundred years. In view of the perceived threat to the habitability of the planet, the latter is the subject of particular attention at present, and improving the predictive models is a priority. Physics-based models should, in principle at least, achieve a seamless transition from the long to the shorter timescale through the current epoch.

Figure 9.2 summarises the probable evolution of the composition of the Earth's atmosphere, with many uncertainties. High concentrations of carbon dioxide in the first billion years kept the surface warm enough, when the Sun was fainter, to keep the oceans liquid. The earliest forms of life produced methane, feeding on hydrogen emitted copiously from the early volcanoes, which warmed the surface through its powerful greenhouse action and so increased the biological action producing more methane. This positive feedback continued until there

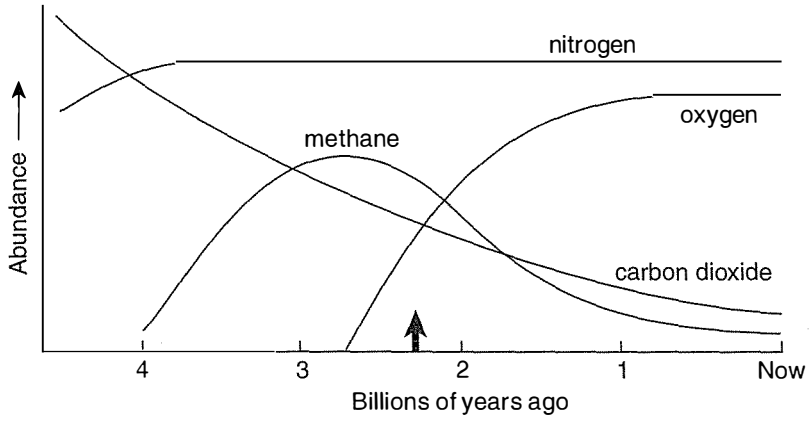

Fig. 9.2
The evolution of the atmospheric composition of the Earth. The absolute amounts of the gases are very uncertain, and the vertical scale is not linear; there may have been around 10 bars or more of carbon dioxide in the first phase. This was consumed first by methane-producing bacteria, and then by photosynthetic organisms that release oxygen deadly to the methanogens. It may be significant that the changeover apparently coincided with the first global ice age 2.3 billion years ago, marked by the arrow.

was so much of it that the Earth may have been covered by an orange smog of hydrocarbons and nitriles, produced by photochemistry from atmospheric nitrogen and methane, much as Titan is now. This would increase the albedo and cool the planet, reducing methane production, and possibly reaching equilibrium where methane and haze production found a balance. Nitrogen amounts increased initially due to outgassing and photolysis of ammonia, but probably levelled out at something close to the present 0.77 bars around about the time that it took over from carbon dioxide as the main constituent.

At some point, which may, according to geological evidence, have coincided with the first severe global ice age about 2.3 billion years ago, oxygen-producing lifeforms that consume carbon dioxide and inhibit methane production started to take over. Methanogens particularly like high temperatures, so the general cooling and freezing of the land masses may have hastened their demise, along with the increasing oxygen levels. Those that survive today do so in anaerobic environments like the guts of cows or decaying vegetation in swamps. Around 2 billion years later, some 500 million years before the present, further global ice ages accompanied a further rise in the oxygen level, and a corresponding fall in carbon dioxide and methane amounts, reaching something like their present levels a few million years ago, where they have remained.

Whether the oxygen-rich regime produced the freezing conditions or vice versa is a moot point: possibly the Earth's Milanković cycles initially triggered the transition. These periodic changes in the elliptical orbit that the Earth describes around the Sun each year are of three kinds, involving:

1. the eccentricity of the orbit,
2. the angle between the equatorial plane and the orbital plane, and
3. the precession of the spin axis around the normal to the orbital plane.

The cycles can be calculated, with some difficulty, since a complex many-body gravitational interaction problem involving all of the large bodies in the Solar System must be solved to obtain accurate results. The orbit-induced changes in the solar flux at the Earth are found to have periods of tens or hundreds of thousands of years, and amplitudes large enough to affect climate significantly, particularly when the three effects combine to reinforce each other. There is some experimental evidence, still incomplete, for a correlation between the Milanković effect and the more recent ice ages on the Earth, suggesting they were produced, or at least provoked, by this mechanism.

The orbital cycles are so slow, however, that forward projections indicate that the next era of significant climate change due to this cause is probably at least 50,000 years in the future. In the shorter term, the threat of climate change is associated with possible changes in the energy output from the Sun itself, and human industrial and agricultural ('anthropogenic') activities. The Sun's output has been measured accurately by satellite instruments orbiting above the atmosphere for the last thirty or forty years. The solar 'constant' is observed to vary by

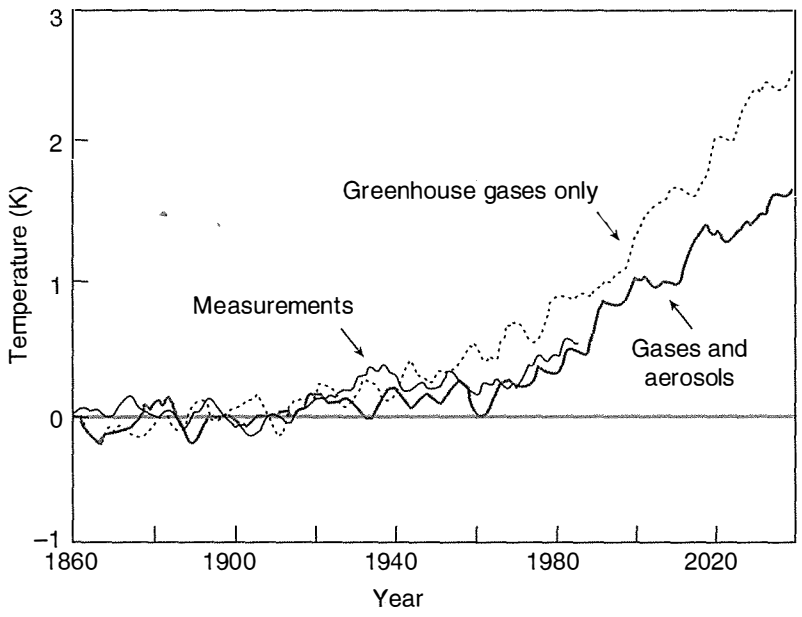

Fig. 9.3
The mean surface temperature of the Earth from 1860 to 2040, as predicted by the Intergovernmental Panel on Climate Change (2001) using an assemblage of sophisticated climate models, and by the present simple model (heavy lines). The inclusion of the effect of 'global dimming' by changes in the aerosol content of the atmosphere ameliorates the effect of increasing warming by greenhouse gases, and produces good agreement with the observed temperature history.

about 0.1%, mostly in response to changes in sunspot number as part of the 22-year cycle in the solar magnetic field. Less reliable evidence from before the space age is interpreted as showing that the solar output has remained constant to within this range for at least the last 1000 years, and probably much longer. In models, changes in solar output of one part in a thousand affect the surface temperature by less than 0.05 K. There remains some debate about whether these small changes might be amplified somehow within the climate system, possibly leading to an observable correlation between solar fluctuations and climate, but this is yet to be resolved.

The greenhouse gases, carbon dioxide, methane, nitrous oxide and a number of others, make up less than 1% of the atmosphere, but have been increasing relentlessly since the industrial revolution. At the same time as the greenhouse gas concentration is growing, industrial emissions are adding to the natural sulphur content of the atmosphere. The effect of this is to increase the concentration of aerosols, tiny, submicron-sized droplets or crystals of various substances, including sulphuric acid and sulphates. This in turn tends to increase cloud cover and thickness by providing additional condensation nuclei, a major factor in cloud droplet formation. Both clouds and aerosols have an effect on the albedo of the planet, that is, the fraction of the incoming solar radiative energy that is reflected back to space without being absorbed.

The difficulty in measuring the albedo of a planet makes monitoring of changes unfeasible, even for the Earth. Attempts have been made using measurements from satellites and of the 'Earthshine' on the dark face of the Moon, but since the reflectivity varies considerably at a single point in space and time it remains difficult to integrate over the whole globe and all solid angles. Still, it seems likely that some secular change is taking place, and if so this leads to 'global dimming' corresponding to about a 1 °C fall in surface temperature for every 1% of

increase in the global mean albedo. The comparisons between data and models shown in Fig. 9.3 appear to demonstrate that greenhouse gas and albedo increases are the dominant factors controlling the changing climate on the Earth, and that these two factors are working against each other.

The estimates in Fig. 9.3 were made by an international panel of experts, the Intergovernmental Panel on Climate Change (IPCC), by combining results from advanced climate models from the world's leading research groups, while the 'measured' curve is their summary of all the available data that is considered reliable. One model curve considers only the warming due to increased greenhouse gas concentrations; the other subtracts from this the estimated cooling effect due to changing cloud and aerosol amounts. The model estimates of global warming and global dimming predict that the former will dominate by an amount that matches the observed temperature trend very well. This increases confidence in the models and what they predict for the future, although of course this depends not only on the models but also on the expected emissions scenario that is adopted. The expectation at the present time, taking all uncertainties into account, is for a rise in mean global surface temperature of between 3 and perhaps as much as 9 degrees before the end of the present century.[82]

Theoretical results for comparison with the data in Fig. 9.3 can also be derived from the simple models discussed in Chapter 5. We saw there that it is possible to use some very basic physics to describe climate in terms of the global and seasonal mean temperature profile.[83] These can be extended to make approximate, but readily understood and informative, predictions about the past and future behaviour of the climate on each of the Earth-like planets. They also give some idea of how they can be expected to respond to perturbations of various kinds, such as changes in solar irradiance or variations in atmospheric composition due to industrial or volcanic emissions.

First it is necessary to be convinced that a 'back of the envelope' model is plausible enough to be useful. In Fig. 5.3 we showed how such a model temperature profile, representing the present-day climate of the Earth, compared to some typical measured temperature profiles. While the model predicts the global mean, and is not expected to be the same as that at any particular time or place, the overall consistency shown there is quite encouraging, suggesting that the model provides a simple tool to look at some aspects of the Earth's climate history. It is also possible to show that results very close to the IPCC synthesis of large, complex models can be obtained with little effort and with complete visibility of the physics used and assumptions made. Results identical to those in Fig. 9.3 are obtained with an increase of 2.5% per decade in the global CO_2 concentration, and 0.0001 (0.3% of its current value) per decade in the albedo, both quite reasonable assumptions in the light of current knowledge. However, this takes no account of how the most powerful greenhouse gas – water vapour – responds in a changing climate, or of the likely, important, but unpredictable effect of changing cloud cover.

[82] See D.A. Stainforth *et al.*, 'Uncertainty in predictions of the climate response to rising levels of greenhouse gases', *Nature*, **433**, 403–406, 2005, for a different prognosis.

[83] See also *Elementary Climate Physics*, chapters 7 and 11.

9.4 The climate of Venus

9.4.1 Early speculation about the climate on Venus

Before the space age, many astronomers expected that the surface environment on Venus would resemble a more tropical version of the Earth. The Swedish Nobel Laureate Svante Arrhenius wrote nearly a century ago that the surface temperature 'is calculated to be about 47 °C', compared to an average of around 26 °C in the Congo on Earth, and he inferred that the humidity on Venus is about six times higher than on Earth.[84] Patrick Moore, in his book *The Planet Venus*, published in 1954, echoed Arrhenius' speculation that Venus could be a world in a 'Cambrian' state, possibly complete with primitive organisms.

Beginning in 1956 at the US Naval Research Laboratory, Earth-based microwave observations of Venus showed that the planet had an equivalent blackbody temperature of about 575 K. The scientists planning the microwave radiometer to be carried on the first spacecraft mission to Venus, *Mariner 2*, took this to be the probable surface temperature of the planet and, weighing up all of the available observational and theoretical evidence, planned their experiment around atmospheric models in which the surface pressure ranged from 2 to 20 bars and the composition was 75% CO_2, 24% N_2, and 1% H_2O. The results from the experiment (§3.8.1) confirmed a high surface temperature, and the first direct measurements by the lander *Venera 4* in 1967 delivered an improved estimate of around 675 K. Modern values for the mean surface temperature on Venus are around 730 K, which is higher than the melting point of the metals lead and tin. Excursions of more than 100 K occur, since the lapse rate is around 10 K km^{-1} and the topography varies by more than 10 km.

[84] Arrhenius was trained as a physicist but received the Nobel Prize for Chemistry in 1903 for his work on the electrolytic theory of dissociation. He is best remembered today for his work recognising the key role of atmospheric carbon dioxide in the terrestrial greenhouse effect. He wrote about Venus in *The Destinies of the Stars*, Putman, New York, 1918.

9.4.2 Surface–atmosphere interactions

As long ago as 1952, by which time it was known that Venus' atmosphere was mainly carbon dioxide, but not how hot or dense the atmosphere is near the surface, Harold Urey[85] suggested that reactions would take place between CO_2 and the common minerals assumed to exist in large quantities on the surface. In particular, he suggested that the exchange

$$CaCO_3(\text{calcite}) + SiO_2(\text{silica}) \leftrightarrow CaSiO_3(\text{wollastonite}) + CO_2$$

might buffer the total amount of CO_2 in the atmosphere. This reaction occurs very efficiently in the presence of liquid water, leading Urey to deduce that the high abundance of carbon dioxide observed spectroscopically in the atmosphere (above the clouds; observations below the clouds were not possible at that time) probably ruled out large amounts of liquid water.[86] A decade later, when microwave measurements had revealed the high surface temperature that definitely precluded the possibility of water oceans on Venus, geochemists noted

[85] Harold Urey (1893–1981) won the Nobel Prize in 1934 for his work on isotopes, especially for deuterium and heavy water. This led him to consider the relative abundances of elements and their isotopes on Earth, and in the Solar System and beyond.

[86] Urey wrote in *The Planets*, Yale University Press, 1952, that 'the presence of carbon dioxide in the planet's atmosphere is very hard to understand unless water were originally present, and it would be impossible to understand if water were present now'.

that the same reaction could proceed efficiently without liquid water, but that a CO_2 partial pressure of 50 bars or more would be required to approach equilibrium, a value that was then still considered unrealistically high. Another decade later, when pressures of nearly 100 bars had been measured on the surface of Venus by landed probes, the possibility that Urey's mechanism might be relevant received renewed attention. In fact, modern data for the thermodynamics of the reaction shows that, within the uncertainty of the measurements, equilibrium is reached at values very close to the mean temperature and pressure found on the surface of Venus.

This may be a coincidence, however. It is unclear how a sufficiently intimate contact between atmosphere and lithosphere is achieved without a much better knowledge of the actual mineralogical composition and physical state of the exposed material on the surface of Venus, and of weathering and possible subduction and effusion rates. Furthermore, although the surface temperature and pressure are indeed at an equilibrium point with the calcite–wollastonite mineral reaction, it is actually an unstable equilibrium, suggesting that unknown mechanisms may be providing the stability, requiring a more complex model of surface–atmosphere interactions that are linked to the history of volcanism and the nature of the interior.

Whether or not the surface of Venus is in equilibrium with the atmosphere, the interaction does provide a plausible explanation for the apparent superabundance of CO_2 on Venus relative to Earth. As a result of long-term carbonate rock formation from dissolved carbon dioxide in the oceans, today, chalk-based formations like coral atolls and the white cliffs of Dover on the Earth collectively hold the equivalent of roughly 100 bars of CO_2. Thus, the water-depleted state of Venus may be responsible for so much of the gas remaining in the atmosphere. Any carbonate that formed in the early wet phase on Venus, if indeed there was one, could have been recycled into atmospheric CO_2 by thermal processes during subduction of the crust.

Carbon dioxide is not the only important atmospheric species that is likely to have important reactions with the surface. Heterogeneous reactions between sulphur dioxide and common minerals proceed rapidly, relative to geologic timescales, in chemical kinetics experiments performed under Venus-like conditions in the laboratory. These show that the deep atmosphere abundance of SO_2 is more than two orders of magnitude higher than can be accounted for by equilibrium with surface minerals. Thus, there must be active sources of reactive sulphur compounds, presumably volcanoes. Any changes in the abundance of atmospheric SO_2 will have an impact on the climate of Venus, the scale of which can be estimated using evolutionary models (§9.4.6).

However, some important factors are difficult to estimate, for instance, the ability of the gas to reach new reaction sites on buried grains once the easily available surface has reacted. Diffusion into porous soil is the only static possibility; otherwise, some erosion or overturning process, likely to be slow, must be invoked. Of course, the whole scenario depends on what minerals are actually present, and in

what amounts. SO_2 at the surface is more than two orders more abundant than required for equilibrium with calcite, but it is close to equilibrium with pyrite and magnetite, minerals which would be much less common if Venus is like Earth.

9.4.3 Recent missions to Venus

Much of our current knowledge of the details of the Venus atmosphere and climate system was accrued by the *Pioneer Venus* orbiter and entry probe missions of the late 1970s and early 1980s. Four probes sounded the clouds and lower atmosphere, returning chemical, physical, and meteorological data on the Venus atmosphere. The orbiter observed the surface of Venus with a radar altimeter and sounded the atmosphere in the infrared and ultraviolet regions of the spectrum. It also provided *in situ* data on the upper atmosphere, ionosphere and solar wind interaction.

The Soviet *Venera* and *VEGA* missions of the early 1980s were followed by the NASA *Magellan* surface mapping mission, which arrived at Venus in August 1990, but there was a gap of two decades before another mission with an atmospheric focus was launched. This was rectified in May 2006 when the *Venus Express* mission of the European Space Agency became the twenty-eighth spacecraft to arrive successfully at Venus since *Mariner 2* in 1962. Its goals were to carry out systematic climate-related remote sensing observations of the Venusian atmosphere below the clouds,

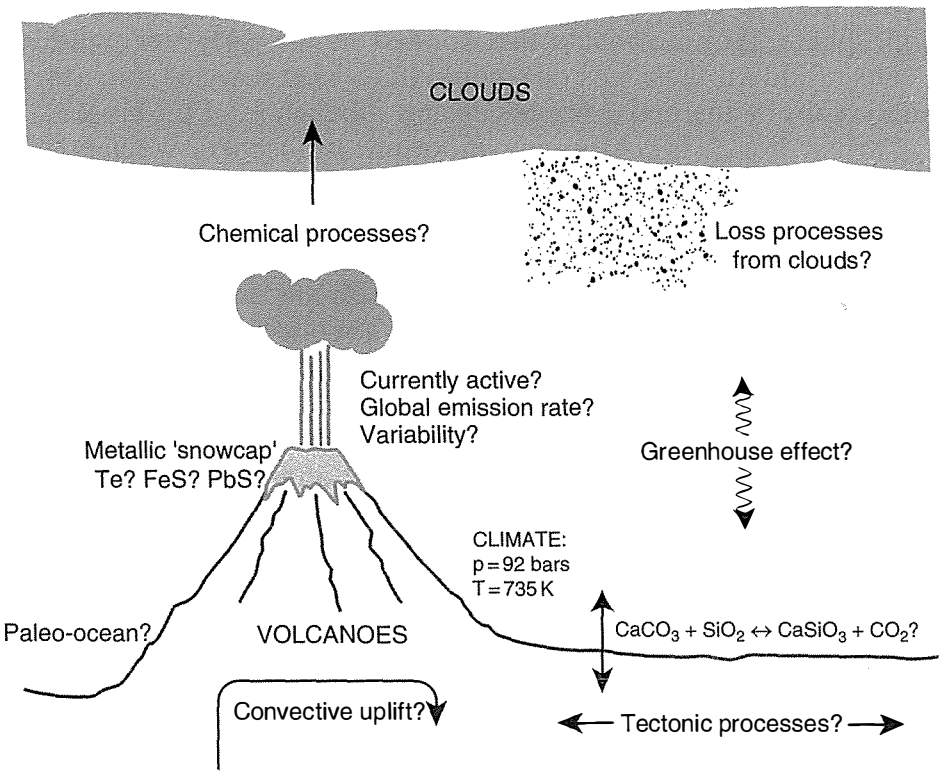

Fig. 9.4
Climate-related processes on Venus investigated from orbit by the *Venus Express* mission. From Taylor (2007).

- producing improved greenhouse models of the energy balance in the lower atmosphere,
- validating and improving general circulation models of the atmosphere, with improved treatment of the zonal superrotation, the meridional Hadley circulation, and the polar vortices,
- generating new climate evolution models, using simple physics and chemistry constrained by measurements, and
- making comparative studies in all three areas with the other terrestrial planets, including Earth.

Close behind *Venus Express* is a Japanese mission called *Venus Climate Orbiter*, the goals of which are summarised in Fig. 9.5. By mapping the thermal structure, cloud properties, and dynamics of the equatorial and midlatitude atmosphere from orbit over an extended period, it aims to clarify the cause of the zonal superrotation (§8.3.2), allowing improvements in time-dependent models of the climate system and more detailed comparisons with the Earth.

There is undoubtedly further evidence in the geological record that will support or eliminate the postulate that Venus once had liquid water on its surface. Finding this is made more difficult by current indications that most of Venus has been resurfaced relatively recently by the flux of lava from the interior. If so, drilling and the return of deep core samples to Earth is called for, a very difficult operation on Venus, where the high temperature prevents the operation of any kind of electronic equipment for more than an hour or so. New generations of high-temperature semiconductors will no doubt resolve this problem in time, and then it will also be possible to explore the surface using rovers, like those currently being developed and deployed on Mars. One of the tasks they will have is to characterise the surface mineralogy, in particular the budgets of carbonates and silicates that may play a key role in stabilising the climate.

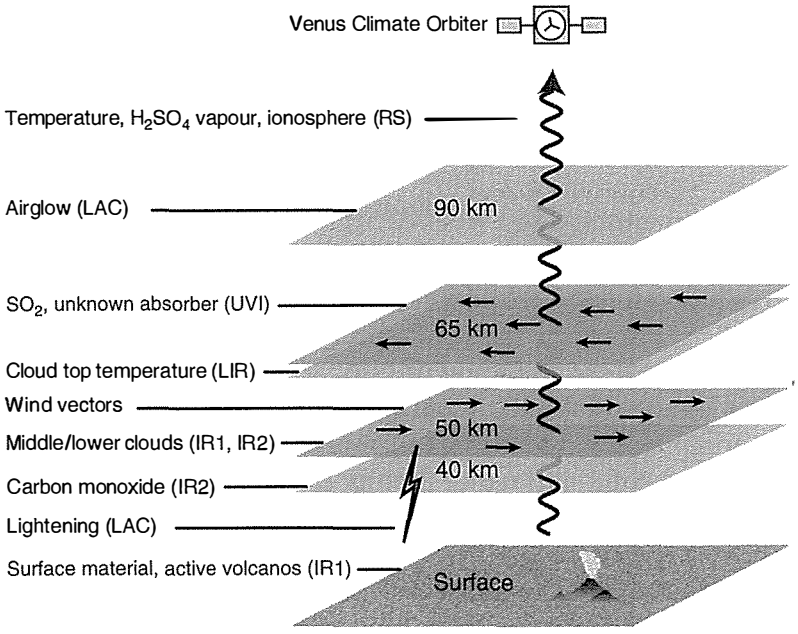

Fig. 9.5
A summary of the goals of the Japanese *Venus Climate Orbiter*, due to reach the planet in December 2010. The abbreviations refer to the instruments in the payload: the Lightning and Airglow Camera (LAC), the Ultraviolet Imager (UVI), the 10 μm Long-wave Infrared Camera (LIR), the 2 μm Camera (IR2), and the 1 μm Camera (IR1). RS refers to the Radio Science (occultation) technique, which uses the communication beam to probe the atmosphere. From Nakamura *et al.* (2007).

9.4.4 Venus climate models: GCMs

Since Venus and Mars are Earth-like in many ways, it is relatively easy to adapt terrestrial general circulation models to these different environments. The ultimate goal is the development of fully three-dimensional, time-dependent models in which all of the relevant sources and sinks, and all radiative, dynamical, and chemical processes, are included with high precision and resolution. This is a goal that is being pursued for terrestrial climate models, which of course are much better tested and constrained by data. Modified, and where necessary simplified, versions of these steadily improving terrestrial GCMs are then available to model the dynamical component of the current climate of Venus.

Generally, considerable additional work is required before a terrestrial GCM with modified input parameters can be made to produce output that even approximately reproduces the observed behaviour on another planet. Stretching the model in this way not only gives insights into what is actually happening on Venus and Mars, but also helps to understand common processes with the Earth. Terrestrial GCMs are 'tuned' to reproduce the observed behaviour of the atmosphere before they are used to make climate forecasts; if they do not adapt without further tuning to the warmer and colder environments of the sister planets, then this suggests that the programming or the physics in the model is inadequate. This is not surprising, of course; the real climate system is too complicated to be programmed reliably on a computer from first principles alone.

There are also problems of understanding, as well as implementation. For Venus, these include the difficulty of accurately computing radiative transfer in a very dense, pure carbon-dioxide atmosphere where poorly understood pressure-induced transitions have a large effect on spectral line formation. There is also limited information on the height distribution of the absorption of solar energy in the clouds. Current models find that the model wind field is a strong function of the heating profile, so this introduces large uncertainties. The clouds themselves clearly have very variable properties, in density, microphysics, and composition, but information on what these are is still quite limited.

Experiments with current models do show that global superrotation tends to develop, consistent with observations. This is a property of optically thick atmospheres on slowly rotating planets, which is also seen on Titan. However, the wind speeds predicted by the models are generally too slow, by a factor of two or more. The features seen in ultraviolet images of Venus rotate around the planet in 4 to 5 days, corresponding to wind velocities of more than $100\,\mathrm{m\,s^{-1}}$ at the cloud tops, while the solid surface of Venus rotates 50 times more slowly, once every 243 days. The models struggle to reproduce such a high level of atmospheric superrotation with realistic inputs and constraints. Cloud variability and wave modes in the atmosphere seen in UV and IR mapping may indicate a role for the surface topography in maintaining or opposing the superrotation, and a role for waves or

eddies in the transport of angular momentum. Both of these are difficult to incorporate realistically in the models.

Eventually, helped by the massive effort being applied to model the changing climate of the Earth, Venus GCMs will incorporate the relationships between dynamics, volcanism, exospheric escape, surface–atmosphere reactions, composition, clouds and radiative balance. Currently, however, while the fledgling GCMs that have been developed for Venus show some features of the real atmosphere, they reproduce little of the detail, and they are not at the stage where they can be used reliably to examine possible variations in climate over time. Although it is important to attempt it, this is a risky practice for the Earth as well.

9.4.5 Venus climate models: Evolutionary models

The complexity and computational requirements of a climate model are greatly reduced if the model is restricted to one spatial dimension (altitude) rather than three. Parameterisations of the global-scale processes that control the origins and evolution of Venus' atmosphere and the complex set of time-dependent feedbacks that control the planetary climate can still be represented. On the other hand, the effect on the climate of the general circulation, and all atmospheric dynamics except for vertical convection, has to be neglected. So also has the problem of accounting for the observed large-scale global variations in cloud structure and optical thickness. The importance of clouds for regulating climate is well known and their role on Venus needs to be analysed statistically, and the overall affect on radiative balance quantified,

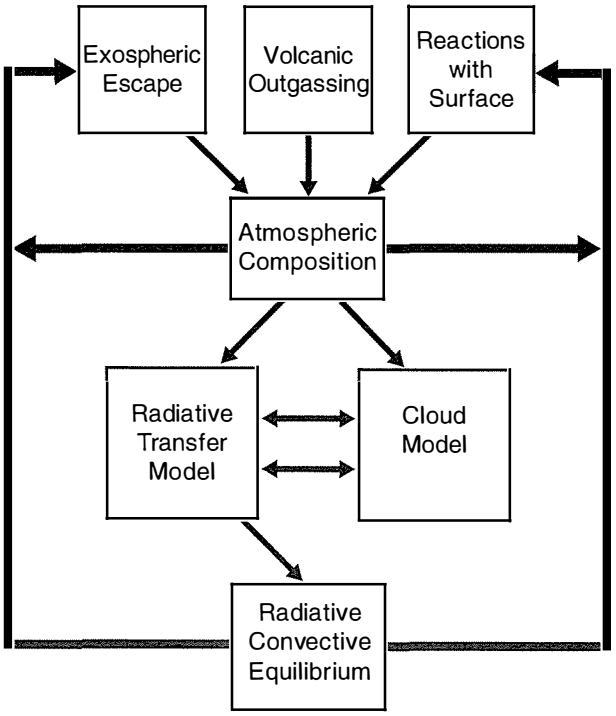

Fig. 9.6
A block diagram of a Venus climate evolution model. At each time step, the atmospheric composition is adjusted for the effects of volcanic exospheric loss, volcanic outgassing, and by reactions with the surface, then the coupled cloud and radiative–convective models are allowed to reach equilibrium.

which is only possible with a three-dimensional, time-dependent model, i.e., a GCM. With those caveats in mind, evolutionary models can be used to begin to understand long-term, large-scale climate change.

The most comprehensive evolutionary model for Venus to date is that of Bullock and Grinspoon,[87] depicted in Fig. 9.6. In this, the climate system is represented by five planetary-scale processes that can be represented by linked mathematical models and sequentially executed. These are:

1. A non-grey radiative transfer code in a one-dimensional, two-stream model to calculate the transport and balance of energy within the atmosphere, and obtains thermal infrared fluxes, heating rates, and radiative–convective equilibrium temperature profiles as a function of atmospheric composition;
2. A cloud chemical and microphysical model to calculate the distribution and transport of H_2SO_4/H_2O aerosols in the atmosphere;
3. A model of volcanic activity to calculate the crustal outgassing;
4. Equilibrium and kinetic models to calculate the reactions of atmospheric gases with surface minerals;
5. An exospheric diffusion model to calculate the loss of atmospheric water due to the escape of hydrogen from the top of the atmosphere.

The model cycles through these calculations until an equilibrium state is found.

The code must be flexible and fast enough to recalculate the fluxes of radiation at all wavelengths many times, since the goal is to follow the evolution of the climate over long time periods, while factors such as volcanic activity and the incoming solar flux are changing. The amount of computation to achieve this requires making some simplifying assumptions and parameterisations, in particular limiting the spectral and vertical resolution and using simple spectral and hemispherical integration schemes. Other approximations include:

1. Radiative–convection equilibrium is assumed, i.e., the lapse rate in the radiative equilibrium temperature profile is reduced to the adiabatic value wherever it tended to be larger.
2. The gaseous absorption coefficients are calculated for just nine of the molecular species found in Venus' atmosphere: CO_2, H_2O, SO_2, CO, OCS, HDO, H_2S, HCl, and HF.
3. The energy deposited in the atmosphere is assumed to be the observed solar net flux profile measured by the radiometer on the *Pioneer Venus* entry probes, although this sample may not be representative of the whole planet.
4. The absorption of UV radiation at wavelengths shorter than 0.4 μm, which occurs mostly above 70 km, is neglected since the *Pioneer Venus* measurements do not extend to such short wavelengths.

[87] M.A. Bullock and D.H. Grinspoon, 'The recent evolution of climate on Venus', *Icarus*, **150**, 19–37, 2001.

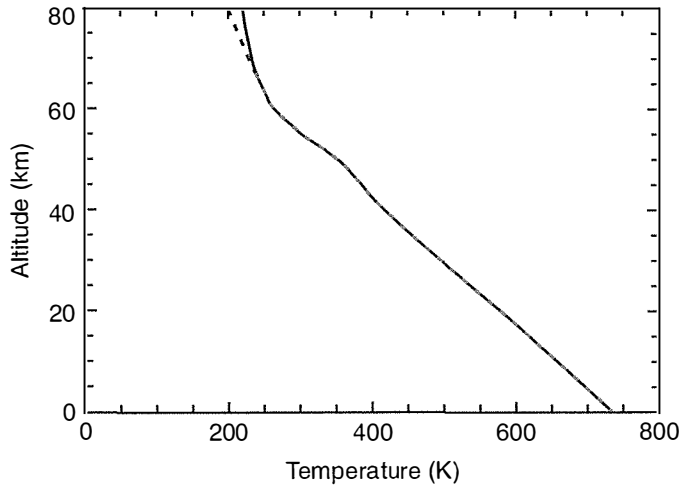

Fig. 9.7
The mean atmospheric temperature profile on Venus calculated with the radiative transfer model of Bullock and Grinspoon (solid line) compared to the mean measured profile from the Venus International Reference Atmosphere (dashed line).

5. Simple models are used to represent the thermochemistry and microphysics of the Venusian clouds, noting that these processes are poorly understood in any case.
6. The kinetics of reactions of atmospheric gases with surface minerals are poorly known, making it difficult to include them; future laboratory experiments to determine these rate constants would allow potentially important improvements to the model.

When the model is run with the inputs (solar constant, volcanic activity, etc.) set to present values, it should of course reproduce the currently observed climate, in particular the measured mean temperature profile. In fact, in order to achieve this, arbitrary changes to the opacity in and above the clouds are found to be necessary, reflecting the incomplete state of current knowledge about atmospheric composition and cloud layering and microstructure. With all of these simplifications and assumptions, the radiative equilibrium profile of temperature as a function of altitude calculated by the model matches reasonably well (Fig. 9.7) the Venus International Reference Atmosphere, a conglomeration of measured temperature profiles.[88]

This sort of validation, although essential, does not of course provide complete confidence in the suitability of the model to represent the time history of Venus' atmosphere, particularly in view of the simplifications that were made and the 'tuning' that was necessary to represent the current, known state. This is a problem for all predictive, and to a lesser extent retrospective, climate models. When extrapolating back into the past, there is at least geological and other paleontological evidence (such as the volcanic record in the crust, and the deuterium-to-hydrogen ratio in the atmosphere) to validate the model 'hindcasts'. When predicting the future, there is no such reassurance. This is one of the arguments why comparative climatology is so valuable, since it allows climate simulations to be carried out for the situations on Venus and Mars that are hotter and cooler, respectively, than the Earth, but still have the major processes in common and are constrained by observations.

[88] International organisations such as COSPAR, the Committee for Space Research, and the space agencies, especially NASA, organise groups to prepare so-called 'reference models' for planetary atmospheres, which are useful for planning missions, as well as for comparisons like these.

9.4.6 Evolutionary model simulations for Venus

Bullock and Grinspoon (1996, 2001) used their model to study the evolution of Venus' atmosphere over the last approximately one billion years. If, as many planetary geologists believe, Venus was resurfaced about 650 million years ago in a massive volcanic event that has since relaxed to a smaller but still significant level of activity, there will have been a surge in the amount of carbon dioxide, sulphur dioxide, and water vapour in the atmosphere at that time. This was modelled as a sudden pulse of outgassing to the atmosphere, in amounts corresponding to a global layer of lava 1 km thick erupting onto the surface, declining exponentially with a time constant of 100 million years. The sulphur dioxide is lost rapidly to the formation of thick sulphuric acid clouds and temperature-dependent reactions with the surface, while atmospheric water is lost more slowly due to its dissociation by solar UV and then exospheric escape. The cloud formation initially cooled the surface by about 100 K due to the increased albedo (Fig. 9.8), but after about 200 million years the water and sulphur dioxide levels fell to the point where the clouds thinned, lowering the albedo, and the residual greenhouse gases raised the surface temperature to around 850 K.

The model results also imply that active volcanism must have continued until recent times, since there must have been large-scale outgassing within the past few million years to replace the sulphur dioxide and water vapour that are being continuously lost. These gases produce the substantial cloud layers found today and give Venus the surface temperature we now observe, which is about 100 K below the maximum reached 550 million years ago in the model (Fig. 9.8).

Interesting as they are, there are many reasons to be cautious about these simulations. In addition to the simplifications mentioned above, there is the common problem for models that the key input data may

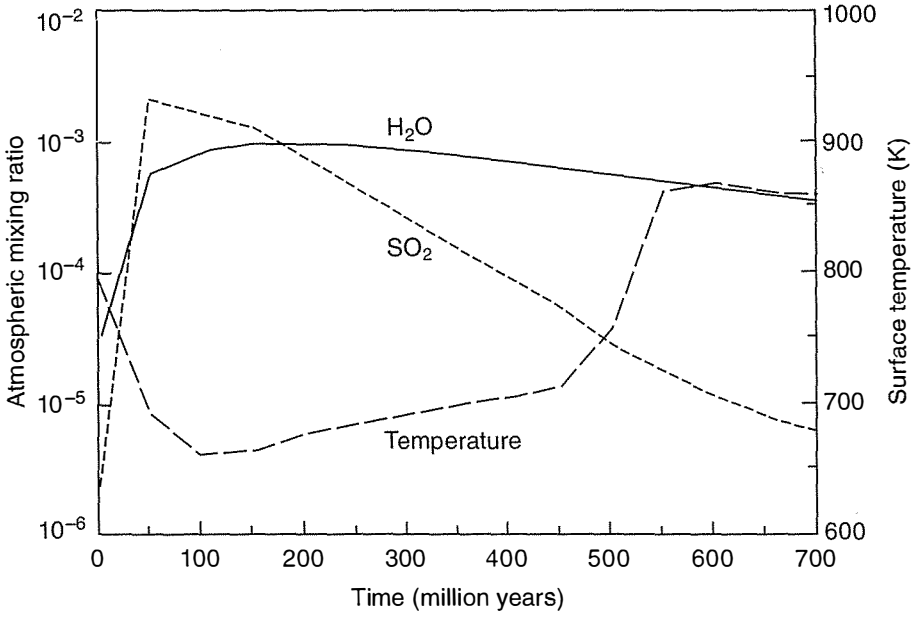

Fig. 9.8
Atmospheric composition and temperature at the surface of Venus in a model experiment (Bullock, 1997) covering the last 700 million years in the evolution of Venus' atmosphere. The premise, based on geological evidence, is that this period started with a very vigorous episode of volcanic activity, which then declined sharply. The steep increase in temperature about 500 years ago, from about the present-day value to something about 100 K hotter, is mainly due to the drop in albedo which accompanied the loss of the sulphuric acid clouds following the decline in sulphur dioxide in the atmosphere. Since that has not actually happened (yet), the implication is that active volcanism is in fact ongoing.

be very uncertain. For instance, very little is known about the composition of the surface material on Venus, and almost nothing is certain about the current level of volcanic activity. Once this and a great deal of other essential basic data about Venus have been gathered by current and planned missions to the planet, much more sophisticated climate models will become possible. With these it will be possible to address the existence of equilibrium states much more realistically, and the conditions and the timescales required to allow transitions between them to occur.

9.4.7 Venus climate models: Simple approaches

Simple models (§5.1) with a stratosphere in radiative equilibrium with the Sun, overlying a deep atmosphere in which the profile follows a dry adiabat, are not time-dependent, so cannot trace the evolution of climate, although they can usefully clarify the basic processes maintaining a particular climatic state. Top of the list might be to investigate the stability of the current climate (as described by its surface temperature and pressure) with respect to the problem posed by Urey more than half a century ago, the equilibration of carbon dioxide with surface minerals.

As in the evolutionary model, we calculate the surface temperature and the surface pressure in a model Venus atmosphere assuming (a) a radiative–convective equilibrium temperature profile, and (b) chemical equilibrium between the atmosphere and the surface.

We assume that the dominant reaction for CO_2 in equilibrium with carbonates on the surface is

$$CaCO_3 + SiO_2 \leftrightarrow CaSiO_3 + CO_2$$

for which thermodynamic data measured in the laboratory suggests a relationship for the temperature dependence of the pressure of CO_2 in the form

$$\log p = \Delta H/RT + \Delta S/R + A + BT + CT^{-2}$$

where ΔH and ΔS are change in enthalpy and entropy, respectively, and A, B and C are constants, all of which are determined from laboratory data. Figure 9.9 shows a plot of this function over the range from 0 to 800 K, along with the result from the radiative–convective equilibrium model for the surface pressure as a function of surface temperature. Since we expect both of these conditions to be satisfied, the model solution is the point where the two curves cross. Figure 9.9 shows that equilibrium is reached at $T = 735$ K and $p = 95$ bars, very close to the mean conditions that are now known to exist on Venus.

Since the equilibrium is unstable, it must be maintained dynamically. It is tempting to conclude that the climate on Venus is held at this hot equilibrium state by vigorous volcanism, in which a copious supply

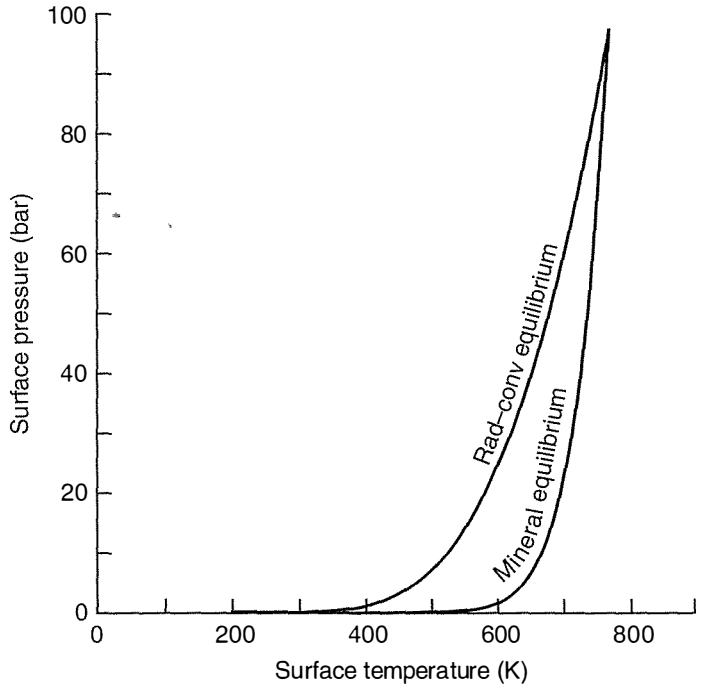

Fig. 9.9
Phase curves for the surface temperature and pressure on Venus, corresponding to radiative–convective equilibrium in the atmosphere (calculated using the simple model described above), and to chemical equilibrium between CO_2 in the atmosphere and in surface minerals (calculated using data from Adamcik and Draper, 1963).

of carbon dioxide is prevented from raising the surface pressure above 95 bars by the capacity of the surface to absorb the excess. If this were so, in the long term, when volcanism subsides, Venus would tend to be held in its present state by releasing carbon dioxide at a rate that maintained the surface pressure.

Some of the experiments with the evolutionary model, with time-dependent volcanism and cloud formation and dissipation, suggested that the unstable nature of the CO_2–$CaCO_3$ equilibrium would produce oscillations before Venus relaxes to lower temperature and pressures. In Fig. 9.10, we explore some of these possible cooler states for Venus, comparing three imaginary scenarios to the current state. The present climate is represented by the solid line, which we saw in Chapter 5 is a reasonable fit to a measured temperature profile for the middle atmosphere of Venus from the *Magellan* radio occultation experiment. This model is calculated by assuming radiative equilibrium in the stratosphere, a dry adiabatic gradient in the troposphere, and allowing for the temperature dependence of the scale height and (through the specific heat) the lapse rate (hence the curvature in the profiles).

A plausible scenario for the future of Venus is if the volcanic activity ceases and the surface pressure and the cloud cover change as a result. It is not difficult to imagine a future Venus in which most of the sulphur is lost from the atmosphere by reactions with surface minerals, after the volcanic source is removed. Then the highly reflective sulphuric acid clouds might be replaced by very sparse water clouds, as on Earth or perhaps more like Mars, when the albedo of the planet as a whole would fall, say from 0.8 to 0.2.[89] If nothing else changes, this will heat the planet by reflecting less sunlight, and the surface temperature rises.

[89] These numbers are fairly arbitrary, chosen to make the calculations easy and to emphasise their approximate nature. They are probably somewhat too high (the best value for the current albedo of Venus is 0.76) and too low, respectively. 0.2 is close to the albedo of present-day Mars, which has almost no clouds and relatively little atmosphere to scatter solar radiation. Raleigh scattering would be important on Venus even if there were no cloud. On the other hand, Mars has airborne dust, polar caps and icy haze layers, which tend to increase its reflectivity.

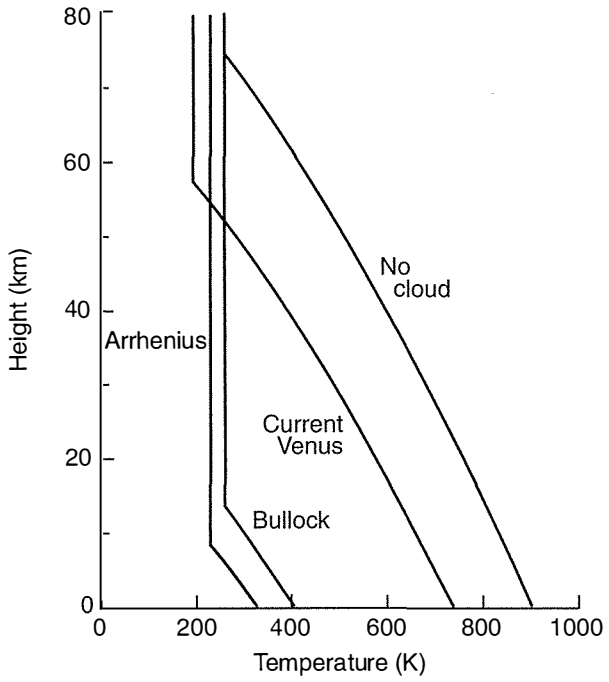

Fig. 9.10
Some examples of (imaginary) future climate scenarios for Venus that are compatible with radiative–dynamical equilibrium, with the current temperature profile ('Current Venus') for comparison. The other profiles are a cloud-free scenario in which the albedo drops to 0.2, but the surface pressure remains at its present value; a low-CO_2 future where the pressure is 43 bars and the temperature 400 K ('Bullock'); and an Earth-like scenario with surface pressure of 1 bar ('Arrhenius').

The amount of the increase can be estimated as before (§ 5.1). If the starting value of the stratospheric temperature T_{strat} is 201 K (Table 5.1) and the albedo changes from 0.2 to 0.8, the new temperature T'_{strat} is given by

$$\left(\frac{T'_{strat}}{T_{strat}}\right)^4 = \frac{(1-0.2)}{(1-0.8)} = 4$$

and $T'_{strat} = 193 \times \sqrt{2} = 273$ K, an increase of 80 K. If nothing else changes, this rise also applies at the surface, giving the curve labelled 'no cloud' in Fig. 9.10.

The other two models reprise the work of Bullock (1997), whose evolutionary model found a stable state with a surface pressure and temperature of 43 bars and 400 K, and Arrhenius (1915), who assumed (from the primitive measurements available at the time) that Venus had an albedo of 0.52 and an otherwise Earth-like atmosphere with a surface pressure of 1 bar. For the 'Bullock' model, the cloud-free albedo of 0.2 is assumed and the tropopause temperature and pressure left as free parameters; they work out to be 260 K and 7 bars, respectively, at a height of 13 km above the surface.

In the 'Arrhenius' model, the tropopause is at 0.43 bars, 230 K, and 8 km, if the surface temperature is fixed at his original estimate of 320 K. If, instead, the tropopause is taken to be at an Earth-like 11 km and 300 mb, the surface temperature is rather higher, at about 350 K. Finally, we note that it is difficult today to see how Venus' surface pressure could ever fall as low as 1 bar, since it contains 3.5 bars of nitrogen, which is difficult to remove by most of the known processes. In this 'modified Arrhenius' scenario, the surface temperature would be over 400 K.

9.5 Climate change on Mars

Of all the planets, including Earth, the clearest indications for large-scale climate change in the past are found on present-day Mars. The most dramatic and large-scale evidence etched in the surface, first identified by *Viking* more than 30 years ago, corresponds to climate change around 4 billion years ago, while the recent discoveries of weeping gullies and variability in the polar ice caps show evidence for change that is very recent, and possibly even current.

The *Mars Exploration Rovers* that landed on the surface in January 2004 found evidence, including aqueous minerals and sedimentary layered deposits, dispelling any remaining doubts that Mars had a warm, wet climate at some time in the past, with liquid water on the surface. Precisely how warm and how wet it was, when these conditions prevailed, and when Mars' atmosphere became too thin to support liquid water, remain subjects of intense debate. In some locations, the water seems to have ebbed and flowed many times in repetitive episodes of flooding, suggesting a complicated climate history.

The present-day atmosphere of Mars is around 10,000 times thinner than that of Venus, with a mean surface pressure of about 6.5 mb, but like Venus is composed mainly of CO_2. The principal candidate as the mechanism responsible for a warmer climate on early Mars is an enhanced greenhouse effect, due to a thicker atmosphere that was produced by exhalation of gases from the interior via the volcanoes still seen, now apparently inactive, on the surface. This early atmosphere appears to have been lost by a combination of processes after the most active phase of volcanism ceased. While it is not too difficult to conceive that, with the scale of volcanism that apparently prevailed on early Mars, the atmosphere was once at least as dense as modern Earth's, it is harder to explain how Mars evolved to reach the state we see today.

Another important unsolved puzzle is whether the present Martian climate is stable, or simply a stage in a gradual (or cyclic) decline in surface pressure and temperature that has been going on since volcanic input declined below the replacement level.

9.5.1 Evidence for climate change

The evidence for climate change on Mars rests principally on the following:

1. Photographs from orbit showing ancient oceans, lakes, and rivers;
2. Other geological records, including aeolian deposits and surface modification;
3. The presence of extensive deposits of aqueous minerals on and just below the surface;
4. The variability of the polar icecaps;
5. The presence of layers in exposed cliff faces etc. on thickness scales from metres to kilometres in different types of terrain, all over the planet;

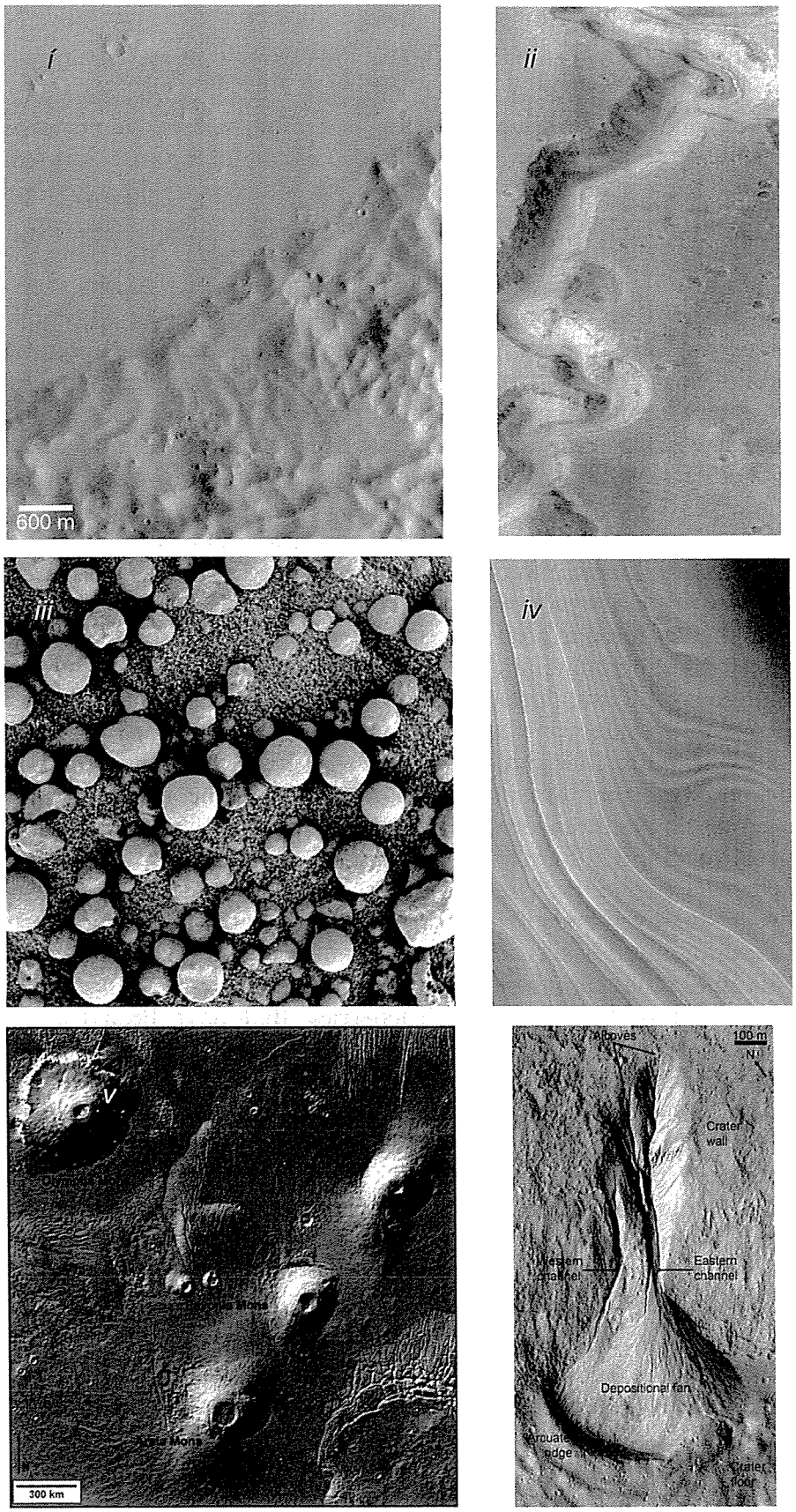

Fig. 9.11
Evidence for climate change on Mars: (i) a section of possible ancient coastline; (ii) a dry riverbed; (iii) 'blueberries', made of the water-deposited mineral haematite; (iv) layered terrain; (v) extinct volcanoes; (vi) a 'weeping' gully.

6. Analyses of the atmospheric composition and isotopic ratios that suggest long-term changes in surface pressure;
7. Extinct volcanoes and signs of recent geothermal activity.

These are illustrated in Fig. 9.11 and discussed in the following sections.

9.5.2 Liquid water on early Mars

Since the *Viking* missions of the mid 1970s, pictures of Mars taken from orbit have revealed giant outflow channels and valley networks, and low-lying regions that look like they may have been lakes and seas. The large, meandering channels that resemble dry river beds, some of them as wide as several tens of kilometres and hundreds to thousands of kilometres in length, are believed to be very ancient, perhaps 3 or 4 billion years old. Many of them feature streamlined islands and terraced walls that suggest scouring by massive amounts of water flowing in enormous floods; others seem to be produced by gradual erosion by drainage and seepage, possibly following rainfall. Features resembling shorelines in the northern hemisphere have been interpreted (controversially) as the boundary of a vast ancient ocean covering the north polar region. In support of this, imaging and altimeter results from *Mars Global Surveyor* showed that the vast northern plains form a bowl nearly four kilometres deep with several large channels disgorging into it from the surrounding highlands. The near-absence of cratering supports the idea that it was once filled with water, protecting the surface and filling with sediment any impact features that did occur.

Any long-lived body of water, for instance, in the northern plains or in the craters and basins with valleys running into them, leaves deposits of sediment that form a record of the climate in that vicinity, like the sulphates and the haematite 'blueberries' that have been found in abundance by the *Mars Exploration Rovers* in the layered terrain that they have sampled. Carbonates have also been found, but sulphates are more common at the sites explored so far. Both form in liquid water but not together, as they are chemically incompatible. The water probably contained dissolved acids from volcanic sulphur dioxide that eliminated, or prevented the formation of, carbonates in favour of sulphates.

While this explains the absence of carbonates where sulphates are found, it makes it harder to understand where the carbon dioxide in the early atmosphere went. It is still possible that carbonates, or some other sink for carbon dioxide, are still undiscovered in large quantities below the surface. If they are not, it lends support to the idea that climate change occurred catastrophically when the early atmosphere was mostly blown away during the bombardment of Mars by one or more large meteorites, asteroids, or comets, since it is difficult to identify any other process that would remove large amounts of carbon dioxide without leaving vast deposits of chalky minerals.

9.5.3 Atmospheric composition, volatiles, and isotopic ratios

Some of the gases in the Martian atmosphere show relative depletion of their lighter isotopes, suggesting that escape processes other than bombardment also contributed to the removal of the thick, early atmosphere responsible for the conditions that formed the water-related features on the surface. Thermal escape or solar wind erosion, for instance, would be expected to result in this sort of fractionation, while the effect would be much smaller if the atmosphere had been simply blasted away.

Measurements of the abundance of the two nitrogen isotopes ^{14}N and ^{15}N find that the heavier isotope, ^{15}N, is enriched by nearly a factor of two relative to ^{14}N when compared with the terrestrial case. It is unlikely that the $^{15}N/^{14}N$ ratio differed from that of the Earth at the time the planets formed, and the enrichment on Mars is probably the result of the more rapid loss of the lighter isotope. A much larger amount of nitrogen must have been present originally to produce the observed enrichment in this way.

The ratio D/H of the heavy to light isotopes of hydrogen, measured spectroscopically in the Martian atmosphere and directly in water contained in Martian meteorites, is found to be five times that of the Earth. A similar, but much larger, enrichment on Venus has been interpreted as fractionation during the removal of water, and Mars probably lost water too, consistent with the decline in the amount of nitrogen.

The krypton and xenon isotopes on Mars are close to the solar values, however, and some of the gas trapped in Martian meteorites has isotopic ratios in nitrogen, oxygen, and carbon that are similar to Earth's and not to Mars' present atmosphere. It is hard to reconcile these findings without assuming that there are at least two reservoirs of these gases on Mars, only one of which was fractionated during the loss of the early atmosphere. The other may have been released from the interior at a later time.

At present, there are too few measurements, and too little knowledge of where on the planet the samples came from, to make full use of the information that these kinds of data obviously contain. However, the analysis of future returned surface materials containing a wider variety and abundance of volatile species (including compounds of elements such as sulphur and chlorine, as well as carbon, oxygen, and noble gases) clearly offers great potential for deciphering the long-term climate history of Mars.

9.5.4 The polar caps

The north residual polar cap, that is, the part that remains at the end of the summer after the seasonal cover of CO_2 frost has evaporated, is made primarily of water ice. This is known mainly from mapping its temperature from orbit. The amount of material that it actually contains is also quite well known now, from measurements of its height profile by the laser altimeter on the *Global Surveyor* orbiter. The cap, which is about 1200 km across, has a maximum depth of 3 km and an average thickness of approximately 1 km, corresponding to a total volume of about a million cubic kilometres.

This is a lot of ice, but less than half that of the Greenland icecap on Earth, and only about 4% of the Antarctic ice sheet. It represents about one tenth of the volume required to fill the ancient Martian ocean basins (if that is indeed what they are), even if the whole cap were melted. The south residual polar cap is colder than the north and most of it, on the surface at least, is CO_2 ice. Water ice is also trapped in the cap, probably in large amounts, but even if it were nearly all water it cannot account for more than another 10% of the capacity of the putative ancient oceans. If the oceans were really there, and if all of the water is still on Mars, then something like 80% of it is hidden below the surface and not in the polar caps.

The north residual polar cap is the most important seasonal source of water vapour in the Martian atmosphere. Large quantities of water vapour sublime from it during late spring and early summer. The southern polar cap, by contrast, produces about half as much. About 3 billion tons of water vapour is released into the atmosphere in the northern summer (§6.6), which is far less than on Earth because the thin, cold atmosphere on Mars can hold and transport much less water, even if it is in contact with a plentiful supply on or underneath the surface.

9.5.5 The layered terrain

The layers that are revealed in cliff faces and valleys, and at the edges of both polar caps, record changes in the amounts and types of airborne material and the deposition processes over long, geologic timescales. At the poles, the dust is trapped by sedimentation as water vapour and carbon dioxide freeze and snow out onto the surface, in cycles with timescales ranging from seasonal to millennial to millions of years. The layers are clearly visible, even from orbit, which would not be the case if they all contained exactly the same material deposited in exactly the same way. The main difference between lighter and darker layers may just be the relative amounts of dust and ice they contain, but it is also possible that different shades are caused by different compositions or particle sizes.

The fact that thick layers are also found at more temperate latitudes (for example, in Meridiani, almost on the equator) has led to speculation that, rather than having simply evolved from a warmer to a colder climate, Mars may actually alternate between having a cold thin atmosphere (as at present) and a warmer thicker atmosphere able to support precipitation from water clouds. This could conceivably happen if water vapour and other atmospheric gases are released from the subsurface deposits and the 'permanent' polar caps at times when the orbital characteristics of the planet change, as they are known to do on very long timescales due to the Milanković cycles (§9.6.2). Such periodic orbital changes are thought to explain the terrestrial ice ages, and are more extreme for Mars because of its more eccentric orbit.

9.5.6 Volcanism on Mars

Most models of the internal structure of Mars suggest that the interior should have cooled and solidified in the distant past, perhaps as long as 2 billion years ago. The main difference between Mars and the Earth in this respect is size: smaller bodies cool much faster. It also depends on the composition of the interior, which affects the conductivity and melting point of the lithosphere, and the release of chemical, radioactive, or potential energy.[90] A cold, solid core appeared until recently to be likely, based on thermal models supported by evidence like the absence of a significant magnetic field. Since the Earth's field is apparently produced by dynamo action in its molten iron core, the absence of similar activity on Mars seemed clearly to indicate that the core had frozen.

In addition, although there is plenty of evidence for volcanoes on Mars, they were thought to have expired once the interior was no longer hot enough for liquid magma. However, recent high-resolution images of the surface show what appear to be quite fresh lava fields, some of which may have occurred in the last few million years. Laboratory analysis of samples of the Martian meteorites support these age estimates by showing that some of the meteors are made of volcanic rock formed only a hundred and fifty million years ago. If Mars experienced volcanism so recently in geological terms, it is unlikely to have stopped entirely. Major eruptions could be rare, perhaps thousands of years apart, which would explain why none has been observed in the forty years or so that imaging from orbit has been possible. Less-energetic subsurface heating could be continuously melting subsurface ice to create ground water that escapes on the surface in a less-dramatic fashion than full-scale volcanoes, an intriguing possibility for which recent evidence has also been accumulating.

[90] Potential energy is released as heat if relatively heavy substances are able to migrate closer to the centre of the planet. This is an important process soon after a planet forms, but it is not known whether it still operates inside Mars to any significant degree.

9.5.7 Evidence for recent surface liquid water

The latest high-resolution photography from orbit reveals erosion features running down the side of gullies on the edges of craters and valleys. The flow features look very young, since they are sharply delineated and free of craters, dust deposits, or signs of erosion, and in some cases they run across recently formed windblown dune fields. They closely resemble some found in cold regions on Earth that are definitely produced by water erosion. On Mars, they may be produced by residual volcanism melting the underground ice and releasing liquid water a few metres below the surface. In crater walls and other near-vertical surfaces this may occasionally break through, causing the flows.

However, it is difficult to explain how liquid water could possibly survive under present conditions on Mars, once exposed to the atmosphere. Even below the surface, water should be frozen to a depth of several kilometres, and if geothermal heating melted and drove it out onto the surface, it should evaporate quickly in the thin Martian

atmosphere, instead of dripping down the crater wall. But the subsurface water is unlikely to be pure, and briny water with very high concentrations of soluble salts can have a freezing point low enough to make a plausible case for survival as liquid on the surface, at least for a while, particularly if it is protected by a layer of ice on top. The time required to produce the gully features, which are only tens or at most hundreds of metres in extent, could be quite short, perhaps less than an hour.

9.6 Mechanisms for climate change

The processes that contributed to climate change on Mars must be the same, although possibly on a different scale, as those for Earth and Venus. The main candidates are:

1. Changes in the output of the Sun over time;
2. Orbit and spin axis cycles and variations;
3. Creation of a dense early atmosphere and flash flooding by volcanism, infall of icy cometary material, etc.;
4. Atmospheric removal by massive meteoritic impacts, solar wind erosion, subsurface sequestering, etc.

These are summarised in the sketch in Fig. 9.12 and discussed below.

9.6.1 Solar variations

According to most current theories of stellar evolution, the Sun has got gradually hotter over its lifetime of about 4.5 billion years, so that, at the time of the formation of the water-related features on Mars, it would have been around 30% less luminous than today. Since the geological and biological evidence suggests that both Mars and Earth were actually warmer than at present, this presents a problem, known

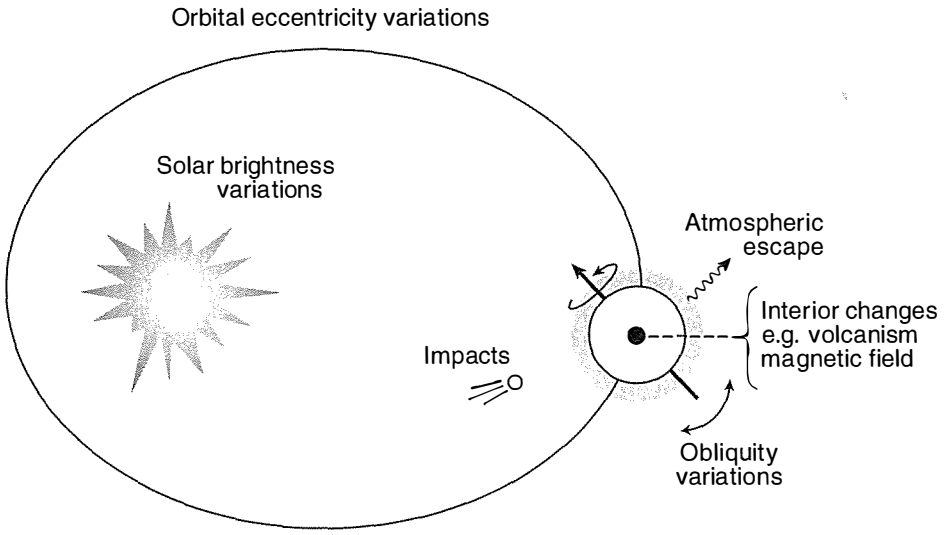

Fig. 9.12
A summary of the key factors thought to have affected the climate of Mars over its 4.5 billion year history.

as the faint young Sun paradox. If Mars received a third less solar energy today, its mean surface temperature would fall below the freezing point of carbon dioxide and most of the atmosphere would condense on the surface, a global version of the phenomenon that presently occurs only in the polar night in the winter. The mean temperature of the whole of Earth would also drop to Arctic levels, around 3° below freezing, and our planet would become icebound.

Since this apparently did not happen, the early weak Sun must have been compensated on both planets by some kind of additional warming at the surface. This was most likely an enhanced greenhouse effect, since Mars and Earth had thicker atmospheres then, which may have contained larger concentrations of ammonia and other strong greenhouse gases that have subsequently vanished. Additional carbon dioxide and water vapour may have been vented from the hot interior of the planet, and this could have been supplemented by impacting icy material on a larger scale than happens now.

Alternatively, it is possible that the early Sun was not as dim as current theories suggest. Recent observations of young stars elsewhere in the universe cast doubt on whether there really is a definite progression in heat output with age, while some models find that the Sun was actually warmer in the very distant past, which would have great significance for Mars, and Earth, if true.

9.6.2 Cyclical variations in Mars' orbital parameters

Mars' equinoxes precess much faster and with greater effect than Earth's do, because Mars' orbit is so non-circular. Other changes in Mars' orbit and inclination occur on longer timescales, and can be calculated with a version of the Milanković model used to explain Earth's ice ages. The latest calculations include the effect on the orbit of Mars of gravitational perturbations by all other planets and the Moon, minor effects due to the polar flattening of the Earth and Sun, tidal dissipation in the Earth–Moon system, and even general relativity.

The most striking feature of the result is an increase about 5 million years ago in the axial tilt (obliquity) of Mars to more than 45°, producing a large increase in insolation at the summer pole. This type of phenomenon may have been responsible for the local release of subsurface water to produce the eroded gullies seen in some, mostly polewards-facing, slopes. Some calculations suggest that obliquities as high as 82° have occurred, in which case the poles would actually point nearly straight towards the Sun, and the ice caps would completely melt or sublime. How much of an effect that had on the mean global climate is debatable, since it is uncertain how much volatile material would be released at the time of formation of the major fluvial features several billion years ago. In any case, the calculations become unstable on such long timescales, and the predicted variations in Mars' orbital parameters become unreliable.

9.6.3 Loss of an early dense atmosphere

A mixture of solar wind sputtering, impact erosion, conversion to carbonate rocks, and deposition in the regolith and polar caps could have reduced a dense early atmosphere to the present state. Currently, there is of the order of one hundredth of a bar in the Martian atmosphere and probably something between 10 and a 100 times as much in the polar caps, regolith and subsurface ices. Modelling suggests that warm, wet early Mars must have had a surface pressure of at least 1 bar and probably more if the warming was by the greenhouse effect alone. If these figures are correct, then at least 2 bars of mostly CO_2 must have been lost in the first billion years or so.

Atmospheric gas could have been lost due to ejection by impacts of large objects in the early days of the Solar System, when there was a lot more randomly drifting debris than there is today. The efficiency of an impact obviously depends on the mass of the object coming in (§2.5.4), but it also depends on the mass of the planet, with more material being removed from a smaller planet because of its smaller gravitational field. Thus, impact erosion is relatively inefficient on Earth and Venus, while the impact of a sufficiently large and fast object (more than 3 km across and travelling at least 14 km s^{-1}) will create a plume on Mars that expands faster than the escape velocity. This could sweep away a large fraction of the atmosphere, especially if the impact is oblique like a brush stroke, rather than a direct hit. However, some researchers dispute whether there were ever enough impacts on Mars to remove several bars of atmosphere.

Mars, like all of the planets, is exposed to streams of protons and helium ions expelled from the Sun to form the solar wind. Since these are charged particles, a planet like the Earth, which has a magnetic field, deflects the solar wind around the planet, and this may also have been the case with early Mars. When Mars' magnetic field disappeared, as the core cooled and stopped acting as a generator, the solar wind could interact more directly with the atmosphere. This would alter the rate at which sputtering took place, a process in which the solar wind particles collide with upper atmosphere atoms or molecules and eject them into space (§2.5.3).

Impacts, especially of icy bodies, can actually supply atmospheric gases, as well as remove them. The large craters and the river valleys on Mars appear to be about the same age, which has led to suggestions that the warming needed to produce the liquid water responsible actually came from the impacts of giant bodies like asteroids and comets. In between such infrequent, catastrophic events, the planet could have cooled back to something like its present austere condition. Some of the geological evidence supports this kind of catastrophic theory of the early Martian climate; for instance, the fact that the river valleys show few tributaries could be explained by flash flooding rather than slow erosion of the kind familiar on Earth.

Atmospheric gases do not have to be lost from the planet in order to escape from the atmosphere. On the Earth, weathering is a very efficient process, which removes carbon dioxide by converting it into

carbonate rock. To work efficiently, the process requires standing water and rain, in which the CO_2 dissolves, forming carbonic acid, which then interacts with silicate rocks, producing carbonates. In this way, the Earth's CO_2 would be removed by the oceans in ~10,000 years if it were not replaced by volcanism and other processes. The crust and the polar caps are also storehouses for atmospheric gases on Mars, not only as ices of water and carbon dioxide, but also by adsorption into minerals.

9.7 Mars climate models

All of the different factors involved in climate change can be evaluated using numerical models of various degrees of sophistication. If the surface pressure is increased to simulate the conditions that might have prevailed on early Mars, we can address whether a thicker atmosphere 4 billion years ago, at the time when the features we interpret as drainage channels and perhaps oceans were produced, would in fact have allowed Mars to be warm and wet.

The simplest model is that discussed in §5.5, with an isothermal stratosphere and a convective troposphere following an adiabatic lapse rate. The surface temperature is calculated assuming a single-slab atmosphere, and a 'perfect' greenhouse effect, in which the atmosphere is transparent to all solar photons and opaque to all those in the thermal infrared at wavelengths longer than about 5 m. This overestimates the greenhouse effect due to Mars' thin atmosphere by giving a

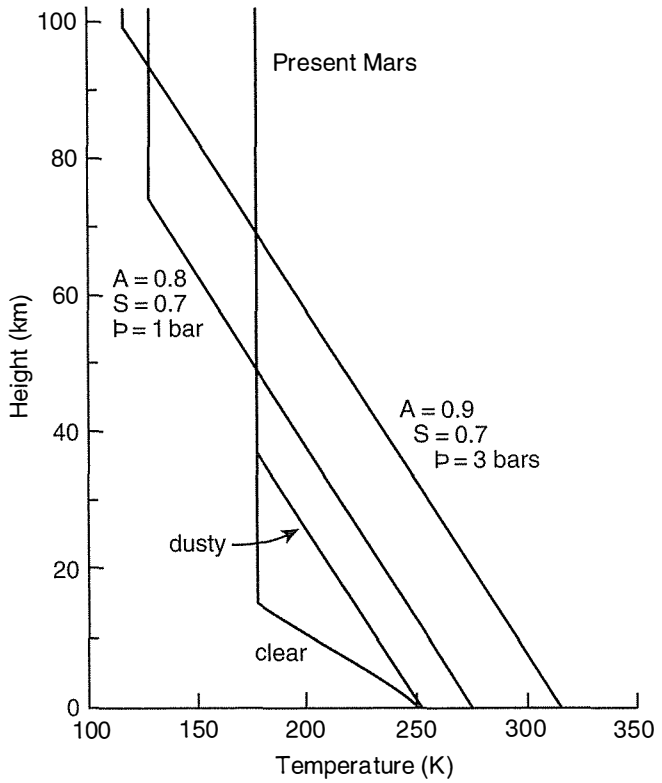

Fig. 9.13
Simple models of the mean temperature profile for present-day Mars with a clear and a dusty atmosphere. The other profiles are a hypothetical early Mars in which the surface pressure p is similar to modern Earth, and a version of early Mars with a Venus-like albedo ($A = 0.8$ or 0.9) due to condensate cloud formation. In both models of the paleoclimate, the Sun is 30% less intense than today ($S = 0.7$).

surface temperature of 250 K, which is too high to be the mean for the entire globe of Mars, but corresponds quite well to typical temperatures at low and mid latitudes. The stratospheric temperature is 177 K, and with a dry adiabatic lapse rate of $g/C_p = 4.5\,\mathrm{K\,km^{-1}}$ and a scale height of 13 km, the tropopause occurs at a height of about 16 km above the surface. This is lower than observed since the model requires modification to allow for the absorption of solar and planetary thermal radiation by airborne dust (§5.5). When the lapse rate is arbitrarily reduced to $2\,\mathrm{K\,km^{-1}}$, this brings the profile more in line with measurements and more detailed radiative transfer calculations (Figs. 9.13, 7.8 and 5.7).

It would be unrealistic to assume Mars' bolometric albedo remains unchanged at the present low value, since it is likely to increase very substantially in a high-pressure atmosphere following the formation of water clouds in the troposphere and CO_2 clouds in the stratosphere. Even without clouds, the albedo would increase due to molecular Rayleigh scattering; according to one estimate, the albedo of a cloud-free Mars with a surface pressure of 2 bars would be 0.38, compared to about 0.25 now. With both kinds of cloud as well, a value close to that of Venus, say 0.8, might be appropriate.

Finally, these high-pressure atmosphere simulations relate to a time when it is believed that the Sun was dimmer by around 30% (§9.6.1). Including this factor in the model as well, the mean surface temperature for ancient Mars with a surface pressure of 1 bar is 274 K, just above the melting point of water ice. For 3 bars, this rises to a positively tropical 314 K, or 41 °C, suggesting that under some circumstances Mars could have had Earth-like temperatures if the pressure was higher in the past.

More detailed models reach similar conclusions, although many uncertainties remain. Some of these work in favour of higher temperatures, for instance, the possibility that the early atmosphere contained other greenhouse gases in substantial quantities, in addition to carbon dioxide and water vapour. One of the prime candidates to produce additional opacity is methane, which was recently detected in the Martian atmosphere in tiny quantities of a few tens of parts per billion, much too small to affect the climate now.

9.8 A sketch of the Martian climate over time

During the first billion years or so of its existence, Mars was volcanically active and large quantities of carbon dioxide, water vapour, and other gases were pumped continuously into the air. At this stage, the Martian atmosphere was much thicker than it is now and the surface pressure may have been several bars. The greenhouse effect associated with carbon dioxide, water vapour, clouds and minor constituents, such as methane, was sufficient to maintain the surface temperature above the freezing point of liquid water. Mars' inventory of water was also not too different from Earth's, in proportion to the size of the planet, and in this early epoch large open bodies of liquid water were

present on the surface, fed by rain and run-off from the highlands via an extensive network of river valleys. The standing water was very salty, using salt in its broader sense to mean any soluble compound and not just sodium chloride, which helped it to stay liquid when cold.

The climate changed dramatically when the interior of Mars began to cool. This had the two-fold effect of first reducing and then eliminating the planetary magnetic field, and of fuelling a declining rate of volcanism. Without its magnetic shield, the rate at which the upper atmosphere lost gases to space as a result of the action of the solar wind increased, while at the same time the lost gas was less-rapidly replaced by the increasingly torpid volcanoes below. Large impacts by stray bodies colliding with Mars were still a common enough occurrence to have a role in further depleting the atmosphere, producing brief warming episodes, even as they helped to produce an overall cooling in the long term.

As the atmosphere got thinner, the surface got cooler and fell below the freezing point of water. When this happened, the oceans froze and the amount of water vapour in the air dropped dramatically, further lowering the mean temperature. Rarely now, large impacts and sporadic eruptions produced local melting on and under the surface, causing a flood of liquid water, lava, and ejecta that would soon, in geological terms, subside. The thin, dry air eroded the exposed rock on the higher mountains and plateaux, producing dust that blew around the planet and gradually covered over the frozen seas. Volcanic eruptions ceased entirely, and the production of atmospheric gas to offset the losses was reduced to low-level seepage through a few remaining active vents. Atmospheric loss due to impacts also effectively ceased. At some point the air became so cold that carbon dioxide, its main constituent, also began to freeze out at high altitudes and in the polar winters, further reducing the pressure and the temperature until Mars reached the state we see today.

9.9 The climate on Titan

The solar irradiance at Saturn's distance from the Sun is only about 1% of that at the Earth ($14\,W\,m^{-2}$). The albedo of Titan has a value of about 0.3, which corresponds to an effective emitting temperature in radiative equilibrium of only 81 K. Measurements by the *Voyager, Cassini*, and *Huygens* probes revealed a mainly nitrogen atmosphere, with methane at about 5%, a significant secondary component. Although the major constituent is the same as that on the Earth, the total amount of N_2 on Titan is about ten times higher. Allowing for the lower gravity (g is about one-seventh of the terrestrial value), this equates to a surface pressure close to 1.5 bars (1.467 bars was measured at the landing site of *Huygens* in January 2005). This gives a small but significant greenhouse warming, largely due to the infrared absorption bands of methane, with important contributions from pressure-induced bands of N_2 and H_2 at the longer wavelengths.

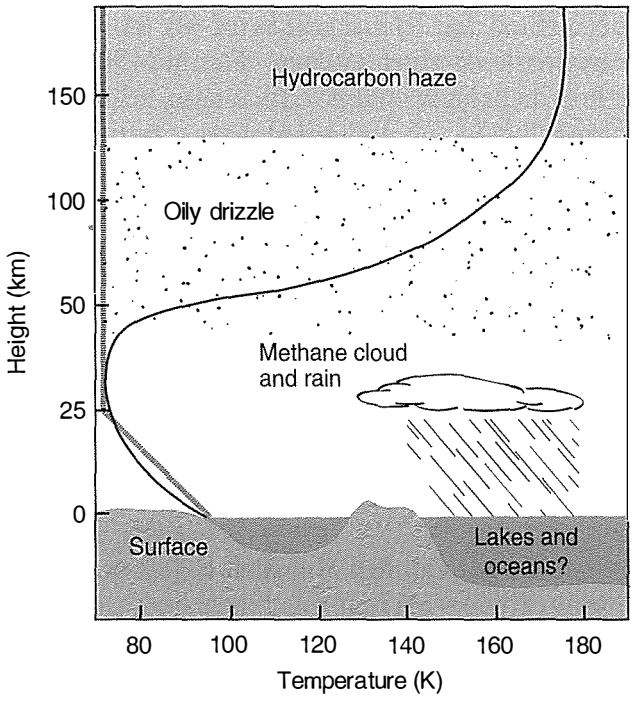

Fig. 9.14
The mean measured temperature–height profile for Titan, compared to a radiative–convective equilibrium model (thick grey line). The simple model takes no account of the heating at higher levels due to aerosols and methane photolysis, and hence is only approximately valid in the lower atmosphere.

Applying the radiative–convective and one-layer greenhouse models (§5.1), we obtain $T_0 = 95\,\mathrm{K}$ for the surface temperature, and $T_s = 68\,\mathrm{K}$ for the stratospheric temperature. The adiabatic lapse rate for an atmosphere consisting primarily of molecular nitrogen, but saturated with condensable methane, on this low-gravity world is just $0.89\,\mathrm{K\,km^{-1}}$, so the tropopause should be approximately 31 km above the surface. Figure 9.14 shows that these global mean values compare reasonably well to the profile measured near the equator by *Voyager 2* in 1980, which in turn is close to that measured by the *Huygens* probe during its descent through Titan's atmosphere (Figs. 5.11 and 5.12).

The second most abundant gas, methane, condenses at the low temperatures on Titan and produces cumulus-type clouds which cover a small fraction of the surface of the moon, especially near the subsolar point, where heating, and therefore convection, is greatest. Photographs of the surface of Titan from *Huygens* suggest that methane precipitates seasonally from these clouds as liquid, producing river-like channels and other features in the terrain.

Above these condensation clouds, methane is dissociated by solar radiation and an orange-tinted photochemical haze forms (§7.4.1). The processes that produce the haze obviously will deplete the atmospheric methane content, and do so at such a rate that it should all be gone after a time of the order of a few million years. The fact that Titan's atmosphere is currently saturated with methane implies the existence of a reservoir on or below the surface. The subsurface supply of methane is probably trapped in water ice, but able to escape in places through fissures via 'cryovolcanoes' into the atmosphere. There are also seasonal liquid reservoirs on the surface, filled by methane rain

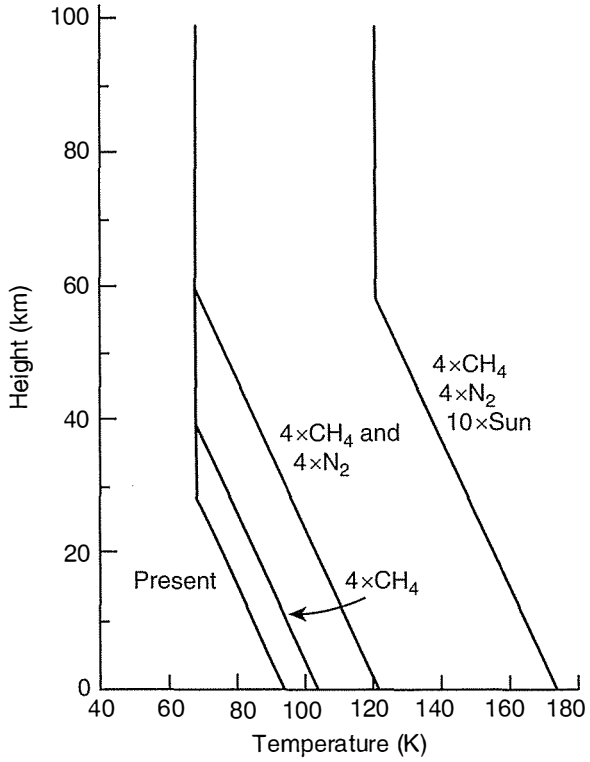

Fig. 9.15
The vertical temperature profile on Titan, according to simple radiative–convective models, for four scenarios: (a) the present day; (b) with abundant methane (4 × present) in a 'runaway greenhouse' scenario; (c) with 4 × nitrogen and 4 × methane; and (d) as (c) but 6Gy hence, when the Sun is a red giant star and the solar constant at Titan is ten times the present value.

from the clouds, and more complex, oily materials from the precipitating haze.

Titan's climate depends critically on these volatile reservoirs, particularly on the methane inventory. Were the supply of fresh methane to the atmosphere to slow down, the reduced greenhouse effect would lower the temperature near the surface and induce negative feedback, since the colder air would hold less methane, analogous to the behaviour of water vapour on Earth. The current temperature profile is not much above the saturation temperature of nitrogen, and so nitrogen cloud formation and rain-out also becomes a possibility. This would lead to further cooling until most of the atmosphere has collapsed and Titan resembles Neptune's large satellite, Triton, which has large amounts of frozen nitrogen on its surface.

Conversely, if the methane supply remains abundant, extra warming of the lower atmosphere from any cause would increase the take-up of methane and enhance the greenhouse warming, leading to further evaporation. This kind of 'runaway' greenhouse could continue indefinitely, or until the supply of methane runs out, and lead to quite high surface temperatures and pressures. Figure 9.15 shows the effect of increasing the methane concentration to four times its present abundance. Also shown is the result of a less plausible change in which nitrogen also increases by a factor of four, perhaps by the escape of ammonia from the interior, which is subsequently converted to molecular nitrogen by photolysis. This takes the surface pressure to 6 bars, and the temperature to over 120 K.

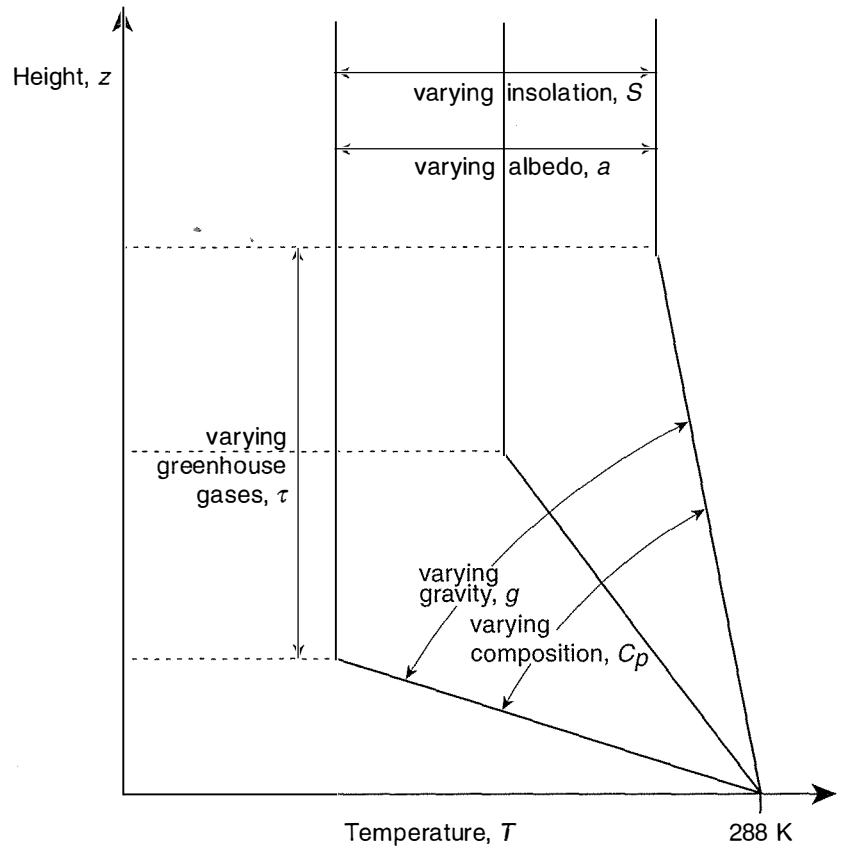

Fig. 9.16
Model atmospheres for exoplanets with Earth-like surface temperature and pressure, achieved with different combinations of surface gravity g, albedo a, solar constant S, specific heat capacity C_p, and greenhouse gas concentration changing the optical depth τ.

Finally, the Sun is expected to become much warmer towards the end of its lifetime, destroying all life on Earth. The model in Fig. 9.14 suggests that a solar flux at Titan which is a factor of 10 times the present value, this being of the order predicted by models of solar evolution reported in the literature, would still only warm the surface to less than 200 K. In order to reach the melting point of water and achieve something resembling Earth-like conditions, the solar constant would have to be more than 100 times what it is now, equivalent to moving Titan into Earth's current orbit.

9.10 Exoplanet atmospheres

Earth-like exoplanets have yet to be discovered, but it must be only a matter of a relatively short time, as observing techniques improve, before they are. What will climatic conditions there be like? Of the infinite number of possibilities, the ones that interest us the most are likely to be those with about the same surface temperature and pressure as the Earth. The same simple models as used above for Venus, Mars, and Titan can be used to analyse situations where this might apply, where the variables are the solar constant, the optical depth due to greenhouse gases, the albedo, the atmospheric composition (through the specific heat and infrared spectral properties) and the size of the planet (through the surface gravity). In fact, there exist a semi-infinite

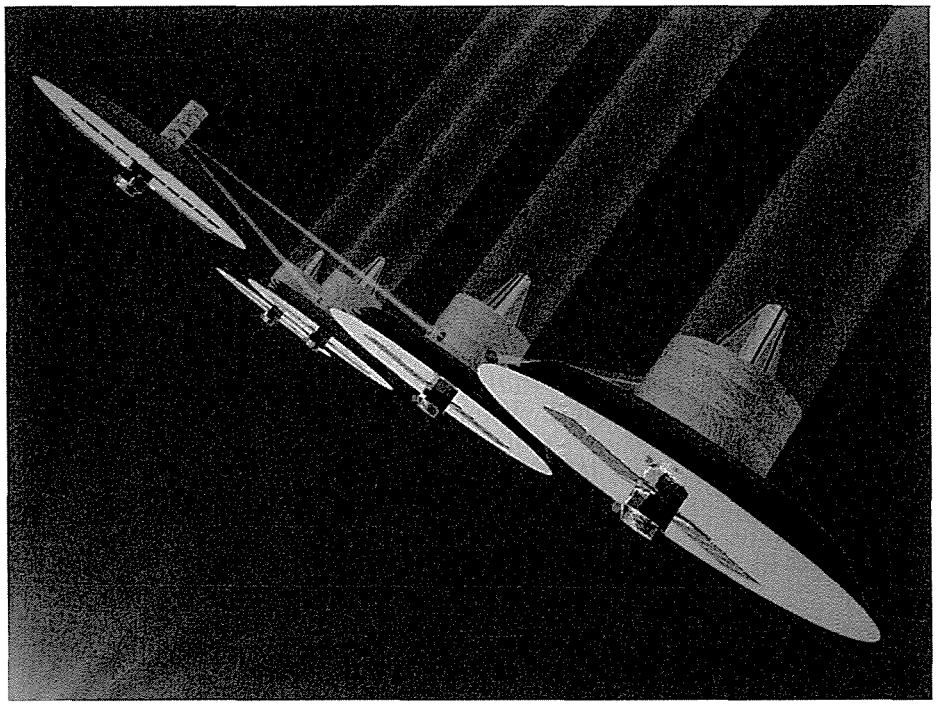

Fig. 9.17
NASA's *Terrestrial Planet Finder*, and its European counterpart *Darwin*, are designed to detect Earth-like planets orbiting nearby stars, and obtain spectra that will elucidate the condition there and perhaps provide evidence of life. The design uses an array of large free-flying space telescopes as an astronomical interferometer, linked by lasers to hold a tight formation. The beams from each are combined in a hub spacecraft, which will contain the spectrometers to analyse the light collected and relay the data to Earth. The array can be extended indefinitely to increase the effective aperture, and thus the resolution and sensitivity.

number of values for these parameters that would give an Earth-like mean temperature and pressure at the surface; Fig. 9.16 shows schematically the envelope of temperature profiles that all have this property.

It follows that a very large number of planets may exist in the universe where humans could reside in reasonable comfort. A subset of these may have really Earth-like atmospheres, through having about the same planetary mass orbiting a similar star, although there will not be much oxygen unless plant life is present. The climate variables, such as albedo, atmospheric composition, and even the surface temperature and pressure, are measurable in principle by spectroscopy from large and sophisticated telescope arrays in orbit around the Sun (Fig. 9.17), so that targets can be selected for interstellar versions of today's interplanetary probes. The Earth and the planets of our Solar System are only the beginning.

9.11 References and further reading

Adamcik, J.A., and A.L. Draper. The temperature dependence of the Urey Equilibrium and the problem of the carbon dioxide content of the atmosphere of Venus. *Planet.Space Sci.*, **11**, 1303–1307, 1963.

Bullock, M.A. The Stability of Climate on Venus. Ph.D. Thesis, University of Colorado, Boulder, Colorado, 1997.

Bullock, M.A., and D.H. Grinspoon. The stability of climate on Venus. J. *Geophys. Res.*, **101**, 7521–7529, 1996.

Bullock, M.A., and D.H. Grinspoon. The recent evolution of climate on Venus. *Icarus*, **150**, 19–37, 2001.

Kasting, J.F. When methane made climate. *Sci. Am.*, 80–85, July 2004.

Kliore, A.D., V.I. Moroz, and G.M. Keating, eds. The Venus International Reference Atmosphere. *Adv. in Space Res.*, **5**, 1–305, 1985.

Forget, F., and R. Pierrehumbert. Warming early Mars with carbon dioxide clouds that scatter infrared radiation. *Science*, **278**, 5341, 1273–1276, 1997.
Laskar, J., B. Levrard, and J. Mustard. Orbital forcing of the Martian polar layered deposits. *Nature*, **419**, 375–377, 2002.
Lorenz, R.D., C.P. McKay, and J.I. Lunine. Photochemically-driven collapse of Titan's atmosphere. *Science*, **275**, 642–644, 1997a.
Lorenz, R.D., J.I. Lunine, and C.P. McKay. Titan under a red giant Sun: A new kind of 'habitable' world. *Geophys. Res. Lett.*, **24**, 2905–2908, 1997b.
Lorenz, R.D., C.P. McKay, and J.I. Lunine. Analytic investigation of climate stability on Titan: Sensitivity to volatile inventory. *Planet. Space Sci.*, **47**, 1503–1515, 1999.
McKay, C.P., J.B. Pollack, J.I. Lunine, and R. Courtin. Coupled atmosphere-ocean models of Titan's past. *Icarus*, **102**, 88–98, 1993.
Nakamura, M., *et al.* Planet-C: Venus Climate Orbiter mission of Japan. *Planet. Space Sci.*, **55**, 12, 1831–1842, 2007.
Taylor, F.W. Climate variability on Venus and Titan. *Space Sci. Rev*,, **125**, 1–4, 445–455, 2007.
Taylor, F., and D. Grinspoon. Climate evolution of Venus. J. *Geophys. Res.*, **114**, E00B40, doi:10.1029/2008JE003316, 2009.

9.12 Questions

1. State briefly how you would account for the following:

(a) A seasonal swing of nearly a third in the mean surface pressure all over Mars.
(b) Venus has between ten and one hundred thousand times less water in its atmosphere than exists in the oceans and atmosphere of the Earth, while deuterium is about one hundred times more abundant on Venus than Earth.
(c) The atmospheres of Venus and Mars are mostly CO_2, despite the fact that solar UV radiation efficiently converts CO_2 to CO and the recombination reaction is spin forbidden.
(d) Primordial argon and neon are orders of magnitude less abundant on Earth than on Venus, and less common on Mars than Earth by a similar large factor.
(e) The ratio of ^{15}N to ^{14}N in the Martian atmosphere is about 1.7 times that on Earth.
(f) The radiative equilibrium temperature of Venus is less than that of the Earth, although the solar constant at Venus is twice the value at Earth.
(g) The temperature in the middle atmosphere tends to be constant with height on Venus and Mars.
(h) The thermospheres of Venus and Mars are cooler than Earth's.
(i) Earth is relatively poor in CO_2 compared to Venus, while the amounts of nitrogen are about the same.
(j) Mars probably undergoes large changes in climate on a range of time-scales.
(k) So far as is known at present, the elemental abundances in Jupiter are the same as in the Sun.
(l) Jupiter has at least three layers of cloud in the region visible to the outside observer. The colours include reds, yellows, and browns.
(m) All of the gas giants have internal heat sources (except perhaps Uranus).
(n) Titan has clouds of oily hydrocarbons, and possibly pools of liquid ethane and other condensable hydrocarbons on the surface.
(o) The radiative equilibrium temperatures of the Jovian planets are significantly smaller than the observed bolometric temperatures.

2. The surface pressure on Venus is nearly 100 times that on the Earth. Outline and sketch a theory, such as that first introduced by Urey that involves interaction between the atmosphere and the surface, which may account for this high surface pressure on Venus. State three of the potential difficulties that theory must overcome before it would be possible to accept it as a realistic physical model of conditions on Venus.

Glossary

Adiabatic lapse rate: the rate at which temperature falls off with height in an atmosphere heated from below, assuming air parcels rise without exchanging heat with their surroundings (i.e., adiabatically).

Aerosols: a dispersion of solid and/or liquid particles suspended in the atmosphere, including cloud and haze particles, but more usually referring to ubiquitous dispersions that are nearly, or actually, invisible except under special observing conditions.

Albedo: reflectivity. See *Bond albedo*.

Baroclinic: a buoyancy driven phenomenon, such as the instabilities that may develop in a fluid after flow over a solid obstacle.

Barotropic: a mechanically driven phenomenon, such as the instabilities that may develop in a fluid where large horizontal shear forces exist, near the edge of a jet, for example.

Beta plane: an approximation to the *Coriolis acceleration*, valid only near the equator, such that the atmospheric variables change only in the vertical direction, allowing a simplified solution to dynamical equations.

Blackbody: an ideal surface that absorbs all photons that fall on it, and emits according to Planck's radiation law with an emissivity of unity.

Bond albedo: the Bond or bolometric albedo is defined as the fraction of the incident radiation of all wavelengths that is scattered in all directions, i.e., the fraction of the total incident energy that is not absorbed by the planet.

Brightness temperature: the temperature of a blackbody that emits the same amount of radiant energy in a defined spectral interval as a planet or other target body.

Coriolis force (acceleration): a virtual force (one that does no work) that results in acceleration at right angles to motion on a rotating platform.

Cyclostrophic balance: the state of balance between the pressure gradient and the centripetal force due to the zonal wind motion.

Dust devils: small, travelling whirlwinds, common on Mars that lift dust to considerable heights in the atmosphere.

Ecliptic plane: the equatorial plane of the Sun, which contains the orbits of all of the planets (or nearly so).

Exosphere: the rarefied region of an upper atmosphere where the mean free path is such that escape from the planet is more likely than a collision with another molecule.

Field of view: usually measured in solid angle units (steradians), this is the cone of acceptance at the entrance aperture of an instrument that encloses those rays that will reach the detector. Defines the *spatial resolution.*

Free modes: waves that are not systematically driven by tidal forcing or some other sustained stress.

Froude number: a dimensionless number comparing inertia and gravitational forces, which determines the behaviour of a fluid as regards the formation of certain wave types and vortices.

GCM: originally General Circulation Model, now often used to mean Global Circulation Model or Global Climate Model. A large and complex numerical representation on a computer of a planetary atmosphere that includes three-dimensional, time-dependent dynamics.

Geostrophic balance: the condition when the horizontal force due to the pressure gradient and the Coriolis force balance.

Gravitational tide: a periodic movement of the atmosphere or ocean in response to the attraction of the Sun or Moon.

Gravity waves: the oscillation of parcels of air with different density to their surroundings moving under the control of buoyancy forces at right angles to the direction of propagation.

Greenhouse effect: the warming of the surface of a planet by infrared radiation from the atmosphere, augmenting direct solar heating.

Hadley cell: an atmospheric circulation regime characterised by global-scale overturning in the equator-to-pole direction.

Homopause: the level in an atmosphere above which constituents are no longer mixed but instead tend to separate by mass under the influence of gravity.

Hydrostatic equilibrium: the condition where the atmospheric pressure balances the weight of the overlying column of air.

Inversion: (i) a temperature profile that changes from increasing with altitude to decreasing, or vice versa; (ii) the art of determining temperature, pressure, composition, and other atmospheric properties from measurements of spectra.

Jet: a region of locally high winds, extended in one dimension (usually zonally) and confined in height and latitude.

Kelvin wave: a type of large-scale, low-frequency gravity wave that propagates around the equator with no polewards velocity component.

Lapse rate: the rate at which temperature T falls off with height z in an atmosphere, i.e., $-dT/dz$.

Limb brightening or darkening: when observing a planet from a distance, the intensity of emission of radiation from a source in the atmosphere tends to increase from the centre of the disc to the edge, due to the longer slant path length; this is limb brightening. The opposite effect is expected for emission from the surface or a cloud top, i.e., limb darkening.

Magellan: A NASA mission to Venus launched in 1989, mainly to study the surface using synthetic aperture radar.

Mariner 2: the first successful planetary mission, to Venus in 1962.

Mariner 4: the first successful mission to Mars, in 1964.

Mariner 6 and 7: identical spacecraft which flew by Mars, over equator and pole, respectively, in 1969.

Mariner 9: the first Mars orbiter, launched in 1971.

Mariner 10: carried out a close Venus fly-by in 1974 and then went on to make three close encounters with Mercury.

Mars Climate Orbiter: an unsuccessful mission to Mars, which crashed on arrival in 1989.

Mars Global Surveyor: a successful Mars orbiter mission, arriving in 1997.

Mars Observer: an unsuccessful mission to Mars, lost shortly before arrival in 1993.

Mars Odyssey: a successful Mars orbiter mission, arriving in 2001.

Mars Reconnaissance Orbiter: a successful Mars orbiter mission, arriving in 2006.

Meridional wind: in the equator-to-pole direction.

Mesopause: the level at the top of the *mesosphere*, above which is the *thermosphere*.

Mesosphere: the region in an atmosphere that lies above the *stratopause*, particularly on the Earth. On other planets, may just mean more generally the 'middle atmosphere'.

Micron: a micrometre, abbreviated μm, one thousandth of a millimetre. The wavelength of visible light ranges approximately from 0.38 to 0.75 μm.

Milankovi cycles: long-term cyclic changes in orbital parameters, such as eccentricity and obliquity, due to gravitational interactions of each planet with other members of the Solar System.

Near infrared: the 'near infrared' is the part of the infrared spectrum of a planet that is mostly dominated by reflected sunlight, which typically means wavelengths from the visible to about 5 μm (2000 cm^{-1}). The 'thermal infrared' is dominated by radiation emitted at the characteristic temperatures of the planet itself and typically ranges from 5 to 1000 μm (2000 to 10 cm^{-1}).

Noise equivalent power: the radiant power that must fall on a detector to produce a signal equal to the intrinsic noise in the detector and its associated electronics.

Noise equivalent temperature: the brightness temperature of a *blackbody* target that produces a signal equal to the intrinsic noise in the detector and its associated electronics.

Obliquity: the angle between the spin axis of a planet and its orbital plane around the Sun.

Optical thickness: the optical thickness τ of an atmosphere, or any other object, is the product of the absorption coefficient and the absorber amount, so that the transmission is given by $\exp(-\tau)$. The medium is said to be optically thick (or thin) at a given wavelength if $\tau \gg$ (or $\ll$) 1, when a photon

of that wavelength has a small (or large) chance of being transmitted without absorption or scattering.

Pioneer 10 and 11: small (260 kg) spin-stabilised spacecraft launched by NASA in 1972 to carry out an initial reconnaissance of the asteroid belt and of Jupiter and Saturn.

Pioneer Venus: a combined orbiter and multiprobes mission to Venus launched by NASA in 1978, mainly to study the atmosphere.

Planetary wave: any organised wave motion whose spatial scale is comparable with the radius of the planet; usually refers to *Rossby waves*.

Planetesimal: a rocky or icy fragment large enough (about 1 km or more in diameter) to interact gravitationally with similar objects and eventually accrete to form a planet.

Pressure-induced spectral bands: normally forbidden transitions that can occur when molecules are distorted by collisions at high pressure, producing temporary, induced dipole moments and transitions between rotational states.

Quadrupole spectral bands: transitions, usually weak but sometimes important over long atmospheric paths, on the outer planets, for instance, that occur in molecules that have an electromagnetic quadrupole moment.

Radiative–convective model: a simplified representation of an atmospheric temperature profile calculated by assuming *radiative equilibrium*, modified in the *troposphere* to allow for convection by adopting an *adiabatic lapse rate* where this is smaller.

Radiative equilibrium: the condition where the net energy as radiation entering a parcel or layer of atmosphere is balanced by the net radiative energy emitted.

Rossby number: the ratio between the acceleration and Coriolis term describing motion of an air mass, used to test for *geostrophic balance*.

Rossby wave: produced when the *Coriolis acceleration* acts as a restoring force on an easterly (but not westerly) zonal flow that is perturbed, for any reason, away from the purely east–west direction.

Shear: the phenomenon that occurs where rapid winds occur close to more static regions of atmosphere, for instance, near the edge of a jet, near a solid surface, or at the belt–zone interface on Jupiter. Shear forces lead to barotropic instabilities and can (inter alia) tend to spin up parcels of fluid and produce eddies.

Signal-to-noise ratio: the dimensionless ratio between the signal produced at the detector when viewing a planet or other target, and the intrinsic noise in the detector and its associated electronics.

Solar wind: a stream of very energetic charged particles, mostly protons, from the Sun.

Spatial resolution: a measure of the ability of an instrument to separate features on a planet, perpendicular to the viewing direction, typically measured in kilometres. Depends on the angular *field of view*; varies with distance from the target.

Spectral resolution: a measure of the ability of an instrument to separate features in a spectrum, measured in wavelength or wavenumber units.

Stratosphere: the region in an atmosphere that lies above the *tropopause*, characterised by radiative equilibrium which tends to give an isothermal *lapse rate*.

Stratopause: the level at the top of the *stratosphere*, above which is the *mesosphere*.

Superrotation: a persistent, large-scale zonal wind field with an angular velocity greater than that of the surface of the planet.

Synoptic scale: in meteorology refers to the typical dimension of a large weather system, such as a depression or an anticyclone. On the Earth it is usually taken to be about 1000 km.

Thermal infrared: see 'near infrared'.

Thermal tide: the periodic heating of an atmosphere, and the dynamical response to this heating, due to the apparent motion of the Sun across the sky.

Thermal wind equation: a relationship between the vertical derivative of the horizontal wind and the horizontal temperature gradient.

Thermosphere: the region of an upper atmosphere characterised by high temperatures produced by dissociation and ionisation of species by solar ultraviolet radiation.

Tidal heating: heating of the interior of a solid planet or moon by flexing induced by gravitational forces acting unequally on different parts of its mass, for instance, if its orbit is eccentric, or regularly perturbed by a third object nearby.

Tropopause: the level at the top of the *troposphere*, above which is the *stratosphere*.

Troposphere: the lowest region in an atmosphere, characterised by convective transfer of heat in the vertical, which tends to give an *adiabatic lapse rate*.

T-Tauri phase (of the Sun): a period in the early stages of evolution of the Sun and other stars, characterised by huge mass losses in the form of a very active solar wind.

Venus Climate Orbiter: a Japanese mission due to reach the planet in December 2010.

Venus Express: the first European mission to Venus, an orbiter which arrived in April 2006.

Viking 1 and 2: twin missions to orbit and land on Mars, in 1976.

Voyager 1 and 2: twin spacecraft weighing 722 kg, launched by NASA in 1977 to explore the outer Solar System. *Voyager 1* visited Jupiter, Saturn, and Titan; *Voyager 2* flew by Jupiter, Saturn, Uranus, and Neptune.

Weighting function: describes the contribution of different levels of the atmosphere to the signal at the detector in an instrument making remote sounding measurements of, for example, temperature. Thus, the weighting function determines the vertical resolution of the measurement.

Whistlers: pulses of electromagnetic waves, produced by lightning, that occur at descending frequencies around 100 Hz, with durations of about one second.

Window (spectral): a range of wavelengths in the infrared spectrum where, for a given planetary atmosphere, the absorption is weak for all constituents. Remote sensing instruments can therefore probe to deep levels from space. Well-known examples occur near 2.3 microns on Venus, near 10 microns on Earth, and near 5 microns on Jupiter.

Zonal wind: parallel to the equator.

Appendix A Some useful data

Radius of the Sun	700,000 km
Effective temperature of Sun	5780 K
Stefan-Boltzmann constant	5.67×10^{-8} W m^{-2} K^{-4}
Constant of gravitation G	6.6×10^{-11} m^3 s^{-2} kg^{-1}

	Mercury	Venus	Earth	Mars	Jupiter	Saturn	Uranus	Neptune
Solar distance	0.387	0.723	1	1.524	5.2	9.5	19.2	30.1
Orbital period	0.241	0.615	1	1.881	11.9	29.5	84	165
Rotational period	58.8	243	1	1.029	0.411	0.428	0.748	0.802
Orbital eccentricity	12.353	0.412	1	5.471	2.824	3.294	2.706	0.529
Obliquity	0	7.548	1	1.023	0.128	1.151	4.179	1.237
Equatorial radius	0.38	0.95	1	0.53	11.2	9.4	4.0	3.9
Mass	0.055	0.816	1	0.107	318	95	14.5	17.1
Density	0.985	0.950	1	0.714	0.241	0.127	0.230	0.319
Surface gravity	0.283	0.877	1	0.379	2.355	0.928	0.887	1.121
Escape velocity	0.384	0.929	1	0.214	5.232	2.955	1.893	2.259

	g m s^{-2}	C_p J gm^{-1} K^{-1}	Dry adiabatic lapse rate K Km^{-1}
Venus	8.89	0.8501	10.468
Earth	9.79	1.0040	9.760
Mars	3.74	0.8312	4.500
Jupiter	24.25	12.3591	1.963
Saturn	10.00	14.0129	0.714
Uranus	8.80	13.0137	0.676
Neptune	11.10	13.0137	0.853
Titan	1.35	1.0440	1.301

	Venus	Earth	Mars	Titan
Mean distance from Sun (108 km)	1.082	1.496	1.524	14.26
Eccentricity	0.0068	0.0167	0.0934	0.0288
Obliquity (deg)	177	23.45	23.98	27
Year (Earth = 1)	0.615	1	1.88	29.41
Rotational period (hours)	5832.24	23.9345	24.6229	382.68
Solar day (Earth = 1)	117	1	1.0287	16
Solar constant ($kW\,m^{-2}$)	2.62	1.38	0.594	0.0156
Bond albedo	0.76	0.4	0.15	0.3
Net heat input ($kW\,m^{-2}$)	0.367	0.842	0.499	0.0122
Atmospheric:				
Molecular weight (g) *dry	43.44	28.98*	43.49	29
Specific heat C_p ($J\,kg^{-1}\,K^{-1}$)	830	1005	830	1000
Surface temperature (K)	730	288	220	95
Surface pressure (bar)	92	1	0.007	1.467
Mass (1016 kg)	4770	530	~1	300
Composition:				
Carbon dioxide	.96	.0003	.95	15 ppb
Nitrogen	.035	.770	.027	.984
Argon	.00007	.0093	.016	.00004
Water vapour	~.0001	~.01	~.0003	8 ppb
Oxygen	~0	.21	.0013	~0
Sulphur dioxide (ppm)	150	.0002	~0	~0
Carbon monoxide (ppm)	40	.12	700	30
Neon	5 ppm	18 ppm	2.5 ppm	~0

	Jupiter	Saturn	Uranus	Neptune
Distance from Sun (km)	7.78×108	1.43×109	2.87×109	4.50×109
Eccentricity	0.0489	0.0565	0.0457	0.0113
Obliquity (deg)	3.13	26.73	97.77	28.32
Orbital period (years)	11.857	29.42	84.01	164.79
Solar day (hours)	9.92	10.65	17.24	16.11
Solar constant ($W\,m^{-2}$)	50.5	14.9	3.71	1.51
Bond albedo	0.343	0.342	0.30	0.29
Total energy output Solar energy input	1.67	1.78	1.06	2.52
Absorbed flux ($W\,m^{-2}$)	9.22	2.88	0.738	0.297
Emitted flux ($W\,m^{-2}$)	14.66	4.89	0.696	0.73
Internal source ($W\,m^{-2}$)	5.44	2.01	0.042	0.433
Radiative equilibrium temperature (K)	113	84	60	48
Observed bolometric temperature (K)	127	96	59	60
Atmospheric:				
Molecular weight (g)	2.22	2.07	2.64	2.6
Temperature at 1 bar (K)	165	134	76	72
Scale height (km)	27	59.5	27.7	20
Composition: (mole fractions)				
Hydrogen	0.898	0.936	0.825	0.80
Helium	0.102	0.325	0.152	0.19
Methane	0.003	0.0045	0.023	0.015
Ammonia	0.000 26	0.000 125	?	?

Appendix B Reference model atmospheres

Venus

z (km)	p (mb)	T (K)	H (km)
0	92100.00	735.00	16.45
2	81338.82	719.20	16.10
4	71634.79	703.40	15.74
6	62904.59	687.60	15.39
8	55069.76	671.80	15.04
10	48056.56	656.00	14.68
12	41795.75	640.20	14.33
14	36222.43	624.40	13.97
16	31275.87	608.60	13.62
18	26899.34	592.80	13.27
20	23039.93	577.00	12.91
22	19648.39	561.20	12.56
24	16678.98	545.40	12.21
26	14089.29	529.60	11.85
28	11840.10	513.80	11.50
30	9895.21	498.00	11.15
32	8221.31	482.20	10.79
34	6787.83	466.40	10.44
36	5566.76	450.60	10.08
38	4532.58	434.80	9.73
40	3662.03	419.00	9.38
42	2934.05	403.20	9.02
44	2329.64	387.40	8.67
46	1831.69	371.60	8.32
48	1424.87	355.80	7.96
50	1095.54	340.00	7.61
52	831.61	324.20	7.26
54	622.42	308.40	6.90
56	458.61	292.60	6.55
58	332.08	276.80	6.20
60	235.80	261.00	5.84
62	163.78	245.20	5.49
64	110.94	229.40	5.13
66	73.01	213.60	4.78
68	46.47	197.80	4.43
70	29.26	193.21	4.32
72	18.43	193.21	4.32
74	11.60	193.21	4.32
76	7.31	193.21	4.32
78	4.60	193.21	4.32
80	2.90	193.21	4.32

Earth

z (km)	p (mb)	T (K)	H (km)
0	1000.00	288.15	8.434
1	882.50	281.65	8.24
2	778.80	275.15	8.05
3	687.29	268.65	7.86
4	606.53	262.15	7.67
5	535.26	255.65	7.48
6	472.37	249.15	7.29
7	416.86	242.65	7.10
8	367.88	236.15	6.91
9	324.65	229.65	6.72
10	286.50	223.15	6.53
11	252.84	216.65	6.34
12	223.13	214.44	6.28
13	196.91	214.44	6.28
14	173.77	214.44	6.28
15	153.35	214.44	6.28

Mars

z (km)	p (mb)	T (K)	H (km)
0	6.5	250.32	13.01
2	5.542	241.32	12.54
4	4.696	232.32	12.07
6	3.952	223.32	11.60
8	3.303	214.32	11.14
10	2.738	205.32	10.67
12	2.251	196.32	10.20
14	1.833	187.32	9.73
16	1.477	178.32	9.27
18	1.188	177.00	9.20
20	0.956	177.00	9.20
22	0.769	177.00	9.20
24	0.619	177.00	9.20
26	0.498	177.00	9.20
28	0.401	177.00	9.20
30	0.322	177.00	9.20
32	0.259	177.00	9.20
34	0.209	177.00	9.20
36	0.168	177.00	9.20
38	0.135	177.00	9.20
40	0.109	177.00	9.20
42	0.087	177.00	9.20
44	0.070	177.00	9.20
46	0.057	177.00	9.20
48	0.046	177.00	9.20
50	0.037	177.00	9.20
52	0.029	177.00	9.20

Titan

z (km)	p (mb)	T (K)	H (km)
0	1460.00	93.21	20.8
2	1320.00	90.54	20.20
4	1190.00	88.20	19.68
6	1070.00	86.47	19.30
8	961.00	84.72	18.91
10	861.00	83.01	18.52
12	763.00	81.56	18.20
14	687.00	80.18	17.89
16	612.00	78.88	17.60
18	545.00	77.59	17.31
20	484.00	76.43	17.06
22	429.00	75.63	16.88
24	381.00	74.55	16.64
26	337.00	73.68	16.44
28	298.00	72.92	16.27
30	264.00	72.34	16.14
32	233.00	71.81	16.02
34	206.00	71.41	15.94
36	181.00	71.17	15.88
38	160.00	70.91	15.82
40	141.00	70.66	15.77
42	125.00	70.64	15.76
44	101.00	70.84	15.81
46	97.20	70.93	15.83
48	85.90	71.11	15.87
50	76.00	71.35	15.92
52	67.30	71.35	15.92
54	59.60	71.35	15.92
56	52.80	71.35	15.92
58	47.00	71.35	15.92

Index

The emphasis of this book is on comparative aspects of planetary atmospheres, generally meaning comparison with the Earth, including atmospheric composition, thermal structure, cloud properties, dynamics, weather and climate, and aeronomy. The goal is to look for common processes at work under different boundary conditions in order to reach a fundamental understanding of the physics of atmospheres. As part of a general physics course, the material is chosen to emphasise certain aspects that will be of broad topical interest:

- evolutionary processes, setting the Earth in its context as a planet and a member of the Solar System
- the properties of atmospheres that affect the climate near the surface of each planet
- measurement techniques and models, where the same experimental and theoretical physics is applied under different conditions to investigate and explain atmospheric behaviour.

These might be thought of as the astronomical, environmental, and technical sides of the discipline respectively.

The book covers the basic physics of planetary atmospheres in a single text for students or anyone interested in this area of science. The approach is the same as in the author's *Elementary Climate Physics*: an overview, followed by a more detailed discussion of key topics, arranged by physical phenomenon and not planet-by-planet as is usually found in this field. There is an emphasis on acquiring and interpreting measurements, and the basic physics of instruments and models, with key definitions and some historical background in marginal notes and in the glossary at the end of the book.

Fredric W. Taylor is Halley Professor of Physics in the Department of Atmospheric, Oceanic and Planetary Physics at the University of Oxford.

PRAISE FOR *ELEMENTARY CLIMATE PHYSICS*

'Fredric Taylor's Elementary Climate Physics *is an easy-to-read and useful introduction for undergraduate and graduate students who are interested in this increasingly important area of physics.'* Physics Today

Cover art by D.J. Taylor

OXFORD
UNIVERSITY PRESS

www.oup.com

ISBN 978-0-19-954742-5
9 780199 547425